Modeling the historical steel-concrete-composite-bridge-decks without shear connectors based on the in-situ-load-test

A.Ouchene

TU Delft Delft University of Technology

TU Delft and Ingenieursbureau Gemeente Amsterdam

Gemeente Amsterdam

Modeling the historical steel-concrete-composite-bridge-decks without shear connectors based on the in-situ-load-test

Insight in the load-bearing capacity of the historical bridge decks based on the in-situ-load-test.

By

A.Ouchene

in partial fulfilment of the requirements for the degree of

Master of Science
in Civil Engineering
at the Delft University of Technology,

to be defended publicly on Friday December 17th, 2021, at 9:30 AM.

Student number:	4325249	
Thesis committee	Dr. ir. M. Hendriks	TU Delft
	Dr. ir. Y. Yang	TU Delft, chair
	Dr. ir. H. van der Ham	TU Delft
	Dr. ir. A. de Boer	Gemeente Amsterdam

TU Delft

Preface

This thesis is written to complete the Master's degree of Technology at Delft University. This research has been performed in collaboration with the municipality of Amsterdam.

I would like to thank my graduation committee, consisting of Dr. ir. M. Hendriks, Dr. ir. Y. Yang, Dr. ir. H. van der Ham, Dr. ir. A. de Boer, for all their assistance during this research project.

I would also like to thank all my colleagues, friends, and family members, which have believed in my capacities to finish this master's study at the TU-Delft University, because it was not easy to combine my study with a part-time job at the municipality of Amsterdam, but I succeeded and therefore I would like to thank especially the following colleagues:
Annemarij Kooistra, Carla Adams, Frank Boerma, Jan Willem Düsseldorf and Ruud van der Meer.

Ali Ouchene
Delft, December 2021

Abstract

Nowadays, most of the historical bridges (Amsterdam, 2019) of Amsterdam do not meet the load-bearing criteria of the current design code (Eurocode: 2012). This has several reasons. It comes partly because of the overdue of the maintenance (Amsterdam, 2019) but also because the traffic load for which the bridge has been designed, is lower than the present traffic load (Amsterdam, 2019). The current Eurocode 4 does not guarantee the safety of this type of bridge decks. To guarantee the safety and the remaining service life of the historical bridges in Amsterdam, the municipality has started an investigation on historical steel-concrete-composite-bridge-decks. The focus in this thesis is on historical steel-concrete-composite-bridge-decks (a.k.a. *Verbundträger brücken in German)* because this type of bridges does not contain shear connectors in their configuration. This leads to the fact that the capacity of the bridge deck is almost not determined in the longitudinal and completely not determined in the transversal direction. The bridge deck in the longitudinal direction satisfies the unity check based on the protocol of the municipality of Amsterdam to check this type of bridges on safety, where they only consider the steel profile to define the capacity of the bridge in this direction. This is very conservative because the concrete is not taken into account during the calculation of the cross-section. In the transverse direction, the bridge deck does not fulfil the necessary unit check limit, because the municipality takes only the shrinkage reinforcement into consideration during their calculations. In addition to this, the state of the bridge decks and relevant research about how the bridge deck is build-up, is investigated. The main conclusion that can be taken from the cross-section of these type of bridge decks is that there is a lot of variation in all the components of the bridge decks.

Furthermore, during the investigation of the bridge decks it is decided to choose three typical bridge decks (A, B, C), which will be simulated to gain more insights about the cross-section of these historical bridge decks. The current Eurocode 4, which is implemented to guarantee the safety of the type of cross-section containing steel and concrete, does not provide an answer to calculate the load-bearing capacity of historical steel-concrete-composite-bridge-decks, because of a significant difference between the designed current Eurocode 4 model and the designed cross section of the historical model.

The behaviour of the bridge is studied in two directions based on the available literature. In the longitudinal direction, the focus is on the interaction between steel and concrete and how this interaction can be described. In the transverse direction, the aim is to find the relevant failure mechanism and corresponding modelling approach to define the behaviour of the bridge deck in the transverse direction of these bridge decks. The failure mechanisms that were evaluated are: Punching shear failure, compressive membrane action, and failure of concrete strut.

The assessment of the aforementioned failure mechanisms is carried out and the most logical model which can be used to validate during the FEA-simulation is the failure of concrete strut which can be modelled by strut and tie model. This model will also be carried out on the other two chosen bridges, next to bridge A on which the in-situ-load-test is done, to validate this model on more than one bridge deck. There was made use of an analytical model based on Eurocode 2, which has been compared the values of the numerical simulations.

To gain insight in the load-bearing capacity of the historical bridge decks in the longitudinal and transverse direction, an in-situ-load-test is set-up and carried out on bridge deck A in Amsterdam. The accentuation of this in-situ-load-test is to gain insight in the transverse direction, where the goal is to look into the collaboration of the steel-girders in combination with the slab. The main conclusion which can be taken from the in-situ-load-tests is that the results are in the non-linear range. For in-situ-load-test 1 and 3, which are both carried out on a symmetrical location on bridge deck A, there is no hard explanation of this non-linearity which has been observed based on the measured results. For the tested mid-span load location, the results are in the non-linear range. The slip occurs from 50 kN until 400 kN, and between 400 kN until 475 kN the deck becomes stiffer which leads to a change in the behaviour of the slip. In the transverse direction the goal is to gain insights in the cooperation between the steel-girders and the concrete slab. From the in-

situ-load-test the bridge deck shows the collaboration which is needed between the steel-girders and the available concrete slab. There is also slip available in the transverse direction and the results are also in the non-linear range.

The longitudinal direction is modelled as a separated beam (The steel-girder 4 is normative beam DIN26). The FEA-simulation and the analytical model of steel-girder 4 (is a composite beam of concrete and a steel girder) is validated and calibrated based on the performed measurements of in-situ-load-tests. The stress state of the separated composite beam is very low, which does not lead to a failure, where the difference ratio between the simulated stress and the allowable stress is about 10 % for steel and concrete.

In the transverse direction the deck is modelled, calibrated and validated to the performed in-situ-load-tests and the inspections which are available for the bridge deck. The information which is obtained from the inspections of bridge deck A has given more insight in the measurements results of the in-situ-load-tests, like the available corrosion between bottom flange of the steel girders and the concrete, which leads to the observation that the concrete is not connected to the steel girder. This validates the occurring of slip in the transverse direction. Based on this information, the goal is to validate the strut and tie model in the transverse direction. The results of the FEA-simulation, analytical model and the made sketch (which illustrates the load transfers in the transverse direction), validate the concept of the strut and tie model. The strut and tie behaviour is applicable in the transverse direction. The stress state in the load transfer region of the simulated beams is very low, which does not lead to a failure.

Finally, the other two similar bridge decks with longer spans, bridge decks B and C are numerical simulated and the results of these bridges are studied. During the modelling of these two bridges B and C in the longitudinal direction the same assumption is made as for bridge deck A. Based on this assumption, bridge decks B and C are simulated. The stress state of bridge decks B and C is very low, which does not lead to any failure. In the transverse direction the strut and tie model is also applicated on the other two bridge decks B and C. This leads to confirm that the strut and tie model is available in the transverse direction of the historical bridge deck for a load level of 475 kN.

Main overall conclusion:
Generally, this study has given more insight in the structural behaviour of the historical composite bridge decks, because the bridge decks have shown more capacity. The main knowledge which can be gained is that slip occurs from 0 kN until 400 kN, and between 400 kN until 475 kN the deck becomes stiffer which leads to a change in the behaviour of the slip. Furthermore, the strut and tie model is applicable and this gives as insight that the loads are transferring directly to the steel girders, specifically to the corner of the steel, flange and web.

Regarding the two directions (longitudinal and transverse) the main conclusions which can be taken for the historical bridge decks, based on the in-situ-load-tests and FEA-simulations, are:

a) The historical steel-concrete-composite-bridge-deck behaves in the non-linear stage, based on the performed in-situ-load-test measurements. The ratio of stresses of the steel girders and concrete slab of the bridge deck is very low compared to the allowable stresses of the Eurocode;
b) In the longitudinal direction, slip occurs from 0 kN until 400 kN, and between 400 kN until 475 kN the deck becomes stiffer which leads to a change in the absolute value of the slip;
c) Slip behaviour occurs in the transverse direction based on the measurement results;
d) In the transverse direction the strut and tie model is applicable on the historical steel-concrete composite bridge deck based on the performed analysis.

Contents

1. Introduction and Objective

This chapter will define the motivation behind studying the actual load-bearing capacity of the historical steel-concrete-composite-bridge-decks without shear connectors and the theoretical background behind it. Furthermore, the problem definition, the main objectives and the research questions will be defined. Finally, the outline of this thesis is described including the methodology.

1.1. Introduction

Most of the historical bridges of Amsterdam do not meet the load-bearing criteria of the current actual Eurocode: 2012, partly due to overdue maintenance that has not been done in the last several decades. Also, the traffic load for which the bridge has been designed, is lower than the present traffic load. To guarantee the safety of the historical bridges of Amsterdam, the municipality has started an investigation based on an in-situ-load-test. The test has been performed on bridge deck A to define the actual bearing capacity for historical bridges. Based on the input of the in-situ-load-test the thesis assignment is set to gain insight into the mechanical behaviour of the bridge deck in the longitudinal and transverse direction. In the longitudinal direction the goal is to define the interaction level between the steel profile and the concrete slab, based on the measurement data from the in-situ-load-test (see chapter 4). When the interaction level is defined, the collaboration between the two-materials, that is steel and concrete, will be properly defined. The results of the FEA-simulations in the longitudinal direction will be used to set-up a numerical formula which gives, in percentage, the composite action. The results of the longitudinal direction will give insight in the capacity of cross-section based on the defined interaction level between the two materials (steel and concrete). In the transverse direction, the focus will be to gain insights from the following checking methods which are applicable in the transverse direction of the historical steel-concrete-composite-bridge-deck:

a) Punching shear failure;
b) The compressive membrane action;
c) The strut and tie model.

The goal is to find out which of the above checking methods are applicable for the transverse direction of the historical steel-concrete-composite-bridge-deck. This is briefly the motivation of the research. The exact problem with which the structural engineers on the municipality are dealing with will be described and explained in the following paragraph.

1.2. Problem definition

At this moment, the structural department of the municipality of Amsterdam uses the Finite Element software tool to model the bridge deck. The concrete slab is modelled as a plane with shell elements. The steel-girders are modelled as line elements. The two elements are modelled at the same neutral axis, which is not realistic as there is partial interaction between them in the longitudinal direction. These results are constructive because the department takes only the steel-girders into consideration. This leads to unrealistic results which underestimate the capacity of the historical bridge deck in the longitudinal direction. See the figure 1-1 (Figure 1-1 The difference between the physical problem and the modelled problem) where the cross-section is modelled. In the transverse direction the department takes only the concrete slab including the shrinkage reinforcement into consideration during the testing of the capacity of the bridge decks, and this is not enough to meet the design load in the Eurocode. Therefore is it suspected that in the transverse direction there is a larger capacity, because by activating the near steel girders in the transverse direction there is a greater capacity out of this deck than the way which is being used now in the department. This leads to unrealistic underestimated conclusions about the cross-section capacity because the true capacity of the cross-section is not taken into consideration. In addition to this, even if the unity check of the bridge deck is larger than 1 in the transverse direction, and for the longitudinal direction the steel girder is enough to meet the unity check of 1, the bridge deck shows clearly defects in the inspections. But the risk of the defects is not high according to RAMSP (definition in paragraph 2.2.3). See figures 1-2 (Inspection of bridge X) below, which for example shows cracks in the longitudinal direction at the fold lines, leakage, and lime bloom on the bottom of the deck. This has consequences for the advice of the structural engineers at the department towards the client. Because the given advice based on the protocol which Amsterdam is using is not matching with the reality of the bridge (which is in better state). Following that, the department wants to check the reliability of these results and to develop a new protocol to gain more insights into the actual load-bearing capacity of these type of bridge decks. The protocol of the department can be found in Appendix A.

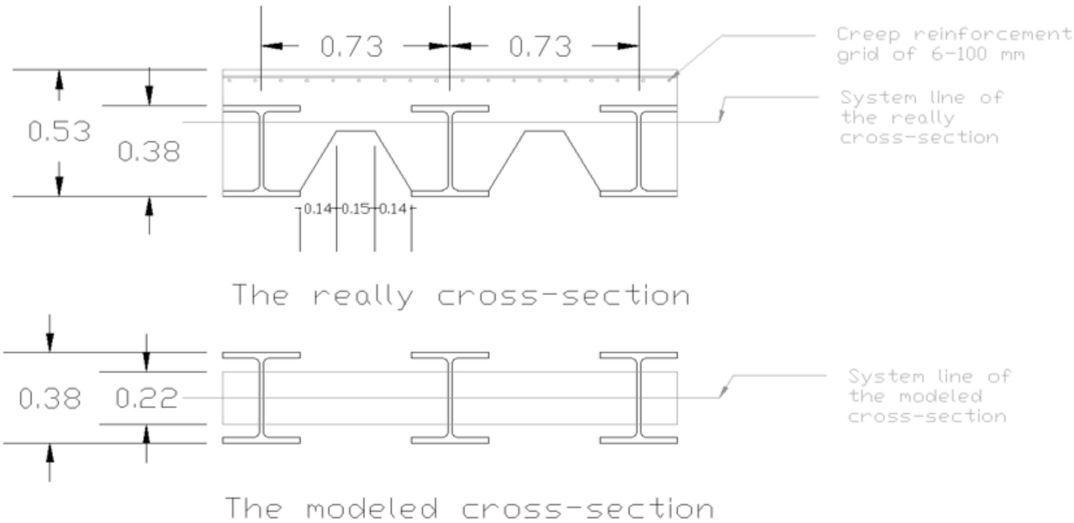

Figure 1-1: The difference between the physical problem and the modelled problem.

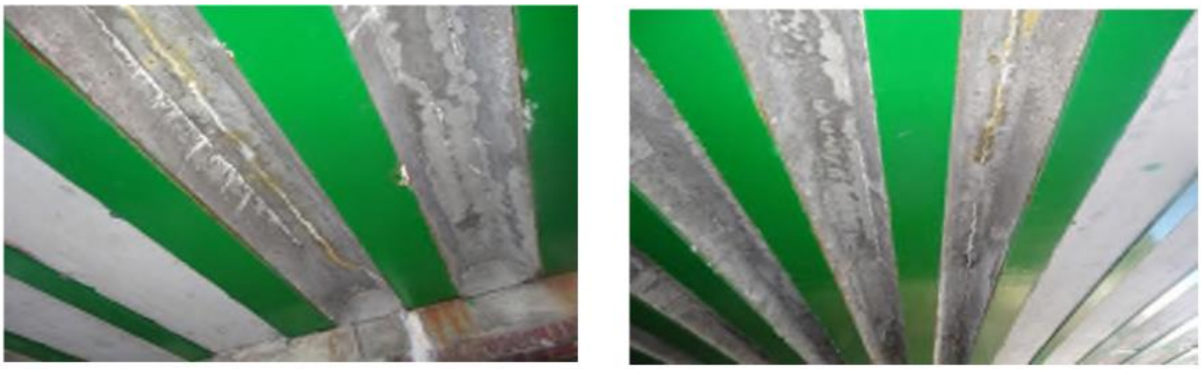

Figure 1-2: Inspection of bridge X (Antea Group B.V., 2016).

The main objective of this research is to gain insight into the actual load-bearing capacity of historical steel-concrete-composite-bridge-decks. This will provide us insights in the mechanical behaviour of the historical bridges in the longitudinal and transverse direction. The results will help us to develop a method which can be used to define the composite action in the longitudinal direction. For the transverse direction the objective is to gain insights into the following mechanical behaviour:

a) The effective width;
b) Punching shear failure;
c) The compressive membrane action;
d) The strut and tie model.

This will be done by using the in-situ-load-test of bridge A and by modelling the historical steel-concrete-composite-bridge-deck in FEA.
In the following paragraph the research questions which will be discussed in this thesis are summed up.

1.2.1. Research questions

The main objective of this research will be investigated by analysing the following research questions:

1. **<u>Main question</u>**

How does the historical steel-concrete-composite-bridge-deck behaves based on the in-situ-load-test in the two directions?

2. **<u>Sub-question</u>**

1. How is the in-situ-load-test of bridge A built-up?
2. What are the conclusions which can be taken from the site (of in-situ-load-test) during the testing of bridge A?
3. How are the composite bridge decks in Amsterdam build-up (geometry/material properties)?
4. What is the current condition of the composite decks in Amsterdam based on the inspections?
5. Is it possible to set-up a FEA-simulations to cover the interaction behaviour between the steel and concrete, based on the condition of historical steel-concrete-composite-bridge-decks from the inspections and the measured results of the in-situ-load-test?
6. Which of the four proposed loadbearing mechanisms can describe the behaviour of the deck in the transverse direction?

1.3. Research methodology and Content of the thesis

First, a background study is presented in chapter 2 and 3. In chapter 2 an overview of the decomposition of the historical steel-concrete-composite-bridge-deck is shown, the overview is done by investigating 32 bridge decks. Furthermore, in chapter 2 an overview of the research relevant for the historical Amsterdam bridge deck is included. This is done by analysing the output from the 32 bridge decks. In chapter 3 theoretical background is reviewed for the most relevant theories which can be applied on the historical Amsterdam bridge decks. An assessment of the theories is done based on different inputs from the investigation of the 32 bridges and the in-situ-load-test. Finally, a total conclusion is included in the chapter.
The second part deals with the in-situ-load-test. To understand the behaviour of the historical bridge decks an in-situ-load-test is done. The in-situ-load-test gives us a practical understanding of the behaviour of the historical Amsterdam bridge decks from the site. The goal is to use the measurements and simulate the behaviour of the historical Amsterdam bridge decks. In chapter 4 the in-situ-load-test is described, and the results are evaluated.

The third part (chapter 5) contains general information about the three chosen bridges. This general information is about the geometry and the other properties which are required to build-up a FEA-model. The bridges will be simulated and described in chapter 6 and 7. Furthermore, in this chapter the calibration process for the 2D linear simulated separated historical beam is described and the results of the 2D numerical simulation of the separated historical beam are presented and discussed. Lastly, conclusions are mentioned in this chapter about the 2D separate beam.

In the fourth part (chapter 6), the 3D linear analysis of the historical bridge deck A is described. The 3D numerical simulations of bridge deck A are presented. Finally, the discussion and conclusions are mentioned in this chapter for bridge deck A in the longitudinal and the transverse direction.
In the fifth part (chapter 7), evaluation of the behaviour of the historical Amsterdam bridge decks based on 3D-lineair simulations (bridge B and bridge C) is described and compared with the numerical simulation of bridge deck A. The numerical simulations of the bridge decks are presented. At last, the discussion and conclusions are mentioned in this chapter for the three bridge decks in the longitudinal and transverse direction.

Finally, the main conclusion and discussion of this thesis is mentioned in chapter 8 for the three bridge decks in the longitudinal and transverse direction. Also, the recommendation which are need to optimize the research in the longitudinal direction are mentioned

2. State of historical bridge decks

The chapter aims to provide a deeper understanding of the historical steel-concrete-composite-bridge-deck. First, the historical background of these bridges and their development over time is described. In addition to this, an overview of the decomposition of the historical bridge decks will be described. At last, an overview of the relevant research will be added.

2.1. Introduction

Amsterdam is one of the oldest cities in the Netherlands. The city contains a lot of old bridges. These bridges had during their lifecycles many construction maintenances, because of the change in the local traffic over the years. Earlier men started with horse wagons, and some bridges are designs for this type of traffic and reconstructed for other local traffic which is developed over the years, like tramway or heavy transport trucks. Because of these issues like traffic load and the reconstruction, the question which can be asked is: are these bridges safe and for how long? This aspect has come forward during the implementation of the Eurocode in 2012. Because the local bridges in Amsterdam does not satisfy the Eurocode, the municipality began with a vast program which is named in Dutch (Programma Bruggen en Kademuren) (Amsterdam, 2019). This program is a project which will research all the traffic bridges and reconstruct the bridges which are beyond lifespan and give an optimal answer about the assets (bridges) of Amsterdam. The focus will be made in this research on the historical steel-concrete-composite-bridge-deck. As mentioned before the bridges are reconstructed during the years and had all lot of changes in their configuration. Due to this issue, there is a need for a broader investigation of the historical composite decks like the interaction between steel and concrete which is unknown. In the figures 2-1-an and 2-1-b the historical bridge A is illustrated into images where the in-situ-load-test is made.

Figure 2-1 a: Bridge A in Amsterdam after the reallocations of the bridge in 1935.

Figure 2-1 b: Bridge A in Amsterdam before reallocations of the bridge in 1935.

Figure 2-1: The historical of bridge A in Amsterdam from 1935 to 2020 illustrated in the images above (Reniers , 2021).

The main question which can be asked:

a) How is the historical steel-concrete-composite-bridge-deck build-up?
b) What type of traffic passes over the historical steel-concrete-composite-bridge-deck?
c) What are the relevant points to research over the historical bridge deck during this thesis?

These questions will be answered in the coming sub-paragraphs.

2.2. Overview of the historical bridge deck of Amsterdam

To address and to gain an overview about the historical steel-concrete-composite-bridge-decks, we need to look for information in the archive of the municipality of Amsterdam. The drawings, calculations and contract drafts there contain a lot of information about the bridges and were created during the design and construction of the bridges. The starting point is a brief description about bridge deck A to illustrate the importance of the drawing and the information they contain:

The historical steel-concrete-composite-bridge-deck of bridge deck A contains two directions, the longitudinal direction, and the transvers direction. The historical steel-concrete-composite-bridge-decks decks can be differentiated based on the following aspects in the longitudinal direction, and the transvers direction:

a) The type of steel profile that has been used;
b) The height of the concrete cross-section;
c) The used material above the steel-concrete deck;
d) The location of the pipes related to the width of the deck.

In the figure 2-2 the variation of the items above can be seen.

The lanes which are available on bridge deck A in the transverse direction are:

a) Foot and/or Bike lanes left and right;
b) Vehicle -lanes;
c) Tramways.

The lanes have also a variation in the transvers direction based on the location of the bridge in Amsterdam and the traffic which belongs to the bridge. In figure 2-3 an illustration of the location of bridge deck A is given to indicate the different lanes on the bridge.

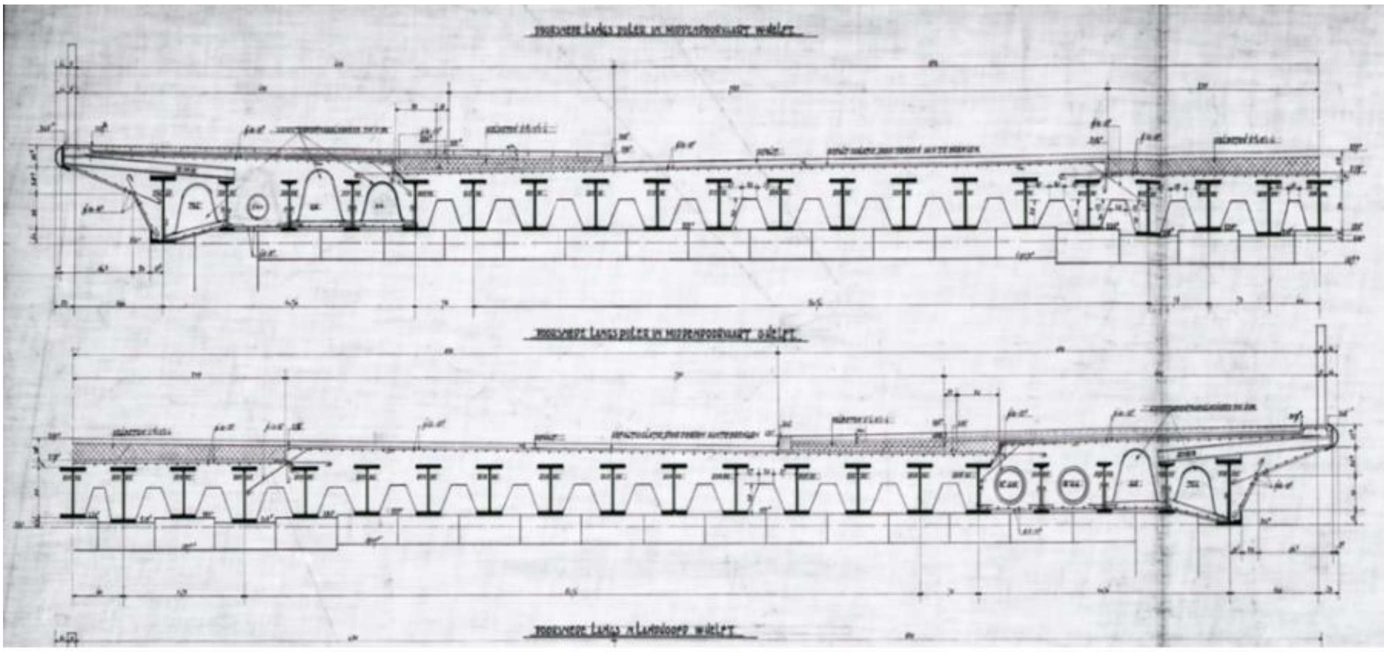

Figure 2-2: Layout of the bridge deck A in the transverse direction (Municipality of Amsterdam, 2019).

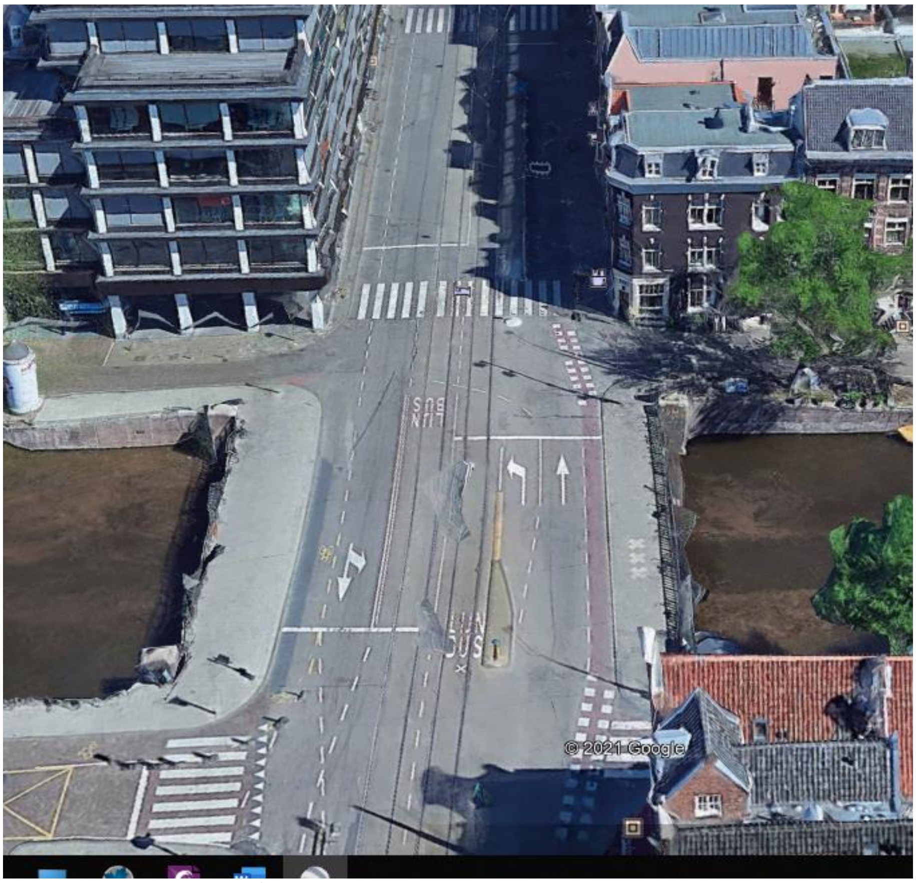

Figure 2-3: Layout of the bridge deck A in the real situation (Google Street View, 2021).

The decision is made to consider 32 bridges in an investigation because all the 32 bridges do not contain shear connectors. The investigation will give an overview about the decomposition of the historical bridge decks and the material properties. The input for the investigation is the drawing of the different bridges. The investigation gives us a global picture of 1/6 assets (bridges) of Amsterdam. In Amsterdam there are circa 150 of historical steel-concrete-composite bridges available. The idea is to select randomly 32 bridges out of 150. The 32 bridges will be researched, and the information will be collected from the drawing and translated into a database. The database is formed to be representative for the transverse direction of the bridge deck. That means that there is a translation from the reality to the database where all the items are stored. The items which have been taken into the database are:

a) Bridge number (are numbers which are introduced for the bridges);
b) Type span (is the span of the bridge (main/side-span));
c) Number of spans;
d) Length span;
e) Total width bridge deck;
f) Construction year;
g) Statically un/determined;
h) Material quality (steel/concrete) (material quality is depended on the dossier of the bridge);
i) Current material quality based on the inspections (steel/concrete);
j) Information of inspection (how is the condition of the bridge);
k) Reinforcement layout of the different lanes;
l) Width of the difference lanes of bridge deck in [m];
m) The minimal height of bridge deck;
n) A center -to-center distance for the difference lanes (is the distance between the steel profile, in the drawing there are more center -to-center distance available there for the number 1 until 3);
o) Steel profile of the bridge for the difference lanes (type/properties).

The 32 bridges in Amsterdam are investigated in the longitudinal as well as the transverse direction. From the investigation the data is obtained. The relevant data will be described for each item.

The 'type span' is the span of the bridge deck in the longitudinal. There are two type of spans, which are the main- and the side-span.

The bridge decks are composed out of one, two and three number of spans in the longitudinal direction. The length of the spans is varying from 5.5 m till 13.5 m. Based on the length of span the effective width is calculated according to the current Eurocode 4 (see the assessment of this part in sub-chapter 2.3.2).

The bridge deck is statically determined, even if it contains more than one span, because the deck contains only shrinkage reinforcement. The amount of reinforcement is not enough to reach a statically undetermined situation.

The minimal height of the cross-section is also added. In the database is only the height of the concrete taken into consideration above the steel.

In the transverse direction the width of the bridge decks is also varying based on the type of traffic which is passing over the bridge deck like a tram, tracks or foot/bike. The variation is from 8 m till 30 m per type of passing traffic over the bridge.

The construction year of the bridges is varying from 1863 till 1954. In this period as mentioned in sub-chapter 2.3.1 the bridges don't contain shear connectors. This is described in sub-chapter 2.3.1.

The steel girders are varying based on the type of traffic and the length of the span of the bridge decks.

The center-to-center distance between the steel profile is also added in the database. This distance is important to compare with the effective width. The comparison can be seen in the sub-chapter 2.3.2. The center-to-center distance has also a variation over the width of the bridge, this variation is analysed and a mean center-to-center distance is chosen, see appendix A.

The reinforcement which has been used on this type of deck is only the shrinkage reinforcement which is a steel bar of 6 over length of 100 mm or steel bar of 8 over length of 100 mm. This amount of reinforcement is not sufficient to reach the needed capacity in the transverse direction as mentioned earlier in the problem definition.

In addition to this, the material properties are obtained from the contracts which describe the amount of the concrete mixture. The concrete mixture contains the following element and the amount of each element is added, cement = 100 Kg, grind 2.4 Kg and sand = 3.8 Kg. This information gives not a view about the situation of bridge deck now, for that an extra investigation is needed. The investigation will be made based on destructive inspections on the bridge deck A where the material properties will be estimated, see sub-chapter 2.3.3. This true also for the steel profiles as well. The strength of the steel profiles is also included in the contract. The strength which holds now will be investigated in the same way as the concrete. The material properties which are investigated based on destructive inspection are added to the database. This will be explained in sub-chapter 2.3.3.

The information about the 32 bridges is added in the database for each item. The database will help with answering many questions about the historical steel-concrete-composite-bridge-deck. The obtained data will also be helpful by addressing the mechanical behaviours which are mentioned earlier in the introduction, like the punching shear for example. In addition to this, the data will be used during the modelling of the FEA-simulations. Furthermore, the data is analysed to check if there is some correlation between the items. The result of this analysis is that the data has no correlation between the different items and for more details see appendix A.

The obtained data is analysed, the conclusion that has been taken is summed up below and for more details see appendix A.

The following conclusion can be taken:

Firstly, the shrinkage reinforcement is not enough to reach the needed capacity in the transverse direction and in the longitudinal the reinforcement doesn't help to reach a statically undetermined system.

Secondly, the center-to-center distance is smaller than the effective width but this will be discussed in the coming sub-chapters 2.3.2.

Thirdly, the material properties must be obtained from the destructive inspections.

Fourthly, the steel profiles are varying over the width of the bridge deck in the transverse direction. This is dependent on the length of the span and the type traffic which is passing over the bridge deck.

At last, three bridges are chosen from the investigated 32 bridges.

After the investigation on the state of the 32 bridges, the bridges are collected in three groups that vary from low to high length in the main span. From each group, a bridge is chosen as the most common bridge to represent that group. So three bridges are chosen for further investigation to define the load-bearing behaviour of these type of bridge decks.

To select these three bridges, the most important criteria was the length of the main span, where the bridge with the highest length inside a specific group was selected. The chosen bridge decks are:

a) **Bridge A** is a representative bridge in the first group (this group contains the lowest length of main spans), because the length on the main span is 7,8 m, but due to sail restrictions of the municipality of Amsterdam during the execution of the in-situ-load-test, it is chosen to use the side-span 6.5 m, and that will be the case also in this thesis assignment;
b) The second bridge is **bridge B**, because this bridge does not contain any tramway and is from the category 10 m span;
c) The third bridge (**bridge C**) is based on the configuration of the cross-section properties and is from the category 13 m span. This is the same for some other bridges in the collection of the 32 bridges.

More information about all the bridges and the population can be found in the appendix A.

For more information about:

a) Overview of the relevant decomposition;
b) Database;
c) Drawing of the selected 3 bridges.

See appendix A.

2.3. Overview of the relevant research over the historical Amsterdam bridge deck

2.3.1. History and Description of steel-concrete cross-section

The origin of the historical steel-concrete-composite-bridge-deck (named also *Verbundträger brücken*) comes from Germany and Austria. These type of bridge decks were constructed before 1950. The bridge decks contain German profile like the DIN or INP as mentioned in the previous figure 2-2. At the concrete part of the deck a minimum of shrinkage reinforcement is present. Later on, the amount of reinforcement was increased from shrinkage reinforcement till top and bottom reinforcement. In 1930 a discussion was started about the minimum of interaction connectors. In 1950 these interaction connectors were incorporated in the concrete design recommendation. In the period between 1950 and Eurocode 4:(NEN-EN 1994-1-1:2005+C1:2009+NB:2012) the interaction behaviour has been updated. In this period (1950 and Eurocode 4:(NEN-EN 1994-1-1:2005+C1:2009+NB:2012)) men began to use shear connectors in the bridge decks, which were still not reliable enough to withstand the needed interaction level between steel and concrete. The reliability of the shear connectors of these type of bridge decks which are designed in this period (1950 – 2012) can be investigated after a solution has been found for the partial interaction of the historical steel-concrete-composite-bridge-decks without shear connector. Nowadays, based on the knowledge and the experience which engineers got, it can be concluded that there is no full interaction between the steel and concrete, but only partial interaction. Based on this conclusion, the following questions can be asked:

a) At which level (maximal applied load) is there a partial interaction available in the longitudinal and transverse direction?
b) Does the effect that the steel profile is embedded in the concrete improve the interaction level?

2.3.2. Assessment of the historical steel-concrete-composite-bridge-deck under the scope of Eurocode 4

Description of the model of the Eurocode 4:

In this paragraph the model of the Eurocode 4 will be described. Eurocode 4 (NEN-EN 1994-1-1:2005+C1:2009+NB:2012) is the recommendation that guarantees the structural safety of the composite steel-concrete cross-sections. In current Eurocode 4 the only model which is taken into account to calculate the steel girder in combination with the concrete slab in the longitudinal direction and the transverse direction is shown in figure 2-4 (Cross-section which is being used in the current Eurocode 4 in the longitudinal direction and the transverse direction). The model in figure 2-4 presents the way to define the loading bearing capacity on the cross-section level for new construction in the longitudinal direction and the transverse direction. In the figure the longitudinal and the transvers direction of the composite model can be seen which is being used in the Eurocode 4. At the top of the steel girder the concrete specimen is positioned with an effective width (see problem definition for more information about the effective width). Furthermore, the steel girder is presented at the bottom side in the figure. At the interface between the steel and concrete, the shear connecters are presented. The shear connectors have the function to let the steel and concrete at the interface collaborate. The amount of them is depending on the external presented force. The total height of the concrete slab begins above the steel flange, under the steel flange there is no concrete available. In short, the decomposition of the cross-section:

a) Steel-girder;
b) Total height of the physical properties of the reinforcement concrete-slab above the flange of the steel-girder;
c) Shear connectors.

The analytical way to calculate the cross-section in this model is presented in the Eurocode 4 *(Het Nederlands Normalisatie-instituut, 2012).*

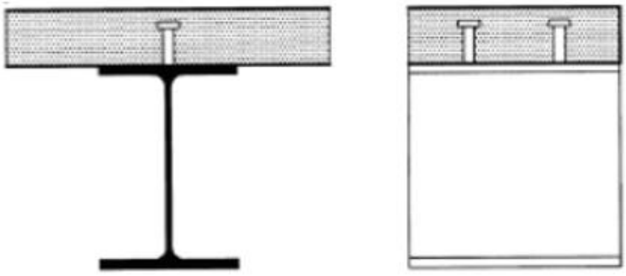

Figure 2-4: Cross-section which is been used in the Eurocode 4 in the longitudinal direction and the transverse direction (Het NederlandsNormalisatie-instituut, 2012).

General description of the historical steel-concrete-composite-bridge-decks in Amsterdam from 1920 until 1950:

The existing calculation and drawing will give more insights in the way which has been used to calculate the historical steel-concrete-composite-bridge-deck. The obtained information will be described in this paragraph and the comparison between the Eurocode 4 and the historical steel-concrete-composite-bridge-decks will be made. In figure 2-5, the longitudinal direction and the transverse direction of the cross-section of bridge deck C is presented. Figure 2-5-a, presents the cross-section in the transverse direction. Figure 2-5-b, presents the longitudinal direction of the bridge deck.

In the transverse direction, at the top side, there is asphalt presented. Under the asphalt begins the historical steel-concrete-composite-bridge-deck. The concrete part contains only shrinkage reinforcement grid at the top of concrete layer. Besides that, the steel girder is also presented in the top figure.

In bottom figure of the longitudinal direction the deck is presented. Furthermore, the abutment and the pillars are also presented in the figure. Last part which is shown in the figure is the height compared to the NAP (Normaal Amsterdams Peil/Normal Amsterdam level).

The cross-section of the historical steel-concrete-composite-bridge-decks which is shown in the previous figures has different components in relation to the Eurocode 4. For example, there is no shear connector, etc. This can be seen in figure 2-5 which shows the decomposition of the historical steel-concrete-composite-bridge-decks in general. In short, the decomposition of the cross-section:

a) Steel-girder;
b) Concrete slab with shrinkage reinforcement grid;
c) No - shear connectors between the steel girder and the concrete slab;
d) Asphalt layer on top of the concrete slab;
e) Hollow tubes for gas, electricity cables.

Besides the drawing information which has been described above, there are also existing calculations. From this document the model is obtained. The model has been used during the calculation of the bridge deck to define the load-bearing capacity of the cross-section in the 1950. This gives an idea about the way men used to ensure the safety of the deck. The model is presented in figure 2-6 (schematic which has been used to design and calculate the bending capacity of the historical steel-concrete-composite bridges). The main difference with the current Eurocode 4 is the embedded geometry of the concrete slab and the steel-girder, and the non-presence of shear connectors. Also the effective width of the historical bridge deck is smaller than the calculated effective width of the current Eurocode 4, which will be addressed in the following paragraph. How the bridge deck is calculated in the past calculation of the capacity of the historical bridge deck based on the way which is made in the past, is added in the coming chapter 2.3.4

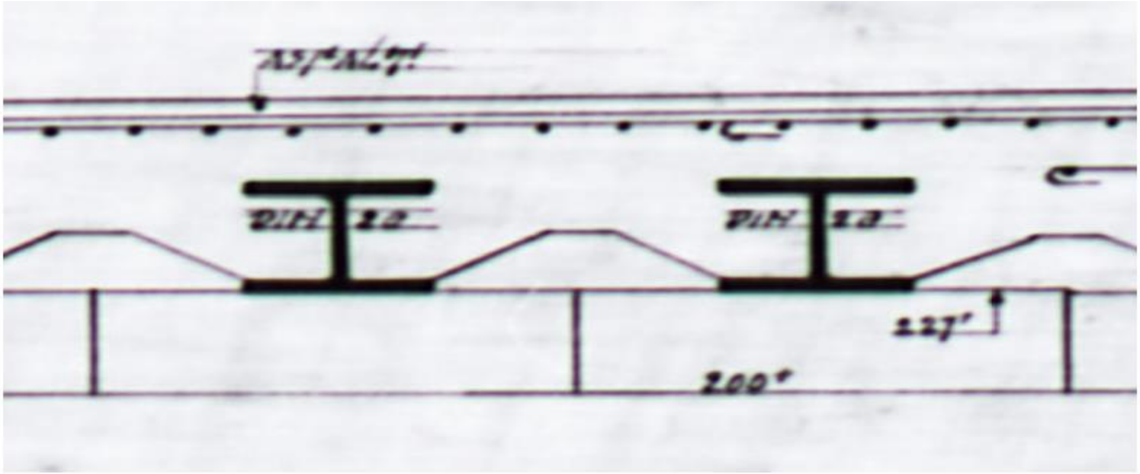

Figure 2-5 a: At the top side, the cross-section in transverse direction (Municipality of Amsterdam, 2019).

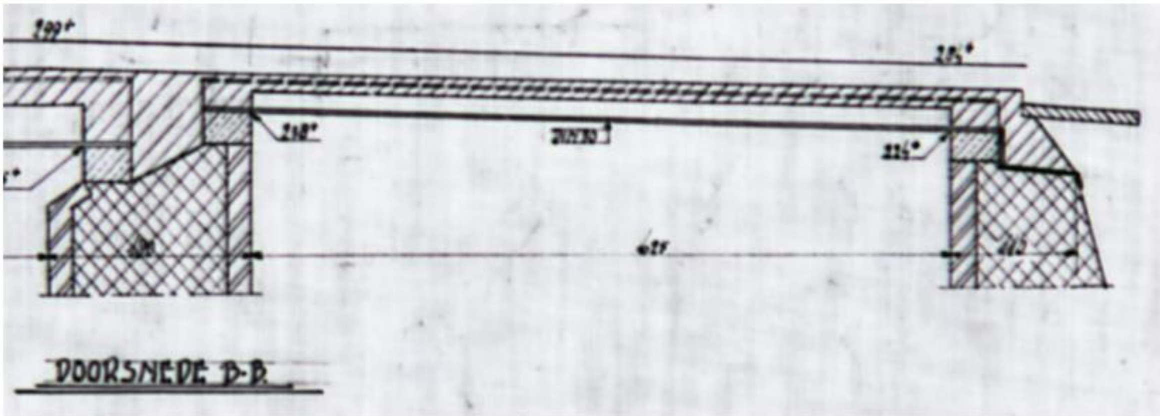

Figure 2-5 b: The bottom the longitudinal direction (Municipality of Amsterdam, 2019).

Figure 2-5 : Cross-section of bridge deck C in Amsterdam in the longitudinal direction(bottom) and the transverse direction(top) (Municipality of Amsterdam, 2019).

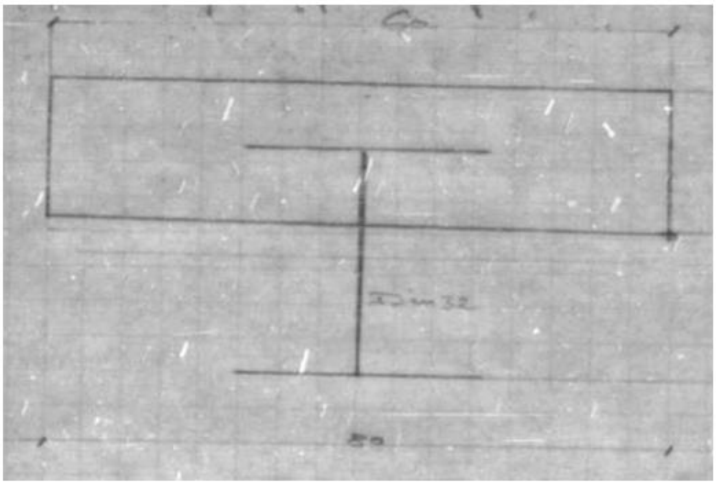

Figure 2-6: Schematic which is been used to design and calculate the bending capacity of the historical steel-concrete-composite bridge deck (Municipality of Amsterdam, 2019).

Differences between the current Eurocode 4 model and the historical model:

The cross-section of the historical steel-concrete-composite-bridge-deck is not described in the Eurocode 4, because it covers only the design of new structures. At the moment, there is no additional specific document available for existing steel-concrete structures in Europe or the Netherlands to check the structural safety of the historical steel-concrete-composite-bridge-decks. The main differences between the two models are:

a) The historical cross-section does not contain the shear-connecters;
b) The historical bridge decks are calculated in the past with the idea that there is a full interaction;
c) The geometry of the concrete slab is embedded in the steel profiles of the historical steel-concrete-composite-bridge-decks and that is not the same as the model of the Eurocode 4.

Besides the geometry and the missing shear-connecters, the engineers before 1950 used the design philosophy where the cross-section is based on a 100% interaction between the steel and concrete. Based on this conclusion, that there is no full interaction, this case study is started. This study will lead to answering the safety and the load-bearing capacity of this type of historical cross-section.

The influence contribution of the effective width on the actual load-bearing capacity of the historical steel-concrete-composite-bridge-deck:

The effective width is calculated based on the Eurocode 4. The value of the effective width is compared with center -to-center distance between the steel profiles. Based on this analysis it is concluded that the value of the center -tot-center distance is smaller than the effective width which is calculated. This gives a positive result, based on the assumption that there is some capacity hidden in the transverse direction. More specific, is that the adjacent steel-girders can take over the load in some percentage. This conclusion can be validated during the numerical modelling. Key 1 is used from the figure 2-7. This model is based on a two-points support beam. The reason why this model is chosen is because there are no assumptions which can lead in the cross-section to use the theory of continuous beams. Because in the longitudinal direction there is only shrinkage reinforcement in the cross-section and that is not enough capacity to transfer the moment distribution from one field to the other. Therefore, model 1 has been used. The figure 2-7 shows the way to calculate the effective width for a steel-composite cross-section. See figure 2-7 (Equivalent spans, for effective width of concrete flange (adapted from Eurocode 4 (Het Nederlands Normalisatie-instituut, 2012)). The calculated values in the database for the effective width have some variation because the effective width depends on the main and side-span value. However, the interesting part is that the center -to-center distance for most bridges is smaller than the calculated effective width as mentioned before. This leads to the conclusion that there is some capacity left to get from the effective width in the cross-section. See figure 2-8: (Analysis of the effective width based on the main span of bridge deck A compared with center -to-center distance of the steel-girders) where the difference can be seen for bridge deck A.

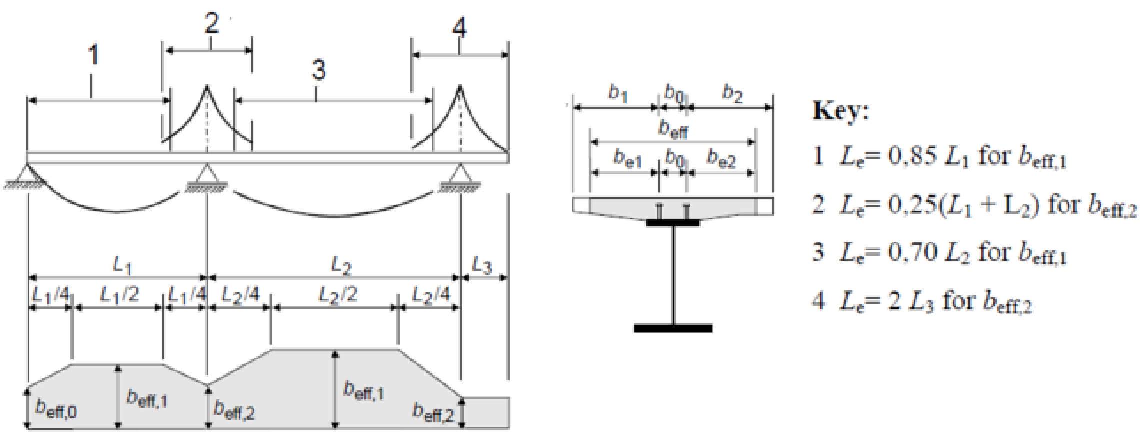

Figure 2-7: Equivalent spans, for effective width of concrete flange (Het NederlandsNormalisatie-instituut, 2012).

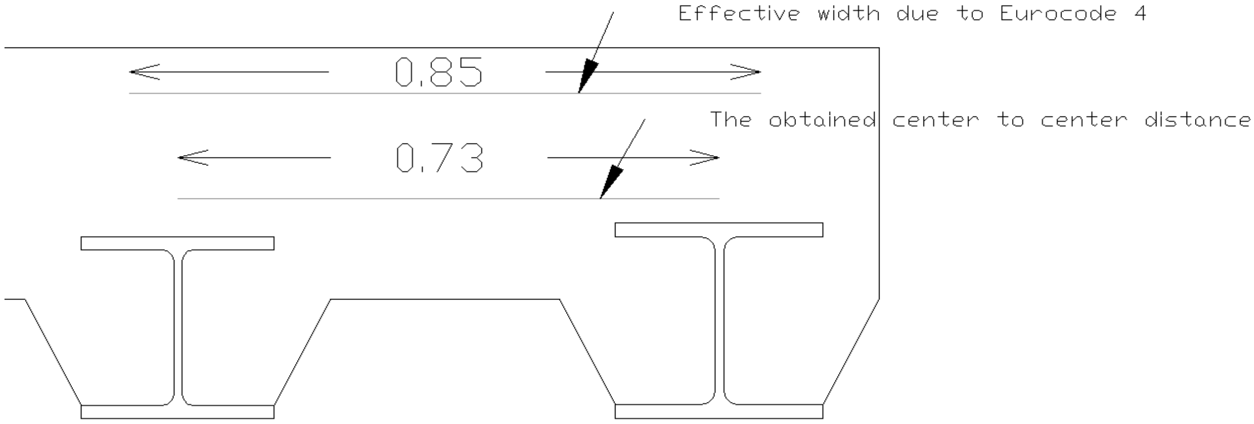

Figure 2-8: Analysis of the effective width based on the main span of bridge deck A compared with center -to-center distance of the steel-girders.

Conclusion:

Based on the assessment about the Eurocode 4 compared to historical bridge decks, the conclusion can be taken that the Eurocode 4 can be useful but the articles don't to guarantee the safety of the historical bridge decks. This is because of the differences and the missing elements (see points which are mentioned in the paragraph of Differences between the current Eurocode 4 model and the historical model) in the cross-section of the historical bridge decks. The cross-section of the historical steel-concrete-composite-bridge-decks is not included in the Eurocode 4. Therefore, there is no guideline available which is representative for the historical steel-concrete-composite-bridge-decks and it is needed to introduce a guideline for these type of bridge decks. Besides the difference between the cross-section which is presented in the Eurocode 4 and the cross-section of the historical steel-concrete-composite-bridge-decks, the engineers before 1950 used the design philosophy that the cross-section is based on a 100% interaction between steel and concrete, which is however not fully available is in the cross-section. Furthermore, the effective width of the historical steel-concrete-composite-bridge-decks is calculated based on the Eurocode 4 formulas. The value of the calculated effective width based on the Eurocode 4 is compared with the center-to-center distance between the steel profiles. Based on this analysis, it is concluded that the value of the center-to-center distance is smaller than the calculated effective width based on Eurocode 4. This conclusion can lead to extra bearing capacity of these type of bridge decks. The strut and tie model underline this conclusion. This conclusion will be validated during the numerical modelling of the transverse direction.

2.3.3. Assessment based on the condition of the bridges from the inspections

The inspections which are used during the analysis are from the year 2016. The information from the inspection gives an overview about the condition of the bridges. This information also gives a risk assessment of the bridge according to the CUR recommendation 72, class 1.2 and the NEN2767-4 system. The detected damages are recorded in a sheet according to the model of the RAMSHEEP risk assessment. The RAMSHEEP will be defined in the following table. All the definitions are included in the table below.

Table 2-1 Definition of the RAMSHEEP.

Letter	Aspect	Description
R	Reliability	The chance that due to the lack of measures the object will be destroyed by the established damage can no longer perform its function in the coming 5 year.
A	Availability	The blocking duration (for road and / or shipping traffic) if the building part / element occurs because of the established damage.
M	Maintainability	The extent to which the part can be reached / maintained / delivered.
S	Safety	The consequences for personal safety if the building part / element occurs.
H	Health	The degree to which the health of the user can be affected.
Ec	Economics	The extent to which the repair costs will increase due to the absence of measures. This partly concerns the damage development, partly it concerns the way in which to recover.
En	Environment	The degree to which the environment is polluted because of the defect.
P	Political	The degree to which the artwork is polluted, and this affects its appearance of the object.

The inspections reports are investigated to get an overview about the different thirty-two bridge decks. The most common defects which are found in the inspection of the different thirty-two bridges are shown in the table 2-2:

Table 2-2 the defect of thirty-two bridge decks.

Bridge name	Cracks are present in the longitudinal and transverse direction in the concrete	The deck shows trace leakage at the underside of the deck	There is lime bloom at the underside	Corrosions of the steel beams	The reinforcement is corroded
Bridge D	Yes	Yes	Yes	Yes	No
Bridge E	Yes	Yes	Yes	Yes	No
Bridge F	Yes	No	No	Yes	No
Bridge G	Yes	Yes	Yes	Yes	Yes
Bridge H	Yes	Yes	Yes	Yes	Yes
Bridge I	Yes	Yes	Yes	Yes	Yes
Bridge J	Yes	Yes	Yes	Yes	Yes
Bridge K	Yes	Yes	Yes	Yes	Yes
Bridge L	Yes	Yes	Yes	Yes	Yes
Bridge M	No	No	No	No	No
Bridge N	Yes	Yes	Yes	Yes	No
Bridge O	Yes	Yes	Yes	Yes	No
Bridge P	No	No	No	Yes	No
Bridge Q	No	No	No	Yes	No
Bridge R	No	No	No	Yes	No
Bridge S	Yes	Yes	Yes	Yes	No
Bridge T	Yes	Yes	Yes	Yes	Yes
Bridge U	Yes	Yes	Yes	Yes	No
Bridge V	Yes	Yes	Yes	Yes	No
Bridge W	Yes	Yes	Yes	Yes	No
Bridge X	Yes	Yes	Yes	Yes	No
Bridge Y	Yes	Yes	Yes	Yes	No
Bridge Z	No	No	No	No	No
Bridge AA	Yes	No	No	Yes	No
Bridge AB	Yes	Yes	Yes	Yes	No
Bridge AC	Yes	No	No	Yes	No
Bridge AD	Yes	No	No	Yes	No
Bridge AE	Yes	No	No	Yes	No
Bridge AF	Yes	No	No	Yes	No

In general, those are the defects which are found in the inspection reports about the thirty-two bridges. The focus will go to the three selected bridge decks A, B and C which are already chosen from the database in the previous chapter. The inspection reports of the three bridge decks will be analysed and the defects will be summed up. The named defects will be taken into consideration during the numerical modelling of the cross-section of the decks. Example given, how to use the output from the inspection reports:
If the bridge deck shows cracks in this case, the elastic module of concrete should be reduced.

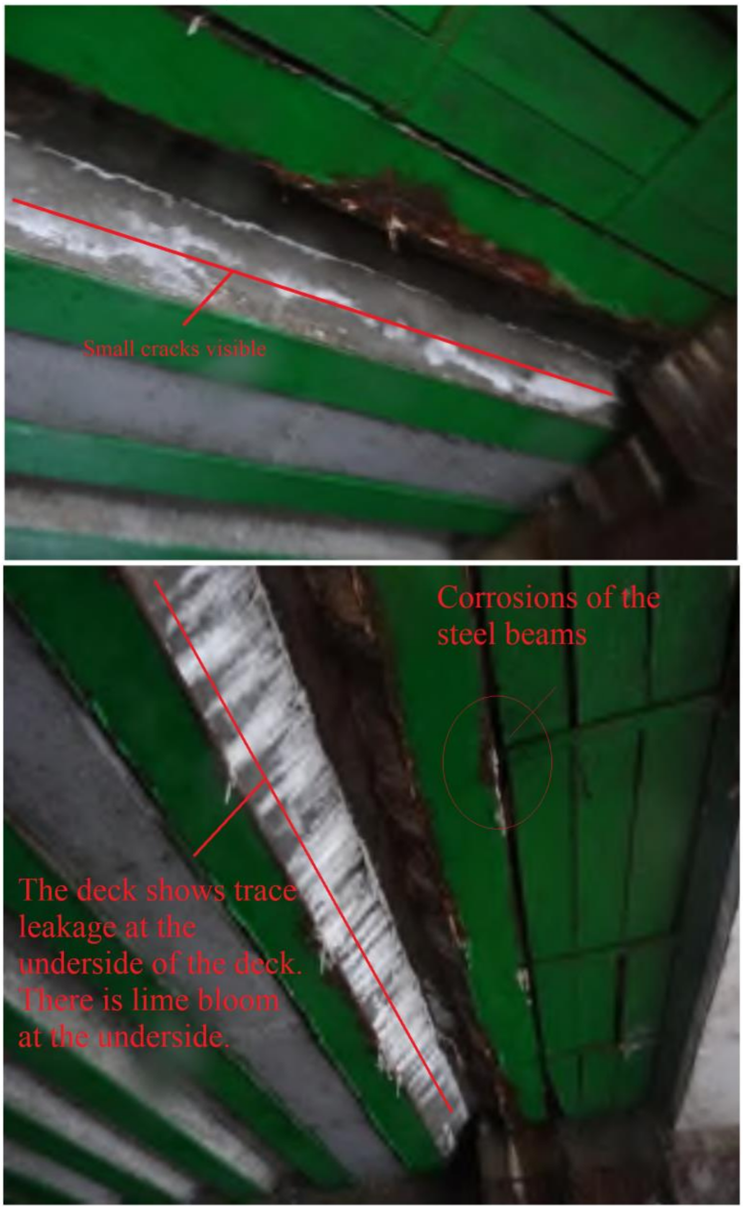

Figure 2-9: Defects which are found in inspection bridge A (Antea Group B.V. 2016).

The defects for bridge deck A are:

a) Corrosions of the steel beams;
b) The material removals steel beams at the bottom flange is about 10%;
c) The deck shows trace leakage at the underside of the deck. There is lime bloom at the underside. This is for 50% of the steel beams;
d) Small cracks visible.

Comment: the bridge deck (side-span) part where the in-situ-load-test is executed there are no defects available from the mentioned defect in the main span. The deck which is tested has a good condition only there is one longitudinal crack available between steel girder 5 and 6 which will be mentioned during the FEA-simulations, see figure 2-10 and see chapter 5.

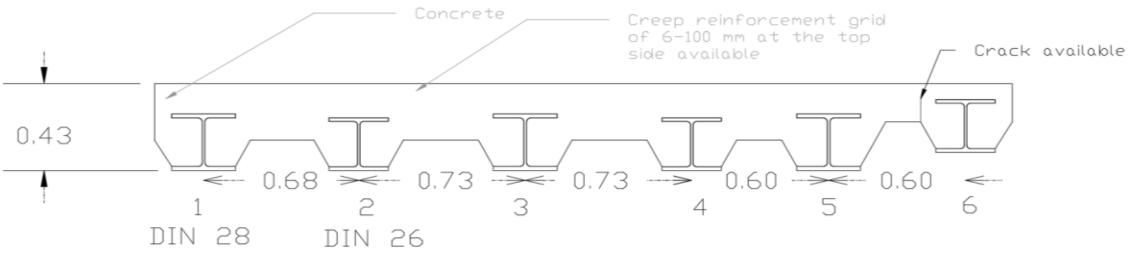

Figure 2-10: Defect between steel girder 5 and 6 by the side-span.

Analysis of the inspection of bridge deck A: From the inspection of bridge deck A, it can be seen that the bridge deck has a lot of defects on the middle of the bridge deck which have consequence and will lead to a reduction of the stiffness of the bridge deck A at the middle of the bridge deck. This is not valid for the bridge deck part where the in-situ-load-test is being executed. At the side-span the condition of the bridge deck is better than the main span see the previous comment. The condition of the bridge deck A, at the main span does not play a role because this side-span is leading and the main span is out of scope of this thesis.

Figure 2-11: Defects which are found in inspection bridge B (Antea Group B.V.2016).

The defects for bridge deck B are:

a) Corrosions of the steel beams;
b) There is no material removal;
c) Small cracks visible.

Comment: bridge deck B is in good condition.

Analysis of the inspection of bridge deck B: From the inspection of bridge B can be seen that the bridge deck has no defects which have high consequence and effect which lead to a reduction of the load-bearing capacity of the bridge deck B. The only defect are the small cracks which maybe have same effect on the stiffness of the concrete but that will be investigated during the FEA-simulations. See chapter 5.

Figure 2-12: Defects which are found in inspection bridge C (Antea Group B.V. 2016).

The defects for bridge deck C are:

a) Corrosions of the steel beams;
b) There is no material removal;
c) Small cracks.

Comment: bridge deck C is in good condition.

Analysis of the inspection of bridge deck C: From the inspection of bridge C can be seen that the bridge deck has no defects which have high consequence and effect which lead to a reduction of the load-bearing capacity of the bridge deck C. The only defect are the small cracks which maybe have same effect on the stiffness of the concrete but that will be investigated during the FEA-simulations, see chapter 5.

Conclusion:

The three bridges show more or less the same defects. The main conclusion which can be taken for the three bridges after the made inspections on the bridge decks is:

Bridge deck A:

a) The condition of bridge deck A is good, besides that there is a crack available in the longitudinal direction between steel girder 5 and 6;
b) There are micro or small cracks visible in the transverse and longitudinal direction in the bottom of the concrete slab;
c) The steel-girders of bridge deck A show 10 % material loss in the bottom flange, but that is not the worst case scenario because this will not have high impact or a decrease in the stiffness of the steel;
d) The main thing which we can conclude from the inspection is that there is corrosion between bottom flange of the steel girder and the concrete slab, which leads to an observation that the concrete and steel are not connected to each other.

Bridge deck B and C:

a) Bridge deck B and C are in good condition;
b) There are micro or small cracks visible in the transverse and longitudinal direction in the bottom of the concrete slab;
c) The steel-girders are not interesting because the material does not decrease based on input of the inspections for the two bridge decks.

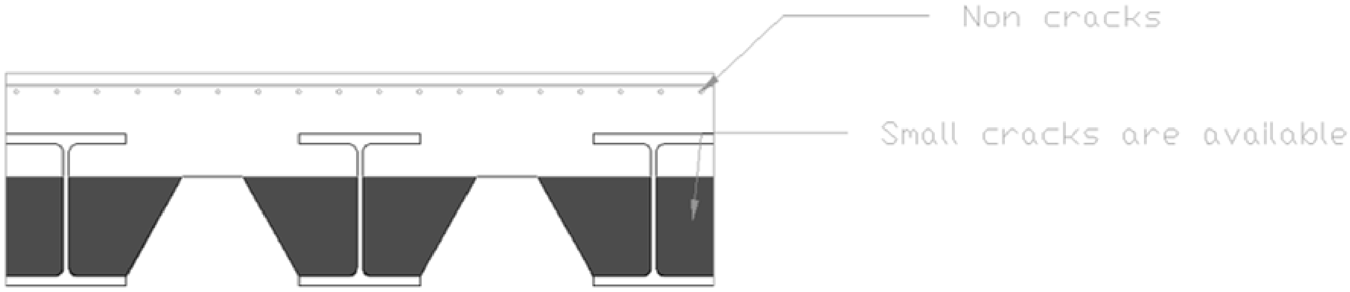

Figure 2-13: Defects which are available in cross-section in the concrete part.

2.3.4. The assessments of the bearing capacity of the historical bridge deck based on the approach in the past by assuming a full interaction

Introduction:
In this chapter the assessment of the load bearing capacity based on the made calculation in the past will be explained and carried out in the steps written below. This assessment explains the way how the bridge decks were developed and calculated in the past. The material properties which have been used in this section are obtained from the destructive inspection. This will be described in the first step. The calculations which are presented in the steps below are made in Excel. The calculation is made on the three selected bridge decks which are also mentioned in the previous chapter. In this chapter the results of the calculation of the three bridge decks will be presented, whereat the geometry and the developed Microsoft Excel can be found in the appendix A. The excel which is developed can be used to validate the output of the numerical simulation by assuming a full interaction between steel and concrete.

Step 1:
The material properties which have been used in this section are obtained from the destructive inspections performed on bridge deck A. The material properties are assumed to be the same for all the three bridge decks. This input will be used to calculate the load bearing capacity of the bridge decks.

Table 2-3: Material properties of the isolated historical beams.

Beams of the cases	Type material	Material properties	
Historical beams of bridges A,B and C	Concrete	Young's modulus	38214 N/mm2
		Density	2.5 x 10-9 T/mm3
		Tensile strength	4.21 N/ mm2
		Compression strength	55 N/ mm2
		Shear strength	7,20 N/ mm2
	Steel	Young's modulus	210000 N/ mm2
		Density	7.85 x 10-9 T/mm3
		Tensile strength	235 N/ mm2
		Compression strength	235 N/ mm2

Step 2:
The cross-section of the historical beam is not uniform. The second step is to define the geometry quantities which will be used during the calculations. The cross-section of the historical beam is symmetrical about the Z-axis. This leads to focus only on the position of the neutral axis (NC) on the Y-axis. First the full cross-section is divided in different heights. This is done in such a way to define the material properties of concrete at the cross-section in a proper way. The different geometric properties are defined in the figure 2-14 for only bridge The rest of the bridge decks are added in the appendix A. In the figure 2-14 the first assumption can be seen:

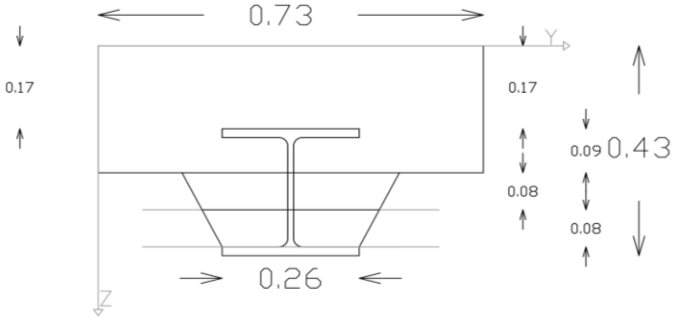

Figure 2-14 The Cross-section of DIN 26 including the different height.

The formulas below are used to calculate the coordinates of the NC of the three cross-sections based on the presented input in the previous figure and table

$$y_{NC} = \frac{E_{concrete}\, S_{y-concrete} + E_{steel}\, S_{y-steel}}{E_{concrete}\, A_{concrete} + E_{steel}\, A_{steel}} \qquad : (2.1)$$

$$z_{NC} = \frac{E_{concrete}\, S_{z-concrete} + E_{steel}\, S_{z-steel}}{E_{concrete}\, A_{concrete} + E_{steel}\, A_{steel}} \qquad : (2.2)$$

Step 3:

In the figure 2-15 the calculated NC including is presented.

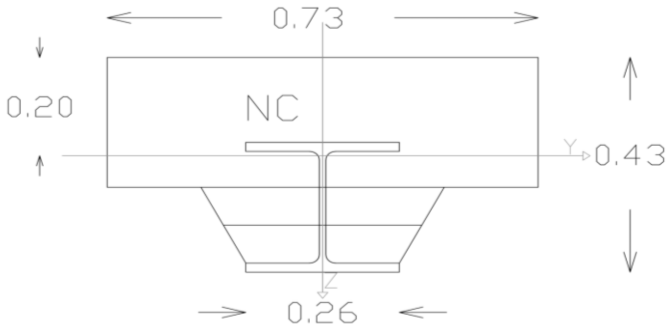

Figure 2-15: The cross-section of DIN 26 including the NC.

The formulas below are used to calculate the stiffness of the three cross-sections based on the presented input in de the previous figures. The stiffens of the bridge can be found in the table 2-4.

$$EA = E_{concrete}\, A_{concrete} + E_{steel}\, A_{steel} \qquad : (2.2)$$

$$EI_{yy} = E_{concrete}\, I_{yy} + E_{steel}\, I_{yy} + E_{concrete}\, A_{concrete}\, a^2 + E_{steel}\, A_{steel}\, a^2 \qquad : (2.3)$$

$$EI_{zz} = E_{concrete}\, I_{zz} + E_{steel}\, I_{zz} + E_{concrete}\, A_{concrete}\, a^2 + E_{steel}\, A_{steel}\, a^2 \qquad : (2.4)$$

Table 2-4: Quantities of the different calculated historical cross-sections.

Bridges	Total EA (N)	NC of the cross-section (mm)	The total EI cross-section (Nmm^2)
Bridge A	1.26E+10	230	2.3E+14
Bridge B	1.13E+10	210	2.08E+14
Bridge C	8.27E+09	187	1.56E+14

As mentioned before by assuming a full interaction between steel and concrete this calculation can be used to validated the FEA-simulations. The validation is made by the validating the vertical displacement of the numerical simulation. The following equations are used during the calculation because the beam is subjected to a traffic load and a dead-load. Therefore, the outcome of the two formulas is used and summed up. So, the total deformation is equal to the sum of the outcome of the below formula's calculation can be find in appendix A

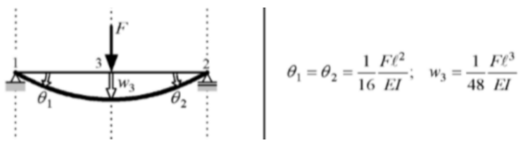

Figure 2-16-a: Forget me nots 1.

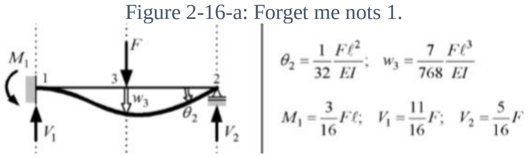

Figure 2-16-b Forget me nots 2.

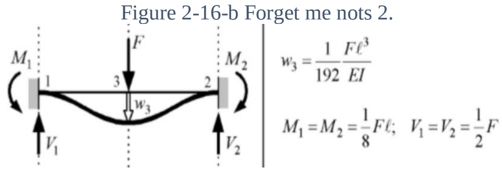

Figure 2-16-c Forget me nots 3.

Figure 2-16: Forget me nots.

2.4. Conclusions

The conclusion that can be taken from the investigation on the state of the 32 historical steel-concrete-composite-bridge-decks is:

a) Firstly, the reinforcement is not enough to reach the needed capacity in the transverse direction and in the longitudinal direction the reinforcement doesn't help to reach a statically undetermined system;
b) Secondly, the center to center distance is smaller than the effective width;
c) Thirdly, the material properties must be obtained from the destructive inspections;
d) Fourthly, the steel profiles are variating over the width in the transverse direction; this depends on the length of the span and the type of traffic which is passing over the bridge deck.

After the investigation on the state of the 32 bridges, the bridges are collected in three groups that vary from low to high length in the main span. From each group, a bridge is chosen as the most common bridge to represent that group. So three bridges are chosen for further investigation to define the load-bearing behaviour of these type of bridge decks.

To select these three bridges, the most important criteria was the length of the main span, where the bridge with the highest length inside a specific group was selected. The chosen bridge decks are:

a) **Bridge A** is a representative bridge in the first group (this group contains the lowest length of main spans), because the length on the main span is 7.8 m, but due to sail restrictions of the municipality of Amsterdam during the execution of the in-situ-load-test, it is chosen to use the side-span 6.5 m, and that will be the case also in this thesis assignment;
b) The second bridge is **bridge B**, because this bridge does not contain any tramway and is from the category 10 m span;
c) The third bridge (**bridge C**) is based on the configuration of the cross-section properties and is from the category 13 m span. This is the same for some other bridges in the collection of the 32 bridges.

Based on the assessment about the Eurocode 4 compared to historical bridge decks, the conclusion can be taken that the Eurocode 4 cannot be useful to guarantee the safety of the historical bridge decks. This is because of the differences and the missing elements (see points which are mentioned in the paragraph of Differences between the current Eurocode 4 model and the historical model) in the cross-section of the historical bridge decks. The cross-section of the historical steel-concrete-composite-bridge-decks is not included in the Eurocode 4. Therefore, there is no guideline available which is representative for the historical steel-concrete-composite-bridge-decks and it is needed to introduce a guideline for these type of bridge decks. Besides the difference between the cross-section which is presented in the Eurocode 4 and the cross-section of the historical steel-concrete-composite-bridge-decks, the engineers before 1950 used the design philosophy that the cross-section is based on a 100% interaction between steel and concrete, which is however not fully available is in the cross-section.

Furthermore, the effective width of the historical steel-concrete-composite-bridge-decks is calculated based on the Eurocode 4 formulas. The value of the calculated effective width based on the Eurocode 4 is compared with the center -to-center distance between the steel profiles. Based on this analysis, it is concluded that the value of the center -to-center distance is smaller than the calculated effective width based on Eurocode 4. This is a good result, because it supports the conclusion of applying the strut and tie model. This conclusion is validated during the numerical modelling of the transverse direction.

The research has been performed based on the three selected bridge decks. The three bridge decks show more or less the same defects. The state of the bridge as observed from the inspections reports are:

Bridge deck A:

a) The condition of bridge deck A is good, besides that there is a crack available in the longitudinal direction between steel girder 5 and 6;
b) There are micro or small cracks visible in the transverse and longitudinal direction in the bottom of the concrete slab;
c) The steel-girders of bridge deck A show 10 % material loss in the bottom flange, but that is not the worst case scenario because this will not have high impact or a decrease in the stiffness of the steel;
d) The main thing which we can conclude from the inspection is that there is corrosion between bottom flange of the steel girder and the concrete slab, which leads to an observation that the concrete and steel are not connected to each other.

Bridge deck B and C:

a) Bridge deck B and C are in good condition;
b) There are micro or small cracks visible in the transverse and longitudinal direction in the bottom of the concrete slab;
c) The steel-girders are not interesting because the material does not decrease based on input of the inspections for the two bridges.

See figure 2-17 for the visualization of the small/micro cracks.

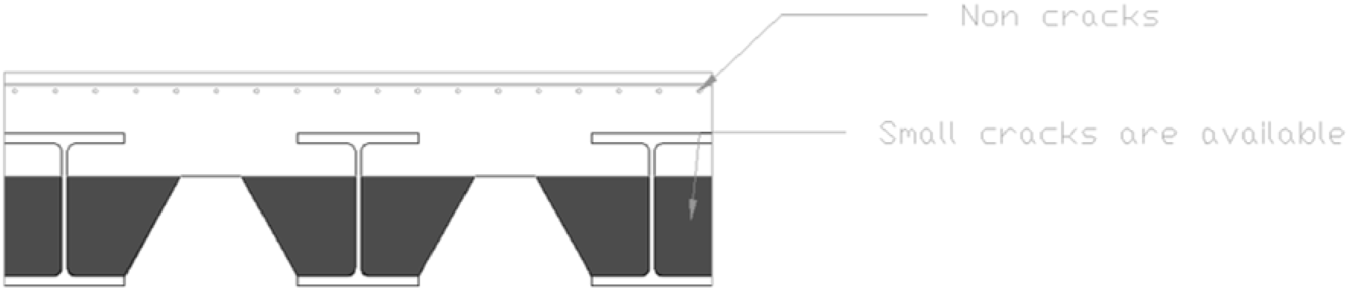

Figure 2-17: Defects which are available in cross-section in the concrete part.

3. Available checking methods and The assessment of the historical bridge deck

3.1. Introduction

In this section methods will be introduced to gain a deep understanding of the behaviour of the historical bridge decks will be explained and carried out, based on an assessment over the selected three bridge decks (A, B and C). The reason why these methods have been introduced is because the Eurocode 4 is not applicable on the historical bridge decks and this leads to investigate other methods to introduce an assessment of these bridge decks. The investigation is applicable on the two directions of the historical bridge decks. In the longitudinal direction the idea is to study the interaction level and make an assessment of the shear stiffness between steel and concrete, which will lead to define the interaction level. The method will be carried out and explained in sub-chapter 3.2. In the transverse direction there are checking methods which will be investigated and an assessment will take place. The quick assessment will help with judging the relevance of the checking methods on the historical bridge decks in the transverse direction.

a) Punching shear failure;
b) The compressive membrane action;
c) The strut and tie model.

In the coming sub-chapters, the description of the checking methods is included.

3.2. The available theoretical method and The assessment of the historical composite bridge deck in the longitudinal direction

3.2.1. Introduction

In this section the various interaction level is defined. Furthermore, the assessment of the longitudinal direction of the historical composite bridge deck will be analysed and the model will be developed and described in this section. The assessment is only done on bridge deck A.

3.2.2. Interaction possibilities to describe the composite action in analytical way

The interaction behaviour in the longitudinal direction will be first investigated in this thesis assignment. In the longitudinal direction, the capacity of the cross-section depends on the interaction level between the concrete and the steel. As mentioned before, the shear connectors are missing in the cross-section which leads to an undefined situation for the composite action. According to the figure 3-1 the interaction between the two materials can be classified under the following categories:

a) No interaction;
b) Partial interaction;
c) Full interaction.

In the case of the historical steel-concrete-composite-bridge-deck, the partial interaction level is interesting. But to a deeper understanding of the interaction behaviour, all the three cases will be described. In the case of “No interaction” between the concrete and the steel profile, the strain of both specimens are not the same because they are acting separately. This aspect has impact on the stresses which are available in the overall cross-section because the stresses are also acting separately which leads to lose of the composite action. This has then also effect on the capacity of the cross-section, because losing the composite action leads to the problem definition which the structural department of the municipality of Amsterdam has. The structural department of the municipality of Amsterdam now only takes into consideration the steel profile in the longitudinal direction and not the concrete. But in this case the historical steel-concrete-composite-bridge-deck satisfies the unity check in the longitudinal direction. In the transverse direction the bridge deck does not satisfy the unity check. In case of “partial interaction”, therefore it can be seen that the strain of the concrete specimen starts to act, and the belonging stress is also added to the steel part. This shows more the results which the department hopes to see. Shortly, the composite action between steel and concrete begins to be present. This leads to increase the capacity of the cross-section and give more realistic results. In an ideal scenario, where everything is perfectly bonded, a complete interaction is present between steel and concrete. In this case the strain as well as the stresses is fully acting on the overall cross-section, where the composite action 100 % present.

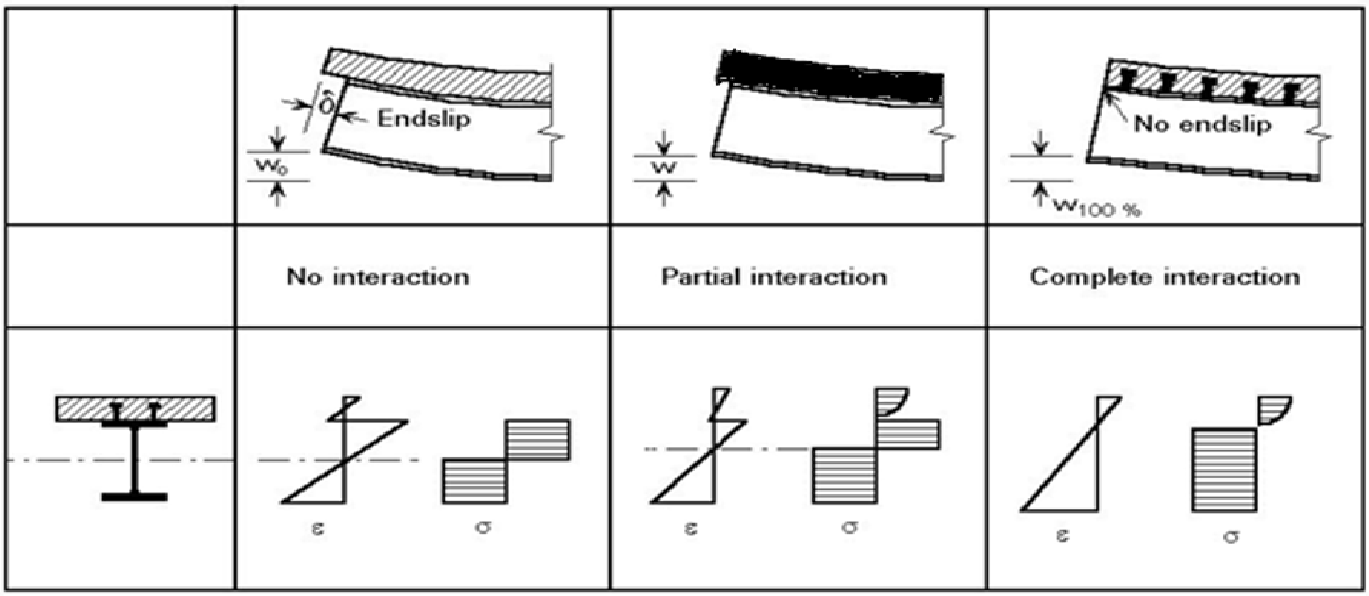

Figure 3-1: Illustration of the interaction between steel and concrete (Het NederlandsNormalisatie-instituut,2012).

In the figure 3-1 (Illustration of the interaction between steel and concrete) on top the interaction between the two materials is illustrated. The parameters **δ**;, W0, W, W100%, ε, σ give an illustration about the level of interaction. The mechanical behaviours are all based on the level of interaction between the two materials, the parameters are:

a) **δ**: gives an illustration of the axial displacement between the concrete and steel partial interaction due to bending;
b) $\mathbf{W_0}$: is the vertical displacement if there is no interaction due to bending;
c) **W**: is the vertical displacement if there is partial interaction due to bending;
d) $\mathbf{W_{100\%}}$: is the vertical displacement if there is complete interaction due to bending;
e) **ε**: is strain in three phases;
f) **σ**: is the stress in three phases.

How to define the composite action analytically?

The analytical model which is presented in the figure 3-2 (Model the interaction between the steel and concrete for a simply supported beam) presents the system which can be used to model the interaction between steel and concrete. The figure is divided in three subfigures (a, b, c), which describe the total analytical model. In the figure (a) the longitudinal and the transverse direction of the simply supported beam is presented, including the point load at the middle. In figure (b) the strain distribution is presented for two separated cases; the case where it is assumed that there is a full composite interaction and in the other case the opposite is assumed (no interaction). For this research the case of the partial interaction between the two materials is important. The model which has been used to model the partial interaction is presented in figure (c). In figure (c) specimen of the longitudinal direction is presented. This specimen presents the model which has been used to model the interaction. In this figure (c), the kinematic relation of the model which has been used, is presented. At the top side, the concrete specimen is presented with Euler-Bernoulli beam bending theory, including the axial deformation action in the beam. At the bottom the steel specimen is shown which presents the same conditions as well as at the concrete. At the interface the interaction is presented with two kinematic relations which are representing the shear stress and the normal stress between steel and concrete. Furthermore, the presented slip between steel and concrete is defined by the symbol s. This in total is the model which can be used to calculate the interaction analytically. Based on this analytical solution, the interaction between steel and concrete will be carried out and presented in the coming paragraph in detail with all the formulas. See appendix's B for the reached which is made by Jianguo Nie1 and C. S. Cai, P.E. (Jianguo Nie1 and C. S. Cai, 2003)

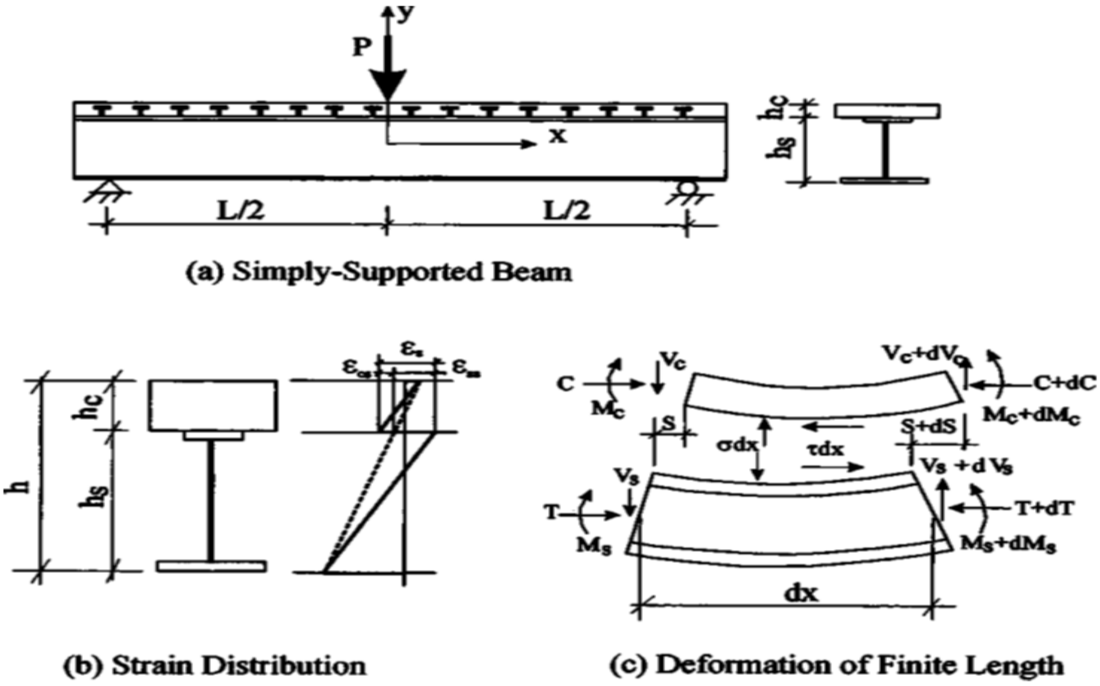

Figure 3-2: Analytical model of the interaction between the steel and concrete for a simply supported beam (Jianguo Nie1 and C. S. Cai, 2003).

Implement the theory on the historical Amsterdam bridge:

The model which is described above will be rewritten and used on the cross-section of the historical steel-concrete-composite-bridge-decks as far it is possible to rewrite it and apply it on the historical steel-concrete-composite-bridge-decks. There is a difference between the two cross-sections, as mentioned before in paragraph 2.3.2. The cross-section which has been used to set-up the analytical model is like the one in the Eurocode 4. The analytical model which is described in the paper "Jianguo Nie1 and C. S. Cai, P.E about" is a model which is being used for the steel-concrete cross-section with shear connectors like the Eurocode 4. The historical deck has no-shear connectors and therefore the shear stiffness is undefined in this case, the shear stiffness which can be applicable to describe the composite action is based on the shear stiffness of the concrete. In the Eurocode 2, concrete has three different ways to judge the shear stress at the interface. This is dependent on the interaction level between the two materials steel and concrete. In the table 3-1 the interaction levels which are defined in the Eurocode 2 are shown.

Table 3-1: Information from the Eurocode about the shear interface.

Interface situation	Information about interface conditions	Cohesion	Friction angle	Factor of static friction
Very smooth	A surface cast against steel, plastic or specially prepared wooden moulds.	c = 0,025 to 0,10	$26{,}5 \leq \theta \leq 45$	$\mu = 0{,}5$
Smooth	A slip formed or extruded surface, or a free surface left without further treatment after vibration	c = 0,20	$26{,}5 \leq \theta \leq 45$	$\mu = 0{,}6$
Rough	A surface with at least 3 mm roughness at about 40 mm spacing, achieved by raking, exposing of aggregate or other methods giving an equivalent behaviour.	c = 0,40	$26{,}5 \leq \theta \leq 45$	$\mu = 0{,}7$
Indented	A surface with indentations complying with.	c = 0,50	$26{,}5 \leq \theta \leq 45$	$\mu = 0{,}9$

To calculate the ultimate shear stress which is acceptable at the interaction level, the following formula will be used, based on the input of the table above and the material properties of the concrete which are available on the cross-section of the historical steel-concrete-composite-bridge-decks:

$$\mathbf{V_{Rdi}} = \mathbf{c} * \mathbf{f_{ctd}} + \boldsymbol{\mu} * \boldsymbol{\sigma_n} \quad : (3.1)$$

a) $\mathbf{V_{Rdi}}$: shear stiffness;
b) $\mathbf{f_{ctd}}$: tensile strength of concrete;
c) $\mathbf{f_{cd}}$: compression strength of concrete;
d) $\boldsymbol{\sigma_n}$: $\sigma n < 0{,}6 *$ fcd is the 60 % of the compression strength fcd if the interaction is in the compressive zone;
e) $\boldsymbol{\mu}$: is Factor of static friction;
f) $\mathbf{c}$: cohesion.

The formula is computed in the table 3-2 for 4 situations. The interesting situation is only the very smooth situation because the interface of steel is smooth and this is the best way to describe the partial interaction way. See the table 3-2 for the results.

Table 3-2: Information from the Eurocode.

Interface situation	Cohesion	Ecm- (N/mm²)	Factor of static friction μ	Compression strength fcd (N/mm²)	Tensile strength fctm (N/mm²)	σn < 0,6 x fcd (N/mm²)	C x fctd (N/mm²)
Very smooth	0.1	37865	0.5	36.70	3.80	0.38	11.39
Smooth	0.2	37865	0.6	36.70	3.80	0.76	13.97
Rough	0.4	37865	0.8	36.70	3.80	1.52	19.14
Indented	0.5	37865	0.9	36.70	3.80	1.9	21.72

As mentioned before the analytical formula is based on a bending situation which can be written based on the presented formulas in the figure 3-3.

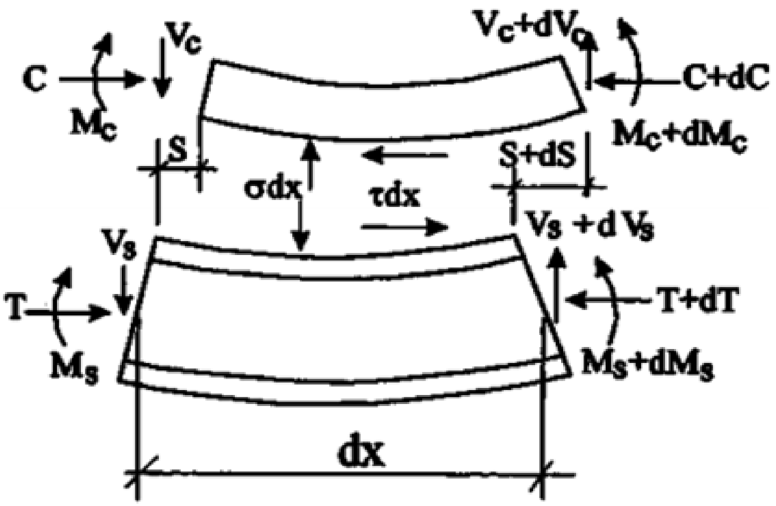

Figure 3-3: Model to describe composite action between steel at the cross-section level (Jianguo Nie1 and C. S. Cai, 2003).

a) $\mathbf{M_c}$: The available moment in the concrete;
b) $\mathbf{c}$: The available normal force in the concrete;
c) $\mathbf{T}$: The available normal force in the steel;
d) $\mathbf{M_s}$: The available moment in the steel;
e) $\mathbf{dM_s}$: The first derivative of the moment in the steel;
f) $\mathbf{dM_c}$: The first derivative of the moment in the concrete;
g) $\mathbf{V_c}$: The shear force in the concrete;
h) $\mathbf{V_s}$: The shear force in the steel;
i) $\boldsymbol{\tau}$: The shear stiffness;
j) $\boldsymbol{\sigma}$: The normal stiffness;
k) $\mathbf{Y_{cb}}$: The coordinate from the neural axis of the concrete part to the interface;
l) $\mathbf{Y_{st}}$: The coordinate from the neural axis of the steel part to the interface.

The material and the geometry properties of bridges are defined in sub-chapter 2.3.4. This will be used also during this assessment. In the first equation the equilibrium of the reaction force is described. The total reaction force in steel and concrete is equal to the applied load.

$$q(x) := \left(tandem_{(traffic\ load)} * Dirac(x - 0.5 * L)\right) + \left(q(x)_{(the\ deadload)}\right) \quad : (3.2)$$

$$\frac{dV_c(x)}{dx} + \frac{dV_s(x)}{dx} = q(x) \quad : (3.3)$$

The total shear force is equal to the total variation of the moment in the two-cross-sections including the shear stress at the interface.

$$\mathbf{V_c(x) + V_s(x) = -\left(\frac{dM_c(x)}{dx} + \frac{dM_s(x)}{dx}\right) + \frac{1}{2}\tau(x) * (y_{cb} + y_{st})} \quad : (3.4)$$

The shear stiffness of the interface is not defined. This part of the analytical model will be an interactive process between the numerical model and the analytical model. When the shear stiffness is defined, the partial interaction level will become clear and will be approximately defined with the following formula.

$$\boldsymbol{\tau}\mathbf{(x) = \frac{G_c * s(x)}{l}} \quad : (3.5)$$

Where:

a) $\mathbf{G_c}$: shear stiffness between steel and concrete (shear stiffness at the contact between two materiaals);
b) $\mathbf{S(x)}$: the available slip over the x-axis;
c) **I**: the length of the beam.

The total moments in the cross-section are equal to the curvature in the x-axis.

$$\mathbf{M_c(x) + M_s(x) = (EI_s + EI_c) * kappa(x)} \quad : (3.6)$$

These equations shown above, describe the model in the longitudinal direction. The shear stiffness is not defined because the goal is to look at the interaction level between steel and concrete. The model is checked by using a full interaction. The result of the vertical displacement of the MAPLE model is compared with the vertical displacement of the in-situ-load-test and the numerical simulation, so therefore the model is validated. The result of the vertical displacement can be seen in the figure 3-4 and in the coming chapter where the numerical simulation of the separated beam is presented. The differential equations are solved in maple. See the figure 3-4 the maximal vertical displacement. The complete solution has been presented in appendix B.

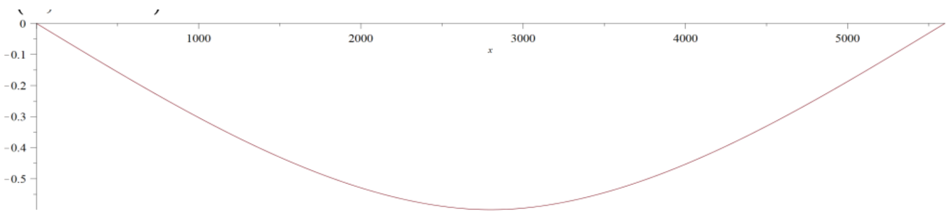

Figure 3-4: Vertical displacement at the mid-span is u = 0.58 mm.

<u>Conclusion:</u>

An analytical model is developed and validated to describe the interaction level between steel and concrete.

3.3. The available checking methods and The assessment of the historical bridge deck in transverse direction

3.3.1. Introduction

In this section the assessment of the three models will be done on the historical bridge deck A. The applicable checking method will be investigated and an assessment will take place. The assessment will help by judging the relevance of the checking methods on the historical bridge decks in the transverse direction. The selected models are:

a) Punching shear failure;
b) The compressive membrane action;
c) The strut and tie model.

3.3.2. The punching shear failure

Introduction:

According to the Eurocode 2 the punching shear is a mechanical behaviour where concrete fails. The failure occurs when a concrete slab is subjected to a high concentrated load. During this aspect of loading a local conical plug is generated out of the slab directly under the load and this causes failure. This behaviour is known as punching. This behaviour is also knowns as the two-way shear. The classification of this behaviour could be:

a) Generally, a brittle punching failure with no warning in advance;
b) Flexural punching where some warning is shown. (1984)

This physical process known as punching is illustrated in the sub-figures 3-5-a and 3-5-b.

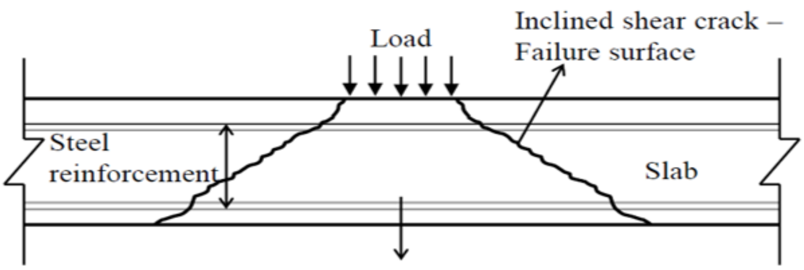

Figure 3-5-a: Conical plug of concrete pushing out of the slab.

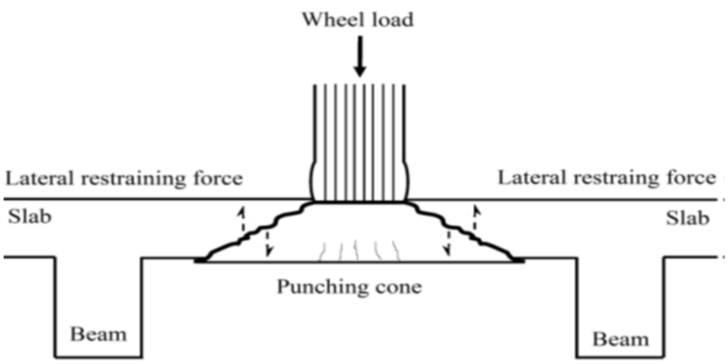

Figure 3-5-b: Punching shear failure in laterally restrained slabs or deck slabs.

Figure 3-5: Illustration of the punching shear mechanism (Kirkpatrick, 1984).

Implement the theory of punching shear on the historical steel-concrete-composite-bridge-deck:

Punching shear as mentioned in the previous paragraph has two categories. In this paragraph the goal is to analysis if the historical steel-concrete-composite-bridge-deck is dealing with this phenomenon or not. Starting point is by applying the mechanical behaviour (punching shear) on the cross-section of the historical steel-concrete-composite-bridge-deck and to take a look if this mechanical behaviour is interesting or not. First step is to use the obtained data from the 32 cross-section of the historical bridges (see chapter 2). The interesting parameters in this case are:

a) The center -to-center distance;
b) The minimal height by included the asphalt.

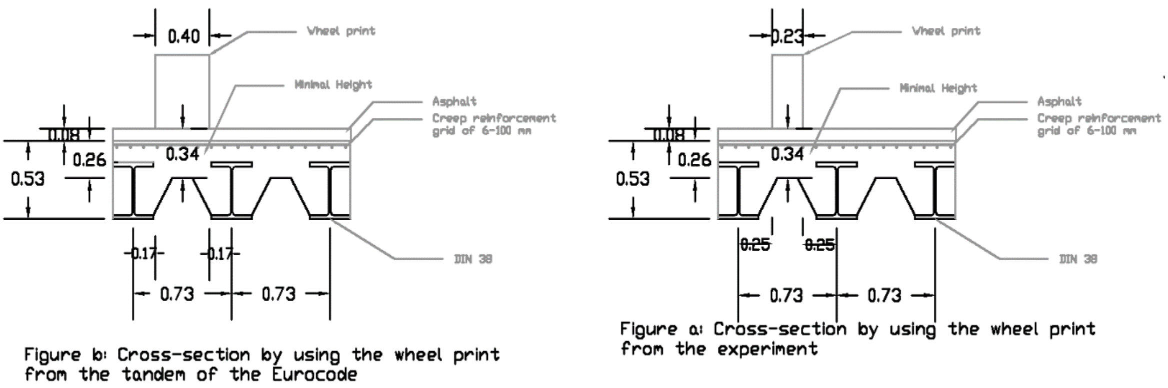

Figure 3-6: Cross-section included the parameters (bridge deck B).

Based on these parameters which are obtained from the thirty-two investigated historical steel-concrete-composite-bridge-decks, a simple analysis will be done to give an illustration of the behaviour of the punching shear failure. The goal is to see if the mechanical behaviour of punching shear plays a role or not in the cross-section of the historical steel-concrete-composite-bridge-decks. To implement the theory there are two-wheel prints used. The first one is from the in-situ-load-test. The dimension of this print is (230x300 mm). The second one is the tandem of the Eurocode. The information about the dimension of the wheel print is obtained from the Eurocode (NEN-EN 1991-2:2003+C1:2015+NB:2011). In the figure 3-7 the configuration of the wheel print is mentioned. This is based on the first model of the Eurocode.

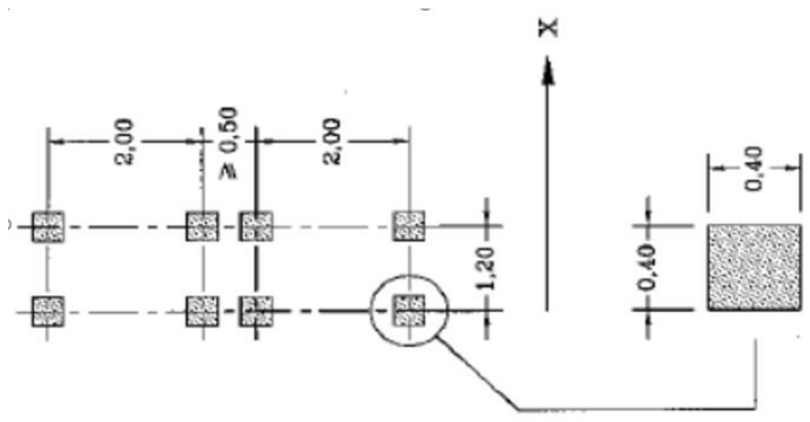

Figure 3-7: The wheel print based on the first model in the Eurocode (Het Nederlands Normalisatie-instituut 2020).

The spreading of the load of the wheel print on the concrete deck will be done based on 45 degrees, which is the maximal rotation which is applicable in the concrete cross-section due to shear. See table 3-1:

Information from the Eurocode about the shear interface. The spreading is illustrated in the figure 3-8.

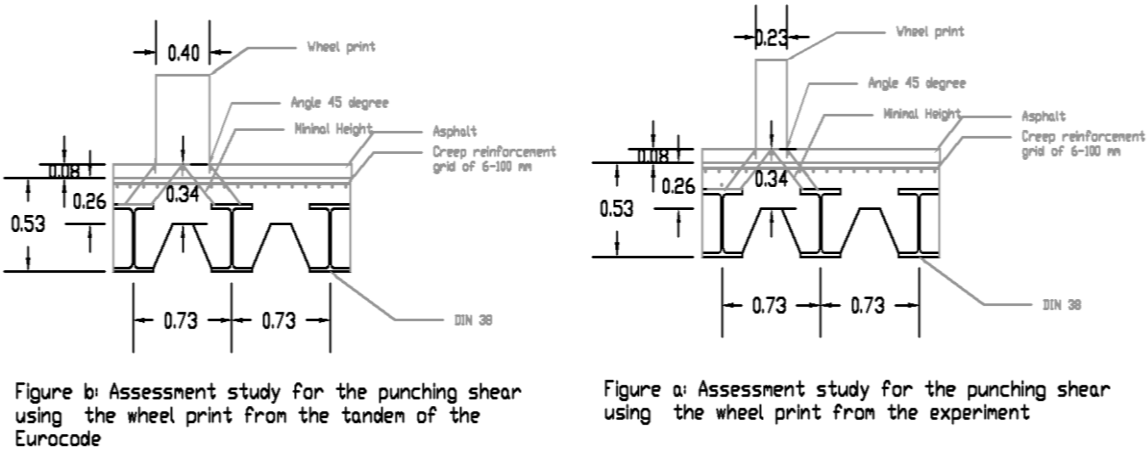

Figure 3-8: The spreading internal concrete bridge deck B due to the two-wheel prints.

Based on the illustration above it can be seen that the punching shear does not play a role in the actual bearing capacity of the historical steel-concrete-composite-bridge-deck. Because the forces are directly transported to the steel-girder. From Figure 3-8 it can be concluded that the punching shear does not play a role in the historical steel-concrete-composite-bridge-deck.

Conclusion:

The conclusion is that the historical steel-concrete-composite-bridge-deck is not subjected to punching shear. This is also a conclusion during in-situ-load-test see paragraph 4.2. Which leads us not take the punching shear into consideration.

3.3.3. The theory of compressive membrane action in concrete

Introduction:

According to Park and Gamble (2000), the compressive member action (CMA) is a phenomenon that occurs in slabs where edges are restrained against lateral movement by stiff boundary elements. The restraints introduce compressive forces in the plane of the slab. The deflection of the slab and the changes in the geometry causes the slab edges to tend to move outward and to react against the boundary elements as shown in figure 3-9 (Compressive membrane action in a reinforced concrete bridge deck slab (Hon, 2005)). CMA leads to an increase in the bearing capacity of the slab, and it fails at a load much higher than predicted by the standard yield line theory (Kirkpatrick et al. 1984, Batchelor 1990, Bakht and Jaeger 1992, Mufti et al. 1993, Fang et al. 1994).

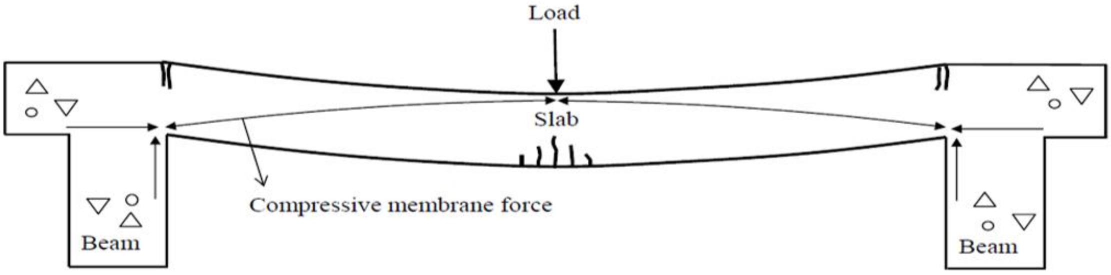

Figure 3-9: Compressive membrane action in a reinforced concrete bridge deck slab (Hon, 2005).

Figure 3-10 shows the load-bearing result of this mechanical behaviour CMA. The result is that the compressive resistance will be higher due to this mechanical behaviour.

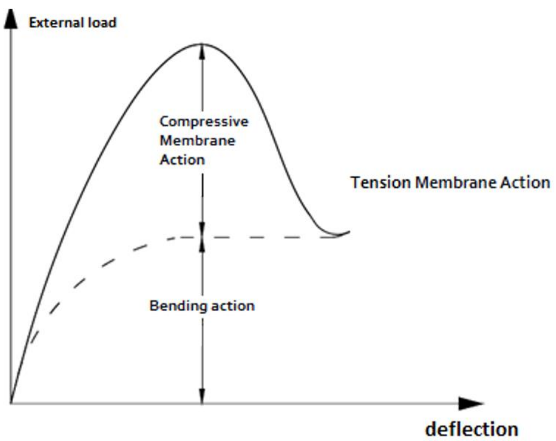

Figure 3-10: Illustration of the effect of the compressive membrane action (adapted from the cement-themas).

Factors affecting compressive membrane action:

According to Hon et al. (2005), the amount of the compressive member action established in the cross-section depends on the horizontal translational restraint stiffness, this lateral restraint depends on:

a) The axial stiffness of the surrounding slab area;
b) The horizontal bending stiffness of the edge beams;
c) The position of the load about the end crossbeams or the diaphragms;
d) The restraint stiffness increases if the loaded area moves toward the ends of the specimen, closer to the diaphragms.

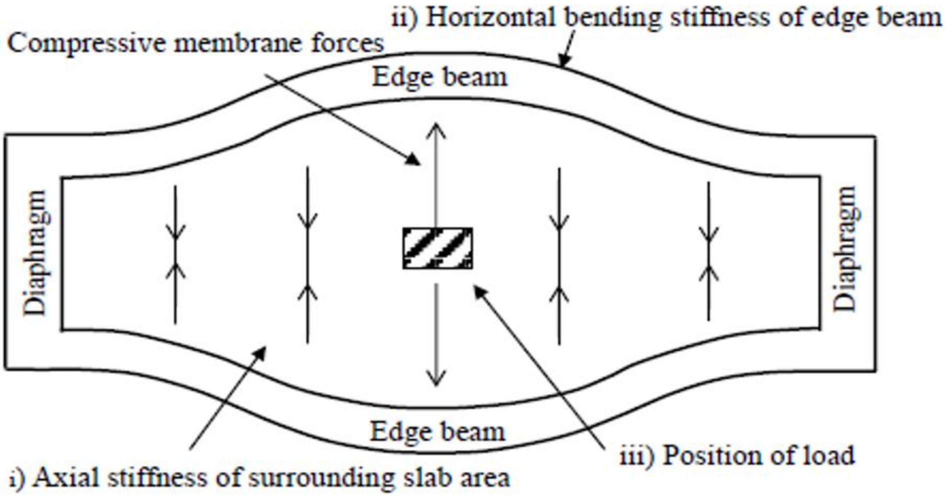

Figure 3-11: Contributions to horizontal translational restraint stiffness according to Hon et al (2005).

Classification of the restraining action:

The restraining action in a slab can be classified by Hewitt and Batchelor (1975) into two parts (Figure 3-12):

a. Compressive membrane action (CMA);
b. Fixed boundary action.

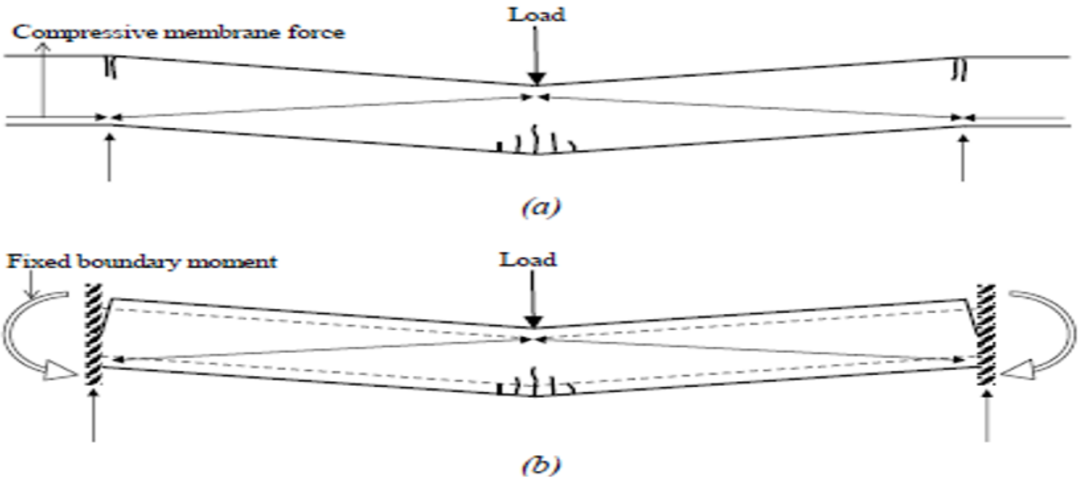

Figure 3-12: Classification of the restrained slab (adapted from Hewitt and Batchelor 1975): a) Compressive membrane action; b) Fixed boundary action.

a) The CMA occurs only in slab which are cracked. This creates a net force in the plane at the slab boundaries. If the strength is the same in tension and compression the mechanical behaviour cannot occur in slabs. The appearance of the reinforcement is not necessary to activate the CMA;

b) The Fixed boundary action occurs in both situations un/cracked slabs (with the appearance of the tensile reinforcement at the slab boundaries) and due to the moment restraint only.

Implement the theory of CMA based on the codes from:

To implement the theory of the CMA on the historical Amsterdam bridges the idea is to use existing codes of the Canada (= New Zealand) and the UK highway agency's. The roles of the existing codes will be applied on the historical Amsterdam bridge decks. The goal is to find out if the deck satisfies the roles of the existing codes. Based on this, it can be concluded that the historical steel-concrete-composite-bridge-deck is dealing with the mechanical behaviour of CMA. The roles of both codes will be addressed in the following:

CHBDC: CAN/CSA-S6-06 (2006):

According to the Canadian code, the following limitations must be satisfied before using the theory. If the historical steel-concrete-composite-bridge-decks satisfied all the limitations, then the CMA can be calculated if it possible according to the Canadian code. (CAN/CSA-S6-06 2006, 2006)

Implementing the limitations of the Canadian code on the historical steel-concrete-composite-bridge-decks:

The check will be done for each point from the set of limitations which are named in the previous paragraph, and are based on the cross-section of the historical steel-concrete-composite-bridge-decks which are obtained from the thirty-two other bridges. In the figure 3-13 the bridge A is presented in the transverse direction to give an illustration of the situation during implementing the theory. (CAN/CSA-S6-06 2006, 2006)

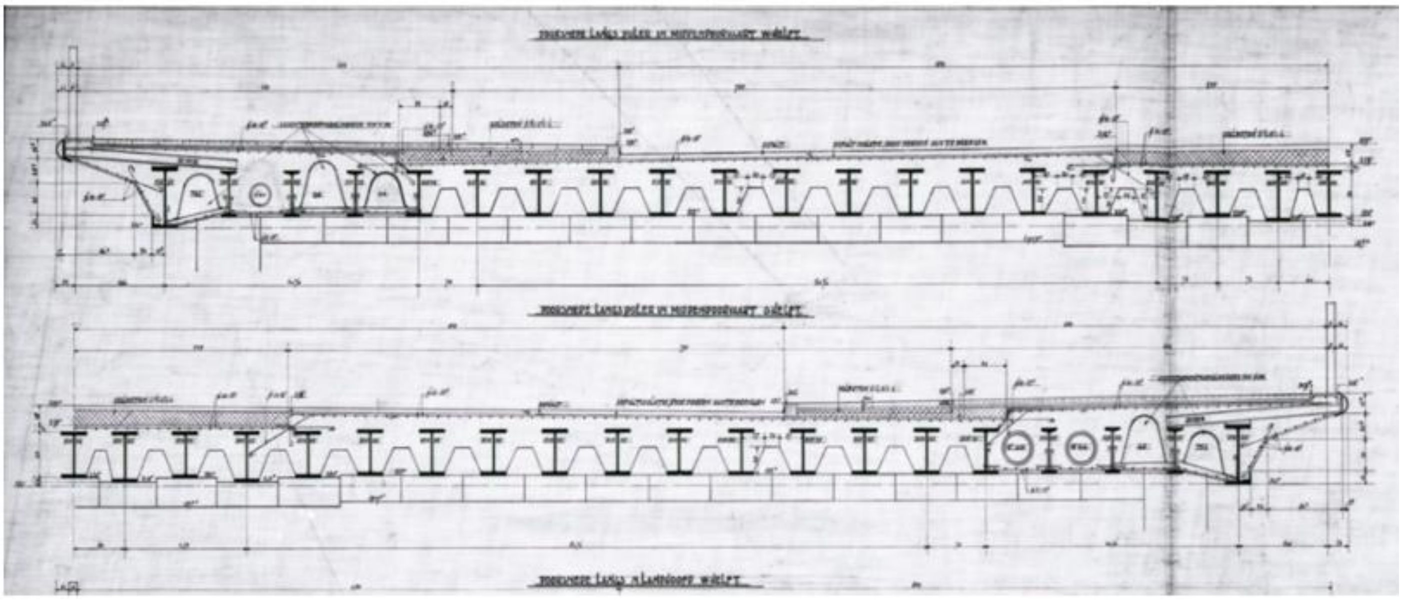

Figure 3-13: Layout of the bridge deck A in the transverse direction (Gemeente Amsterdam).

The center -to-center spacing of the supporting beams for a slab panel does not exceed 4,5 m and the slab extends sufficiently beyond the external beams to provide full development length of the bottom transverse reinforcement:

The bridge deck satisfies the first rule because the maximal center -to-center spacing of the historical steel-concrete-composite-bridge-deck is 0,8 m, which is lower than 4,5 m. The second condition is not interesting because external beams are not on the foot/bike lane. Only the vehicle lane is the main focus for this research.

The ratio of the spacing of the supporting beams to the thickness of the slab does not exceed 20:

The center -to-center of the supporting beams is as mentioned before in point 1 0,8 m. The minimal thickness of the bridge deck is 0.4 m. The ratio is than 2, which is smaller than the 20, so the historical steel-concrete-composite-bridge-deck satisfies the second rule.

The minimum slab thickness of sound concrete is at least 150 mm (with the minimum slab thickness used for slabs of variable thickness):

The minimal thickness of the historical steel-concrete-composite-bridge-deck by the most interesting lane (vehicle) is 400 mm, which leads that the historical steel-concrete-composite-bridge-deck satisfies the rule. The foot and bike lane have a minimal thickness of 100 mm but are not of interest in this analysis because the load is smaller than the vehicle lane.

All cross-frames or diaphragms extend throughout the cross-section of the bridge between external girders and are provided at support lines. The maximum spacing of such cross-frames or diaphragms in case of steel-girders or box girders does not exceed 8.0 m c/c:

The center -to-center of the supporting beams is 0,8 m. So, the historical steel-concrete-composite-bridge-deck satisfies this rule.

The transverse free edges of all deck slabs shall be stiffened by composite edge beams and shall be proportioned for the effects of wheel loads:

This point is not applicable for the historical steel-concrete-composite-bridge-deck. Because the outside steel-girders are not stiffened.

Calculating the resistance based on the Canadian code if the theory will be applied:

In this paragraph the calculation of the capacity of the CMA conform the Canadian code will be carried out on the historical steel-concrete-composite-bridge-deck to check if it is possible to use this code. In the previous chapter the limitations are conducted and checked on the deck. Following the code, the theory can be used if the limitations are all satisfied. But not all limitations are satisfied. Therefore, we cannot use the Canadian code. But if it would have been possible to use the Canadian code, the resistance Rr of the deck could be calculated based on the formulas from the Canadian code which are:

$$\mathbf{R_r = \varphi_{md} * R_n\ [kN]} : (3.7)$$

Were, $\varphi_{md} = 0{,}5$

The value of Rn for both composite and non-composite concrete deck slabs is calculated as follows:

$$\mathbf{R_n = R_d F_q F_c\ [kN]} : (3.8)$$

<u>According to Canadian code (CAN/CSA-S6-06 2006, 2006):</u>

a) $\mathbf{R_d}$: is taken from a particular deck thickness d (or t in Figure 2-42) and the corresponding deck span;
b) $\boldsymbol{F_q}$: is a correction factor based on the reinforcement ratio.

$$\boldsymbol{q = 50\left(\frac{A_{sl}}{b * d_l} + \frac{A_{st}}{b * d_t}\right), \text{with } 0.2\% \le q \le 1\%;} : (3.9)$$

a) $\boldsymbol{A_{sl}}$ **and** $\boldsymbol{A_{st}}$: are the longitudinal and transverse bottom steel areas;
b) **b**: is the width and dl and dt are the longitudinal and transverse effective depths of the deck slab, respectively;
c) $\boldsymbol{F_c}$: is a correction factor based on fc', the specified concrete compressive strength measured on cylinders ($20\ MPa \le fc' \le 40MPa$).

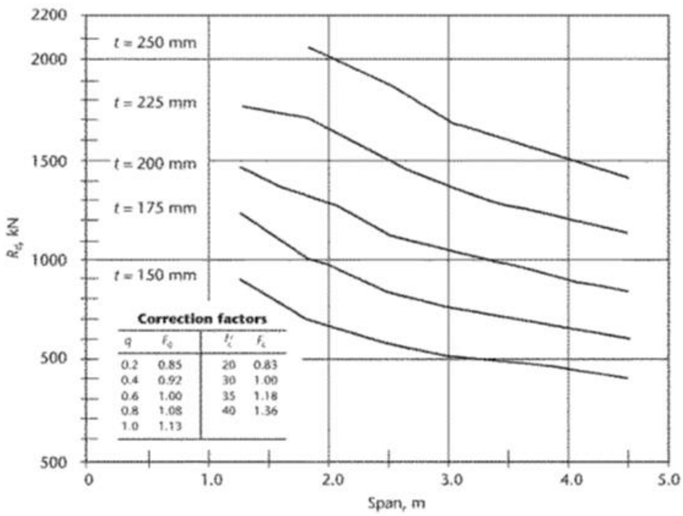

Figure 3-14: Deck punching shear capacity for composite slab (CAN/CSA-S6-06 2006, 2006).

Fq and **Fc** are obtained from the figure 3-14 by linear interpolation. For deck thicker than those shown in figure 3-14. The value of Rn can be obtained by linear interpolation. There is limitation because the resistance of the slab can be defined by the graph 3-14, but the restriction is that the wheel print must be 250 x 250 mm.

Conclusion about the use of the Canadian code:

In this case the Canadian code is not applicable on the historical bridge decks, because the wheel print in the Eurocode is 400 x 400 mm2 or 320 x 600 mm2. Whereas the in-situ-load-test has used a wheel print of 230 x 300 mm2. In addition to this, the thickness of the deck of the historical bridge decks is thicker than the mentioned thickness in figure 3-14. These factors leads to the fact that the theory is not applicable on the historical bridge deck.

UK HA BD81/02 (2002):

According to the UK highway agency's design manual for roads and bridges, the following limitations are implemented in UK for the CMA phenomena. If the historical steel-concrete-composite-bridge-decks satisfied all the limitations, then the CMA can be calculated if it possible according to the UK highway agency's. ((2002), 2002)

Implementing the limitations of the UK highway agencies on the historical steel-concrete-composite-bridge-deck:

The set of rules of the UK highway agency's will be checked in this paragraph. Based on the cross-section which is mentioned in the figure 3-13.

The slab should be at least 160 mm thick and of at least grade 40 MPA concrete.

The slab has minimal thickness of 400 mm at the vehicle lane. This satisfies the rule of the UK highway agency's. The second condition is about the strength of concrete, which must be at least 40 MPA. Based on the inspections which are made for the bridges, the quality of the concrete is 55 MPA which does satisfy the condition of at least 40 MPA.

The minimum steel area provided in the deck slab at each face in each direction should be at least 0.3% of the gross concrete section.

The historical steel-concrete-composite-bridge-deck does not satisfy this rule because the only reinforcement, which is present, is the shrinkage reinforcement.

The transverse (primary) span length of a slab panel perpendicular to the direction of the traffic should not be more than 3.7 m.

The rule is satisfied because the maximal width of the lane is 3 m, where the vehicles pass on the bridge.

The slab should extend at least 1.0 m beyond the center line of the external longitudinal supports of a panel.

This is not relevant for the historical steel-concrete-composite-bridge-deck.

The span length to thickness ratio of the slab should not exceed 15.

The historical steel-concrete-composite-bridge-deck does not satisfy this rule because the ratio is more than 15. The maximal span length in meter is 13,5 m and the thickness deck are 400 mm.

Transverse edges at the ends of the bridge and at intermediate points where the continuity of the slab is broken should be supported by diaphragms designed for the full effects of the wheel loads.

It is not relevant for the historical steel-concrete-composite-bridge-deck.

Cross-frames or diaphragms should be provided at the support lines of all bridges. Bridges with steel beams should have cross-frames or diaphragms at centers not exceeding 8 m or half the span of the bridge. Bridges with concrete beams other than prestressed beams, should have at least one intermediate diaphragm in each span.

It is not relevant for the historical steel-concrete-composite-bridge-deck.

If all the limitations are satisfied, the ultimate capacity can be calculated as follow:

The plastic strain of an idealized elastic plastic concrete ε_c is calculated as:

$$\boldsymbol{\varepsilon_c = \left(-400 + 60f_c - 0.33{f_c}^2\right) * 10^{-6}} \quad : (3.10)$$

The non-dimensional parameter for the arching moment of resistance R is given by:

$$\mathbf{R = \frac{\varepsilon_c * L_r^2}{h^2}} \quad : (3.11)$$

For the deck slab to be treated as restrained, R must be less than 0.26. If this condition is not met, the deck slab is considered unrestrained and the benefit from the compressive membrane action to enhance the load capacity of the slab cannot be assumed. The non-dimensional arching moment coefficient k is given by:

$$\mathbf{k = 0.0525\left\{4.3 - 16.1\sqrt{3.3 * 10^{-4} + 0.1243 * R}\right\}} \quad : (3.12)$$

The effective reinforcement ratio $\boldsymbol{\rho_e}$ is given by:

$$\boldsymbol{\rho_e = k\left(\frac{f_c}{240}\right)\left(\frac{h}{d}\right)^2 \; [Nmm]} \quad : (3.13)$$

The ultimate load $\mathbf{P_{ps}}$ can be calculated as:

$$\mathbf{P_{ps} = 1.52(\phi + d)d\sqrt{f_c}(100 * \rho_e)^{0.25} \; [Nmm]} \quad : (3.14)$$

Where a deck is subjected to axial loading, either two wheels on one slab or two wheels on adjacent axles, the ultimate predicted wheel load $\mathbf{P_{pd}}$ is taken as:

$$\mathbf{P_{pd} = 0.65P_{ps} [Nmm]} \quad : (3.15)$$

Where, d is the average effective depth, the concrete cylinder strength is $\mathbf{f_c} = \frac{0.8\text{fcu}}{\gamma\text{m}}$

a) $\mathbf{f_c}$: is the characteristic concrete cube strength in MPa;
b) $\boldsymbol{\gamma_m}$: is the characteristic concrete cube strength in MPa;
c) **h**: is the overall slab depth;
d) $\mathbf{L_r}$: is half the span of the slab strip with boundary restraint;
(Clear span for slabs monolithic with beams; distance between beam web center lines for slabs supported on steel or concrete girders);
e) $\boldsymbol{\varphi}$: is the equivalent diameter of the loaded area.

Conclusion about the use of the UK highway agency's:

The historical steel-concrete-composite-bridge-decks do not satisfy the limitations of the UK highway agency's. This leads us not to take the CMA into consideration based on the UK highway agency's.

Total conclusion:

Both codes (UK highway agency's and Canadian code) are applied on the cross-section of the historical steel-concrete-composite-bridge-decks. The conclusions which are derived from each theory is that the CMA cannot be applicable on the cross-section of historical steel-concrete-composite-bridge-decks. This means that the codes are not applicable on the historical bridge decks, but it doesn't mean that the CMA is not present in the cross-section. The scope is to apply the codes only and not to research if the CMA is available in the cross-section form the numerical simulations, that is out of the scope.

3.3.4. Strut and Tie model

Introduction:

Deep beams and console are elements which are loaded in their plane. The characteristics of deep beams and console are defined based on the ratio between shear span and depth. The ratio of the deep and console beams is less than or twice the depth of the beam. Based on this the deep beams and console behaves different from a slender beam. The response of this structures is characterized by non-linear strain distributions even in the elastic range. Furthermore, the deep beams and console have a significant direct load transfer from the loaded point to the support. The strut and tie model is applicable in this case. This model will be addressed in detail in this paragraph. In figure 3-15 (The components of a strut-and-tie model.) the transformation path of the load and the concept of strut and tie can be seen. The model will be used in the transverse direction of the historical steel-concrete-composite-bridge-deck to check if the deep and console beams is applicable on the cross-section of the historical steel-concrete-composite-bridge-deck (Asin, 2000).

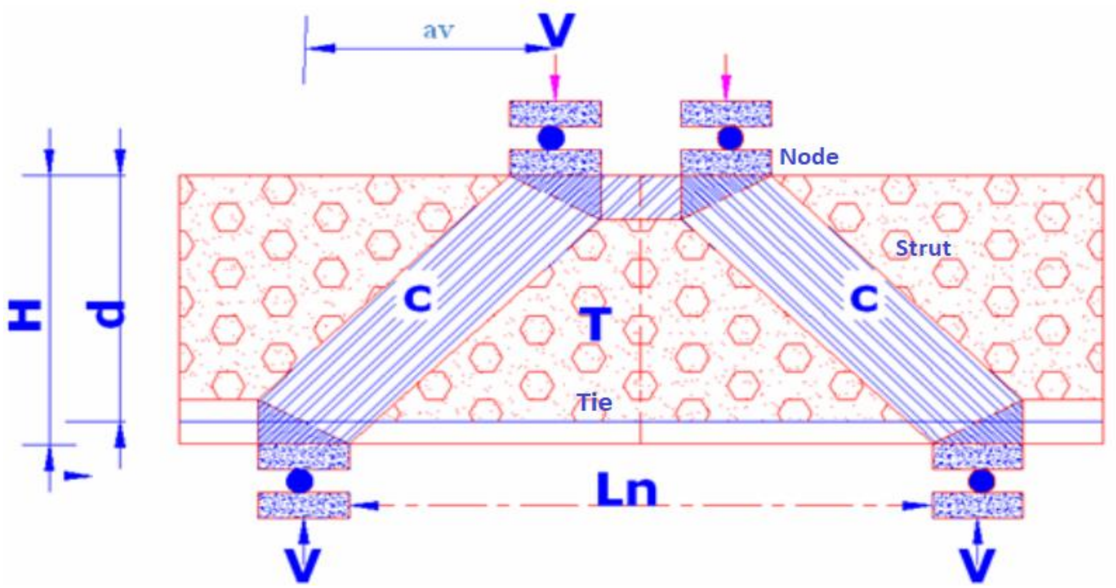

Figure 3-15: The components of a strut-and-tie model.

The strut and tie model (STM) is an approach to design discontinuity regions (D-regions) in reinforced concrete structures. A STM helps to get more insight in the transportation of the structural forces by reducing the complex states of stress within a D-region of a reinforcement concrete member into a truss or uniaxial stress paths. Each path of the uniaxial considers a member of the STM. The STM has a tensile member which is named the tie. The member which is subjected to compression is named struts. The model also contains nodes where the interaction of the different force paths is possible. The forces can be determined using the simple truss mechanics concept (Dr. C. C. Fu, August 21, 2001). See figure 3-15

Implementing the concept on the historical steel-concrete-composite-bridge-deck:

The concept of the deep beams and console has some limitations as named before in the introduction. The depth of the beam must be twice the length. This will be checked on the historical steel-concrete-composite-bridge-deck by using the information and the geometry model which is obtained during the investigation of 32 bridge decks. The properties which will be used during studying this mechanical behaviour is:

a) Material quality (Steel/concrete) (material quality is depended on the dossier of the bridge);
b) The minimal height of bridge deck;
c) A center -to-center distance for the difference lanes (is the distance between the steel profile, in the drawing there are more center -to-center distance available there for the number 1 until 3);
d) Steel profile of the bridge for the difference lanes(type/properties).

Checking the restriction:

The concept will be applicable on the section of transverse direction between two steel profiles and the concrete slab above, see the red frame in figure 3-16 (Distance in the historical steel-concrete-composite-bridge-deck). The rule will be tested by using two distances, which are:

a) Center -to-center distance;
b) HC (the high of the concrete).

The focus is only on the three bridges which are chosen in the assessment study. These bridges will be tested since the case study is based on the results of these bridges, see table 3-3 (Testing the restriction of the deep and console beams)

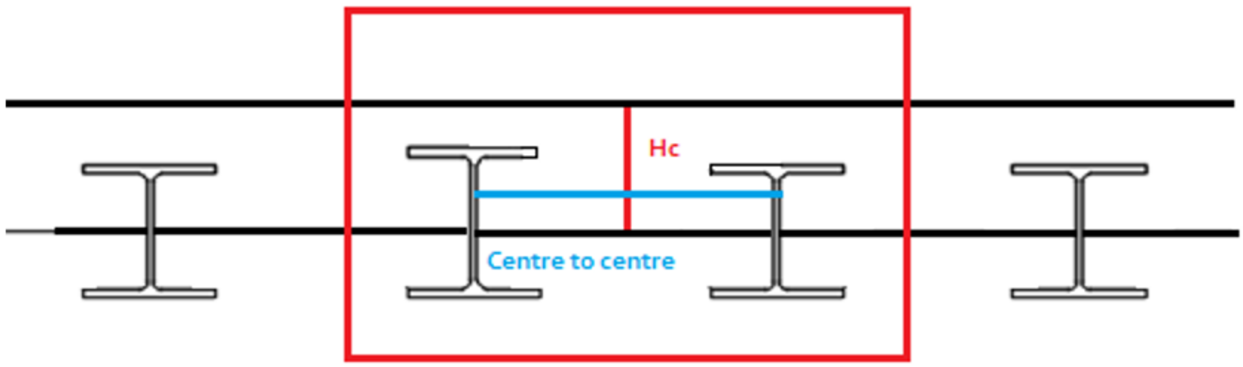

Figure 3-16: Distance in the historical steel-concrete-composite-bridge-decks.

Table 3-3: Testing the restriction of the deep and console beams.

Bridge number	Type span	Deep of the beam H_c in (cm)	Center -to center distance in (cm)/ (is the shear L_N)	Testing the concept
Bridge A	Main span	35	73	The concept is satisfied
Bridge B	Main span	31	73	The concept is satisfied
Bridge C	Main span	24	73	The concept is satisfied

In the table 3-3 it can be seen that all the bridges satisfy the rules. In this case the concept of the deep beams and console can be used by applying the strut and tie model to give an indication about the load transfer in the historical steel-concrete-composite-bridge-deck.

Before implementing the concept there are some assumptions made, which are:

a) The width of the wheel print;
b) The minimal height of bridge deck in included asphalt (cm);
c) The angle transfers the load path in concrete structure is 45 degrees.

Based on this information the force transportation in concrete layer is sketched and is presented in figure 3-17. From figure 3-17 (Implementing the strut and tie model on the historical steel-concrete-composite-bridge-deck) the load transformation can be seen. The strut and tie model are applied on the cross-section of the historical steel-concrete-composite-bridge-deck. The results are that the forces are fully transformed to the two steel-girders. This mechanical behaviour will be modelled in FEA in detail.

Description of the figure 3-17:

The concept of the deep beams and console is implemented in the figure 3-17. The concept is implemented by using the mentioned assumptions above. This shows us the transportation of the load path in the concrete to the steel-girders. Also, the figure shows the geometry of the wheel print which is conform the Eurocode 1990-2.

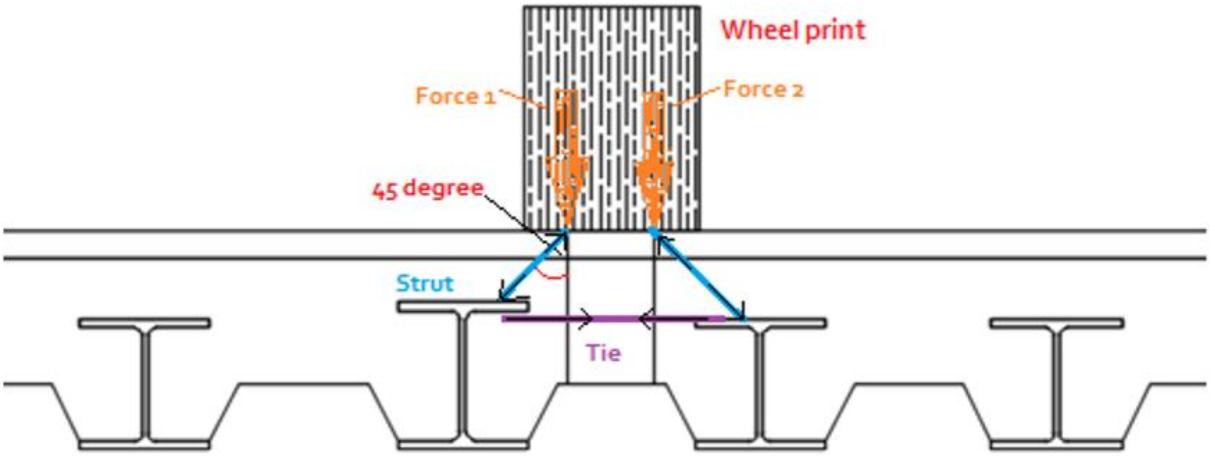

Figure 3-17: Implementing the strut and tie model on the historical steel-concrete-composite-bridge-decks.

Conclusion:

The strut and tie model is applicable on the historical steel-concrete-composite-bridge-deck. This concept will be researched during the FEA-simulations based on the cross-section of the historical bridge. The goal is to get more insight in the behaviour of the historical steel-concrete-composite-bridge-decks.

3.4. Conclusions

The chapter summarizes the conclusions about the reviewed literature and the assessment of it on the historical steel-concrete-composite-bridge-deck. The most important conclusions are listed below:

a) An analytical model is developed and validated to describe the interaction level between steel and concrete;
b) The historical steel-concrete-composite-bridge-deck is not subjected to punching shear. This is also a conclusion during in-situ-load-test, see paragraph 4.2. Which leads us not take the punching shear into consideration;
c) The Canadian code is not applicable on the historical bridge decks, because the wheel print in the Eurocode is 400 x 400 mm2 or 320 x 600 mm2. Whereas the in-situ-load-test has used a wheel print of 230 x 300 mm2. In addition to this, the thickness of the deck of the historical bridge decks is thicker than the mentioned thickness in figure 3-14. These factors leads to the fact that the CMA theory is not applicable on the historical bridge deck. The historical steel-concrete-composite-bridge-decks do not satisfy the limitations of the UK highway agency's. This leads us not to take the CMA into consideration based on the UK highway agency's. Both codes (UK highway agency's and Canadian code) are applied on the cross-section of the historical steel-concrete-composite-bridge-decks. The conclusions, which are derived from each code, is that the CMA cannot be applicable on the cross-section of historical steel-concrete-composite-bridge-decks. This means that the codes are not applicable on the historical bridge decks, but it does not mean that the CMA is not present in the cross-section. The scope is to use the codes only and not to research if the CMA is available in the cross-section. This is out of the scope of this study. During the numerical simulation and from the in-situ-load-test, some conclusions can be made about the CMA but not in detail, because this aspect is out of scope;
d) The strut and tie model is applicable on the historical steel-concrete-composite-bridge-deck. This concept will be researched during the FEA-simulations. The goal is to get more insight in the behaviour of the historical steel-concrete-composite-bridge-decks.

4. In-situ-load-test of historical bridge deck A

4.1. Introduction

The in-situ-load-test is done for bridge A and is executed by four companies. The goal of the in-situ-load-test is to give insight in the actual load-bearing capacity of the bridge deck. However, the in-situ-load-test will gain us more insight in the transverse direction than in the longitudinal direction, because the configuration is set-up for 6-girders behind each other. This is done because we want to check if there is collaboration between the steel-girders in the transverse direction. In addition to this, the in-situ-load-test will be used to validate and to calibrate the FEA-simulations in both directions. The implementation of the in-situ-load-test will be described in this paragraph. The in-situ-load-test is existing out of three separate tests, each of the three tests will be added in the sections below. At last the evaluation of the results will be described for each test and the conclusions and discussion of the results will be added.

4.1.1. Set-up the in-situ-load-test at location of bridge deck A

The in-situ-load-test is set-up by the structural engineering department, at the municipality of Amsterdam, in cooperation with four external companies. Those companies are:

a) TNO Research, coordination;
b) MAX BOGL and K-Dekker, the contractors;
c) Mammoet, load equipment;
d) MFPA Leipzig and Bouwrisk, in-situ measurements.

Each company had a task during the execution of the in-situ-load-test on bridge A. Figure 4-1-a (The plane of the in-situ-load-test from top view of bridge A) shows the top view plane which indicates the location of the places where the test is made for piece B1. In red is the position of the loaded points during the execution of the in-situ test. In green, orange and blue are the locations where the sensors are placed which received the measurement of the in-situ-load-test. Figure 4-1-b (live measurement during the in-situ-load-test) shows the measurement of one of the applied loads and the obtained result during the load. The obtained results are the displacement and the strain of the steel-girders (because the sensors are placed at the bottom of the steel-girders). Also, the dependent time between the un/reloading is given during the in-situ-load-test.

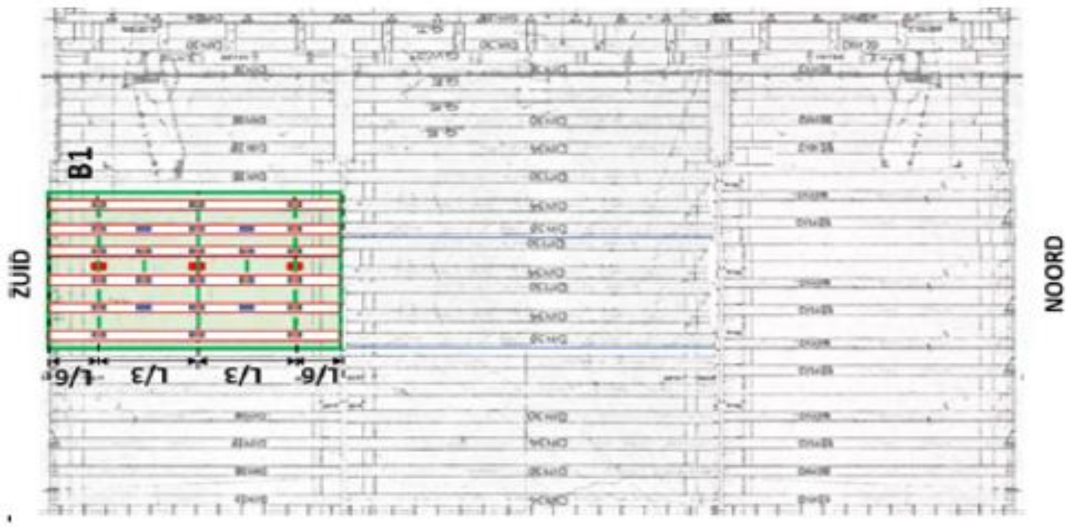

Figure 4-1-a: The plane of the in-situ-load-test on the top view of bridge A.

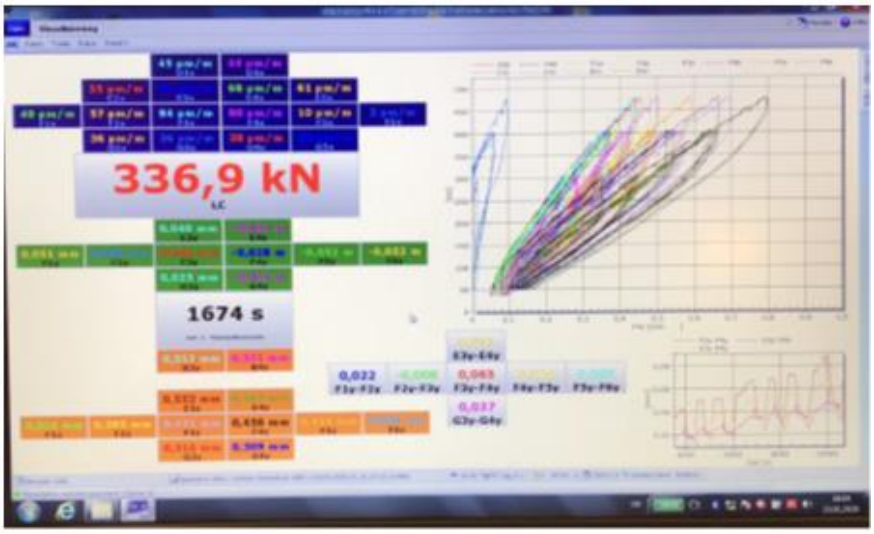

Figure 4-1-b: Live measurement during the in-situ test.
Figure 4-1: Plane In-situ-load-test and the measurement results.

Figure 4-2 (Instrument used during the load test) is composed by three sub-figures. Each of the figures gives an illustration of the component of one of the equipment which have been used during the in-situ-load-test. In figure 4-2 a, the wheel-print which has been used during the test is shown. The size of the wheel print is 300 mm x 230 mm. In figure 4-2-b, the top view of the location of bridge A in Amsterdam and the location where the in-situ-load-test took place is presented. In figure 4-2-c, the location of the placed sensors under the steel-girders is shown. The sensors are placed only to the steel-girders, to avoid measurement errors during the load test, because the concrete can be cracked, and this can lead to errors in the measurement. Furthermore, the in-situ-load-test will be described in detail in the coming paragraphs.

Figure 4-2-a: Equipment of the load pressure and the wheel-print which has been used during the in-situ-load-test.

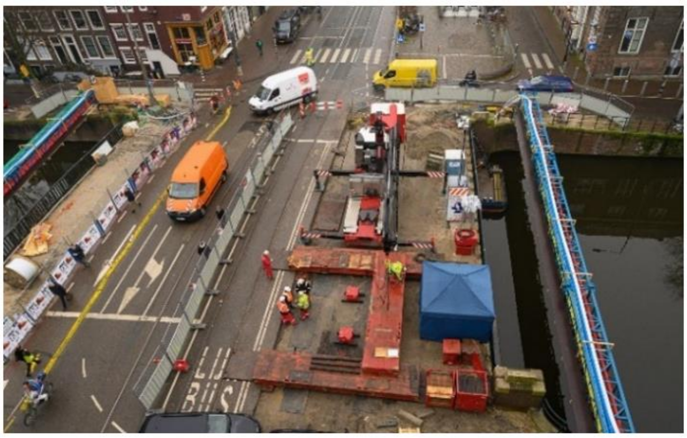

Figure 4-2-b: Top view of in-situ-load-test on the location of the bridge deck A.

Figure 4-2-c: The placed sensors under the bridge deck A.
Figure 4-2: Instruments used during the in-situ-load-test.

4.1.2. Description of the tested specimen of the bridge deck A

Figure 4-1-a, indicates the part (B1) where the in-situ-load-test has been performed for bridge A. The in-situ-load-test is performed on the side-span due to restrictions regarding the fairway below the mid-span of the bridges for boats, so the mid-span isn't used for the experiment of the in-situ-load-test. The plate field contains 6 adjacent steel-girders including the corresponding effective width of the concrete slab. The beams are imposed on natural stone elements, which are placed on the masonry walls of the abutments and the intermediate pillars. Test piece B1 is made up of three steel profiles of type DIN 26 and 3 steel profiles DIN 28. There is no reinforcement mesh at the bottom, only at the top. The reinforcement at the top side was meant to prevent the shrinkage effect in the concrete. The layout of the tested specimen can be seen in the figure 4-3.

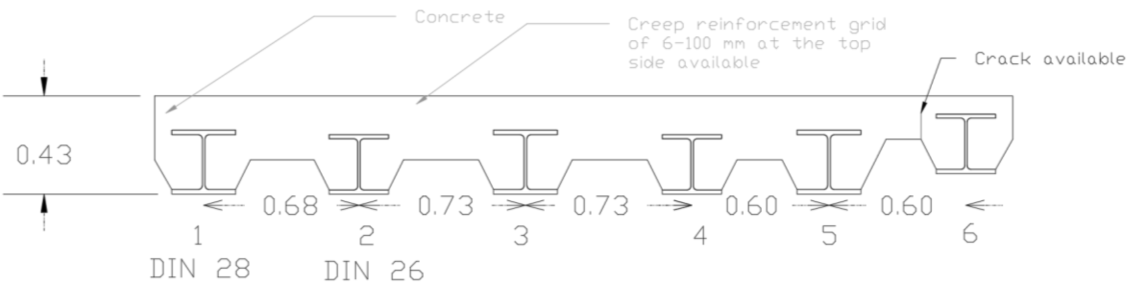

Figure 4-3: Location of the test pieces.

The span of the test piece B1 is approximately L=6.5 m, the width of the test pieces is 4.2 m and the girders are supported on the side of the abutment on a height of 195 cm + NAP, except for the DIN 26 edge beam which is imposed at the height of 204 cm + NAP. On the side of the intermediate pier the beams are imposed at a height of 217cm + NAP. See figure 4-4.

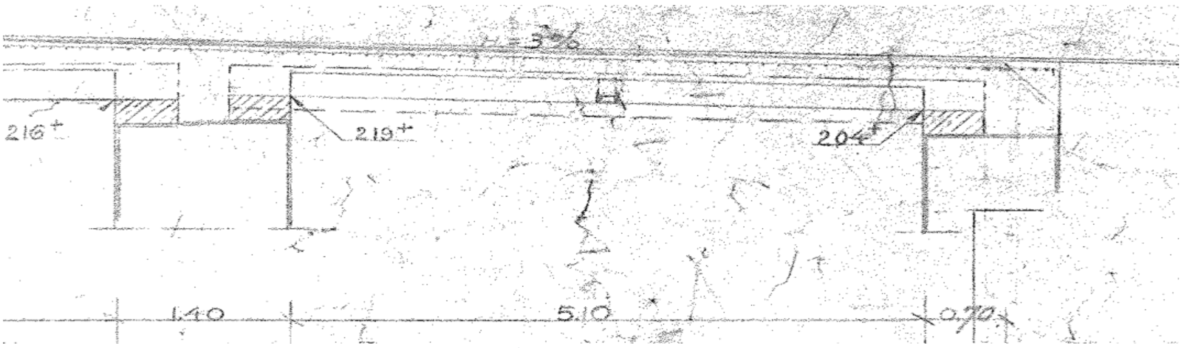

Figure 4-4: Location of the test pieces (Gemeente Amsterdam).

Sawing off the test specimen (tested deck) from the restrained parts in the bridge:
Test piece B1 is sawn loose from the rest of the bridge deck. This is done to create a statically determined plate field. Test piece B1 contains two sets of six steel-girders which are supported both by the existing supports abutments and intermediate pillars.

Description used loads and the position of the load:
Three tests are done for piece B1. Piece B1 is loaded by point load in the middle of the two sets of the six steel-girders. This is done to show the effects of the transverse direction and if there is some load transfer to the adjacent girders. The load plate which has been used during the test has a surface of 230 x 300 mm^2. The size of the load plate is not equal to the wheel print of the traffic load in the Eurocode 1991-2 (Het Nederlands Normalisatie-instituut, 2020) for the traffic load (tandem). The reason for choosing this wheel print is to have an effective spread of the load on the deck to gain an optimal result. The wheel print of the Eurocode will not be sufficient to use during the load test, because the wheel print is larger than the mentioned load plate, which will not be effective enough to show all the load-bearing behaviour of the historical bridge deck. The configuration of the load plate which presents the wheel print is a practice and common wheel print of a loaded truck (Het Nederlands Normalisatie-instituut, 2020). Before starting with the test it is assumed to load the test piece B1 with load that is 475 kN. The made assumption is based on the Eurocode 1 (Het Nederlands Normalisatie-instituut, 2020) where the maximal traffic load is defined for the different models LM1 and LM2 for the impact classes CC2, CC3 and test levels (renovation and rejection). At last the piece B1 is also loaded with a cyclic loading. The resultant effect of the cyclic loading will be not taken into consideration. This will be discussed during the evaluation of the results.

See figure (Figure 4-5: The position of the load in the longitudinal as well as transverse direction) below for illustrations, and the tables for the information about the position and information obtained from the Eurocode.

The loaded positions and the amount of loading which has been used during the in-situ-load-test can be seen in table 4-1 and table 4-2.

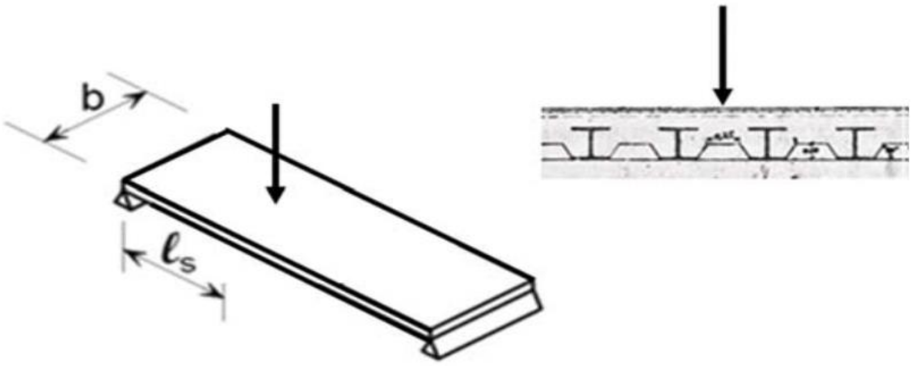

Figure 4-5-a: The position of the load in the longitudinal as well as transverse direction.

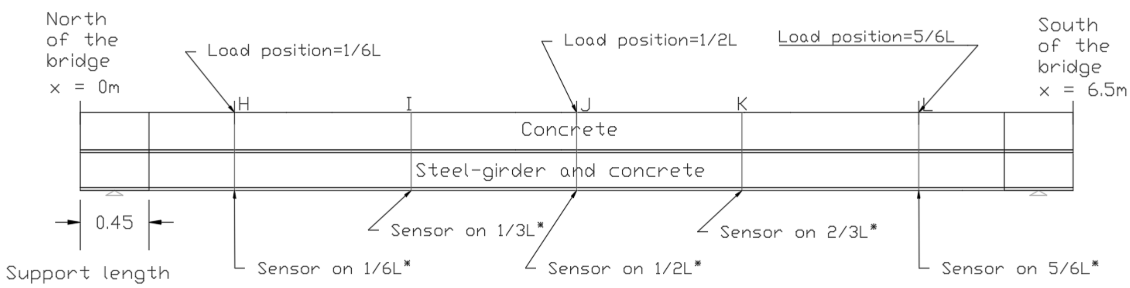

Figure 4-5-b: The position of the loads in the longitudinal on one beam.

Figure 4-5: The position of the load in the longitudinal as well as transverse direction.

Table 4-1: The Longitudinal load positions for five tests.

Location	Profile-type	Longitudinal load positions for five tests		
		ls = 1/6	**ls = 1/2**	**ls = 5/6**
South side	DIN26/28	First	Second	Third

Table 4-2: Load size of Load Models, Consequence Class and test levels (renovation and rejection).

	CC2		CC3	
	Renovation [kN]	**Rejection [kN]**	**Renovation [kN]**	**Rejection [kN]**
LM1	**259**	**224**	**294**	**275**
LM2	**339**	**293**	**384**	**360**

<u>Measurement locations and the quantities which are measured during the load tests:</u>

The position of the sensors which measures the displacement and strain is shown in figures 4-6-an and figures 4-6-b, for more detail see the coming section 4.2 about the three tests. In the figure 4-6-the sensor are placed at the bottom of the steel girders the length which is been used is different from the total length of the bridge deck which is been added as L^*

The following quantities are measured:

a) Applied load (Newton);
b) Vertical displacement of steel profiles (mm);
c) Strain at the bottom of steel profiles in longitudinal direction (micro strain);
d) Relative horizontal displacement of adjacent steel sections in width direction (mm);
e) Cracks under the load (punching through the load) (for signal and stop criterion).

The symbols of the measured quantities are available in the table 4-3.

Table 4-3: Sensor type and symbols.

Quantities to be measured	Sensor type and symbols
1	Load
2	Vertical displacement of steel profiles
3	Strain of the steel profiles
4	Relative horizontal displacement of steel profiles
5	Visually via camera images (Webcam)

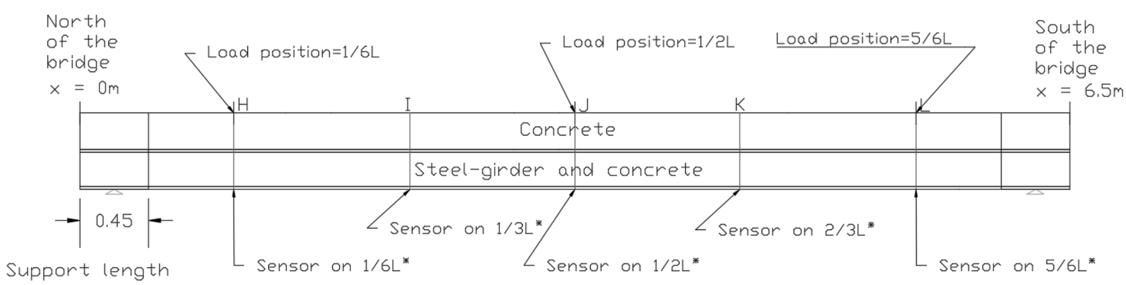

Figure 4-6-a: The position of the loads in the longitudinal and the positions of the sensors on one beam.

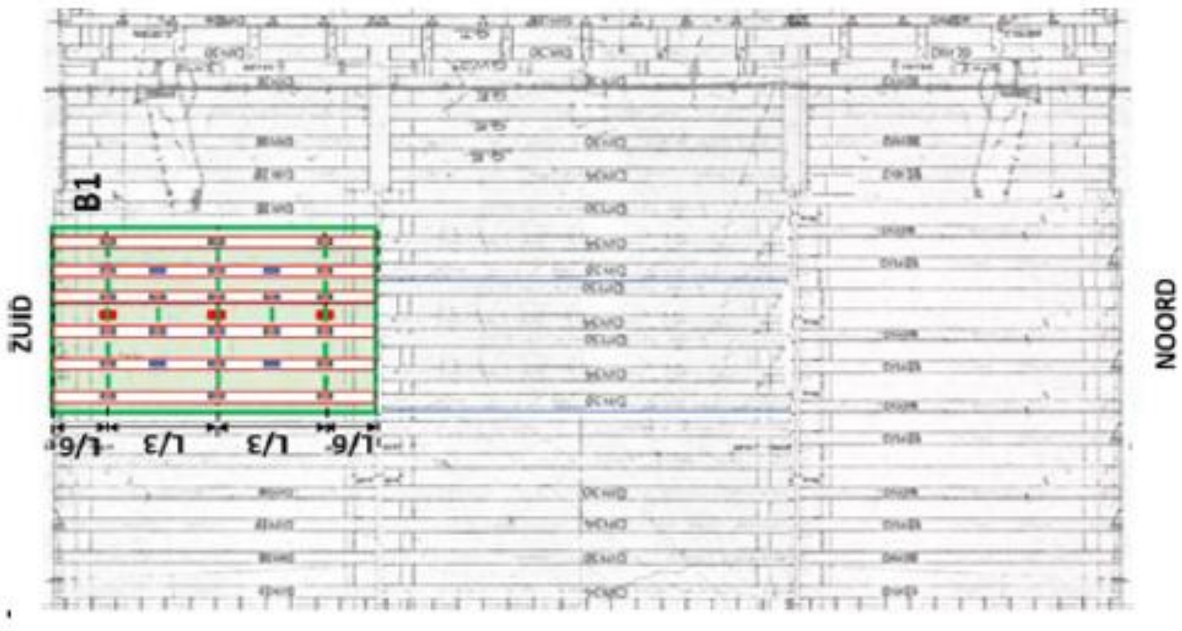

Figure 4-6-b: The position of the loads and the sensors on bridge deck.

Figure 4-6: The position of the sensors.

4.2. Description of the three in-situ-load-tests of the historical bridge deck A and discussion of their results

In this section the goal is to focus mainly on three in-situ-load-tests. First, one of the schema will be described in detail (the rest can be seen in the figures). Then the results will be discussed for each position and evaluated. The evaluation and discussion of the results is done based on analysis of the measured data from each sensor. The sensors are placed on more than one location which will be presented in the coming scheme. The scheme of loading position 1 will be described.

In this case the load is put on the bridge deck with length of L = 1.54 m. The load can be seen in red in Figure 4-7(The configuration of the three tested locations). The sensors are placed on the steel girders (see figure 4-7) at positions in the longitudinal and transverse direction to measure the following quantities:

a) Vertical displacement of steel profiles
b) Strain of the steel profiles
c) Relative horizontal displacement of steel profiles

The sensors are indicated with letters in the transverse direction and with numbers in the longitudinal direction. The configuration of each in-situ-load-test is different for each situation. In the sub-figures 4-7-an until 4-7-c the three tested configurations are presented.

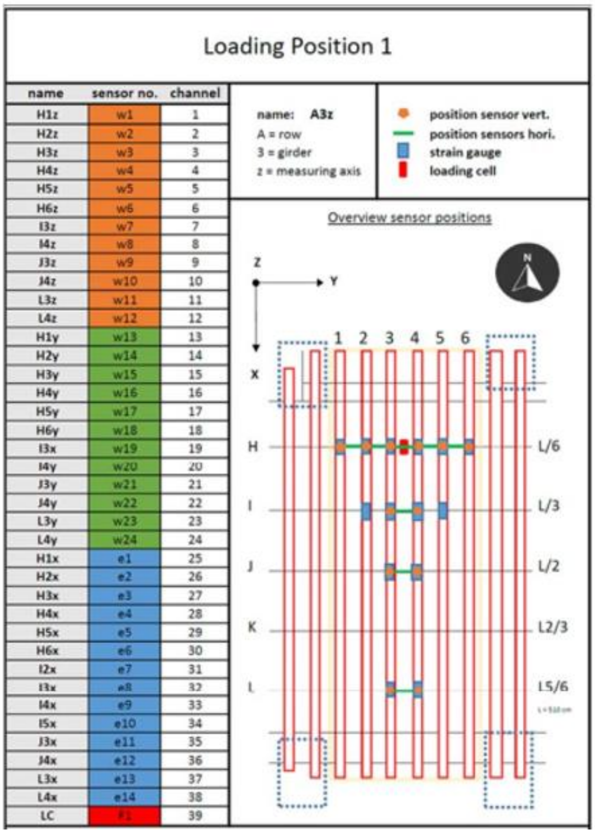

name	sensor no.	channel
H1z	w1	1
H2z	w2	2
H3z	w3	3
H4z	w4	4
H5z	w5	5
H6z	w6	6
I3z	w7	7
I4z	w8	8
J3z	w9	9
J4z	w10	10
L3z	w11	11
L4z	w12	12
H1y	w13	13
H2y	w14	14
H3y	w15	15
H4y	w16	16
H5y	w17	17
H6y	w18	18
I3x	w19	19
I4y	w20	20
J3y	w21	21
J4y	w22	22
L3y	w23	23
L4y	w24	24
H1x	e1	25
H2x	e2	26
H3x	e3	27
H4x	e4	28
H5x	e5	29
H6x	e6	30
I2x	e7	31
I3x	e8	32
I4x	e9	33
I5x	e10	34
J3x	e11	35
J4x	e12	36
L3x	e13	37
L4x	e14	38
LC	F1	39

Figure 4-7-a: First in-situ-load-test 1 on position L = 1.54 m.

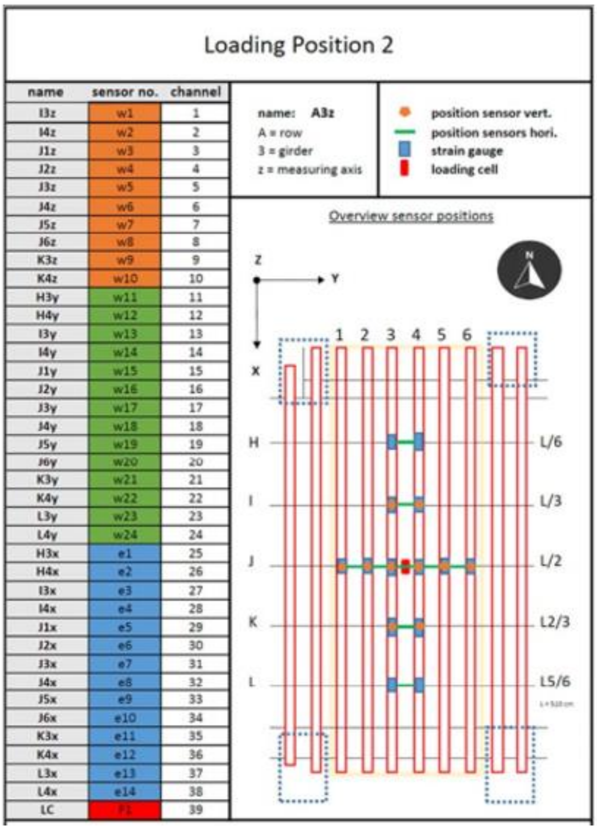

name	sensor no.	channel
I3z	w1	1
I4z	w2	2
J1z	w3	3
J2z	w4	4
J3z	w5	5
J4z	w6	6
J5z	w7	7
J6z	w8	8
K3z	w9	9
K4z	w10	10
H3y	w11	11
H4y	w12	12
I3y	w13	13
I4y	w14	14
J1y	w15	15
J2y	w16	16
J3y	w17	17
J4y	w18	18
J5y	w19	19
J6y	w20	20
K3y	w21	21
K4y	w22	22
L3y	w23	23
L4y	w24	24
H3x	e1	25
H4x	e2	26
I3x	e3	27
I4x	e4	28
J1x	e5	29
J2x	e6	30
J3x	e7	31
J4x	e8	32
J5x	e9	33
J6x	e10	34
K3x	e11	35
K4x	e12	36
L3x	e13	37
L4x	e14	38
LC	F1	39

Figure 4-7-b: Second in-situ-load-test 2 on position L = 3.25 m.

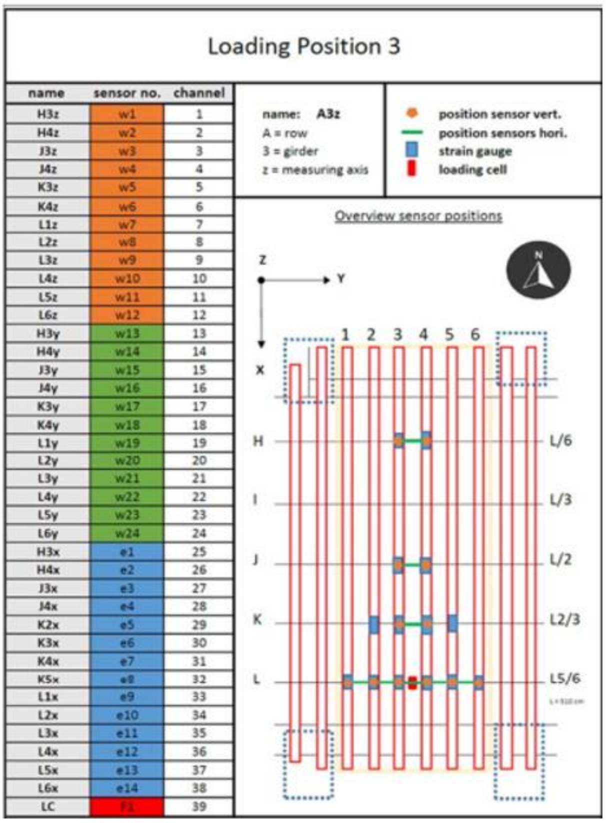

name	sensor no.	channel
H3z	w1	1
H4z	w2	2
J3z	w3	3
J4z	w4	4
K3z	w5	5
K4z	w6	6
L1z	w7	7
L2z	w8	8
L3z	w9	9
L4z	w10	10
L5z	w11	11
L6z	w12	12
H3y	w13	13
H4y	w14	14
J3y	w15	15
J4y	w16	16
K3y	w17	17
K4y	w18	18
L1y	w19	19
L2y	w20	20
L3y	w21	21
L4y	w22	22
L5y	w23	23
L6y	w24	24
H3x	e1	25
H4x	e2	26
J3x	e3	27
J4x	e4	28
K2x	e5	29
K3x	e6	30
K4x	e7	31
K5x	e8	32
L1x	e9	33
L2x	e10	34
L3x	e11	35
L4x	e12	36
L5x	e13	37
L6x	e14	38
LC	F1	39

Figure 4-7-c: Third in-situ-load-test 3 on position L = 4.96 m.

Figure 4-7: The configuration of the three tested locations.

4.2.1. Effect of the cyclic loading on three tests

The three tests are loaded with cyclic loading. The evaluation of this effect will be done only for test 2, because the same procedure is used also on the other tests. The measurement data of test 2 is filtered on several aspects. The cyclical effect of the load procedure (see Figure 4-8: The configuration of the cyclic loading) has been filtered from the data. This means that after each measuring point, only a higher measured maximum load is considered. As a result, the data from unloading and reloading to an earlier reached branch during a repeated tax cycle is filtered and aggregated. An example of this cyclical effect is shown in figures 4-9 until 4-11 for the steel girder 4 for all the three tests.

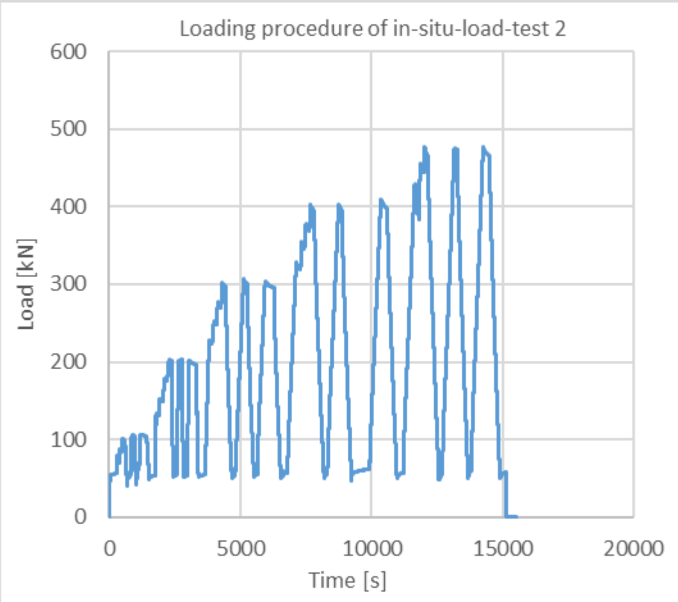

Figure 4-8: The configuration of the cyclic loading.

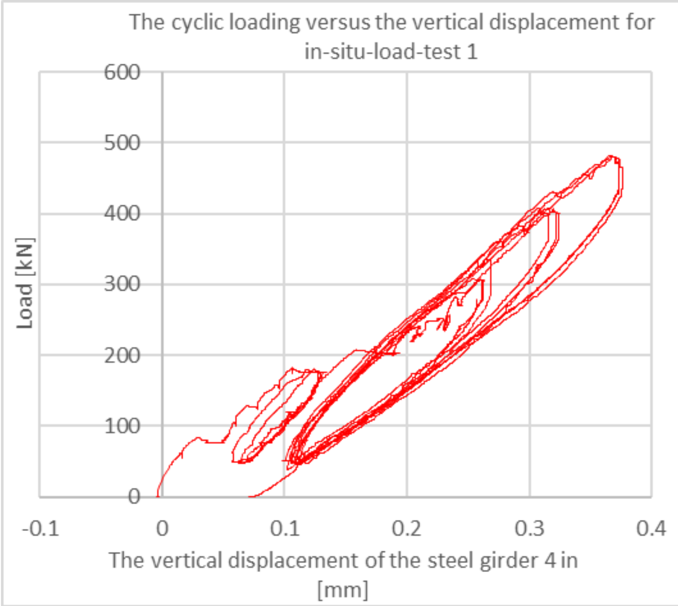

Figure 4-9: The effect of the cyclic loading for test 1.

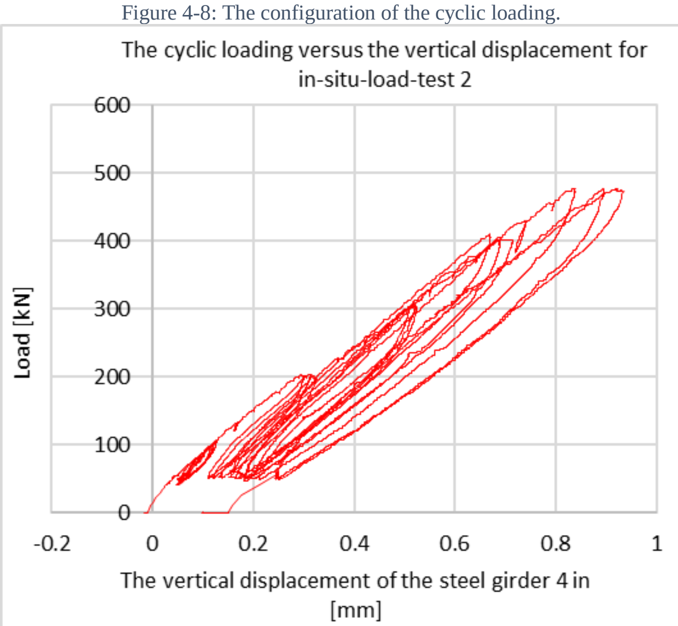

Figure 4-10: The effect of the cyclic loading for test 2.

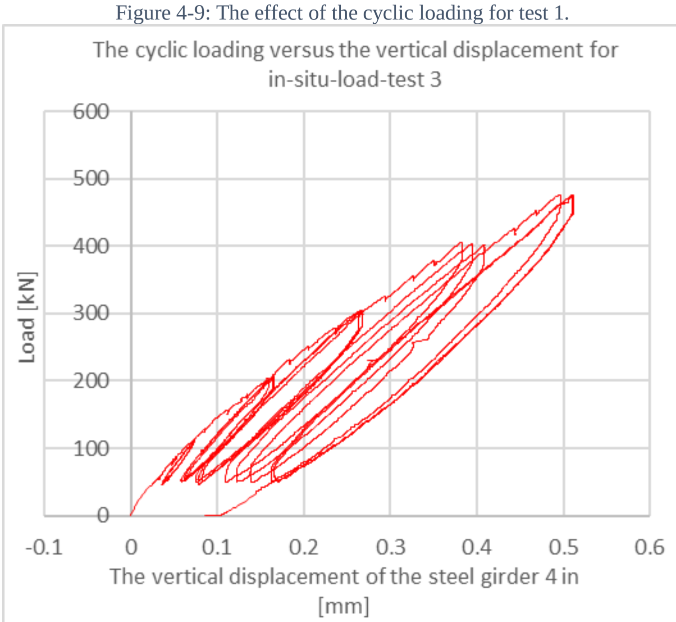

Figure 4-11: The effect of the cyclic loading for test 3.

4.2.2. Evaluation of the results of the first position of the in-situ-load-test 1

The test is made on L = 1.54 m of the span on the bridge deck. The bridge deck is loaded until 475 kN on point H between the steel-girders 3 and 4, see figure 4-7-a: (First in-situ-load-test on position L = 1.54 m). The bridge is loaded with a cyclic load. The effect of the cyclic load is filtered as mentioned in the previous paragraph. During the loading and unloading stages, the measured quantities (strain and displacement) are composed from two components. The components are:

a) In the loading stage the measured quantities are composed by strain and displacement due to the load and due to the residual strain and displacement;
b) In the unloading stage the measured quantities include only the residual strain and displacement.

These two components are subtracted from each other and the resultant displacement and strain will be used during calibrating and validating the FEA-simulations. This is done for the three tests. The main reason of subtracting the two components from each other is to consider the effect of the load on the historical bridge deck without considering the residual deformations which are effecting the measurement results of the in-situ-load-test. The residual deformations can be taken into account in the model by adding extra displacement-load on the structure to take the effect of the residual deformations. But this will be excluded in this thesis because the focus is only to simulate the effect of the used load and to gain insight in the behaviour of these type of bridges.
The bridge at position 1 is loaded with a maximum load of 481.1 kN. There is no occurrence of punching shear failure behaviour or other failure during the loading of the bridge deck. In the figures 4-12 until 4-17 the results of the strain and displacements are plotted. It can be seen that most measured strain and displacement are acting in the non-linear range, but there is no hard explanation of this non-linearity which has been observed. Furthermore, there is also no crack in the concrete observed, based on the inspection and afterwards from the in-situ-load-test. The maximum measured displacement by a load of 475 kN for steel-girders 3 and 4 in row H, is respectively 0.25 mm and 0.27 mm. The maximum strain is 70.7 µm/m respectively 71.5 µm/m. The rest of the measured points are presented in the figures 4-12 until 4-17 based on the configuration of tested position 1 in figure 4-7-a. The measured horizontal displacements between the steel-girders are small. The horizontal displacement is also in the non-linear range, but there is no hard explanation of this non-linearity which has been observed. See figure 4-17 (Measured horizontal displacement in row H during test 1). In appendix C all the tables of the three tests are available.

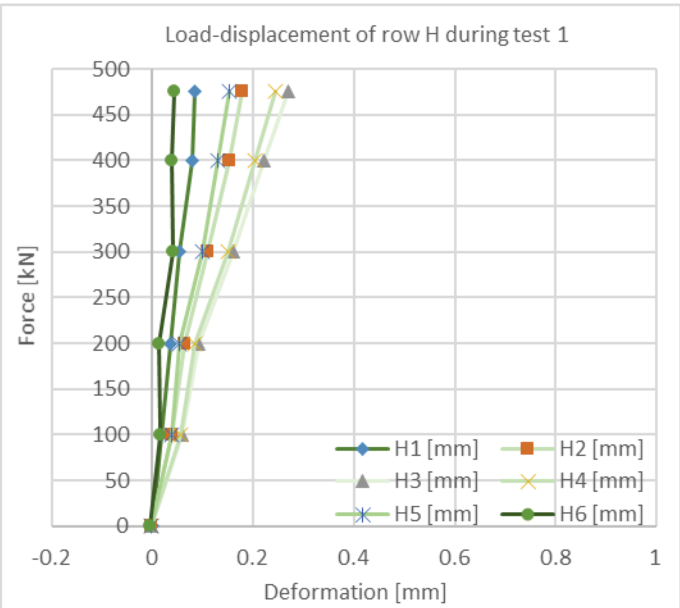

Figure 4-12: Load-displacement of row H during test 1.

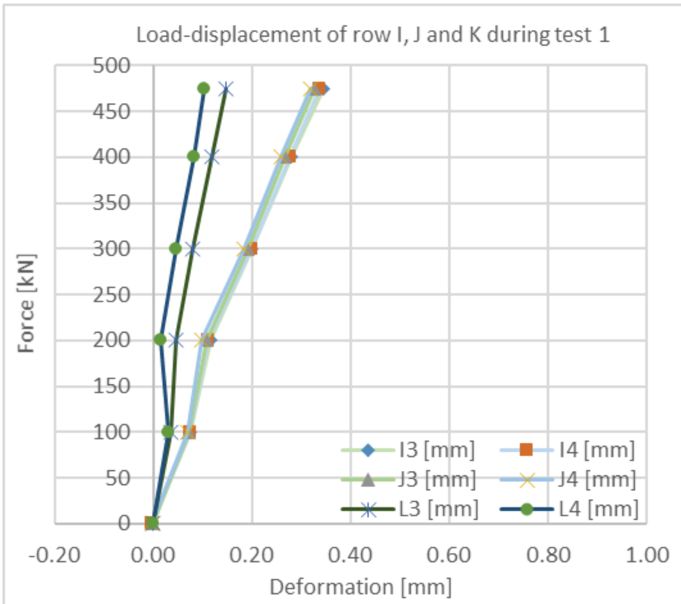

Figure 4-13: Load-displacement of row I, J and L during test 1.

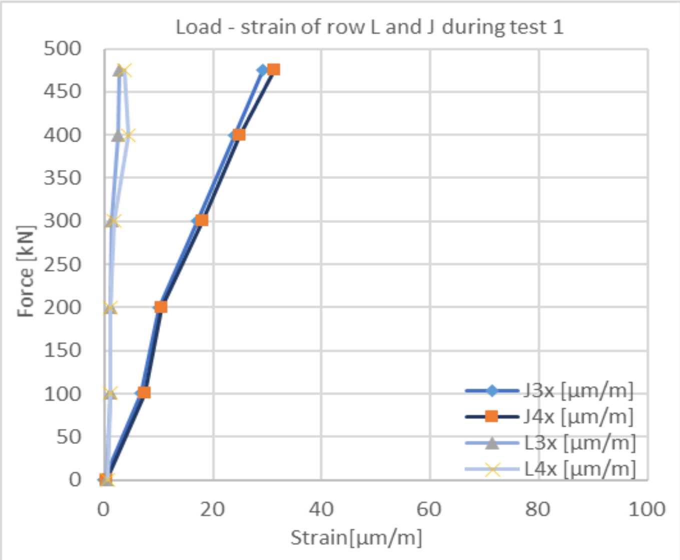

Figure 4-14: Load-strain of row J and L during test 1.

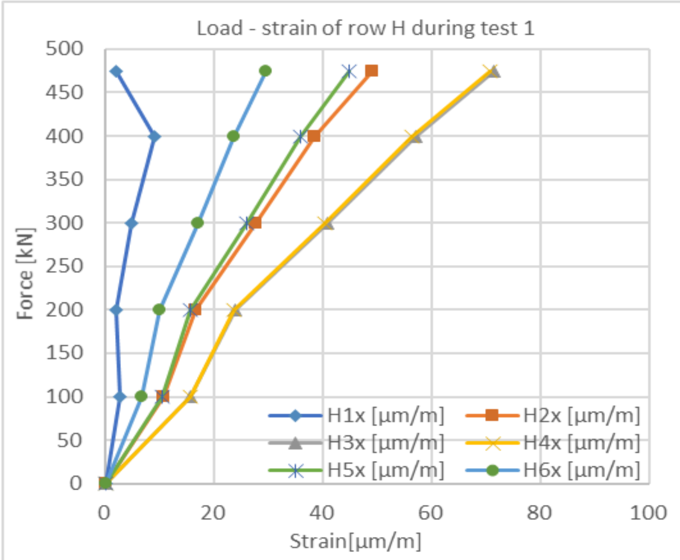

Figure 4-15: Load-strain of row H during test 1.

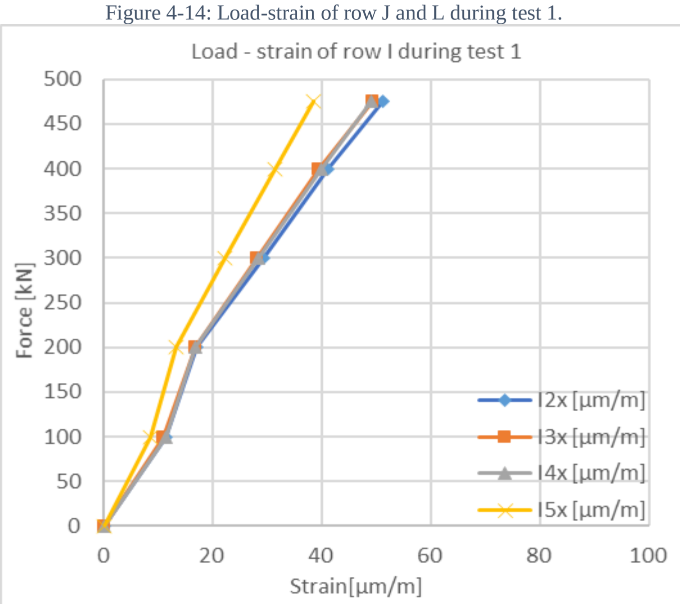

Figure 4-16: Load-strain of row I during test 1.

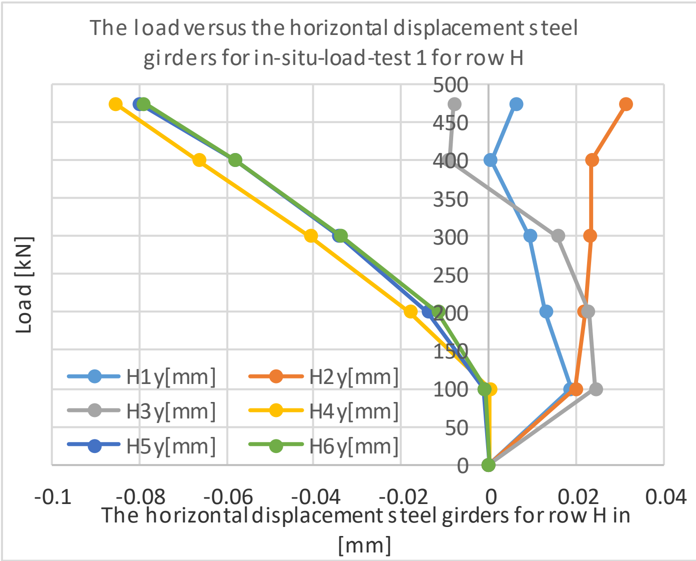

Figure 4-17: Measured horizontal displacement of the steel-girders for row H of test 1.

4.2.3. Evaluation of the results of the second position of the in-situ-load-test 2

Test 2 is the only test with the load in the middle of the span (L=3.25 m) and the measuring points are symmetrical. The expectation from this is that the response left and right and respectively north and south of the load is the same. The test configuration can be seen in figure 4-7-b: (Second in-situ-load-test on position L = 3.25 m). The maximum load which has been used on the bridge deck in this case is 477.4 kN. There is no occurrence of punching shear failure behaviour or other failure during the loading of the bridge deck. Furthermore, there is also no crack in the concrete observed based on the inspection and afterwards from the in-situ-load-test. The results of the displacement and strain are in the non-linear range. From the figures, 4-18 until 4-23 it can be seen that there is a distortion of the displacements from the load of 400 kN until 475 kN. This is valid only for the horizontal and vertical displacement. The most logical interpretation for the horizontal displacement is that the steel girders *(upper flanges)* are sliding until they reach the concrete *(the gap between the flange and the embedded concrete has been assumed to be very small because the measured horizontal displacement is also small),* where the two materials in the transverse direction will be in contact and this leads to activate the concrete where the beam becomes stiffer. This is the explanation of the change in the stiffness of the curve in the horizontal displacement.

In other words, the concrete and steel girders aren't working together until 400 kN, after 400 kN until 475 kN the cooperation between the two materials is activated. See figure 4-23 (Measured horizontal displacement in row J during test 2).

In the longitudinal direction the vertical displacement has also a change in stiffness like the horizontal displacement has from 400 kN. The bridge deck begins to be stiffer than before and this leads to have the same interpretation as in the horizontal displacement. There is slip available until 400 kN, after 400 kN until 475 kN the slip has other behaviour. The sliding between the two materials is very small and not visible. This will be investigated in the numerical simulations (Chapter 5) and also in subchapter 4.2.5.
The maximum measured displacement by a load of 475 kN for beams 3 and 4 in the lane of J is respectively 0.58 mm and 0.58 mm. The maximum resultant strain is 101.4 µm/m respectively 102.7 µm/m. The rest of the measured points are presented in figures 4-18 until 4-23 based on the configuration of tested position 2 in figure 4-7-b.

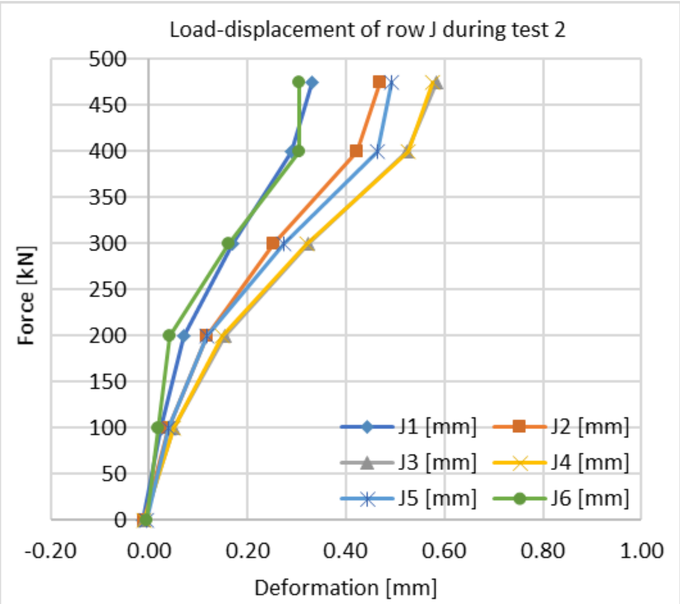

Figure 4-18: Load-displacement of row J during test 2.

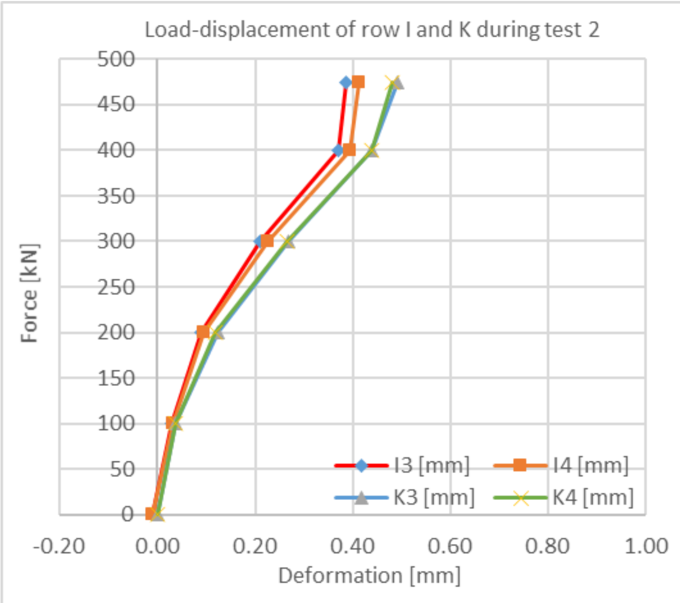

Figure 4-19: Load-displacement of row I and K during test 2.

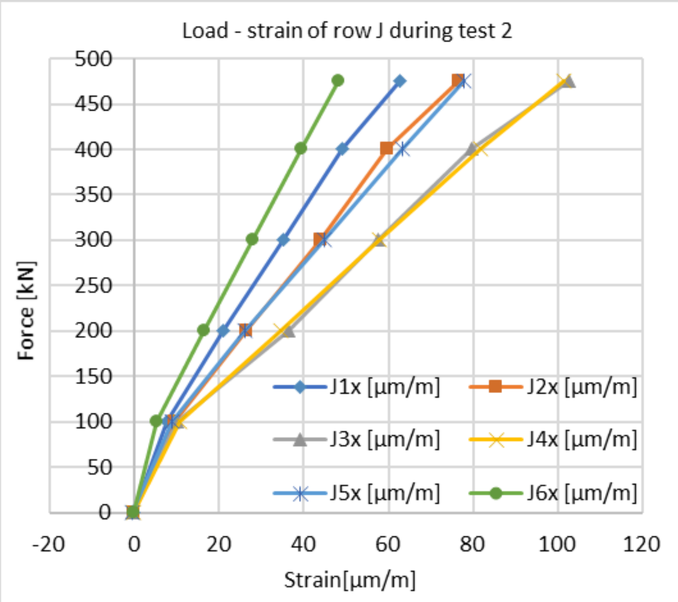

Figure 4-20: Load-strain of row J during test 2.

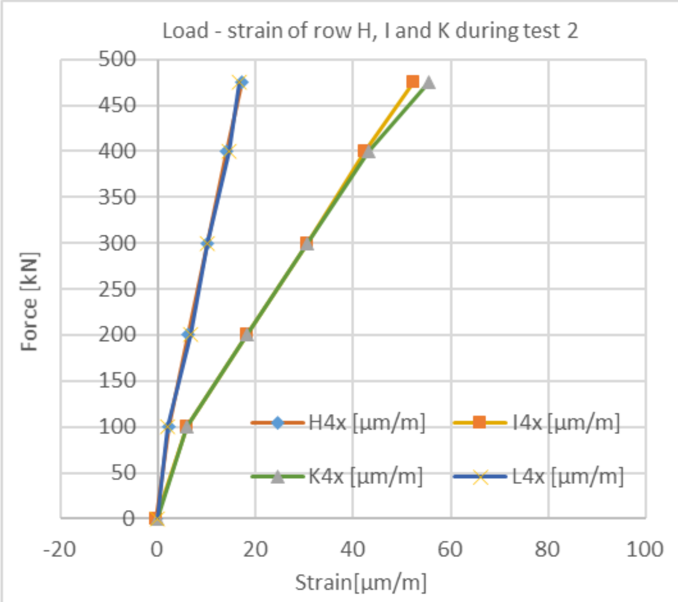

Figure 4-21: Load-strain of row H, I and K during test 2.

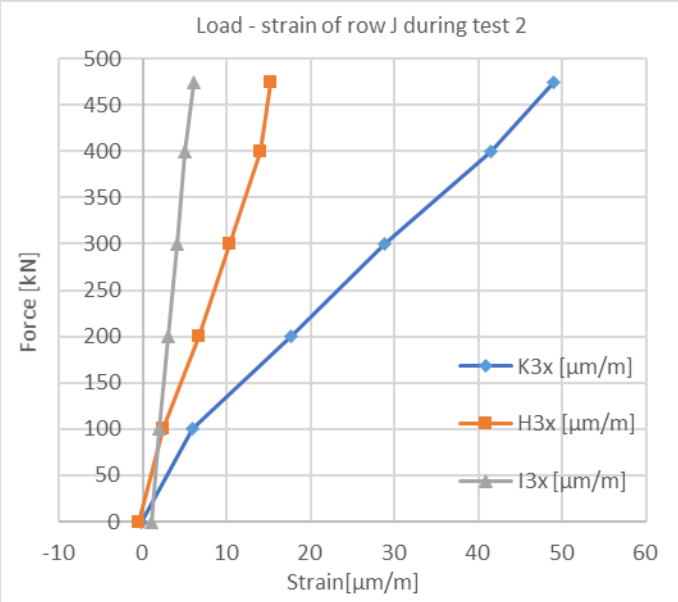

Figure 4-22: Load-strain of row H, I and K during test 2.

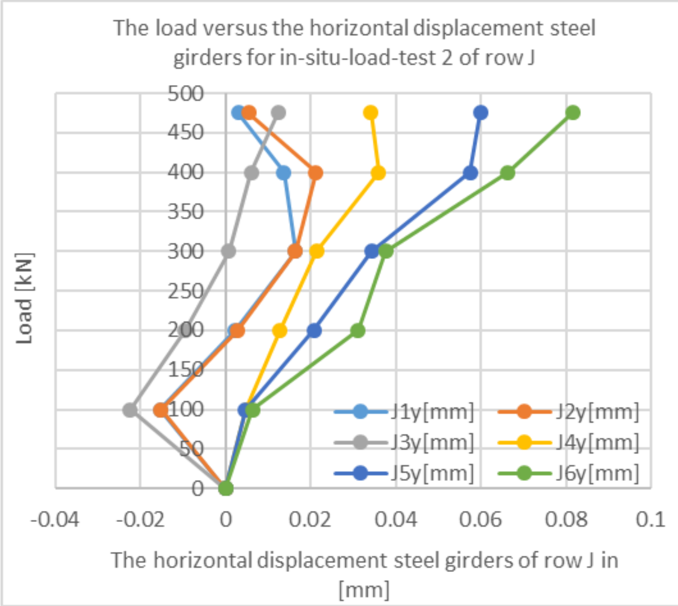

Figure 4-23: Measured horizontal displacement of the steel-girders for row J of test 2.

4.2.4. Evaluation of the results of the third position of the in-situ-load-test

Test 1 and 3 are symmetrical. Test 3 is done to prove that the bridge deck is symmetrical. Test 3 is done on the span of L=4.96 m and the measuring points are symmetrical with test 1. The expectation from this is that the response of test 1 and 3 must be the same. The test configuration can be seen in figure 4-7-c: (Third in-situ-load-test on position L=4.96 m). The maximum load which has been used on the bridge deck in this case is 476.2 kN. There is no occurrence of punching shear failure behaviour or other failure during loadings on the bridge deck. Furthermore, there is also no crack in the concrete observed based on the inspection and afterwards from the in-situ-load-test. The measured results of the vertical displacement and strain are in the non-linear range, but there is no hard explanation of this non-linearity which has been observed. The maximum measured vertical displacement by a load of 475 kN for beams 3 and 4 in the lane of L is respectively 0.33 mm and 0.38 mm. The maximum strain is 44.1 µm/m respectively 64.7 µm/m. The rest of the measured point are presented in the figures 4-18 until 4-23 based on the configuration of the tested position 3 in figure 4-7-c. The measured horizontal displacements are small, but there is no hard explanation of this non-linearity which has been observed. See Figure 4-29 (Measured horizontal displacement during test 3).

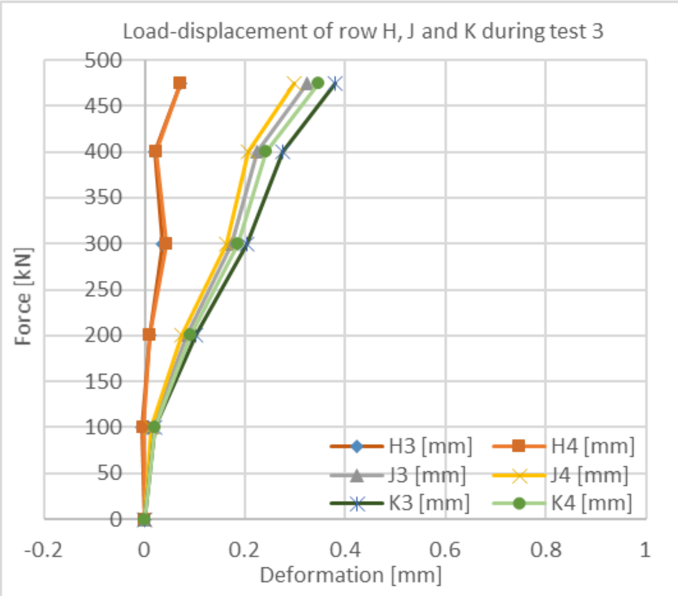

Figure 4-24: Load-displacement of row H, J and K during test 3.

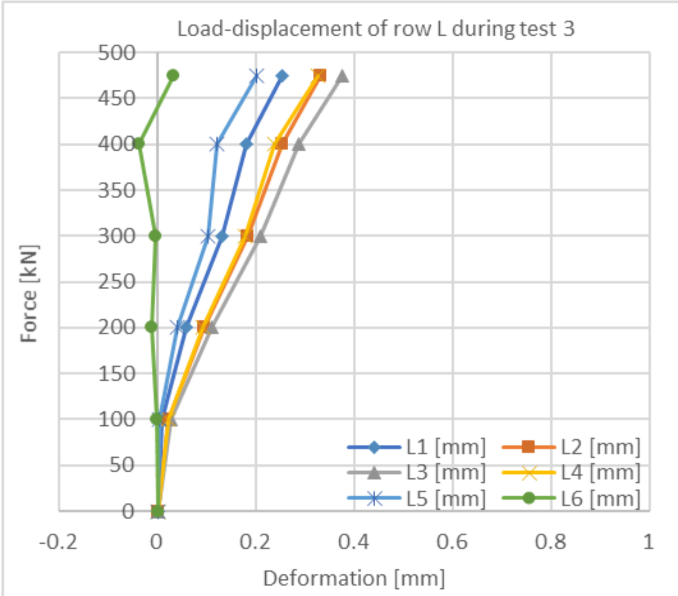

Figure 4-25: Load-displacement of row L during test 3.

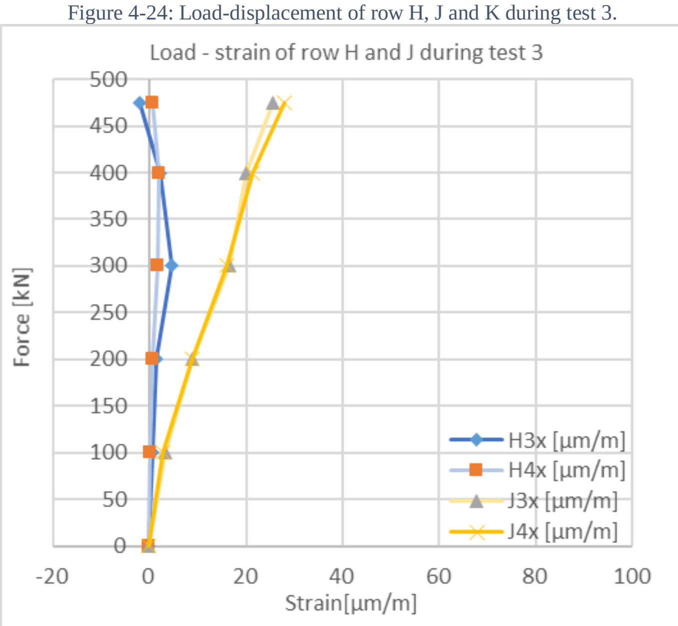

Figure 4-26: Load-strain of row H and J during test 3.

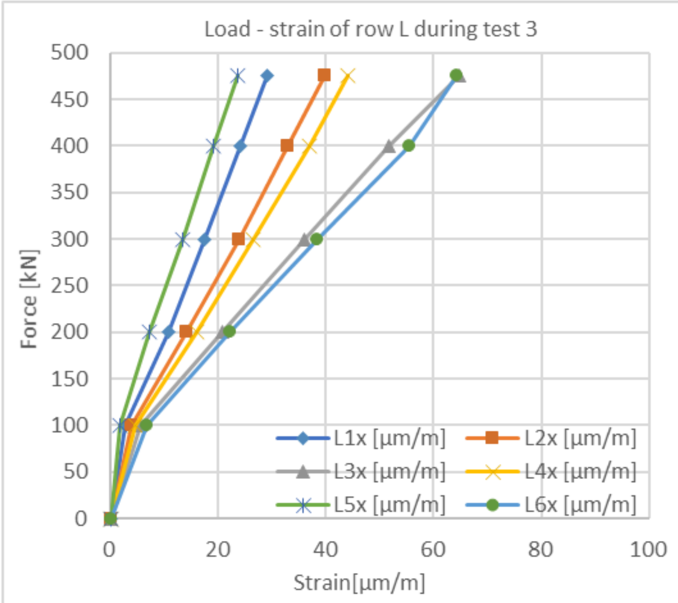

Figure 4-27: Load-strain of row L during test 3.

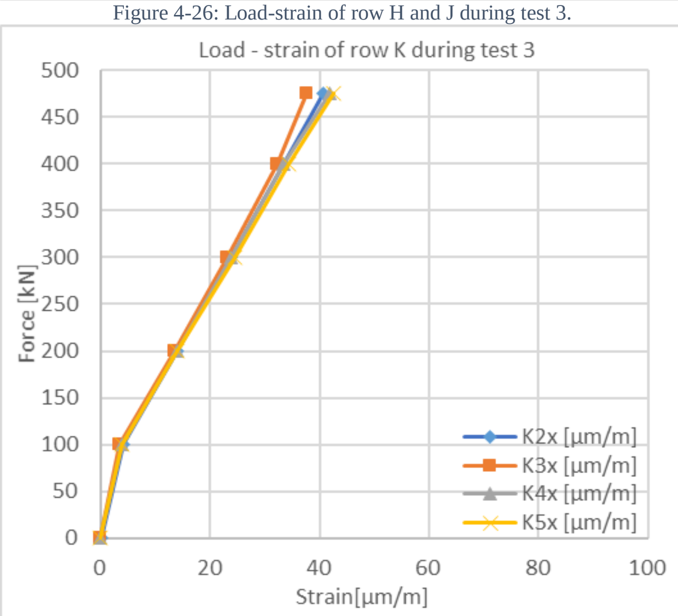

Figure 4-28: Load-strain of row K during test 3.

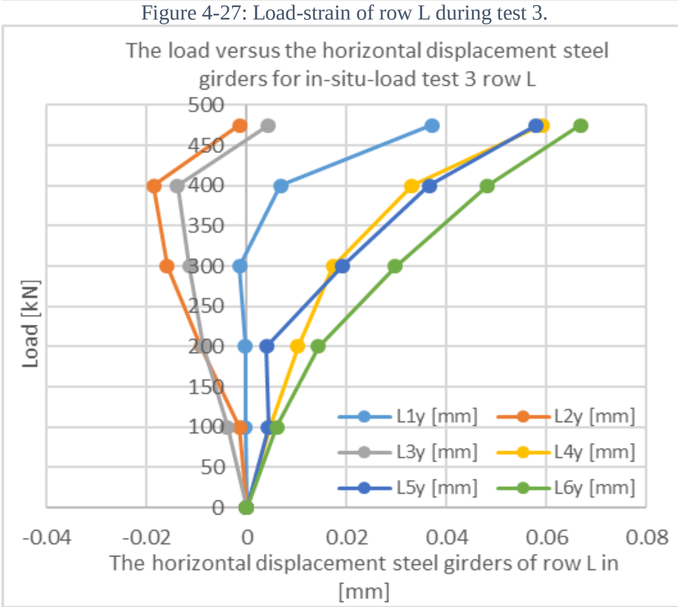

Figure 4-29: Measured horizontal displacement of the steel-girders for row L of test 3.

4.2.5. Evaluation of results of the in-situ-load-tests 2 versus the analytical model

The evaluation of the measured results will also be done with an analytical calculation. The analytical calculation is also done to check which parameters will be used during the numerical simulations to calibrate the FEA-models. The input of the analytical calculation is obtained from sub chapter 2.3.4. Where all the input, including the analytical model, is described and carried out. In this chapter the focus is to compare the results of the analytical calculation with the measured results of the mid-span for in-situ-load-test 2 for only point J. The comparison will be done by comparing the vertical displacement which is obtained from the analytical calculation and the in-situ-load-test. The calculated stiffness of beam 4 in sub-chapter 2.3.4 is presented in table 4-4. The calculated stiffness is based on an assumption of a full interaction between steel girder and the concrete. The total span is 6500 mm but there is a support length of 450 mm for each side of the bridge deck. See figure 4-30. The support length is used as a parameter to calibrate the analytical model and the FEA-model. If we assume that there is a clamed moment available in the bridge deck, then the span will be 5600 mm by removing both support lengths at both sides of the bridge deck from the total span. Furthermore, the force which has been used during the analytical calculation, is obtained from the total force of 475 kN which has been used during the in-situ-load-test. The used support length and load are described in chapter 5. The results of the analytical calculation will be presented in the coming tables. In table 4-4 the input of the analytical model is presented. The results including the analytical models (forget me nots) are added in tables 4-5 until 4-8 and figures 4-31 until 4-34.

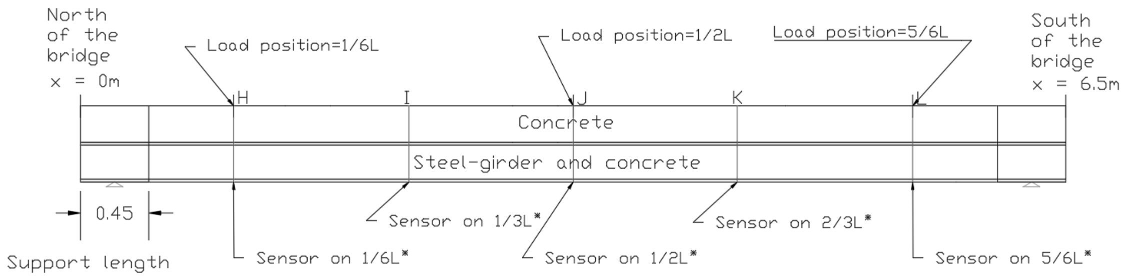

Figure 4-30: Information of used beam in the made calculation.

Table 4-4: The configuration of one beam of the historical bridge deck.

Bridges	The total EI of the composite cross-section [Nmm2]	Length Span [mm]	F [N]
Bridge A	2.30E+14	5600 to 6500	83000

The analytical model which has been used is presented in figures 4-31 until 4-34. In these figures there are three models (forget me nots) presented, first one is supported by hinged and the second one is both with clamped side and a hinged. The last model is clamped by both sides. These three models are being used to calculate the vertical deformation of the bridge deck at the mid-span. This is done to get an idea and feeling about the measured results from the in-situ-load-test on the mid-span position. The calculated results are presented in the tables 4-5 until 4-8 for the three chosen models (forget me nots).

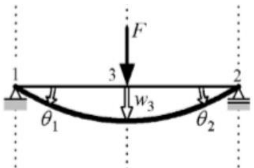

$$\theta_1 = \theta_2 = \frac{1}{16}\frac{F\ell^2}{EI}; \quad w_3 = \frac{1}{48}\frac{F\ell^3}{EI}$$

Figure 4-31: Forget me nots 1.

Table 4-5: The vertical deformation by using forget me nots 1.

Verification with forget me nots 1						
F [N]	**Length Span [mm]**	**L^3**	**7xFxL^3**	**The total EI of the composite cross-section [Nmm2]**	**48xEI**	**W1 [mm]**
83000	6050	2.21E+11	1.84E+16	2.30E+14	1.10E+16	1.66
83000	5600	1.76E+11	1.46E+16	2.30E+14	1.10E+16	1.32

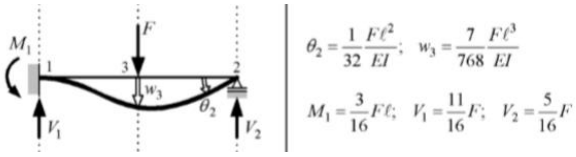

Figure 4-32: Forget me nots 2.

Table 4-6: The vertical deformation by using forget me nots 2.

Verification with forget me nots 2						
F [N]	**Length Span [mm]**	**L^3**	**7xFxL^3**	**The total EI of the composite cross-section [Nmm2]**	**48xEI**	**W2 [mm]**
83000	6050	2.21E+11	1.29E+17	2.30E+14	1.77E+17	0.73
83000	5600	1.76E+11	1.02E+17	2.30E+14	1.77E+17	0.58

In figure 4-33 the illustration of the developed moment due to the support length is given. In this figure the needed forget me nots which will be used to calculate the produced moment is illustrated. The vertical deformation is zero because the abutment is stiff enough. In table 4-7 the calculated moment is given.

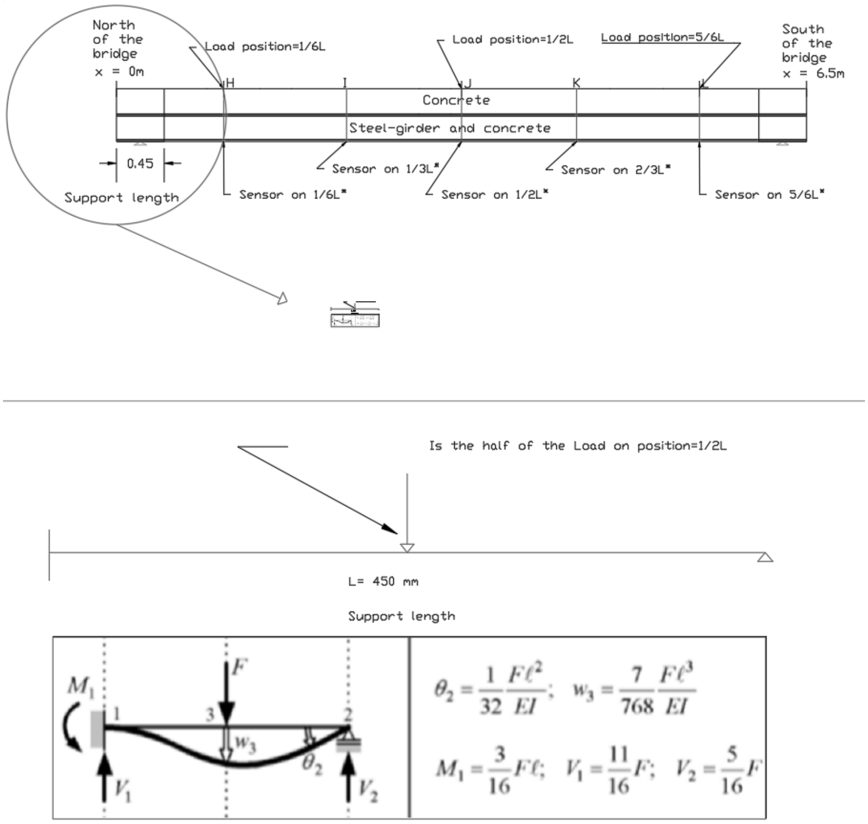

Figure 4-33: The moment which is developed due to the support length.

Table 4-7: The calculated moment which is developed due to the support length.

Verification with forget me nots 2		
F [kN]	**Length Span [m]**	**Moment = (3/16) x F x L [kNm]**
83	0.45	7.00

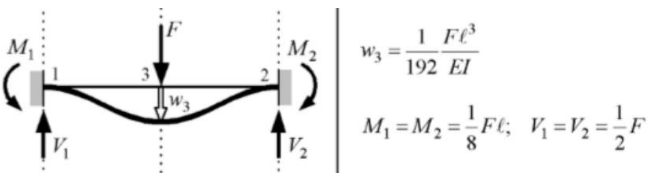

Figure 4-34: Forget me nots 3.

Table 4-8: The vertical deformation by using forget me nots 3.

Verification with forget me nots 3						
F [N]	**Length Span [mm]**	**L^3**	**7xFxL^3**	**The total EI of the composite cross-section [Nmm2]**	**192xEI**	**W3 [mm]**
83000	6050	2.21E+11	1.84E+16	2.30E+14	4.42E+16	0.42
83000	5600	1.76E+11	1.46E+16	2.30E+14	4.42E+16	0.33

From the in-situ-load-test the normative steel girder is steel girder 4. The measured vertical deformation is presented in the table 4-9.

Table 4-9: Measured result of the steel girder 4.

Load [kN]	**J4 [mm]**
475	0.58

The observation and evaluation which can be made from the presented results in the tables 4-5 until 4-9 is:

The measured vertical displacement shown in table 4-9 is more or less close to the results in table 4-5 and 4-7. As mentioned before in the evaluation of the measured results of in-situ-load-test 2, that there is sliding available between steel girder and concrete, the measured vertical displacement is more or less close to forget me nots 2 and 3, which suggest that there is a calmed moment available in the measured result, which will be studied during the numerical simulations. The main observation is: Nonlinearity is local, the majority of the beam might still be in the linear region, but this will also be validated during the FEA-simulations. The results will be discussed in the coming sub-chapter by taking a conclusion.

4.3. Conclusions and discussions of the results of the in-situ-load-tests of the historical bridge deck A

4.3.1. Introduction

The accentuation of the in-situ-load-tests is to gain insight in the transverse direction, where the goal is to focus on the collaboration of the steel-girders in combination with the slab. The longitudinal direction of the bridge deck will be derived from the normative steel girder 4. The results of the in-situ-load-test will be used to calibrate and to validate the FEA-simulations. In this sub-chapter all the discussions and conclusions from the three tests will be included. Finally, the discussion and conclusion of the analytical results will be added.

4.3.2. Discussions and conclusions of results of the in-situ-load-tests 1 and 3

The goal of performing tests 1 and 3 is to prove that the bridge deck is symmetrical. During the execution of the tests, and the demolition of the bridge deck after the tests were performed, a note can be made. That is that the bridge deck was stuck to the abutment with a block of concrete. This means that the bridge deck behaves slightly less than when freely imposed. This makes the comparison difficult. The effects which are named in the previous part are reflected in the maximum vertical displacement and strain of both tests which are included in the figures 4-35 until 4-38 for the beams 3 and 4 over the length of the tested bridge deck. In the figures 4-35 until 4-38 it can be seen how the displacement and the strain are propagating over the length of the beam. As indicated in the figures 4-35 and 4-36 the vertical displacement for beams 3 and 4 in the main row H is measured as 0.25 mm and 0.27 mm, where the vertical displacement for beams 3 and 4 in main row L is measured as 0.33 mm and 0.38 mm. This difference can be explained by the asymmetrical behaviour of the deck. The measured results of both tests are in the non-linear range, but there is no hard explanation of this non-linearity which has been observed based on the measured results. In figure 4-39 the measured results of the transverse direction are added. The results of the transverse direction show that the adjacent steel-girders are activated.

The main conclusions derived from the results:

Both in-situ-load-tests 1 and 3 show non-linear curves and based on this, the results can be considered to be in the non-linear stage, but there is no hard explanation of this non-linearity which is been observed based on the measured results. In addition to this, the values of the displacements and strain are small. Therefore, the in-situ-load-tests will not give a full picture about the load-bearing capacity of the historical bridge decks and the conclusion which can be taken from these in-situ-load-tests about the behaviour of the historical bridge deck is not complete. Furthermore, there is a difference in the stiffness between steel girder 3 and 4. Steel girder 4 is a Din 26 and steel girder 3 is a Din 28. This has also influence on the results of the beams. At last, the in-situ-load-test does not show any defects during the loading procedure. See the figures 4-35 until 4-38 for a comparison of the two leading beams 3 and 4. There is no occurrence of punching shear failure behaviour or other failure during loading the bridge deck. Furthermore, there is also no crack in the concrete observed based on the inspection and afterwards from the in-situ-load-test.

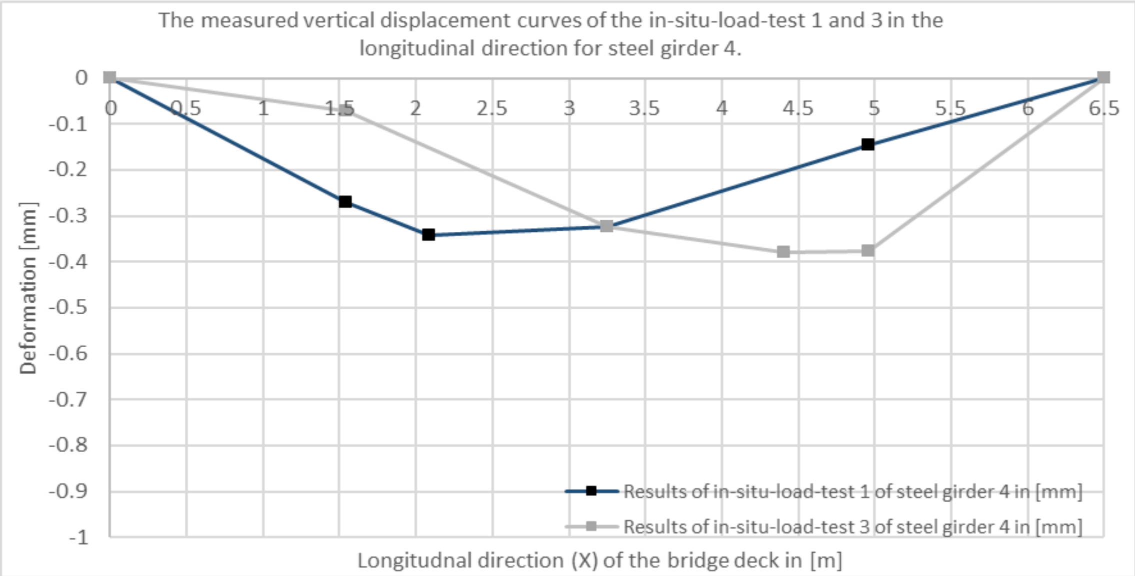

Figure 4-35: The measured displacement curves of the steel-girders 4 for tests 1 and 3.

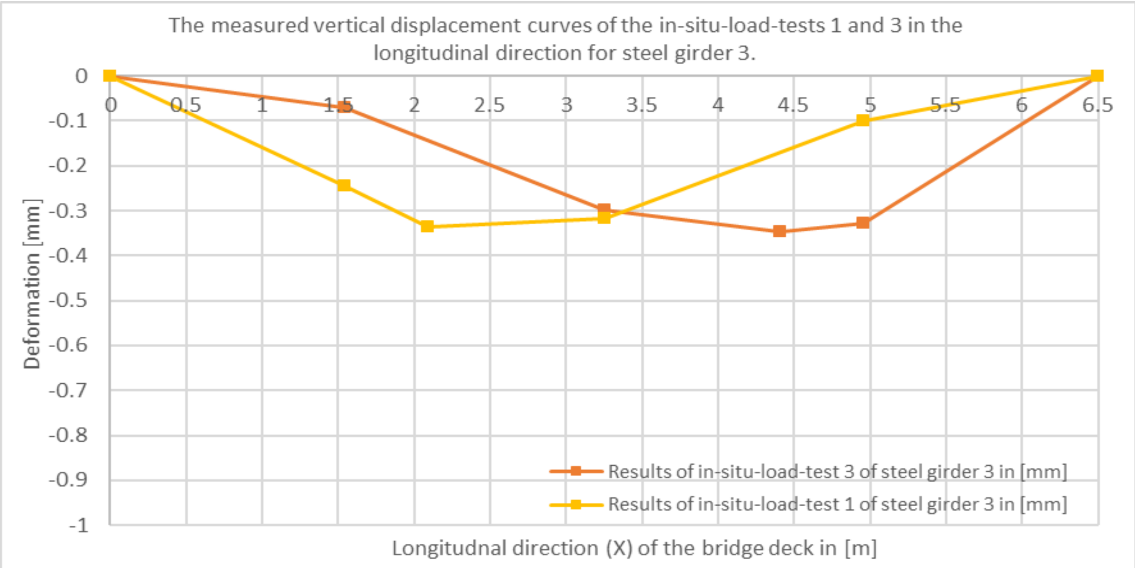

Figure 4-36: The measured displacement curves of the steel-girders 3 for tests 1 and 3.

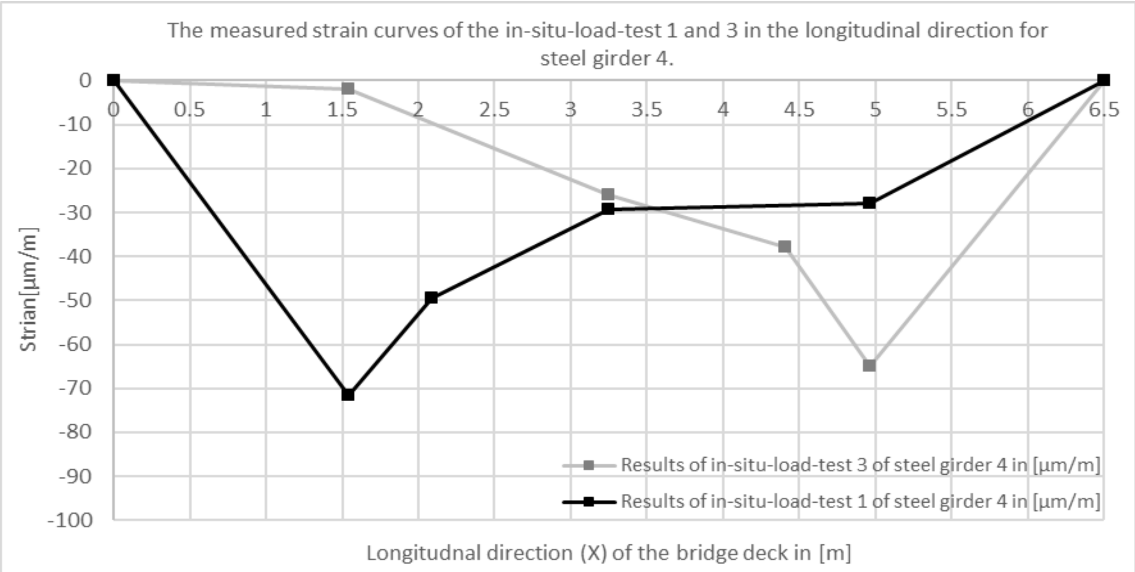

Figure 4-37: The measured strain curves of the steel girder 4 for tests 1 and 3.

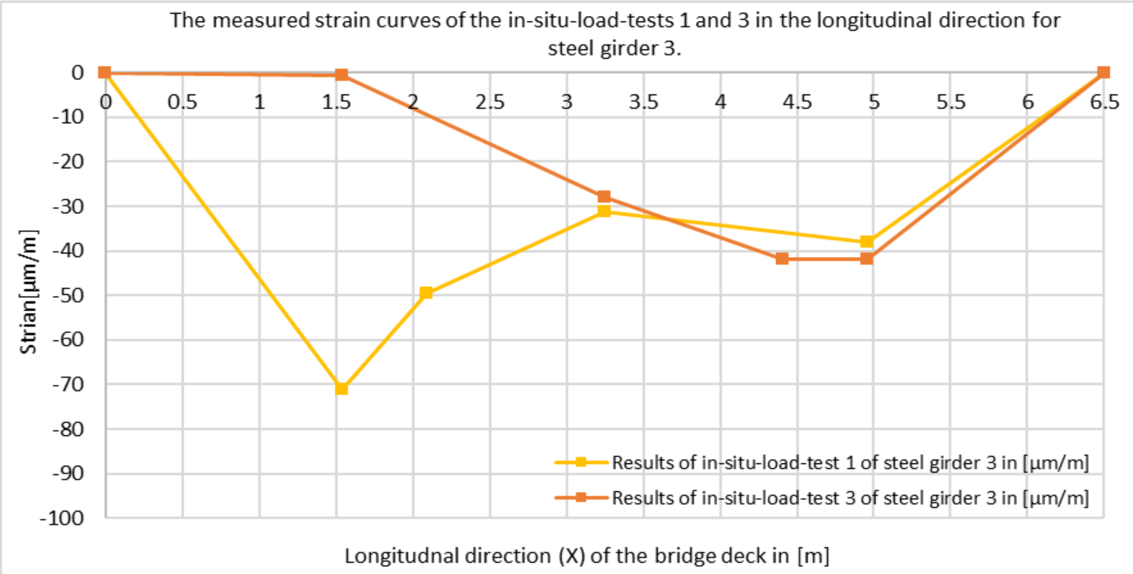

Figure 4-38: The measured strain curves of the steel girder 3 for tests 1 and 3.

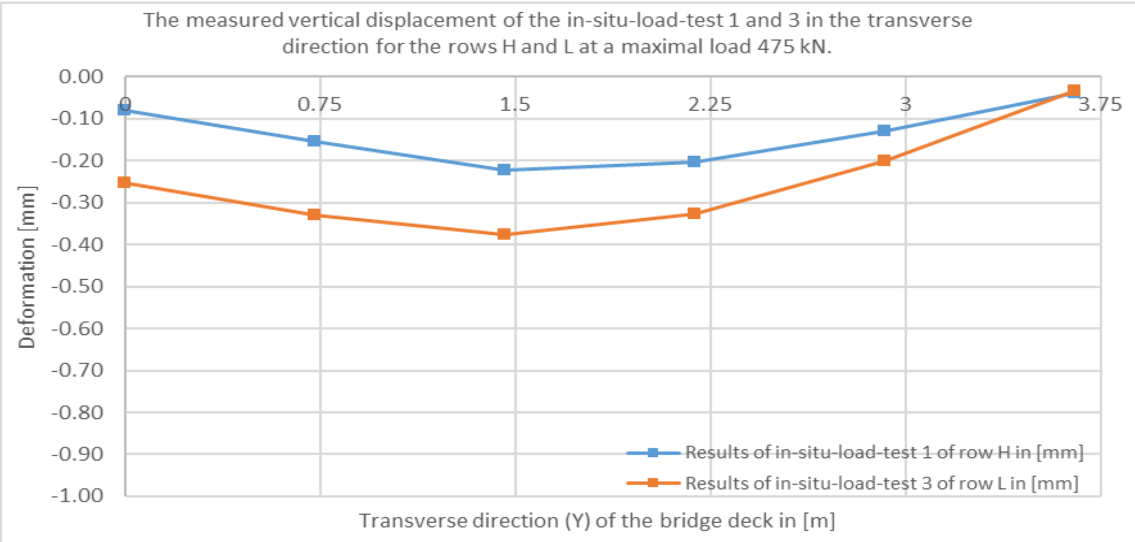

Figure 4-39: The measured deflections in the transverse direction in [mm].

4.3.3. Discussion and conclusions of results of the in-situ-load-test 2

The results of the displacement and strain are in the non-linear range. From the figures, 4-18 until 4-23 it can be seen that there is a distortion of the displacements. This is due to the available slip in the horizontal displacement as well as the vertical displacement. In the previous section some comments were mentioned, the comments are also valid for test 2. In the figures 4-40 and 4-41 the response of the beams 3 and 4 in the longitudinal direction can be seen. The results of point I and K for both beams are not symmetrical. This is due to the asymmetrical behaviour of the bridge deck due to the block concrete which was stuck to the abutment. This explains the difference between beams 3 and 4. Furthermore, there is a difference between stiffness of the two girders as mentioned before and this has influence on the response of the deck. See figures 4-40 and 4-41. The result of the transverse direction shows that the adjacent steel-girders are activated. See figure 4-42.

The main conclusions derived from the results are:

The results can be considered in the non-linear stage. Slip occurs from 0 kN until 400 kN, and between 400 kN until 475 kN the deck becomes stiffer which leads to a change in the behaviour of the slip. In addition to this, the same conclusions of in-situ-load-test 1 and 3 are also valid for the in-situ-load-test 2.

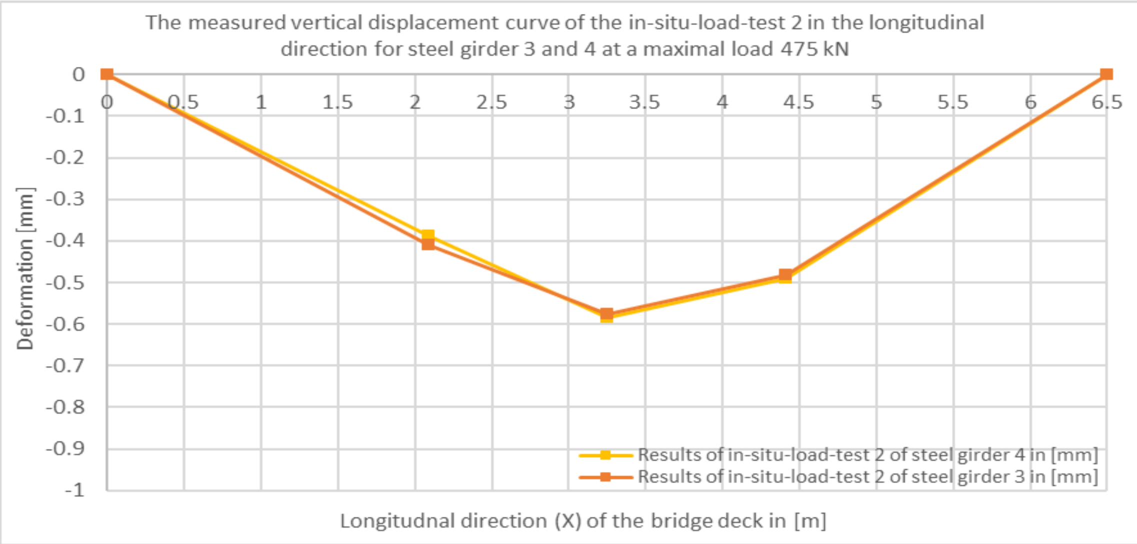

Figure 4-40: The measured displacement curves of the steel-girders 3 and 4 for test 2.

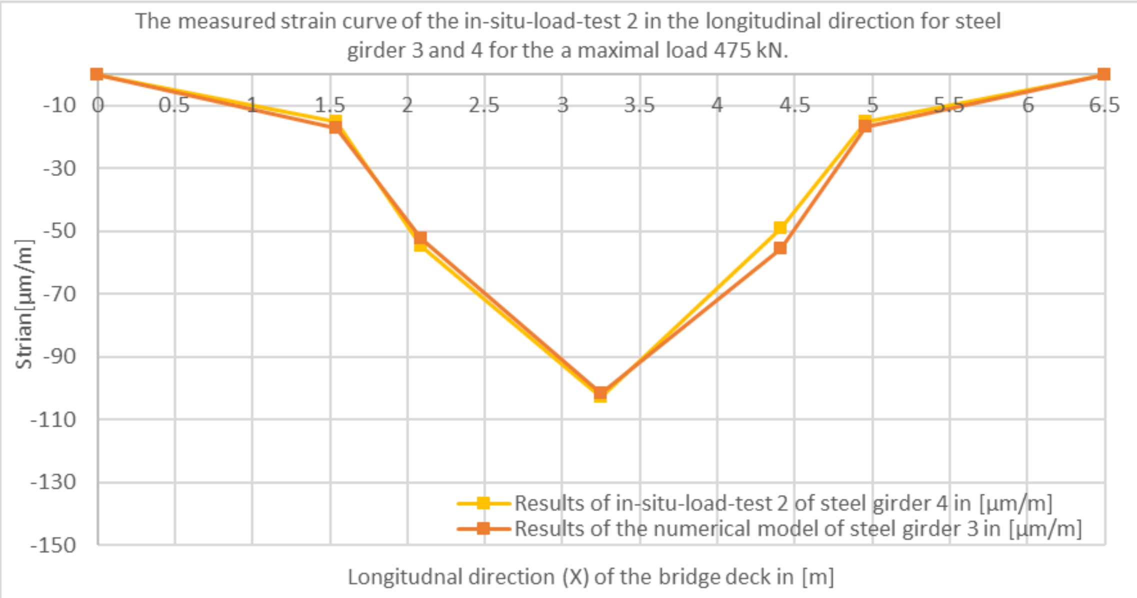

Figure 4-41 The measured strain curves of the steel-girders 3 and 4 for test 2.

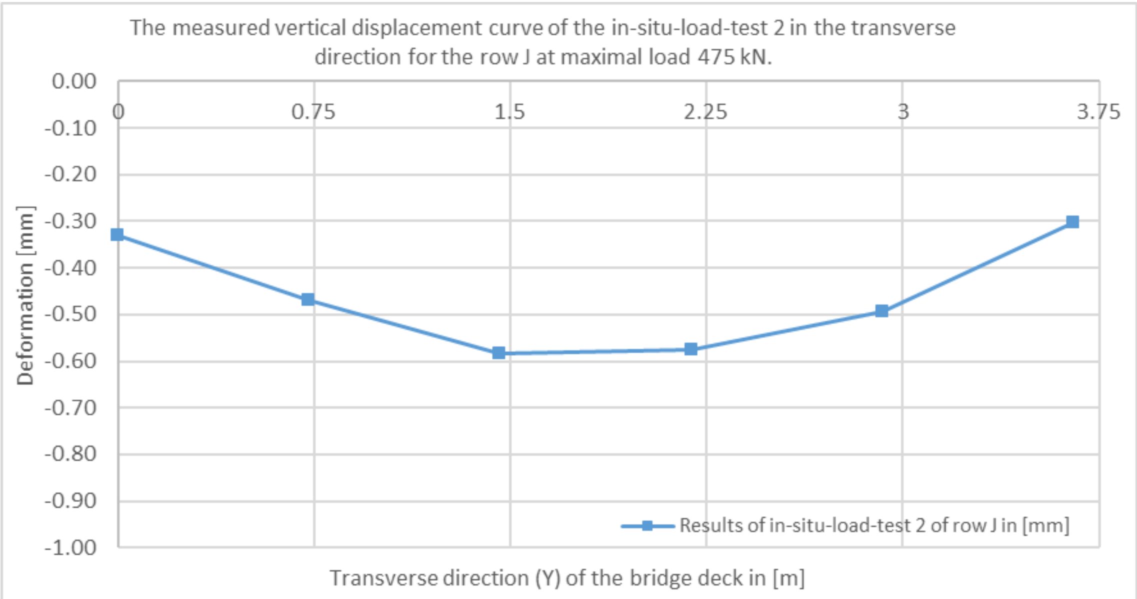

Figure 4-42: The measured deflections in the transverse direction in [mm].

4.3.4. Discussion and conclusions of results of the in-situ-load-tests 2 versus the analytical model

The measured vertical displacement shown in table 4-9 is more or less close to the results in table 4-5 and 4-7. As mentioned before in the evaluation of the measured results of in-situ-load-test 2, that there is sliding available between steel girder and concrete, the measured vertical displacement is more or less close to forget me nots 2 and 3, which suggest that there is a calmed moment available in the measured result, which will be studied during the numerical simulations. The main observation is: Nonlinearity is local, the majority of the beam might still be in the linear region, but this will also be validated during the FEA-simulations. In table 4-10 the results including the ratio between the values is shown.

Table 4-10: Measured result of the steel girder 4 versus the analytical model.

Length Span [mm]	Analytical calculated vertical deformation W2 [mm]	Analytical calculated vertical deformation W3 [mm]	measured vertical deformation [mm]	Ratio between W2 and the measured vertical deformation	Ratio between W3 and the measured vertical deformation
6050	0.73	0.42	0.58	126 %	72 %
5600	0.58	0.33		100 %	57 %

The results are summed up in table 4-10 by taking into consideration the influences of the length. These results are compared with the measured vertical displacement. The strange thing which can be observed is that the results of the analytical calculation and the measured result by taking into consideration the influence of the span, are the same or higher. This leads to an observation that the measured result does not contain occurrence of sliding phenomena or that there is sliding but not by the maximal load of 475 kN which has been used. But this will be studied during the numerical simulations.

The main conclusions derived from the results are:

The conclusion that can be taken is that the measured result shows that that there is a clamed moment available, because the two analytical models are nearby the results of the measured results. In addition to this, the results of the analytical models do not show occurrence of sliding phenomena or that there is sliding but not by the maximal load of 475 kN which has been used. But this will be studied during the numerical simulations.

5. 2D-linear simulations of the historical bridge beam A in the longitudinal direction

5.1. Introduction

In this chapter, the development and the results of the FEA-simulation of decisive separated bridge beam in the longitudinal direction will be described. In addition to this, the parameters which have been used to set-up all the FEA-models are described in this chapter. Furthermore, the calibration process and the sensitivity of the model due to the measurement of the in-situ-load-test is discussed in detail. The simulated and calibrated model to describe the behaviour of the historical bridge deck will be presented. The result of the FEA-simulation of the separated beam will be discussed and the conclusion of the behaviour of the separated beam in the longitudinal direction is added.

5.2. General input for the FEA-simulations

In this section the general input to develop the FEA-models will be added and described. In the previous chapters it is mentioned that there are three bridges chosen to use during the FEA-simulations. Furthermore, the geometry and the properties of the bridge decks will be presented in the coming sub-chapter. The bridges are:

a) **Bridge A: span** = 6.5 m: (the bridge where the in-situ-load-test is done);
b) **Bridge B: span** = 10 m: (from the category of the 10 m span);
c) **Bridge C: span** = 13 m: (from the category of the 13 m span).

Bridge A will be simulated in two ways. The first case is to simulate a normative linear 2D plane stress separated beam (steel girder 4). The simulated and calibrated decisive beam of bridge A will be used to set-up the other FEA-models. The second case is to simulate a linear 3D volume model of bridge deck A. This will be described and discussed in chapter 6. The third case is similar to the second case simulation but then for the other two bridge decks (B and C). This will be presented in chapter 7. The goal is to simulate the behaviour of the three bridges based on the measurement of the in-situ-load-test of bridge A. See the figures 5-1-a, 5-1-b and 5-1-c of the three bridges (A, B and C).

Figure 5-1-a: The photo of the bridge A.

Figure 5-1-b: The photo of the bridge B.

Figure 5-1-c: The photo of the bridge C.

Figure 5-1: The photos of the three chosen bridge decks. (Reniers , 2021)

5.2.1. Constitutive models, material properties and Finite element types

Constitutive model of the steel and concrete:
The material model is linear elastic isotropic for both materials (concrete and steel). The material properties which have been used for concrete and steel are presented in the table 5-1. The presented material models will be used for the 2D separated beam and the other 3D bridge decks.

Table 5-1: Material properties of the three bridges and the separated beam based on the destructive inspections.

Concrete	Young's modulus	38214 N/mm^2
	Density	2.5 $x10^{-9}$ T/mm^3
	Poisson's ratio	0.15
	Tensile strength	4.21 N/mm^2
	Compression strength	55 N/mm^2
	Shear strength	7,20 N/mm^2
Steel	Young's modulus	210000 N/mm^2
	Density	$7.85x10^{-9}$ T/mm^3
	Poisson's ratio	0.3
	Tensile strength	235 N/mm^2
	Compression strength	235 N/mm^2

<u>Interface element of the boundary:</u>
There is a boundary interface present in the FEA-simulation between steel girder and steel plate at the abutment and the pillar. This interface is modelled in the linear stage. The reasonable material properties of this interface are defined based on the presented calculations below.
The stiffness can be calculated following the guidelines provided by the DIANA FEA. According to the information given (FEA), the normal stiffness K_n and shear stiffness K_t can be calculated respectively as:

$$K_n = \frac{E_s}{l_e}$$

$$K_t = \frac{K_{n-steel}}{\alpha}$$

In which l_e is the height which is equal to 1 mm, E_{steel} is the average elastic modulus between the elements and α is a parameter that varies between 10 and 100.

So, the material properties of the boundary interface are:

Table 5-2: Stiffness of the interface boundary.

	Normal stiffness N/mm3	Shear stiffness N/mm3
Interface boundary	$K_n = \frac{E_s}{l_e} = \frac{210000}{1} = 210000 \frac{N}{mm^3}$	$K_t = \frac{K_{n-steel}}{\alpha} = \frac{210000}{10} = 21000 \frac{N}{mm^3}$

Finite element types:

The properties of the finite element which have been used during the modelling of the separated beam and the bridge decks are presented in the tables 5-3 and 5-4:

Table 5-3: Finite element types and properties for the beam.

	2D plane stress elements	2D plane stress elements	1D Interface element (line element)
Type of finite element	CQ16M	CT12M	CL12I
Degree of freedom of element	16	16	12
Interpolation scheme	Quadratic	Quadratic	Quadratic
Dimension	2D	2D	2D

Table 5-4: Finite element types and properties for the bridge deck.

	3D solid brick elements	3D solid pyramid	3D solid pyramid	3D Interface element	3D solid wedge
Type of finite element	CHX60	CPY39	CTE30	CL12I	CTP45
Degree of freedom of element	60	39	30	48	45
Interpolation scheme	Quadratic	Quadratic	Quadratic	Quadratic	Quadratic
Dimension	3D	3D	3D	3D	3D

5.2.2. Geometry

In this sub-chapter the geometry of the three bridges will be described. The form of the geometry which will be described in this sub-chapter is derived from the drawing of each bridge deck. The focus in this chapter is to simulate the behaviour of the separated beam.

Description of the geometry of bridge A:

The deck of bridge A which will be described now, is the side-span of bridge deck A, because as mentioned before in chapter 4 the in-situ-load-test is made on the side-span. The specimen is composed of 6 steel-girders in the transverse direction. This configuration will be used for all the bridges with only one difference, which is the span. The steel-girders which are available in bridge deck A are DIN 26 and DIN 28. The properties of the steel-girders are presented in the table 5.5. Furthermore, the width of the bridge deck is 4.07 m and the length is 6.5 m. The center -to-center distance between the steel-girders is 0.73 m. The total height of the bridge deck is 0.43 m. At last, the support-length of the bridge deck is 0.45 m on both sides. The bridge deck is supported by an abutment and a pillar. In the transverse direction over the width of the bridge deck, there is a continuous beam available. The form of this beam can be seen in the figure 5-2.
The decisive beam of the bridge A is DIN26 (steel girder 4). This beam will be modelled. See figure 5-2.

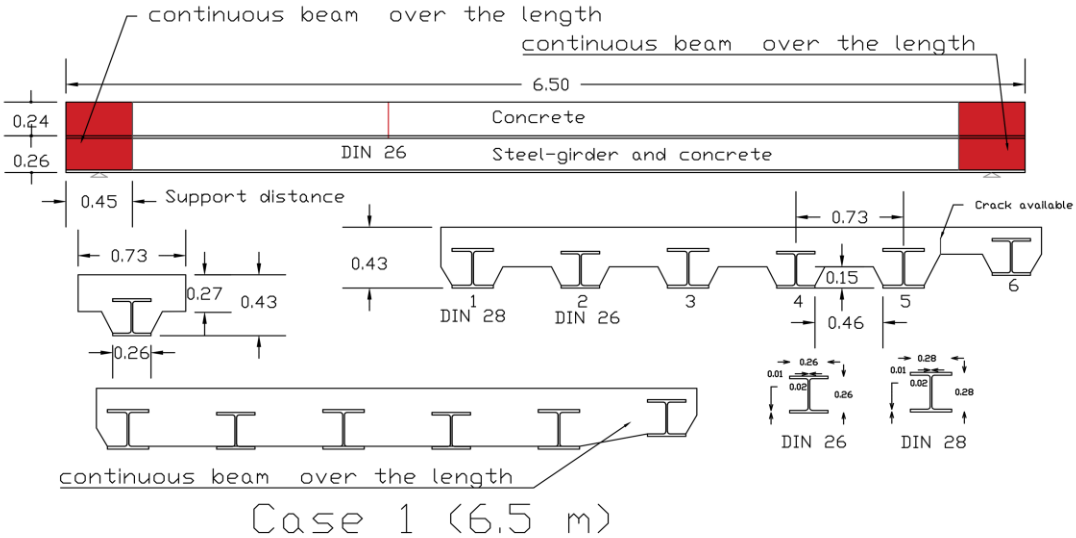

Figure 5-2: The total geometry of bridge deck A.

Table 5-5: The properties of the steel-girders.

Profile	H [mm]	B [mm]	t_w [mm]	t_f [mm]
Din 26	260	260	11	18
Din 28	280	280	12	20

Description of the geometry of bridge B:

The width of the bridge deck B is 4.07 m and the length is 10 m. The bridge deck contains the same steel profile over the width which are DIN 38. The properties of the steel-girders are added in the table 5-6. The support length of the bridge deck is 0.5 m on both sides. The bridge deck is supported by an abutment and a pillar. In the transverse direction over the width of the bridge deck, there is a continuous beam available. The form of this beam can be seen in the figure 5-3.

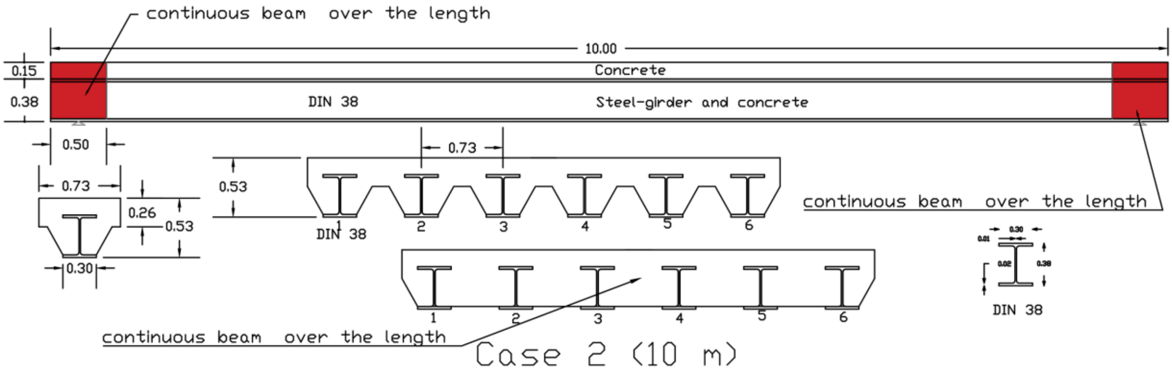

Figure 5-3: The total geometry of bridge deck B.

Table 5-6: The properties of the steel-girders.

Profile	H [mm]	B [mm]	t_w [mm]	t_f [mm]
Din 38	380	300	14	24

Description of the geometry of bridge C:

The width of the bridge deck C is 4.07 m and the length is 13 m. The bridge deck contains different steel profile over the width which are DIN 50 and DIN 55. The properties of the steel-girders are added in the table 5-7. The support length of the bridge deck is 0.4 m on both sides. The bridge deck is supported by an abutment and a pillar. In the transverse direction over the width of the bridge deck, there is a continuous beam available. The form of this beam can be seen in the figure 5-4.

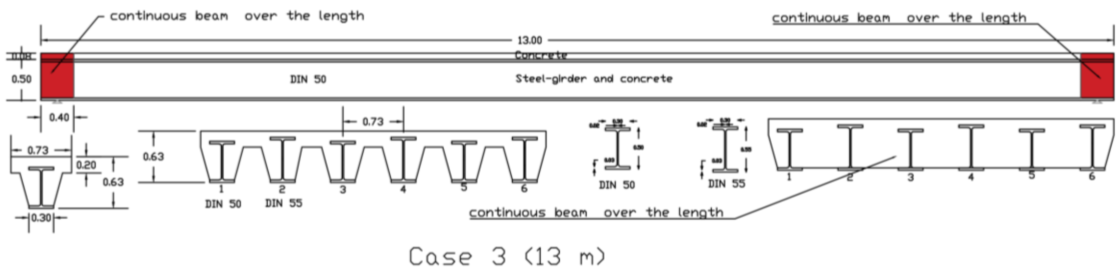

Figure 5-4: The total geometry of bridge deck C.

Table 5-7: The properties of the steel-girders.

Profile	H [mm]	B [mm]	t_w [mm]	t_f [mm]
Din 50	500	300	16	30
Din 55	550	300	16	30

5.2.3. Boundary conditions

The boundary conditions which have been used in the FEA-models in the figures 5-5 and 5-6 are based on the following two informative conditions:

a) The support length from the drawing of the three bridge decks;
b) The available restrain in the x-axis based on the information which is obtained from the in-situ-load-test (see chapter 4).

From the in-situ-load-test it is already mentioned that concrete beam is stacked at the abutment which leads to have the restrain in the x-axis over a height of 150 mm. At the abutment and the pillar in the vertical direction the y-axis is restrained over the support-length of 450 mm on both sides for bridge A. The other bridges have other support length; the length is mentioned in the section of geometry. In addition to this there is one point supported in x-axis at the left of the beam where the abutment is available. The supports which are defined in this section, will be used for the three cases which are defined in the introduction (3D-bridge deck FEA-simulations). The boundary conditions which are defined in this section are also calibrated based on the data from the in-situ-load-test. The calibration process is described in the coming paragraph. See figures 5-5 and 5-6 and the tables for the used restrain during the FEA-modelling.

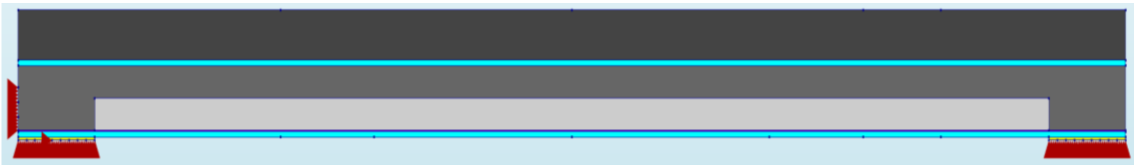

Figure 5-5: Boundary conditions of separated beam (DIN 26 including the concrete).

Table 5-8: Boundary conditions of the separated beam.

Supports on the beam	Abutment	Pillar
X-axis	Fixed point and over the height 150 mm	No restrain
Y-axis	The support length is restrained	The support length is restrained

This boundary condition is also used for the 3D slab FEA-model, but in the topological dimension of a 3D model, see the table 5-9 and the figures:

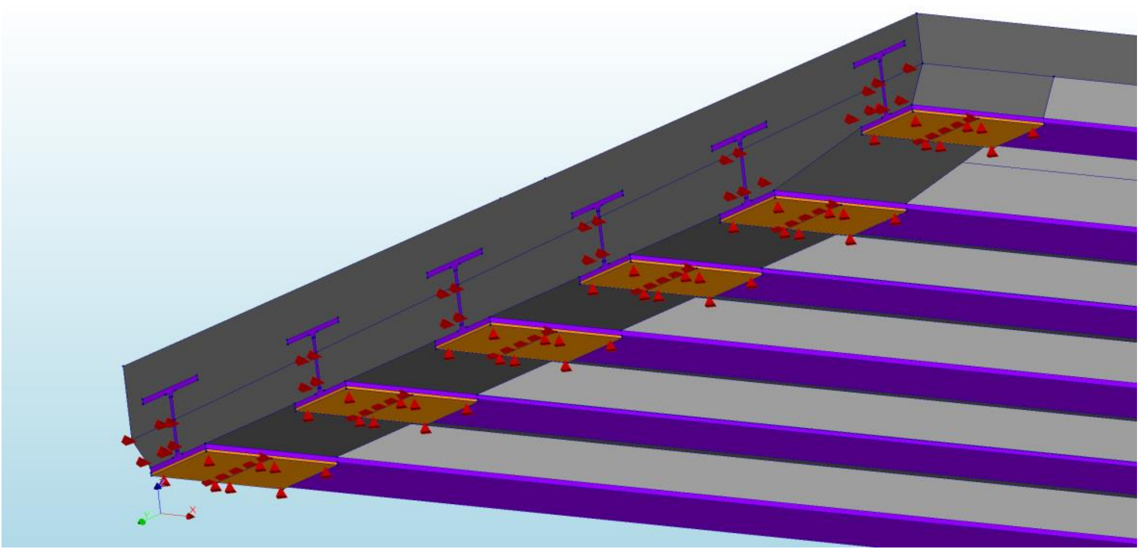

Figure 5-6: Boundary conditions at the abutment.

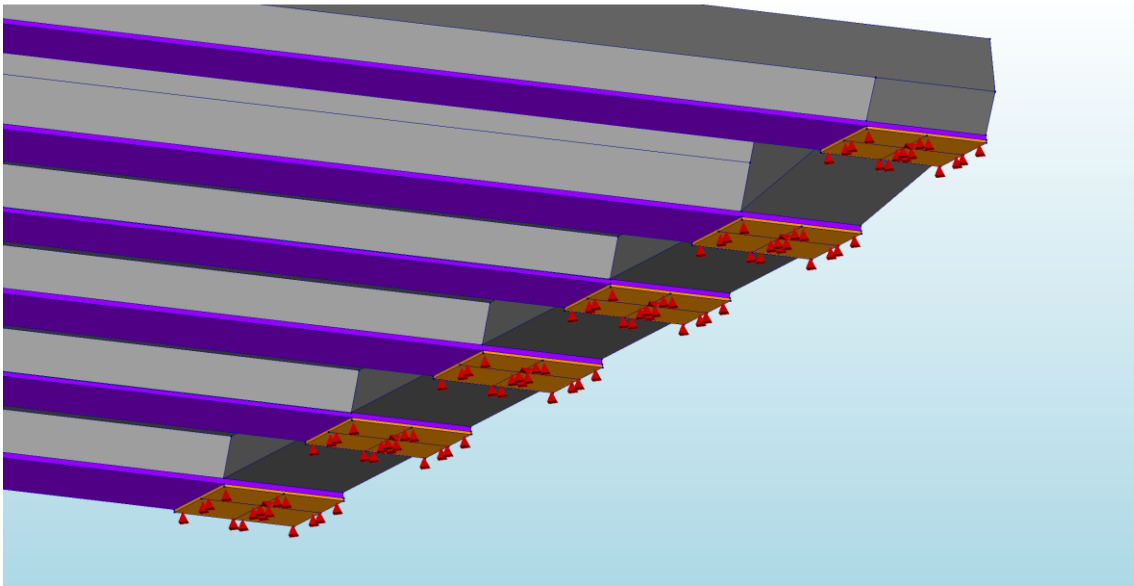

Figure 5-7: Boundary conditions at the pillar.

Table 5-9: Boundary conditions bridge deck.

Supports on the beam	Abutment	Pillar
X-axis	Fixed line over the length of the beams The concrete is supported in the x-direction over the height 150 mm.	No restrain
Y-axis	One point is fixed for each beams	One point is fixed for each beams
Z-axis	The support face is restrained	The support face is restrained

5.2.4. Mesh size of the numerical model

The mesh size is defined based on the instruction from the guidelines of **RTD** (Rijkswaterstaat Technical Document) (Roosen, 2020). In the **RTD** table 5-10 it is shown how the mesh size of the elements of a beam and a slab can be defined. The mesh size which is needed, is the mesh size of beam structure 2D modelling and slab structure 3D modelling. In table 5-10 the size of the mesh for the beam as well as for the slab is defined for all three bridges. In the figures 5-8 and 5-9 the mesh of the beam and slab can be seen. The mesh size of the other slabs is not shown in a figure, but is the same as for bridge A.

Table 5-10: The mesh size by definition from the RTD (Rijkswaterstaat Technical Document) (Roosen, 2020).

Beam Structure	Maximum element size
2D modeling	$\min\left(\frac{l}{50}, \frac{h}{6}\right)$
3D modeling	$\min\left(\frac{l}{50}, \frac{h}{6}, \frac{b}{6}\right)$
Slab Structure	**Maximum element size**
2D Modeling	$\min\left(\frac{l}{50}, \frac{b}{50}\right)$
3D Modeling	$\min\left(\frac{l}{50}, \frac{b}{50}, \frac{h}{6}\right)$

Table 5-11: The size of the mesh element which is been used in FEA-models for all bridge decks.

Type bridge	Type of structure	L [mm]	h [mm]	b [mm]	Mesh size for a 2D-model in[mm]	Mesh size for a 3D-model in[mm]
Bridge A	Beam	6500	430	730	Min = 70	is not needed
	Slab	6500	430	4070	NO is not needed	Min = 70
Bridge B	Beam	10000	530	730	Min = 105	is not needed
	Slab	10000	530	4070	NO is not needed	Min = 82
Bridge C	Beam	13000	630	730	Min = 105	is not needed
	Slab	13000	630	4070	NO is not needed	Min = 82

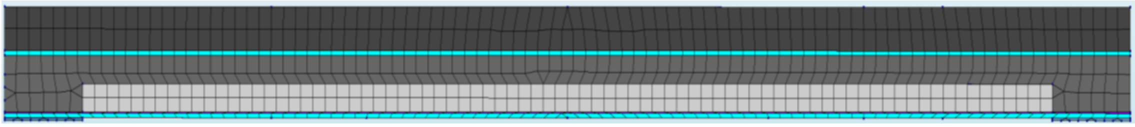

Figure 5-8: The mesh size of beam (steel girder 4) bridge deck A.

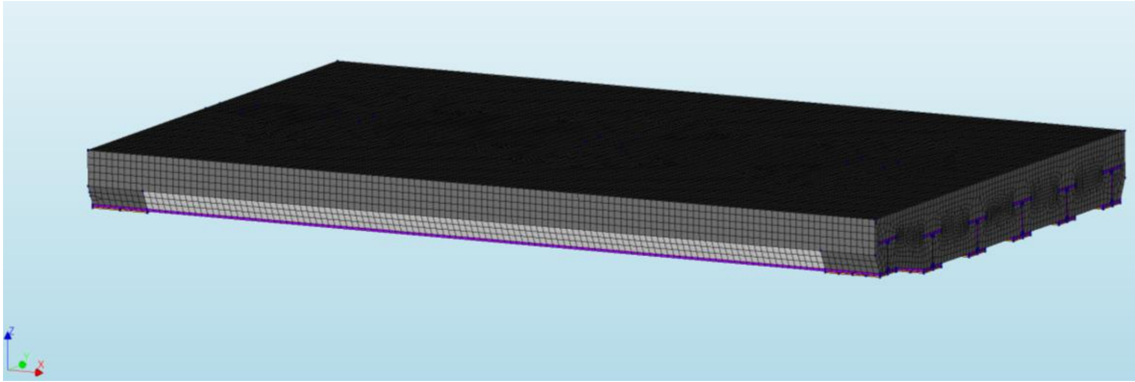

Figure 5-9: The mesh size of the bridge deck A is the same for the other two bridge decks (B and C).

5.2.5. Load conditions

The load for the 2D beam is defined by using the input from the in-situ-load-test. The decisive beam as mentioned before is steel girder 4 from the in-situ-load-test. The calculation which is made to obtain the percentage and precise load which has been used can be found in appendix D. In the table 5-12 the load which is used during the modelling of the 2D beam and the 3D slab on the positions of H, J and L is defined with different percentages. The percentage is obtained as mentioned before from the in-situ-load-test. See appendix D. The figures 5-10, 5-11 and 5-12 show the positions where the load is placed in 2D and 3D. In the table 5-12 the coordinate in the x-direction is mentioned. The load is applied as a point load on the 2D separated beam and as an area load on the 3D bridge deck. See figures 5-10 until 5-12.

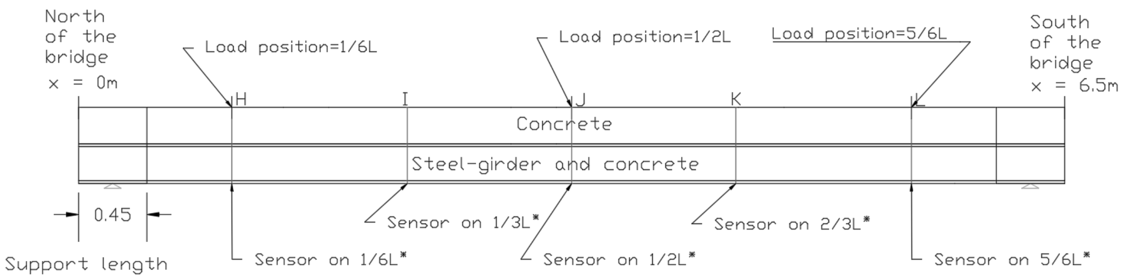

Figure 5-10: The load positions on the beam.

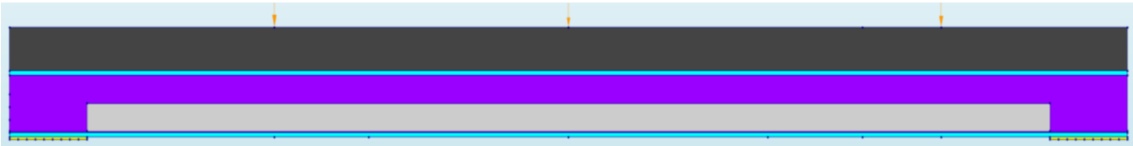

Figure 5-11: The load positions on the beam in the FEA-model.

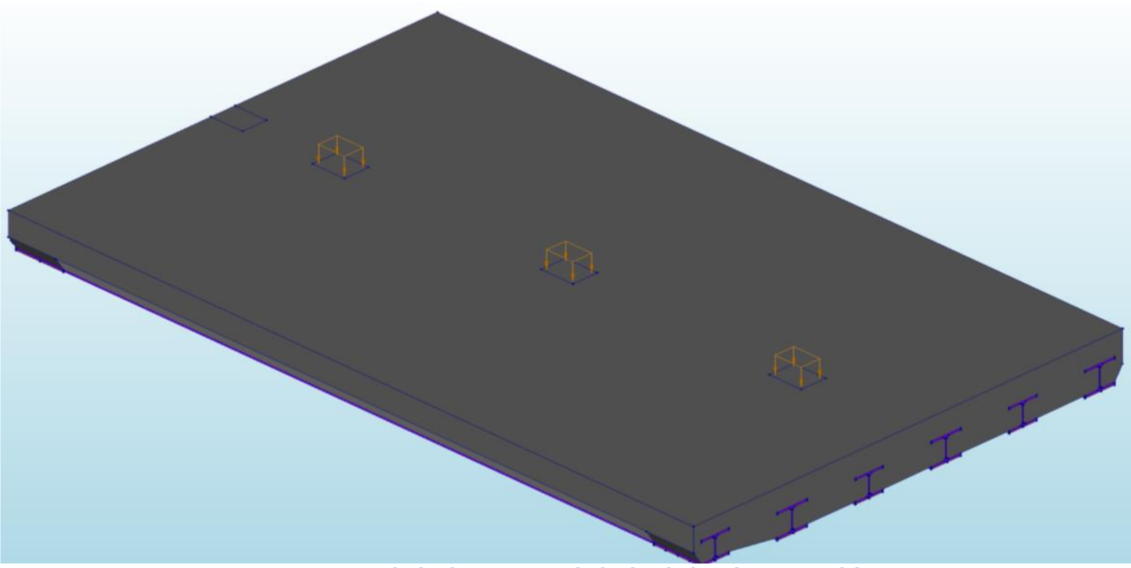

Figure 5-12: The load positions on the bridge deck in the FEA-model.

Table 5-12: The value of the load on each position.

Load level [kN]	Type of struct ure	Size of the loaded wheel-print		Percentage of the used load for each loaded point based on the measurement of in-situ-load-test			Load of the 2D-model [N]			Load of the 3D-model [N/mm²]		
		L [mm]	b [mm]	H	J	L	H [N]	J [N]	L [N]	H [N/mm²]	J [N/mm²]	L [N/mm²]
400	Beam	300	230	27%	20%	28%	108000	83000	112000	-		
	Slab	300	230	100%	100%	100%	`-			5.80		
475	Beam	300	230	28%	20%	25%	132000	100554	118000	-		
	Slab	300	230	100%	100%	100%	-			6.88		

Table 5-13: The position in the x-direction for each loaded point H, J and L of the three bridge decks.

Bridge	Position of the loaded points		
	H [m]	J [m]	L [m]
Bridge deck A	1.54	3.25	4.96
Bridge deck B	2.37	5.00	7.63
Bridge deck C	3.08	6.50	9.92

5.3. Approach of calibrating the FEA-simulations using the in-situ-load-test

The 2D FEA-model is calibrated based on the measurement of the three in-situ-load-tests. The calibration is done by taking three aspects into consideration. In-situ-load-test 2 is normative because it is made on the mid-span. The aspects which have been used during the calibration, are:

a) Support length;
b) The boundary interface;
c) The stiffness of concrete.

The calibration process of each aspect will be described and the results will be discussed. The obtained model from this calibration process will also be used for the 3D-models of the three bridge decks (A, B and C) to gain insight in the load-bearing capacity of the historical composite bridge deck without shear connectors.

5.3.1. Support length

The support length is used to calibrate the model. The support length is 450 mm for bridge deck A. This length is divided in lengths of 50 mm for each side (abutment and pillar). The total length results in 9 lines which must be supported for each side.
The calibration process is to support the beam with divided lengths of 50 mm for each side. This process will be repeated in steps of 50 mm until the maximum support length of 450 mm is reached. The goal is to reach the values of the measured strain and vertical displacement of the points H, I, J, K and L on steel girder 4 for the three in-situ-load-tests. See the figure 5-13 for the support length and the measured points. The conclusion which can be taken from the calibration process by using the support length, is that the separated beam is not calibrated. Because of this, we cannot define the best FEA-model which can be used to give insight in the load-bearing capacity of the historical beam. In the tables 5-14 and 5-15 the definitive results of the last 50 mm are shown. The development of the strain and vertical displacement can be seen in appendix D for the other supported lines.

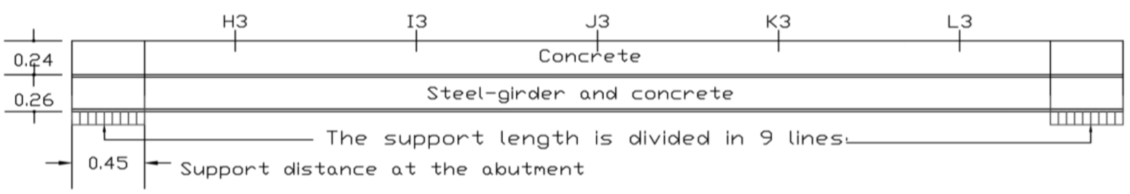

Figure 5-13: The support length of bridge deck A.

Table 5-14: Results of the calibrated vertical displacement due to the support length of line 9 (last 50 mm of the total support length).

Point	X	Vertical displacement from the numerical model by constraining line 9 of the support length in [mm]	Deformation results of in-situ-load-test 2 of steel girder 4 in [mm]	Ratio
***	0	0	0	0 %
I	2.09	-0.43	-0.37	116 %
J	3.25	-0.63	-0.53	120 %
K	4.41	-0.43	-0.44	98 %
***	6.5	0	0	0 %

Table 5-15: Results of the calibrated strain due to the support length of line 9 (last 50 mm of the total support length).

Point	X	Strain from the numerical model by constraining line 9 of the support length in [µm]	Strain results of in-situ-load-test 2 of steel girder 4 in [µm]	Ratio
***	0	0	0	0 %
H	1.54	-8.6	14	61 %
I	2.09	21.9	44.4	49 %
J	3.25	81.1	79.7	102 %
K	4.41	21.9	41.5	53 %
L	4.96	-8.6	14	61 %
***	6.5	0	0	0 %

5.3.2. The boundary interface

The properties of the boundary interface are defined based on the information which is available in paragraph 5.1.1. After that the length has been calibrated, and the results are not good enough. The goal is to use the boundary interface to check if it has some influence on the vertical deformation. The result is that the interface boundary has not high influence and effect on the results of the strain and vertical deformation. This can be seen in the table 5-16 where a small analysis is made by using the following aspects:

a) No interface boundary;
b) Calculated boundary.

The two situations, which are named above, have been studied and this does not result in relevant conclusions. Based on this, the boundary interface has no high influence in calibrating the beam. Therefore, it is chosen to use the calculated interface boundary to finish the calculations, because there is not a lot of difference in the results and that can be seen in the table 5-16.

Table 5-16: Results of the calibrated vertical displacement due the boundary interface of concrete at load of 400 kN.

Point	X [m]	Displacement of the In-situ-load-test 2 in [mm]	Displacement no interface boundary in [mm]	Displacement calculated interface boundary in [mm]
J	**3.25**	-0.52	-0.51	-0.52

5.3.3. The stiffness concrete

The material properties of concrete are defined in paragraph 5.1.1. The material properties of concrete and especially the elastic modulus have been used to calibrate steel girder 4 based on the measured strain and vertical deformations from the in-situ-load-tests. The result of this approach was successful because the beam has reached the best results of the vertical deformation. However, the strains are stiffer, but this has an explanation which will be explained in the discussion and conclusion part of this chapter. In the table 5-17 and 5-18 the definitive stiffness of concrete is shown which has been used to calibrate steel girder 4.

Table 5-17: Results of the calibrated vertical displacement due the stiffness of concrete.

Point	X	Vertical displacement in [mm] from the numerical model by using the stiffness of (50000 N/mm^2)	Deformation results of in-situ-load-test 2 of steel girder 4 in [mm]	Ratio
***	**0**	0	0	0 %
I	**2.09**	-0.36	-0.37	97 %
J	**3.25**	-0.52	-0.53	99 %
K	**4.41**	-0.36	-0.44	82 %
***	**6.5**	0	0	0 %

Table 5-18: Results of the calibrated vertical displacement due to the stiffness of concrete.

Point	X	Strain(in [μm]) from the numerical model by using the stiffness of 50000 N/mm^2	Strain results of in-situ-load-test 2 of steel girder 4 in [μm]	Ratio
***	**0**	0	0	0%
H	**1.54**	-7.5	14.0	-52%
I	**2.09**	18.3	44.4	43%
J	**3.25**	68.4	79.7	88%
K	**4.41**	18.6	41.5	46%
L	**4.96**	-7.0	14.0	-52%
***	**6.5**	0	0	0%

5.3.4. Discussion and conclusion of the calibration process

5.3.4.1. Discussion

The calibration is made by taking three aspects into consideration. The aspects which have been used during the calibration, are:

a) Support length;
b) The boundary interface;
c) The stiffness of concrete.

The separated beam is not calibrated correctly by using the support length, because this does not result in acceptable values. The next step is to use the boundary interface. The goal is to use the boundary interface to check if it has some influence on the vertical deformation. The result is that the interface boundary has not high influence and effect on the results of the strain and vertical deformation see the table 5-16. Besides the boundary interface, it is chosen to use the stiffness of concrete, especially the elastic modulus has been used to calibrate the steel girder 4 based on the measured strain and vertical deformations which are obtained from the in-situ-load-tests. The result of this approach was successful because the beam has reached the best results of the vertical deformation. However, the strains are stiffer, but this is due to the restrained supports which have been used. The effect of the restrained support has influence on the strain which leads that they act stiffer than necessary.

5.3.4.2. Conclusion

The calibrating process as mentioned before is done by using the three components which are:

a) The supported length;
b) Stiffness of concrete;
c) Boundary interface.

These three components have been used to calibrate the beam to obtain the best model which will be simulating the behaviour of beam based on the in-situ-load-test. This FEA-simulation will give an answer for the load-bearing capacity of historical bridge deck A. This results in a beam which is presented in the figure 5-14:

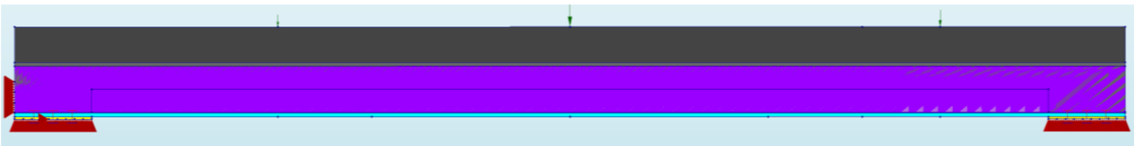

Figure 5-14: The best model to simulate the in-situ-load-test for the separated beam.

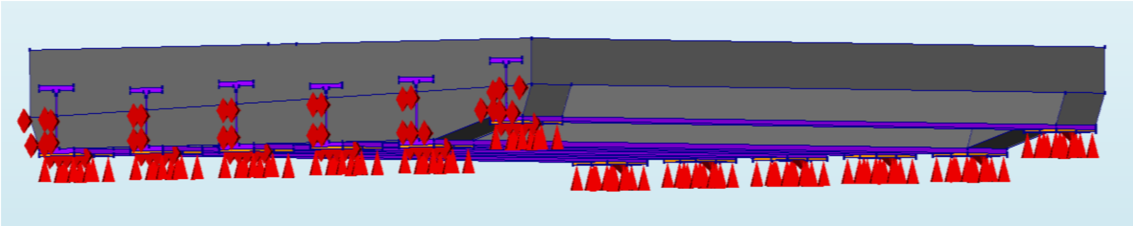

Figure 5-15: The best model to simulate the in-situ-load-test for the bridge deck.

5.4. Numerical result of one separate bridge beam in the longitudinal direction

In this section the results of steel girder 4 will be presented and validated with the measurements results from the executed in-situ-load-test 2 and the analytical model which is carried out in chapter 3.2.2. The load which has been used is obtained from the total load of 400 kN until 475 kN based on the calculation in the previous section 5.1.5 where the load is defined. The configuration of the beam can be seen in the figure 5-16. This configuration is obtained from the in-situ-load-tests, see chapter 4. In the figures 5-17 and 5-18 the numerical results of the vertical displacement and strain of the numerical simulation of the separated beam 4 loaded on point J from 400 kN to 475 kN are presented. In tables 5-21 and 5-22 the numerical simulated values of vertical displacement and strain are presented and the difference with the measured results from the in-situ-load-test and the analytical model is compared (presented by a ratio). In figures 5-19 and 5-20 the numerical simulation of the vertical displacement and the strain in the longitudinal direction of the separated beam over the measured points is given. The difference between the numerical simulated values and measured points is included with a ratio in tables 5-19 and 5-20.

In addition to this there are plots added from excluded FEA-models in Diana to illustrate the vertical displacement and strain for the two load from 400 kN and 475 kN. The principal stress and shear stress of concrete are added in the figures 5-25/5-26/5-27/5-28. The maximal values of the principal stress and shear stress are in tables 5-23 and 5-25. The rest of the numerical results of loaded points H and L are added in the appendix D with the same layout and presentation which is applied in this section. The results of the mid-span are leading.

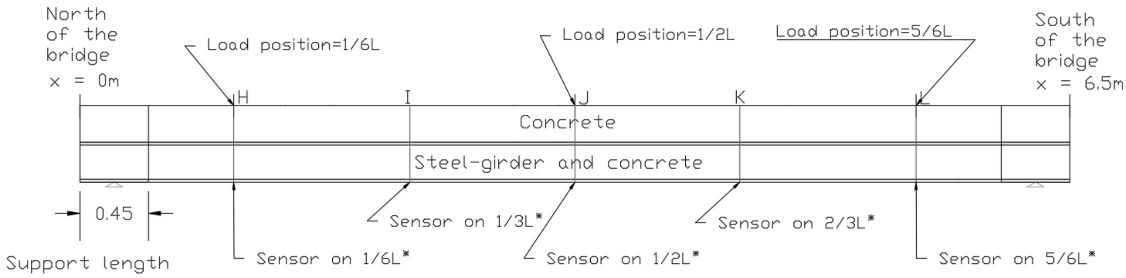

Figure 5-16: The loaded point J on the beam.

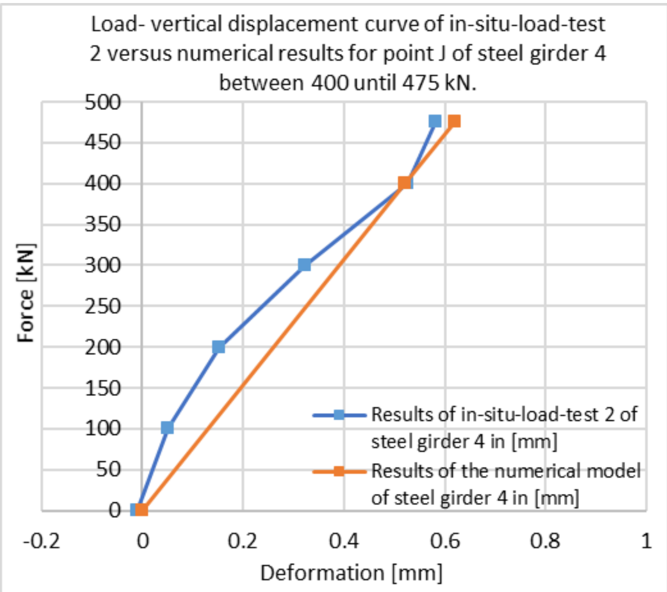

Figure 5-17: Load-displacement curve of in-situ-load-test 2 versus numerical results for point J of steel girder 4 between 400 until 475 kN.

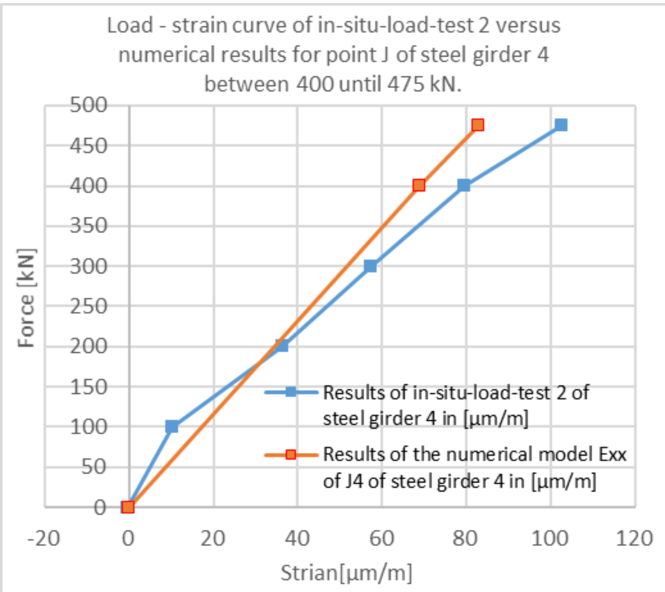

Figure 5-18: Load - strain curve in-situ-load-test 2 versus numerical results for point J of steel girder 4 between 400 until 475 kN.

Table 5-19: Load-displacement of in-situ-load-test 2 versus numerical results for points of steel girder 4.

Point	X	Deformation results of in-situ-load-test 2 of steel girder 4 in [mm]	Deformation results of the numeric model of steel girder 4 in [mm]	Ratio
***	0	0	0	0 %
I	2.09	-0.39	-0.40	103 %
J	3.25	-0.58	-0.62	106 %
K	4.410	-0.49	-0.44	88 %
***	6.5	0	0	0 %

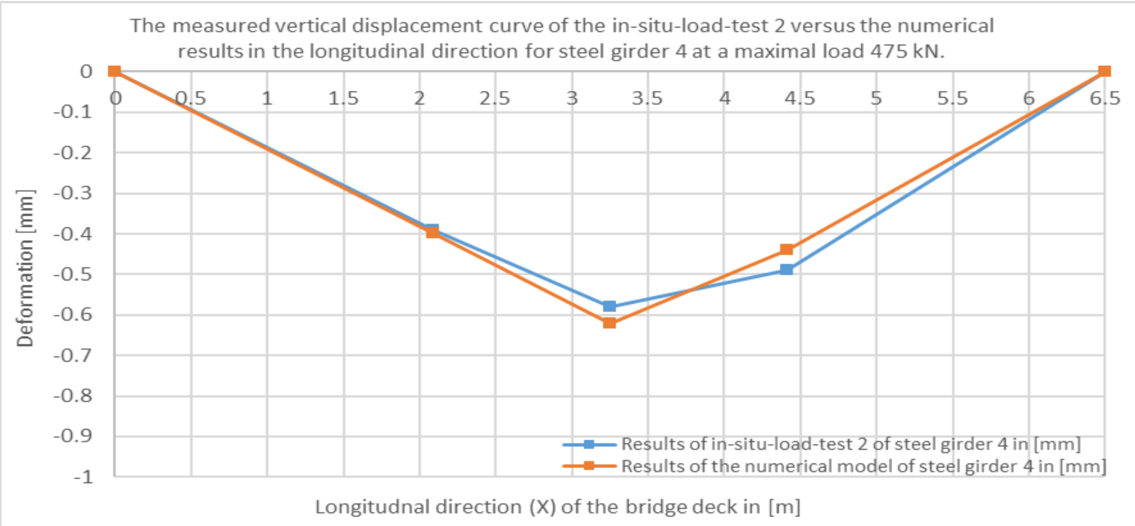

Figure 5-19-a: The measured displacement curves for in-situ-load-test 2 versus the numerical results at load of 475 kN.

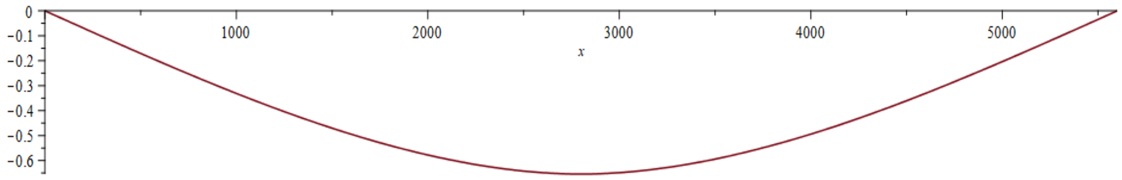

Figure 5-19-b: The analytical results at load of 475 kN (the maximal vertical displacement is u=0.63 mm).

Figure 5-19: The measured displacement curves for in-situ-load-test 2 versus the numerical results and the analytical curve at load of 475 kN.

Table 5-20: Load-strain of in-situ-load-test 2 versus numerical results for points of steel girder 4.

Point	X	Results of in-situ-load-test 2 of steel girder 4 in [µm/m]	Results of the numerical model of steel girder 4 in [µm/m]	Ratio
***	0	0	0	0%
H	1.54	-15	-9	62%
I	2.09	-55	-22	40%
J	3.25	-103	-83	81%
K	4.41	-49	-23	47%
L	4.96	-15	-9	56%
***	6.5	0	0	0%

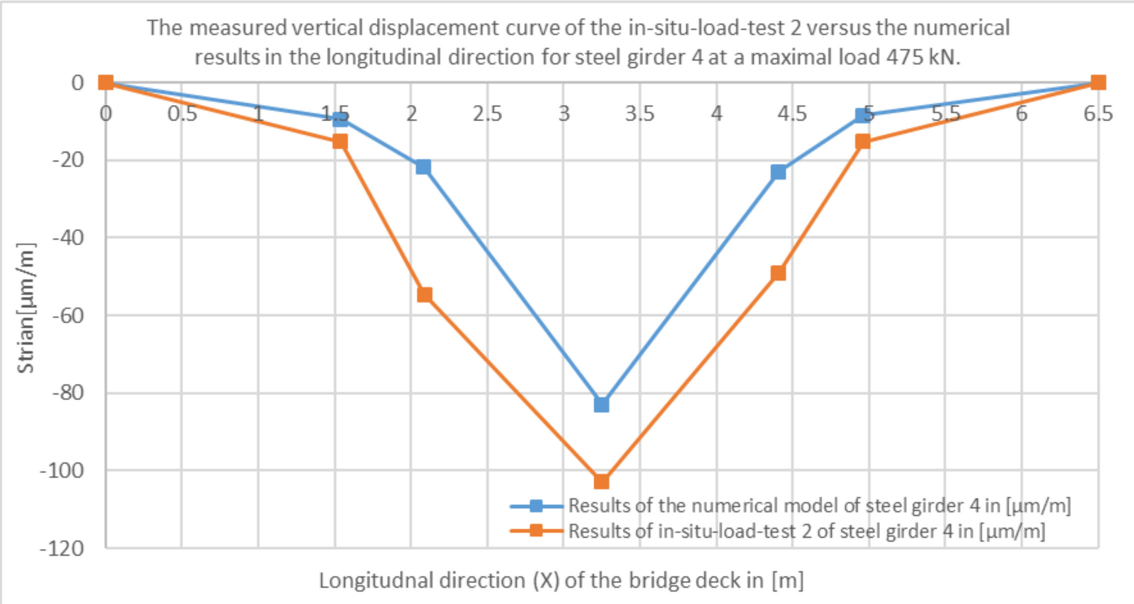

Figure 5-20: The measured strain curves for in-situ-load-test 2 versus the numerical results at load of 475 kN.

Table 5-21: The maximal vertical displacement of the in-situ-load-test 2 versus the numerical results and the ratio.

load	**Results of in-situ-load-test 3 of steel girder 4 on point J in [mm]**	**Results of the numerical model of steel girder 4 on point J in [mm]**	**Results of the numerical model of steel girder 4 on point J in [mm]**	**Ratio between in-situ-load-test and the numerical simulations**	**Ratio between the numerical simulations and the analytical**
0	0	0	0	0 %	0 %
400	-0,53	-0,52	-0.53	99 %	102 %
475	-0,58	-0,62	-0.63	106 %	102 %

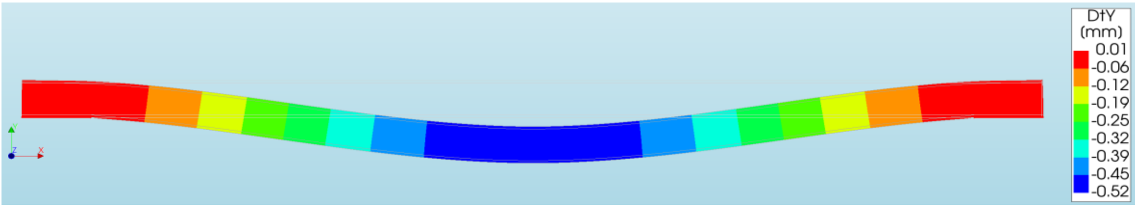

Figure 5-21: The numerical results of the displacement for a load of 400 kN at the mid-span.

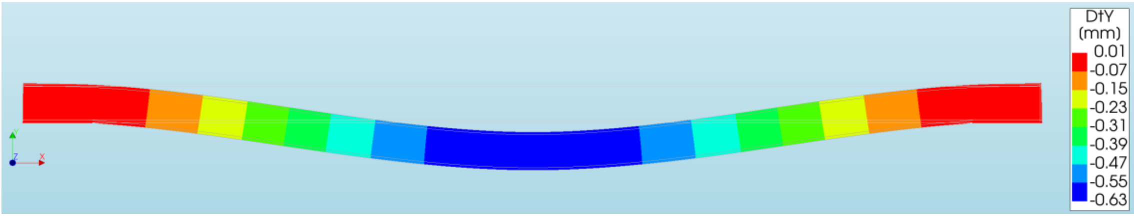

Figure 5-22: The numerical results of the displacement for a load of 475 kN at the mid-span.

Table 5-22: The maximal strain of the in-situ-load-test 2 versus the numerical results and the ratio.

load	Results of in-situ-load-test 3 of steel girder 4 on point J in [µm/m]	Results of the numerical model of steel girder 4 on point J in [µm/m]	Ratio
0	0	0	0 %
400	80	69	87%
475	103	83	81%

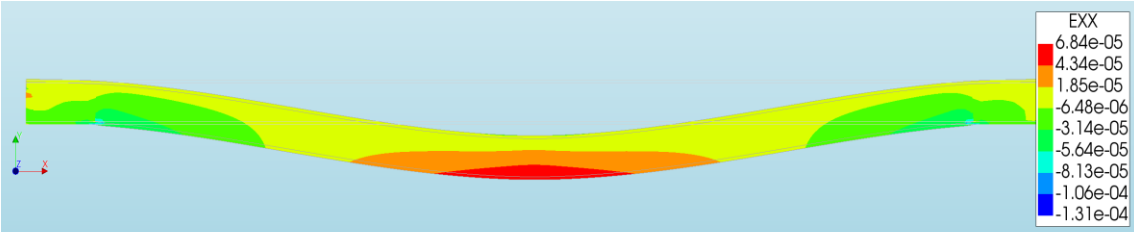

Figure 5-23: The numerical results of the strain for a load of 400 kN at the mid-span.

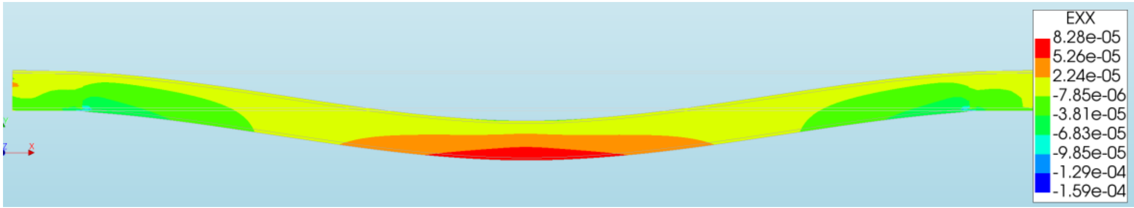

Figure 5-24: The numerical results of the strain for a load of 475 kN at the mid-span.

Table 5-23: The maximal principal stress of concrete at point J.

load	The numerical results of the principal stress of the concrete on point J in [N/mm^2]	Maximal allowable tensile stress of concrete in [N/mm^2]	Ratio
0	0	0	0%
400	3.09	4.2	72 %
475	3.73	4.2	88 %

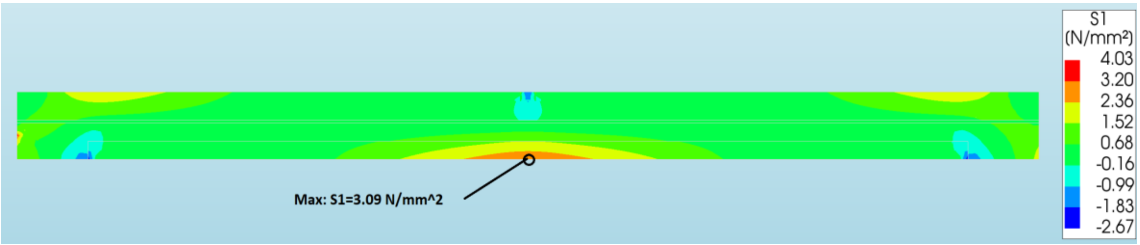

Figure 5-25: The numerical results of the principal stress in the concrete S1 for a load of 400 kN at the mid-span.

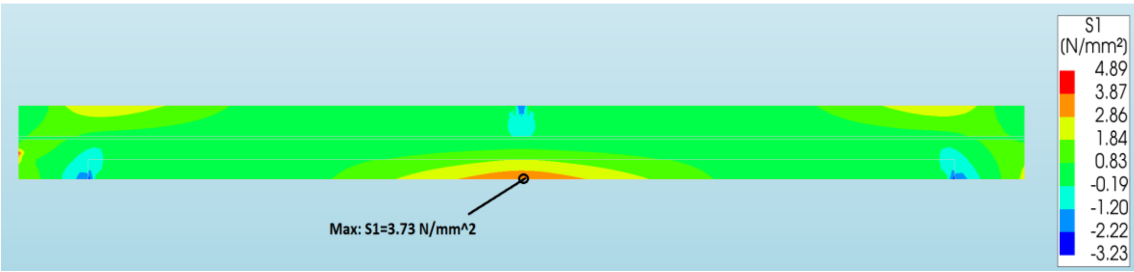

Figure 5-26: The numerical results of the principal stress in the concrete S1 for a load of 475 kN at the mid-span.

Comment: The principal stress is under the maximal tensile stress of steel-girders.

Table 5-24: The maximal principal stress of the steel at point J.

load	The numerical results of the principal stress of the concrete on point J in [N/mm^2]	Maximal allowable tensile /compressive stress of steel in [N/mm^2]	Ratio
0	0	0	0
400	14.4	235	55 %
475	17.4	235	66 %

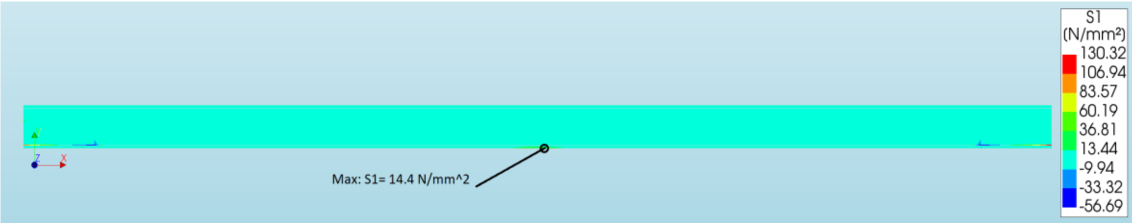

Figure 5-27: The numerical results of the principal stress in the steel S1 for a load of 400 kN at the mid-span.

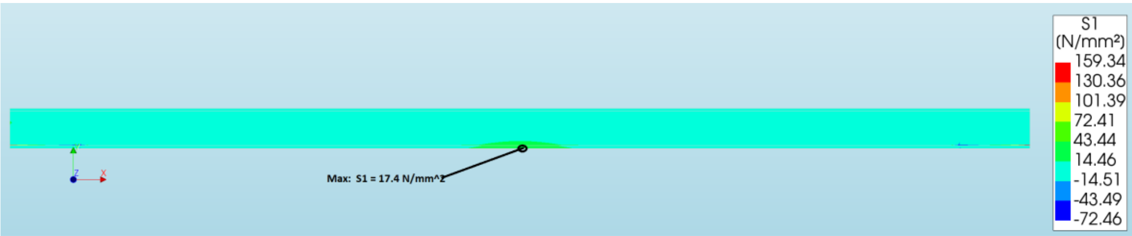

Figure 5-28: The numerical results of the principal stress in the steel S1 for a load of 475 kN at the mid-span.

Comment: The principal stress is under the maximal tensile stress of steel girder 4.

Table 5-25: The maximal shear principal stress of the concrete at point J.

load	The numerical results of the principal stress of the concrete on point J in [N/mm^2]	Maximal allowable shear stress of concrete in [N/mm^2]	Ratio
0	0	0	0
400	1.61	7.2	22 %
475	1.95	7.2	28 %

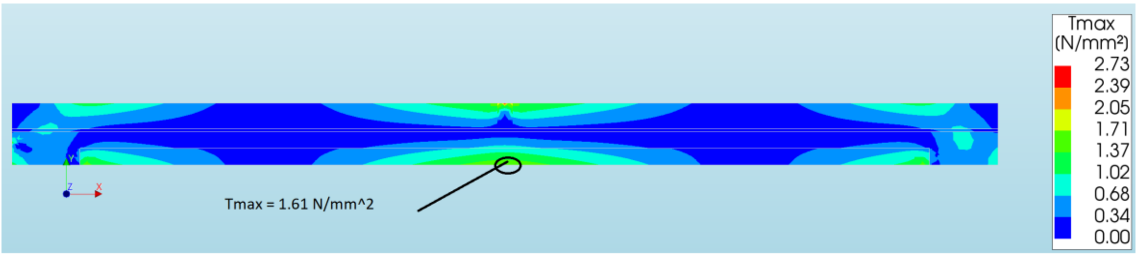

Figure 5-29: The numerical results of the principal stress in the concrete Tmax for a load of 400 kN at the mid-span.

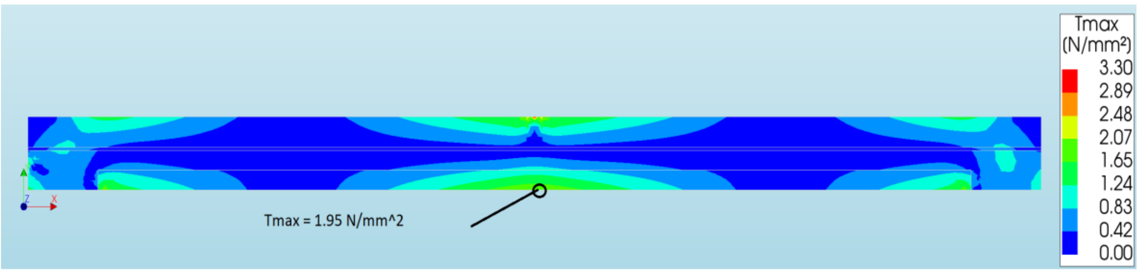

Figure 5-30: The numerical results of the principal stress in the concrete Tmax for a load of 475 kN at the mid-span.

Comment: The shear stress is under the maximal shear stress of concrete.

5.4.1. Discussion of the linear analysis

The geometry of the beam is obtained from the drawing which is mentioned earlier in sub-chapter 5.1.2. The material properties are defined based on destructive inspections and also from the available archive information of the municipality of Amsterdam. The material properties can be seen in the previous sub-chapters. The FEA-simulation process is started by calibrating steel girder 4 based on the measured data from the in-situ-load-tests. The process of calibrating steel girder 4 is made by using three parameters:

a) Support length;
b) The boundary interface;
c) The stiffness of concrete.

The calibration process by using the support length didn't validate the measured vertical displacement and strain of the three in-situ-load-tests. After the support length has been used, the values aren't validated. The boundary interface has been used. The boundary interface had not a very high influence on the results. This resulted to use the stiffness of concrete, and especially the E-modules of concrete which has been used to calibrate and to validate the obtained values from the in-situ-load-tests. The E-modules of concrete which has been used is 50000 N/mm^2. The vertical displacement is validated for the three in-situ-load-tests. However, the strain is stiffer, but this is due to the restrained supports which have been used. The effect of the restrained support has influence on the strain, which leads that they act stiffer than necessary. Based on these results, the best obtained model which will be used to gain more insight in the load-bearing capacity of one separate bridge beam in the longitudinal direction is visualized in the figure 5-31:

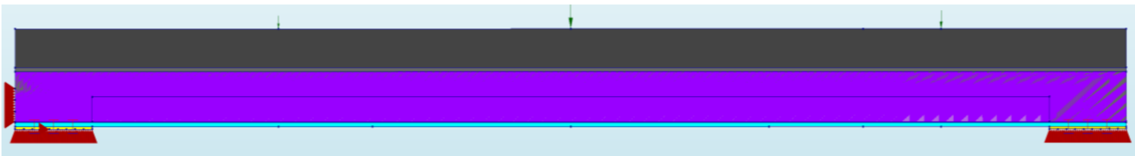

Figure 5-31: The best model to simulate the in-situ-load-test.

In figures 5-17 and 5-18 the vertical displacement and strain of the numerical simulations versus the measured vertical displacement and strain is presented. The ratio between the in-situ-load-test and the numerical simulations is 5%, which is acceptable. The ratio between the numerical simulation and the analytical model is also the same. These values can be seen in tables 5-21 and 5-22. In the figures 5-19 and 5-20 the vertical displacement and strain of the numerical simulations versus the in-situ-load-test 2 is presented in the longitudinal direction for all the points which have been measured. The values are added in tables 5-19 and 5-20. What can be seen is that the ratio between the vertical displacement of the numerical simulations and the in-situ-load-test 2 is in the range of 5%, only one point has a higher ratio of 10%, which is also acceptable because the majority of the ratio is in the range of 5%. For the strains this is a bit different, because the values show a higher ratio, but this has an explanation. The strain is stiffer due to the restrained supports in the numerical simulation. The ratios are in between 20% until 40%. These are the results for the mid-span of bridge deck A at point J. The models are validated based on the acceptable ratio which is 5%. This is done for point J at the mid-span. In the figure 5-32 the numerical simulation of vertical displacement versus in-situ-load-test 1 and 3 is presented for the points H and L. The two tests are set-up to validate the symmetry condition as mentioned before in chapter 4 (the in-situ-load-test). During the in-situ-load-test the measured vertical displacement is not symmetrical at all, this is due to the staked concrete beam at the abutment. During the simulation this is also considered and the results are therefore not symmetrical. The results of linear FEA-models of loaded points H and L for the in-situ-load-tests 1 and 3 are validated mostly with the same ratio like in point J for the vertical displacement, and the strain holds the same explanation like for the mid-span (The strain are stiffer due to the restrained supports in the numerical simulation.). The numerical results are presented in appendix D. See figure 5-32.

.

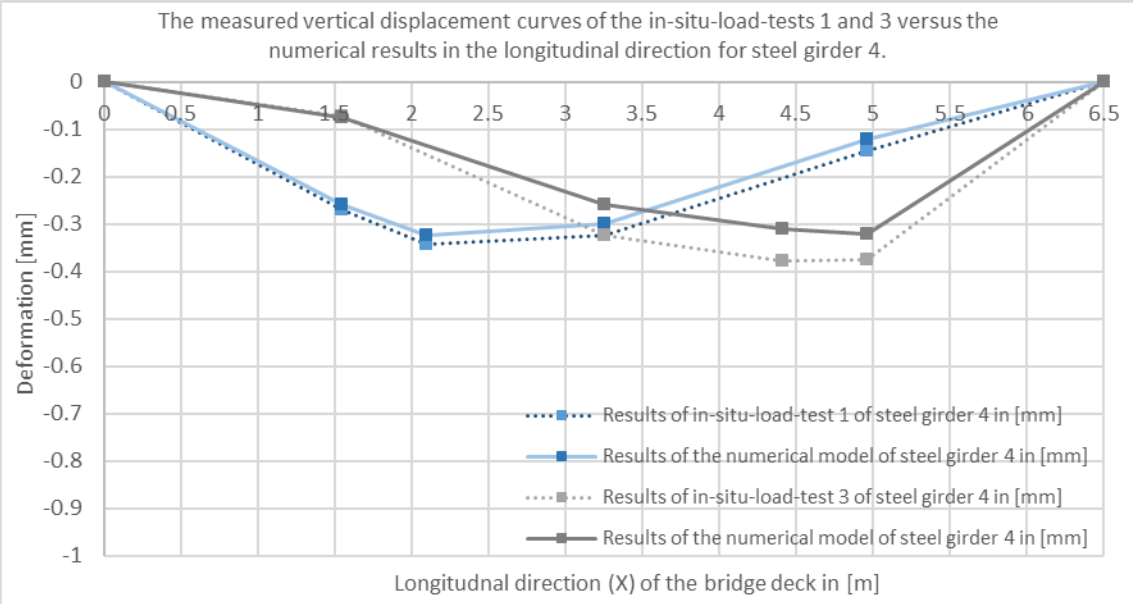

Figure 5-32: The measured vertical displacement curves for the in-situ-load-test 1 (loaded point H) and in-situ-load-test 3 (loaded points L) versus the numerical results in the longitudinal direction for steel girder 4.

After calibrating and validating the model, the results confirm the measured vertical displacement and strain from the in-situ-load-tests. Furthermore, the goal is to gain more insight in the load-bearing capacity of the beam and to test the stress based on the maximal material properties. First of all, the beam is modelled in the linear stage without using any interface between steel and concrete, in addition to that, there is use of incremental load from 400 until 475 kN. This is done based on the input of the measured results from the in-situ-load-tests. The initial idea is to look if there is sliding between steel and concrete. The first observation is that the results of the linear FEA-simulation are nearby or deviate from the measured non-linear results of the in-situ-load-test in a range of 6 % for the used point loads in the numerical simulation between 400 to 475 kN. This can be seen in the table 5-26.

Table 5-26: The maximal vertical displacement of the in-situ-load-test 2 versus the numerical results and the ratio.

load	Results of in-situ-load-test 2 of steel girder 4 on point J in [mm]	Results of the numerical model of steel girder 4 on point J in [mm]	Ratio
0	0	0	0 %
400	-0,53	-0,52	99 %
475	-0,58	-0,62	106 %

From the in-situ-load-test is already mentioned that there is a difference in behaviour from the 0 kN to 400 kN and from 400 kN to 475 kN.

For the first part (from 0 kN until 400 kN) the results of the linear numerical simulations deviate more from the non-linear measured in-situ-load-test results than for the second part (from 400 kN until 475 kN). This is due to the available slip between the steel and concrete.

For the second part (from 400 kN until 475 kN), the non-linear measured in-situ-load-test results are almost the same as the linear numerical simulation results. There is sliding available between 400 kN and 475 kN for the position of the mid-span between steel girder 4 and concrete, but the slip has other behaviour, because the deck becomes stiffer. In addition to this, from the inspection there is corrosion between the bottom of the steel flange and the concrete. This gives symptoms that the concrete and steel are not embedded to each other.

In addition to this, the second step is to analysis the stress of concrete and steel and gain insight in the load-bearing capacity of the beam and to define the failure which is available in the concrete and steel.

Furthermore, the third step is to make a comparison between the inspections, in-situ-load-test and the numerical simulations. This will be discussed.

According to the inspection of bridge deck A and specifically on the side where the in-situ-load-test is done, the following aspects are not found:

a) Corrosions of the steel beams and specially between above the under steel flange and concrete;
b) The material removals;
c) Leakage;
d) Small cracks.

There can be some micro cracks available in the concrete which are not visible from the inspections and during the in-situ-load-test. In addition to this, the numerical results of the tensile principal stress of concrete, which are presented in figures 5-25 and 5-26, are lower than the mean tensile stress of the assumed concrete from the destructive inspections. The compressive principal stress of concrete which is obtained from the numerical model is also lower than the compressive strength of the assumed concrete from the destructive inspections. This is the reason why the numerical results are not presented because the compressive stress is very low and it can be ignored. This observation is made for the maximal load which has been used during the in-situ-load-test of 475 kN. The observation is validated based on:

a) In-situ-load-test;
b) Inspection of bridges;
c) FEA-models.

See previous paragraph how the load is obtained for the three test.

The principal maximal shear stress of concrete which is presented in figure 5-29 and 5-30 is also small, and therefore it does not lead to punching shear or other shear failure. This is also validated from the in-situ-load-tests, where during the in-situ-load-tests there is no observation of punching shear failure in the longitudinal direction. This is the case for the three test of the in-situ-load-tests and the modelled FEA-simulations.
Steel girder 4 is analysed with the help of FEA-simulations. From the FEA-simulations it follows that the principal tensile, compression and shear stress is lower than the maximal stress of the steel S235. The principal stress can be seen in figures 5-25 and 5-26. The other stress states are ignored. In addition to this it is observed from the inspection that the material loss of steel is less than 2 %, which is not high. This will not reduce the capacity of the steel-girder. Furthermore, there is no-corrosion of steel available in the part where the in-situ-load-test is performed, but the rest of the bridge, and especially at the other spans, the bridge deck has shown defects which are mentioned in the chapter 2.3.3, but this is not relevant for the comparison with the made in-situ-load-test and FEA-simulation of the separated beam.

The last point, which is interesting to mention, is that there are singularities available in the model which is visible in the stress pattern at the point load and the supports. The stress which is developed due to the singularities is also not that high that it can lead to a failure. And if it still leads to failure, this is not realistic because we are dealing with singularities. This can be seen in the figures from 5-25 until 5-30.

5.5. Conclusions of the linear analysis of the separated beam

Based on the 2D linear analysis which is done for the separated beam the following conclusion can be taken for the longitudinal direction of bridge deck A:

The beam is calibrated and the results are validated, during the validation process the chosen model (see Figure 5-31) is realistic to use.

The first part (from 0 kN until 400 kN) shows that there is sliding available. This means that there is no full interaction between that the between steel girder and concrete.

In the second part (from 400 kN until 475 kN) the deck becomes stiffer which leads to a change in the behaviour of the slip.

These conclusions are validated only for the single point load at the mid-span.

The stress state of the separated beam is also studied and tested to the assumed material properties from the destructive inspections of bridge deck A. The difference between the obtained stresses from the numerical simulations and the allowable stresses of concrete is very low, which will not lead to failure. This result is also validated based on the input from the in-situ-load-tests and the inspections of bridge A, where the bridge deck in total does not show any defects during the execution of the in-situ-load-test and during the made inspection.

6. 3D-linear simulations of the historical steel-concrete-composite-bridge-deck A

6.1. Introduction

The general input of the 3D FEA-models is already presented in chapter 5. In this chapter the results of the simulated FEA-model on bridge deck A will be presented. In addition to this, the simulated numerical results will be validated based on the measured results of the in-situ-load-tests. Furthermore, the results of the simulated 3D FEA-models will be compared with the results of the 2D separated beam. Also, the results of the numerical simulations will be discussed and conclusions will be taken. In the transverse direction the goal is to validate the most logical checking method as presented in chapter 3.3.

6.2. Numerical result of historical steel-concrete-composite-bridge-deck A

In this section the results of bridge deck A will be presented and validated with the measurements of the in-situ-load-tests in the longitudinal and transverse direction. In addition to this, the results will be compared to the results of the simulated separated beam. The load which has been used is obtained from the total load of 400 kN until 475 kN based on the calculation shown in the previous sub-chapter 5.2.5 where the load is defined. The load configuration and the position on the bridge deck A can be seen in the figures 6-1 and 6-2. This configuration is obtained from the in-situ-load-test, see chapter 4. In the figures 6-3/6-4/6-9 and 6-10 the numerical simulated results of the vertical displacement and strain of the device steel-girders 3 and 4 (of point J) loaded on point J from 400 kN to 475 kN are presented. The values including the ratios are added in the following tables 6-1/6-2/6-6 and 6-7. This describes only the vertical displacement and strain of the loaded point J at the mid-span. In figures 6-5/6-6/6-11 and 6-12 the results of the numerical simulations of the longitudinal direction are presented for the vertical displacement and strain of the two steel girders 4 and 4 respectively versus the in-situ-load-test 2. In the tables 6-3/6-4/6-8 and 6-9 the numerical values including the ratios are presented. In figures 6-8 and 6-13 the results of the numerical simulations of transverse direction is given versus the in-situ-load-test 2. The numerical values of it are presented in the tables 6-5 and 6-10, including the ratios. At last, the figures 6-14 until 6-17 give an illustrative presentation of the FEA-model. This is done for the two loads 400 kN until 475 kN.

The principal stress and shear stress of concrete are also added in the figures 6-18/6-19/6-22 and 6-23. The values which are obtained from the numerical simulations are tested to the maximal allowable stress of concrete which can be found in tables 6-11 and 6-13. This is also done for the steel, where the results can be seen in figures 6-20 and 6-21 and table 6-12.

The rest of the numerical results of the loaded points H and L is added in appendix E in the same way point J is presented in this chapter. The results of the mid-span are leading in this investigation of bridge deck A.

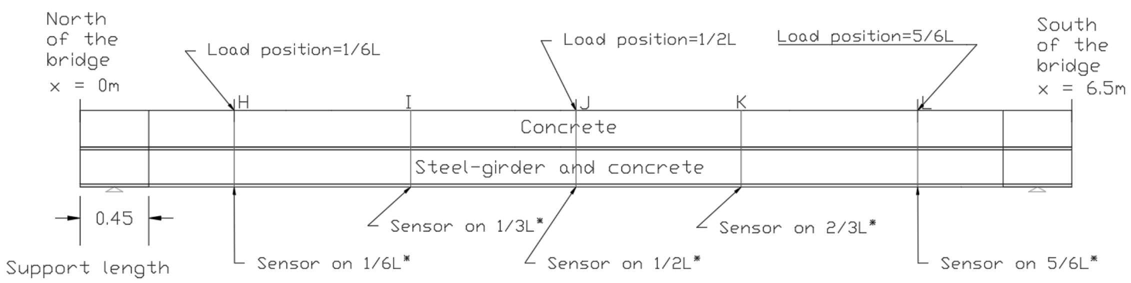

Figure 6-1: The loaded points (H, J and L) on the bridge deck in the longitudinal direction of the bridge deck.

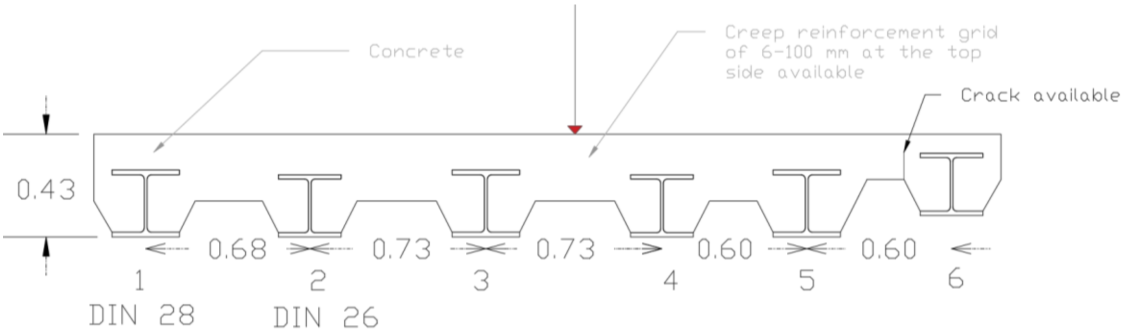

Figure 6-2: The loaded points (H, J and L) on the bridge deck in the transvers direction of the bridge deck.

Table 6-1: Load-displacement of in-situ-load-test 2 versus numerical results for point J of steel girder 4.

load	**Results of in-situ-load-test 2 of steel girder 4 on point J in [mm]**	**Results of the numerical model of steel girder 4 on point J in [mm]**	**Ratio**
0	0	0	0 %
400	-0.53	-0.51	97 %
475	-0.58	-0.61	105 %

Table 6-2: Load-displacement of in-situ-load-test 2 versus numerical results for point J of steel girder 3.

load	**Results of in-situ-load-test 2 of steel girder 3 on point J in [mm]**	**Results of the numerical model of steel girder 3 on point J in [mm]**	**Ratio**
0	0	0	0 %
400	-0.53	-0.52	99 %
475	-0.58	-0.59	101 %

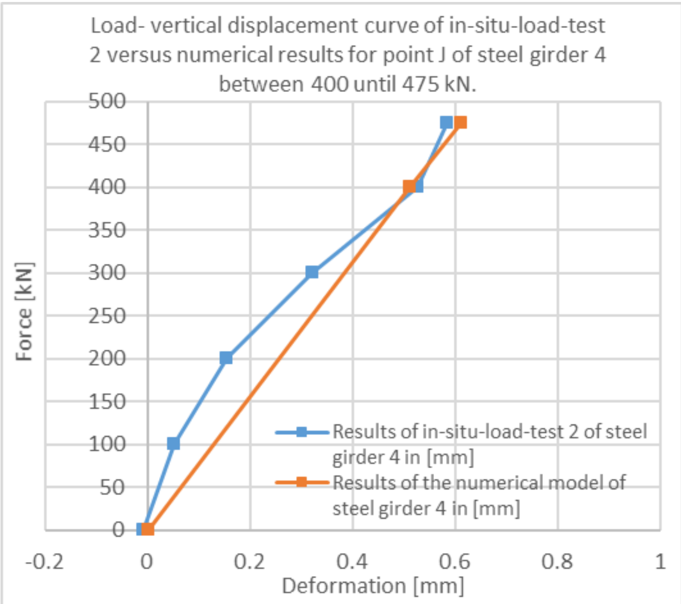

Figure 6-3: Load-displacement curve of in-situ-load-test 2 versus numerical results for point J of steel girder 4 between 400 until 475 kN.

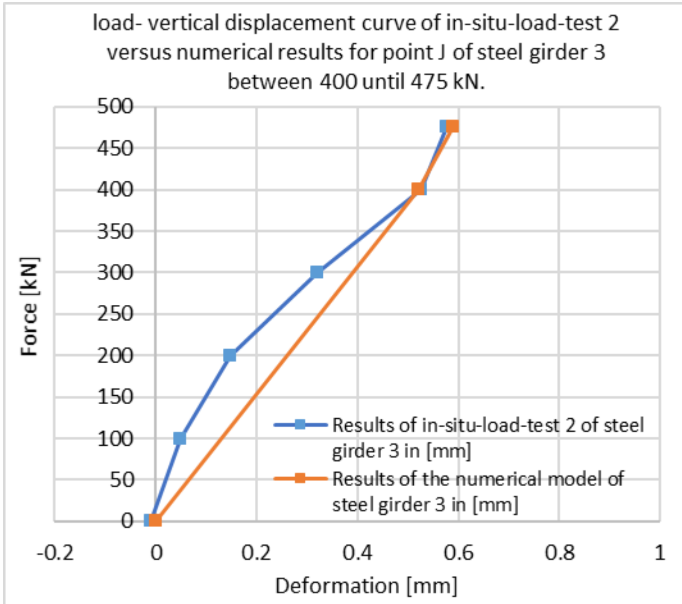

Figure 6-4: Load-displacement curve of in-situ-load-test 2 versus numerical results for point J of steel girder 3 between 400 until 475 kN.

Table 6-3: Load-displacement of in-situ-load-test 2 versus numerical results for points of steel girder 4.

Point	**X**	**Results of in-situ-load-test 2 of steel girder 4 in [mm]**	**Results of the numerical model of steel girder 4 in [mm]**	**Ratio**
***	**0**	0	0	0%
I	**2.09**	-0.39	-0.40	103%
J	**3.25**	-0.58	-0.61	105%
K	**4.41**	-0.49	-0.44	90%
***	**6.5**	0	0	0%

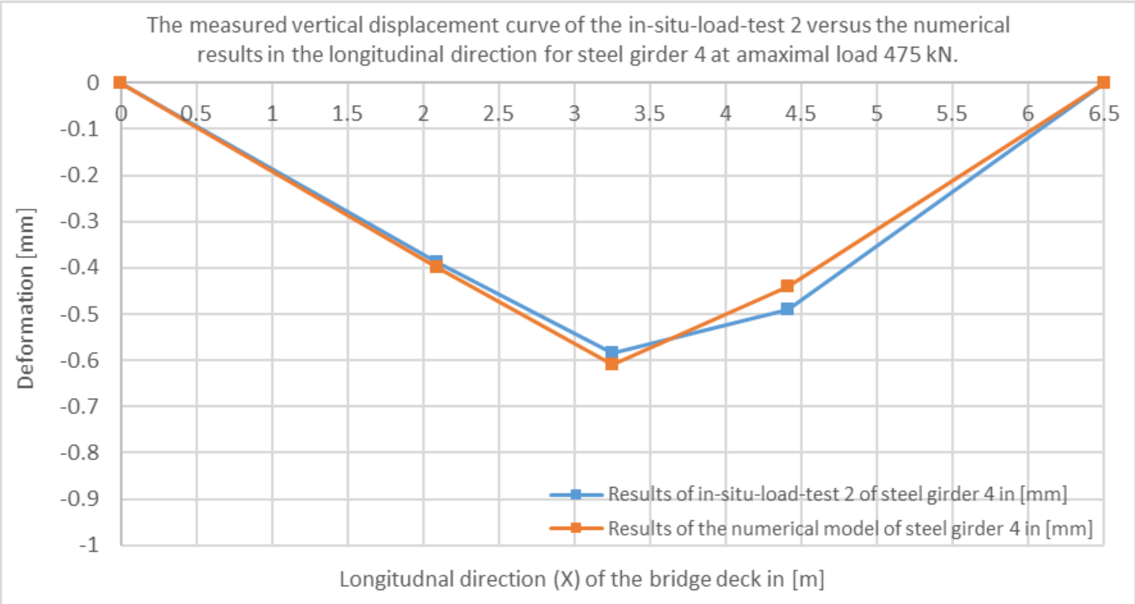

Figure 6-5: The measured vertical displacement curves for in-situ-load-test 2 versus the numerical results for the steel girder 4 in the longitudinal direction of the load 475 kN.

Table 6-4: Load-displacement of in-situ-load-test 2 versus numerical results for points of steel girder 3.

Point	X	Results of in-situ-load-test 2 of steel girder 3 in [mm]	Results of the numerical model of steel girder 3 in [mm]	Ratio
***	0	0	0	0%
I	2.09	-0.41	-0.39	95%
J	3.25	-0.58	-0.59	102%
K	4.41	-0.48	-0.43	89%
***	6.5	0.00	0	0%

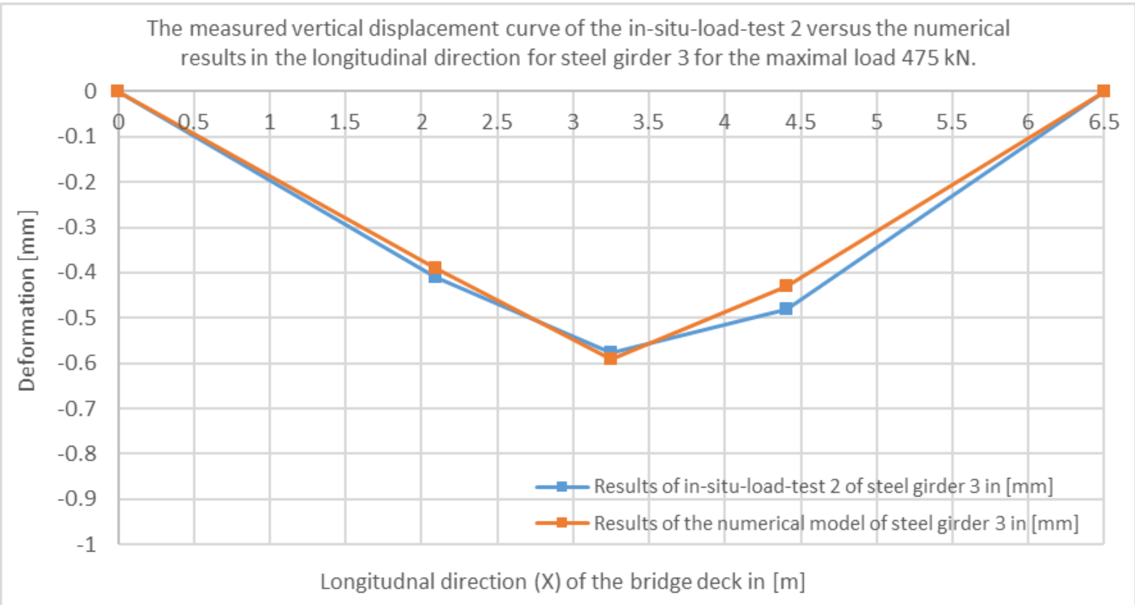

Figure 6-6: The measured vertical displacement curves for in-situ-load-test 2 versus the numerical results for the steel girder 3 in the longitudinal direction of the load 475 kN.

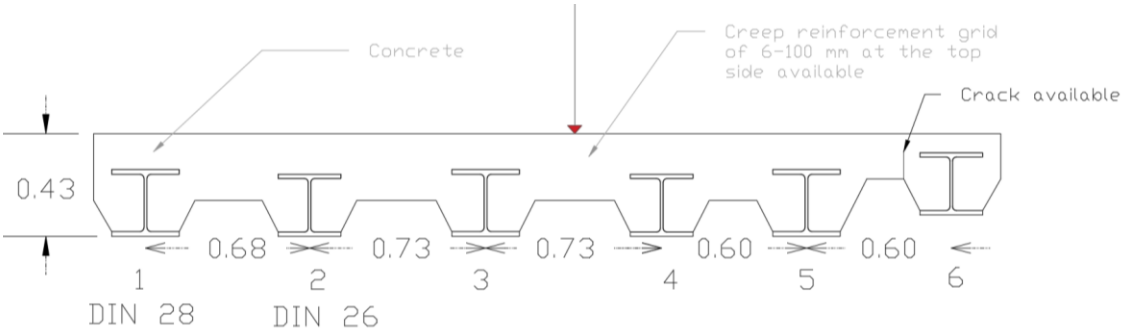

Figure 6-7: The loaded points (H ,J and L) on the bridge deck in the transvers direction of the bridge deck.

Table 6-5: Load-displacement of in-situ-load-test 2 versus numerical results of the row J.

Point	Y	Results of in-situ-load-test 2 of row J in [mm]	Results of the numerical model of row J in [mm]	Ratio
J1	**0**	-0.33	-0.34	103 %
J2	**0.73**	-0.47	-0.45	96 %
J3	**1.46**	-0.58	-0.61	105 %
J4	**2.19**	-0.58	-0.60	104 %
J5	**2.92**	-0.49	-0.40	81 %
J6	**3.65**	-0.30	-0.26	86 %

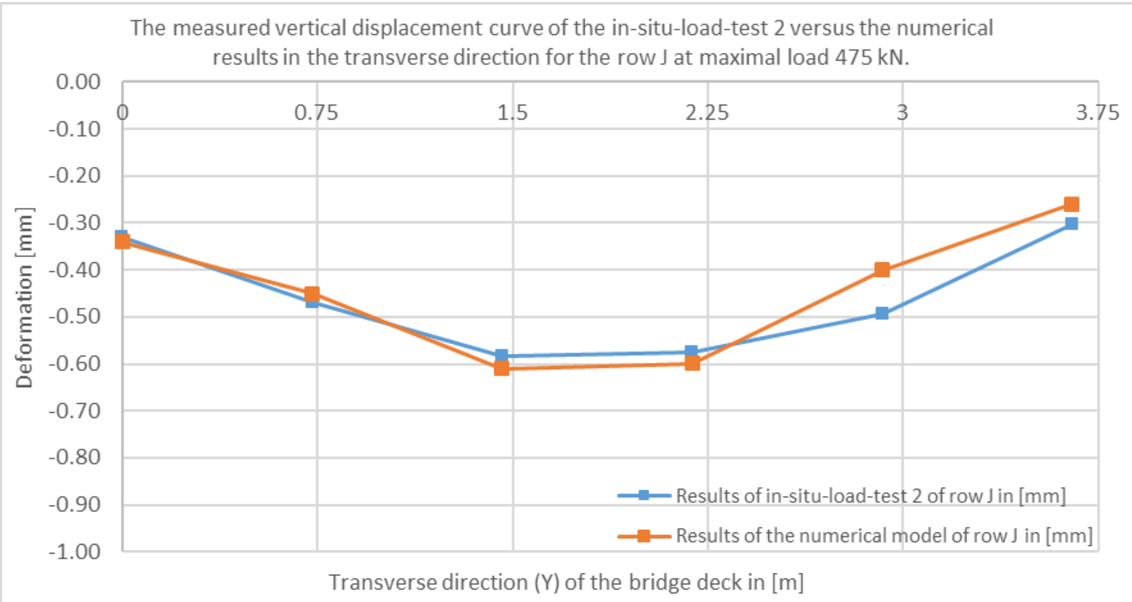

Figure 6-8: The measured vertical displacement curves for in-situ-load-test 2 versus the numerical results in the transverse direction for the row J of the load 475 kN.

Table 6-6: Load-strain of in-situ-load-test 2 versus numerical results for point J of steel girder 4.

Load	Results of in-situ-load-test 2 of steel girder 4 in [µm/m]	Results of the numerical model Exx of J_3 of steel girder 4 in [µm/m]	Ratio
0	0.00	0	0%
400	68.07	81.8	120%
475	80.45	101.4	126%

Table 6-7: Load-strain of in-situ-load-test 2 versus numerical results for point J of steel girder 3.

Load	Results of in-situ-load-test 2 of steel girder 3 in [µm/m]	Results of the numerical model Exx of J4 of steel girder 3 in [µm/m]	Ratio
0	0.00	0	0%
400	69.29	79.7	115%
475	81.77	102.7	126%

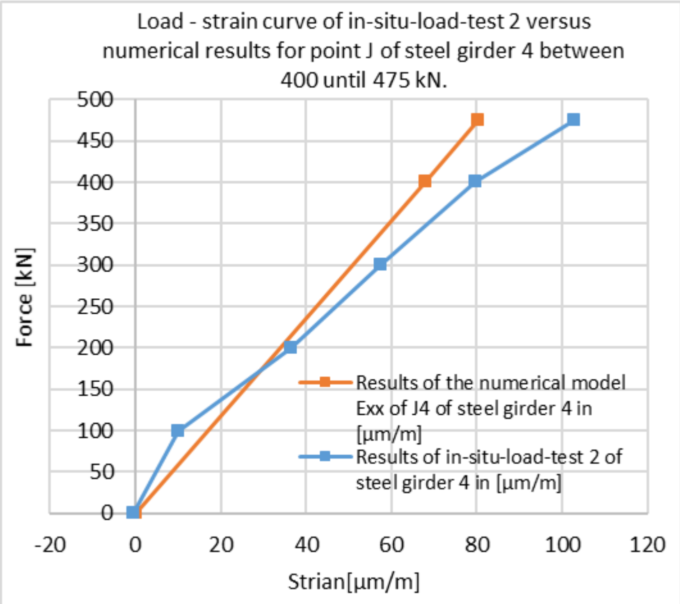

Figure 6-9: Load-strain curve of in-situ-load-test 2 versus numerical results for point J of steel girder 4 between 400 until 475 kN.

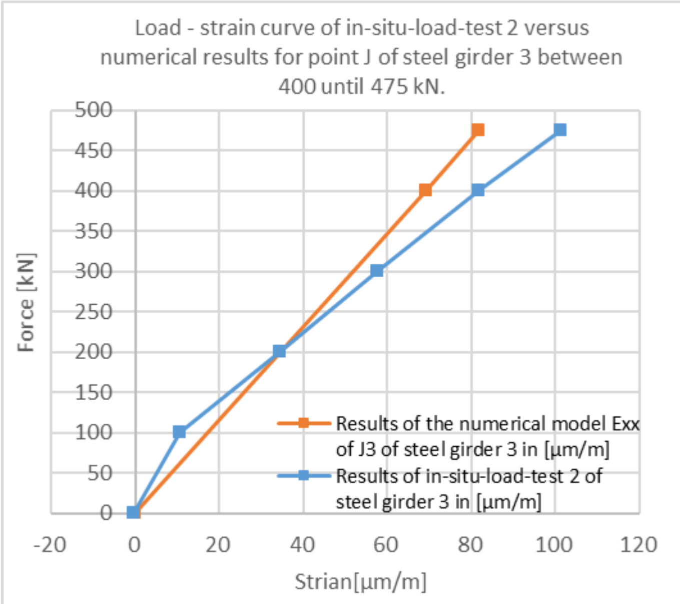

Figure 6-10: Load-strain curve of in-situ-load-test 2 versus numerical results for point J of steel girder 3 between 400 until 475 kN.

Table 6-8: Load-strain of in-situ-load-test 2 versus numerical results for points of steel girder 4.

Point	X	Results of in-situ-load-test 2 of steel girder 4 in [µm/m]	Results of the numerical model of steel girder 4 in [µm/m]	Ratio
***	0	0	0	0%
H	1.54	-15.20	-6.98	46%
I	2.09	-54.70	-13.4	25%
J	3.25	-102.70	-69.3	67%
K	4.41	-49.00	-28.7	58%
L	4.96	-15.20	-5.8	38%
***	6.5	0	0	0%

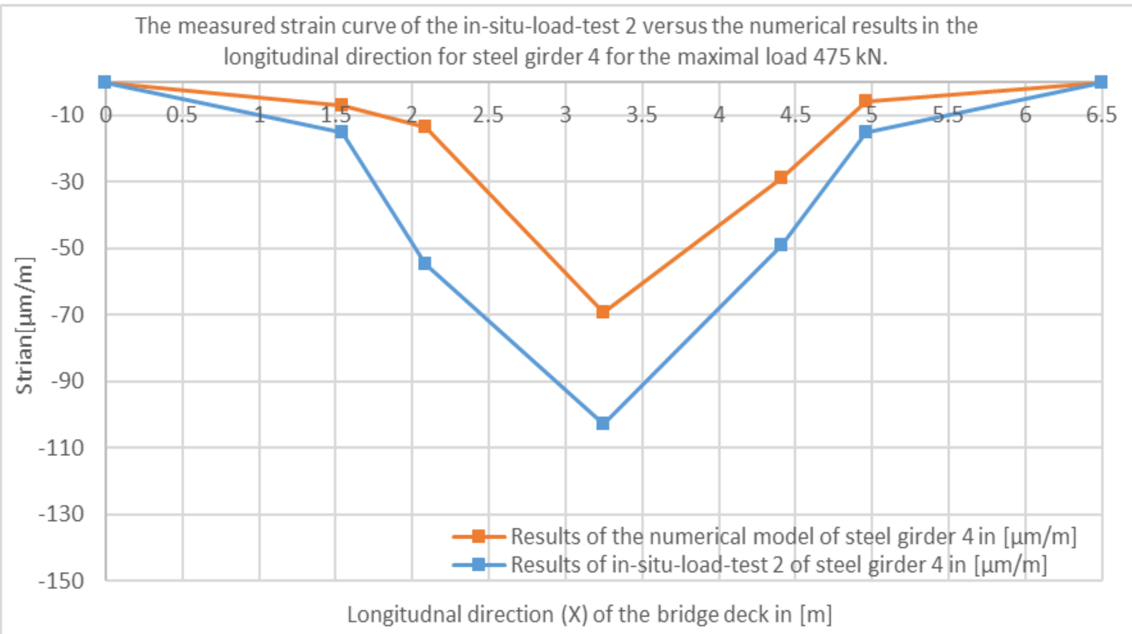

Figure 6-11: The measured strain curves for in-situ-load-test 2 versus the numerical results for the steel girder 4 in the longitudinal direction of the load 475 kN.

Table 6-9: Load-strain of in-situ-load-test 2 versus numerical results for points of steel girder 3.

Point	X	Results of in-situ-load-test 2 of steel girder 3 in [μm/m]	Results of the numerical model of steel girder 3 in [μm/m]	Ratio
***	0	0	0	0%
H	1.54	-17.3	-6.5	38%
I	2.09	-52.4	-13.1	25%
J	3.25	-101.4	-68.1	67%
K	4.41	-55.4	-27.9	50%
L	4.96	-16.6	-5.6	34%
***	6.5	0	0	0%

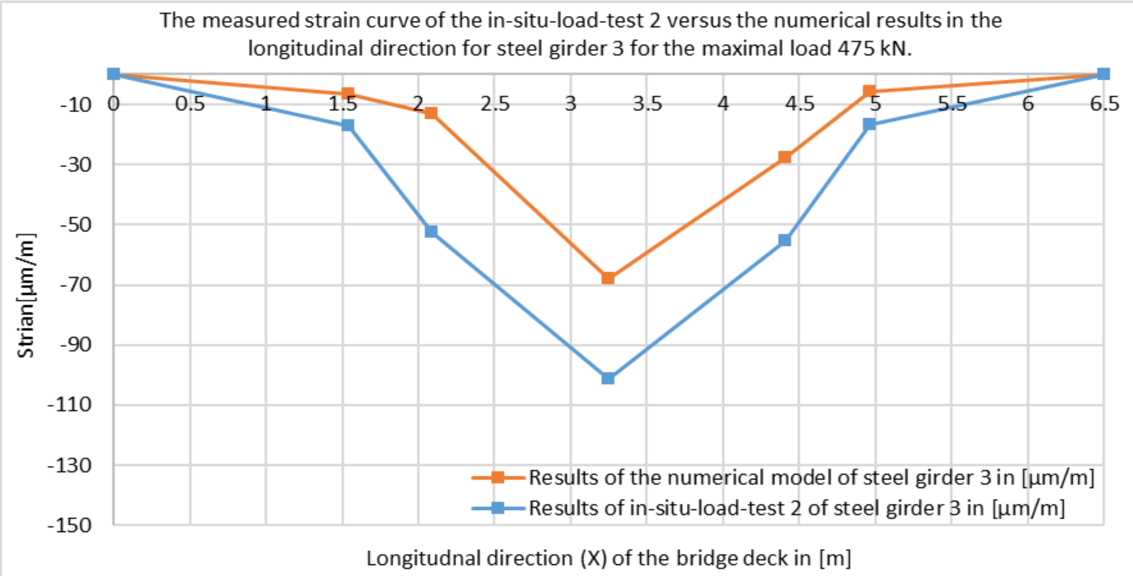

Figure 6-12: The measured strain curves for in-situ-load-test 2 versus the numerical results for the steel girder 3 in the longitudinal direction of the load 475 kN.

Table 6-10: Load-strain of in-situ-load-test 2 versus numerical results for the row J in the transverse direction.

Point	Y	Results of in-situ-load test 3 of row J in [μm]	Results of the numerical model of row J in [μm]	Ratio
J1	0	-62.80	-23.63	38%
J2	0.73	-76.70	-47.10	61%
J3	1.46	-102.70	-69.29	67%
J4	2.19	-101.40	-68.07	67%
J5	2.92	-77.70	-36.72	47%
J6	3.65	-48.30	-24.53	51%

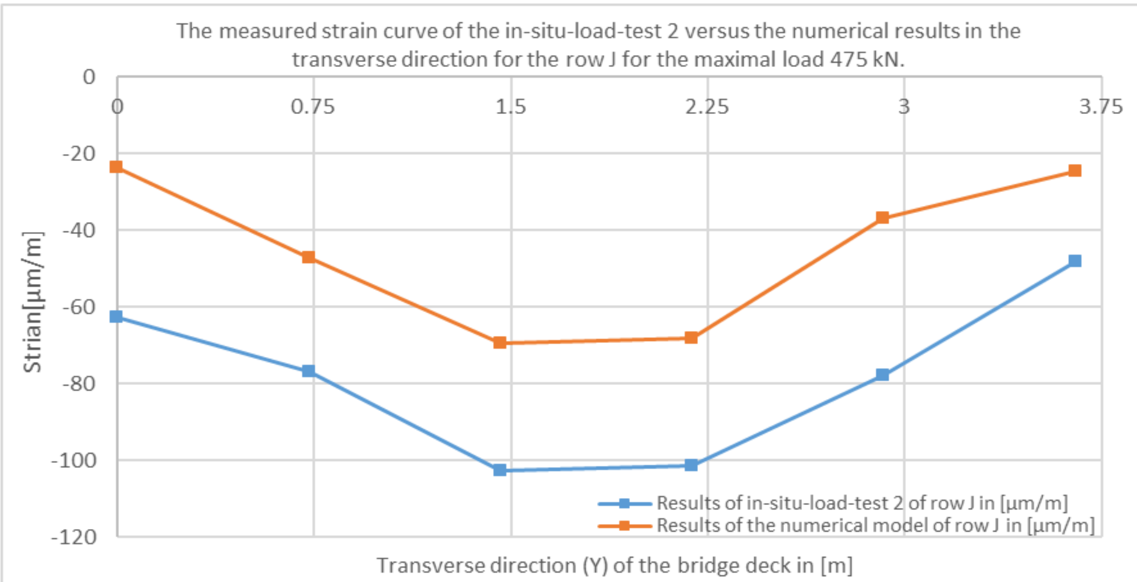

Figure 6-13: The measured strain curve of the in-situ-load-test 2 versus the numerical results in the transverse direction for the row H for the maximal load 475 kN.

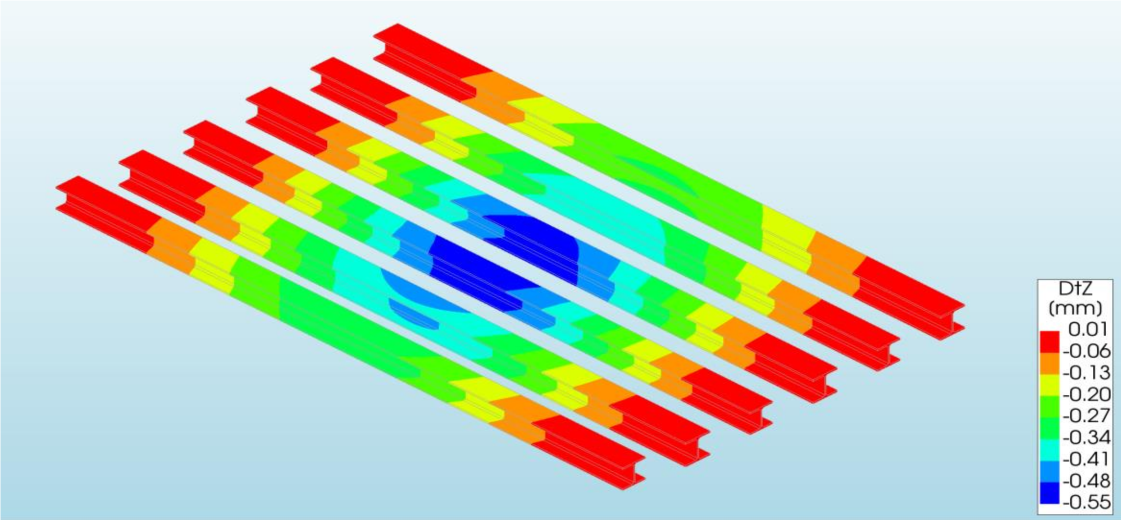

Figure 6-14: The numerical results of the vertical displacement of steel-girders for a load of 475 kN at point J.

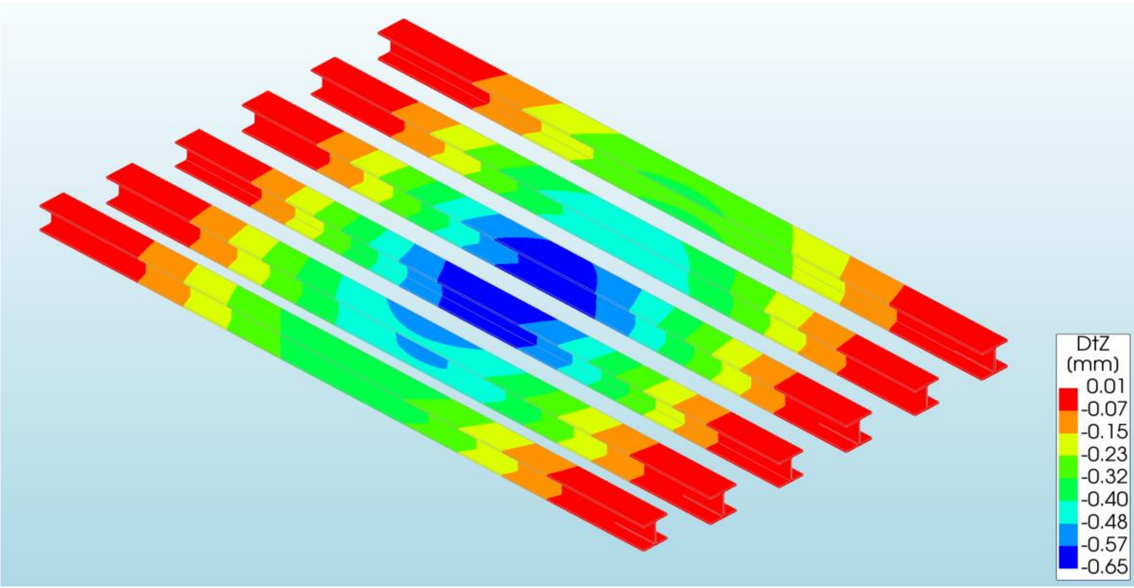

Figure 6-15: The numerical results of the vertical displacement of steel-girders for a load of 475 kN at point J.

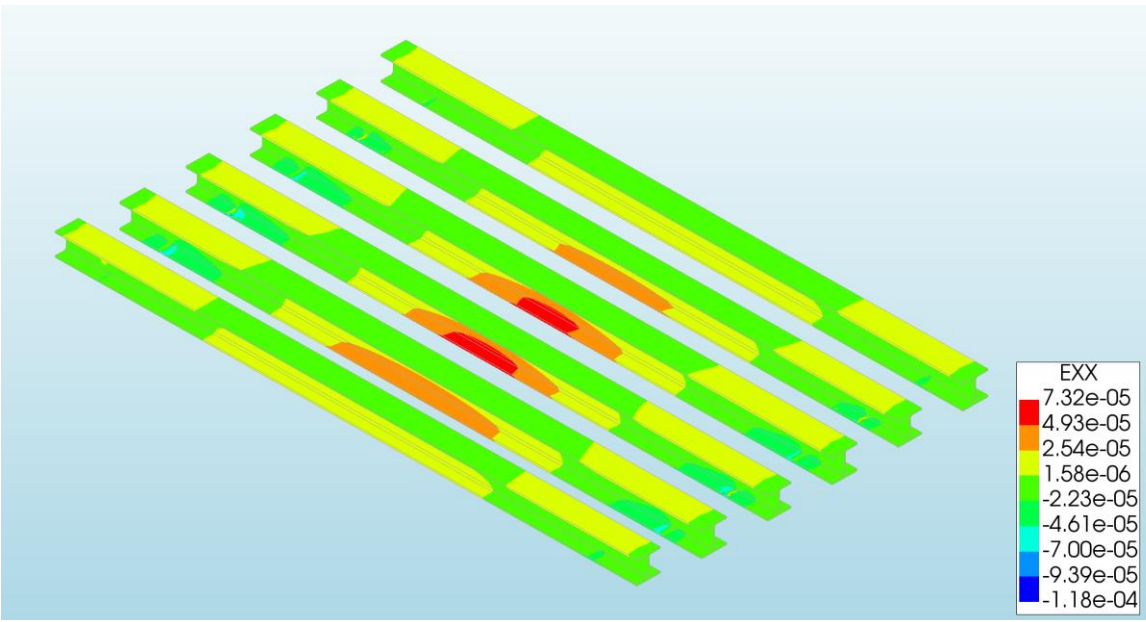

Figure 6-16: The numerical results of the strain of steel-girders for a load of 400 kN in the point J.

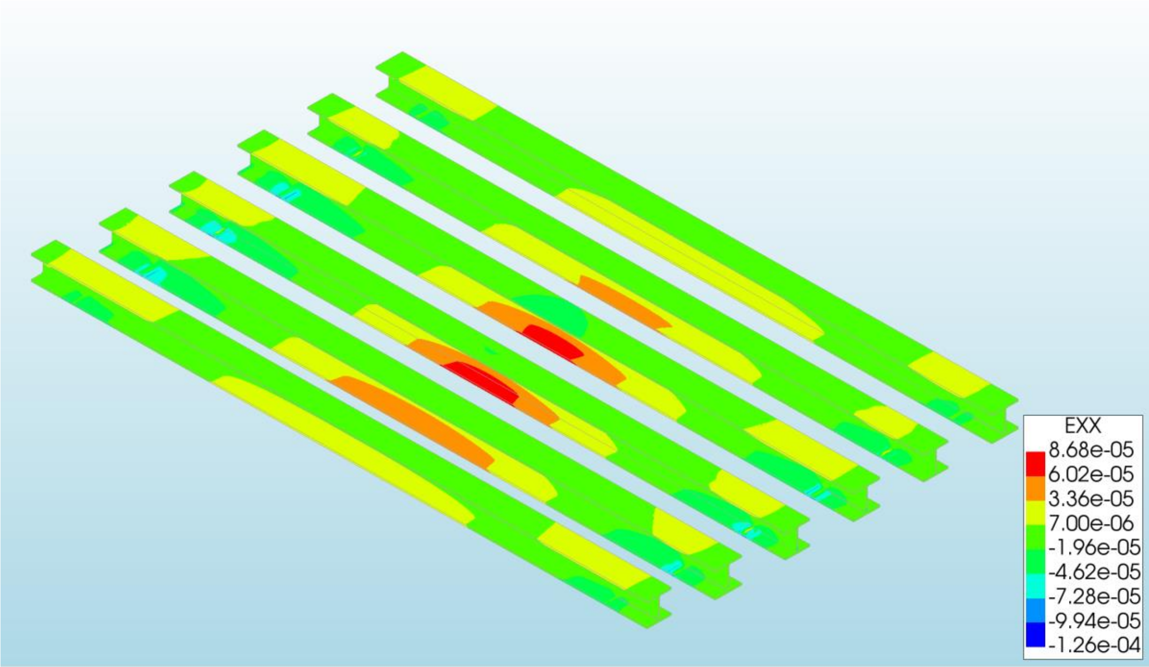

Figure 6-17: The numerical results of the strain of steel-girders for a load of 475 kN in the point H.

Comparing the results of 2D separated beam 4 and steel girder 4 of the 3D model:

In the following tables 6-11 and 6-12 a comparison is made between the vertical displacement and strain of the 2D model (separated beam) versus the 3D volume model of bridge deck A, the results are presented in the tables 6-11 and 6-12. This will be discussed in the discussion part of this chapter.

Table 6-11: Load-displacement of numerical results of the 2D separated beam 4 versus numerical results of steel girder 4 at point J.

load	Results of the numerical model of separated beam 4 on point J in [mm]	Results of the numerical model of steel girder 4 on point J in [mm]	Ratio
0	0	0	0 %
400	-0,52	-0.51	101 %
475	-0,62	-0.61	101 %

Table 6-12: Load-strain of numerical results of the 2D separated beam 4 versus numerical results for point J of steel girder 4.

Load	Results of the numerical model Exx of J_4 of separated beam 4 in [µm/m]	Results of the numerical model Exx of J_4 of steel girder 4 in [µm/m]	Ratio
0	0	0	0%
400	69	81.8	88 %
475	83	101.4	82 %

The stress state is presented in the following figures and tables:

Table 6-13: The maximal principal stress of concrete at point J.

Load	The numerical results of the principal stress of the concrete on point J in [N/mm^2]	Maximal allowable tensile stress of concrete in [N/mm^2]	Ratio
0	0	0	0%
400	3.03	4.2	72 %
475	3.60	4.2	85 %

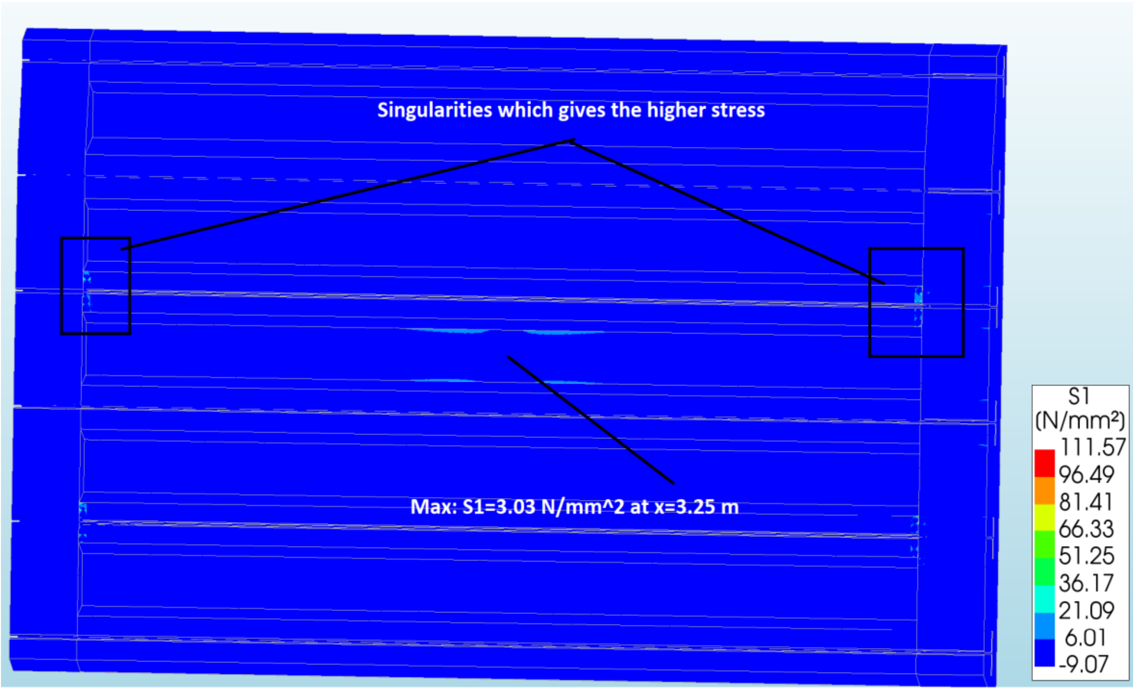

Figure 6-18: The numerical results of the principal stress in the concrete for a load of 400 kN at the point J.

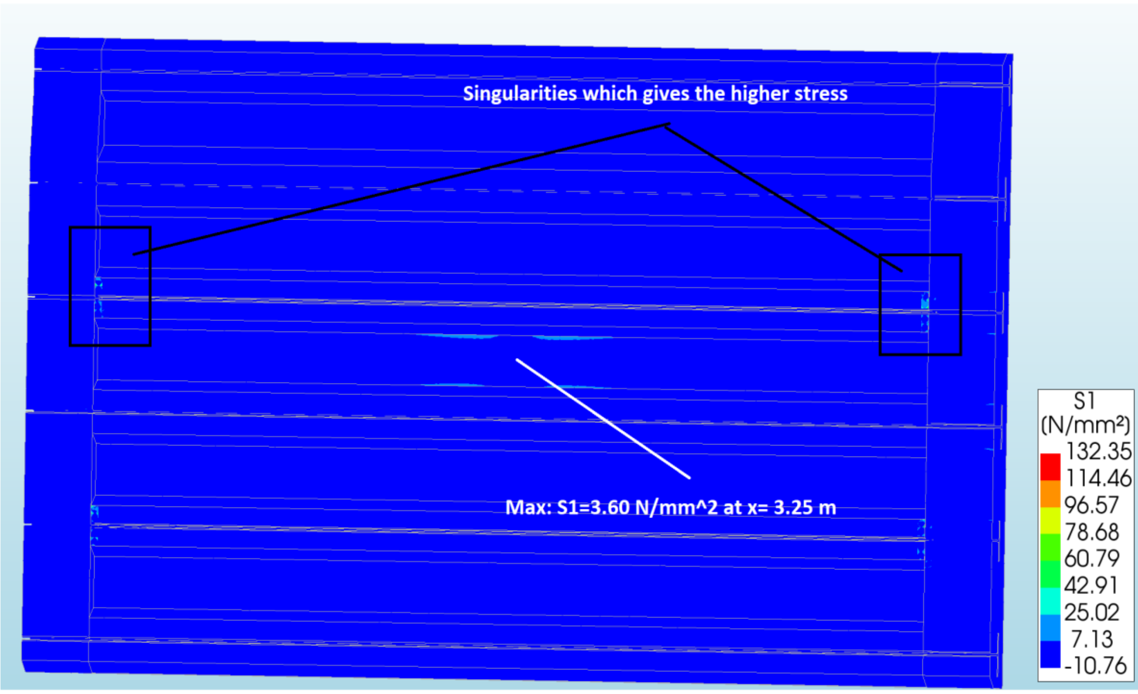

Figure 6-19: The numerical results of the principal stress in the concrete for a load of 475 kN at the point J.

Comment: The principal stress is under the maximal tensile stress of concrete.

Table 6-14: The maximal principal stress of steel at point J.

Load	The numerical results of the principal stress of the concrete on point J in [N/mm^2]	Maximal allowable tensile /compressive stress of steel in [N/mm^2]	Ratio
0	0	0	0
400	18	235	7.7 %
475	21	235	8.9 %

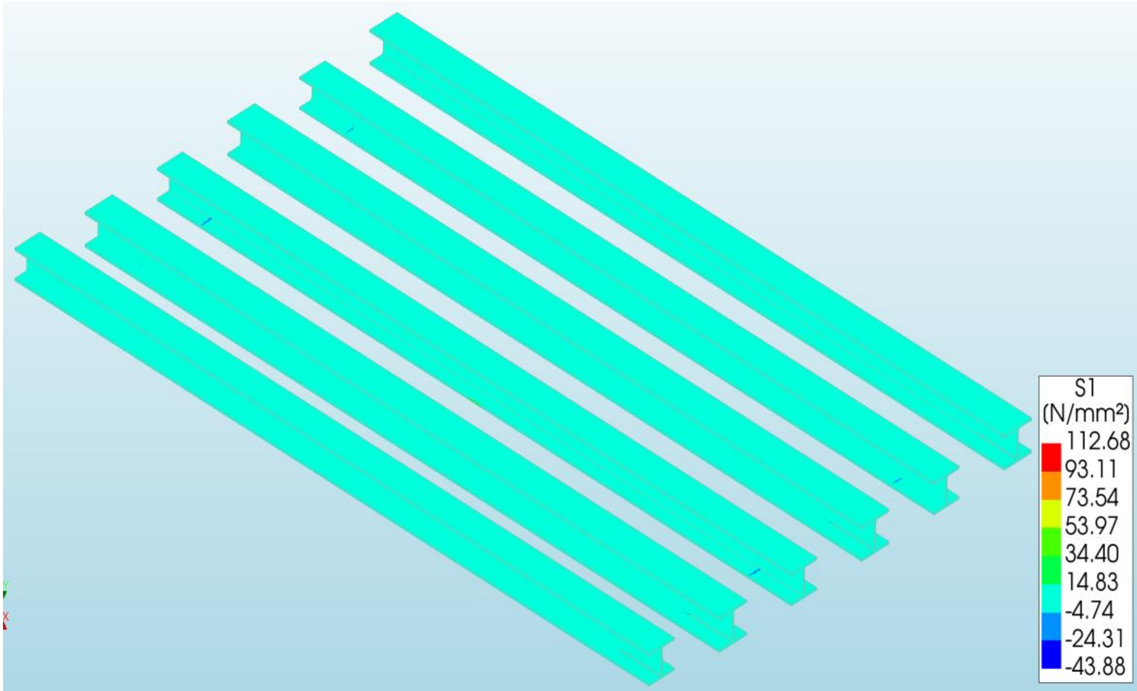

Figure 6-20: The numerical results of the principal stress in the steel for a load of 400 kN at the point J.

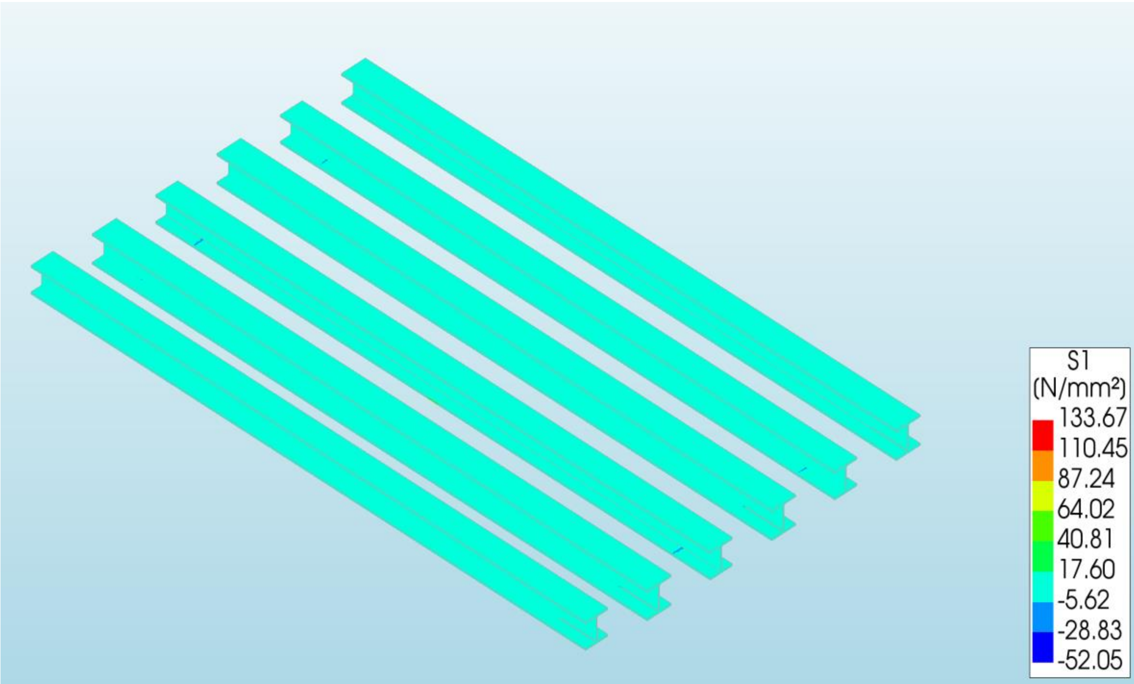

Figure 6-21: The numerical results of the principal stress in the steel for a load of 475 kN at the point J.

Comment: The principal stress is under the maximal tensile stress of steel-girders.

Table 6-15: The maximal shear stress in concrete at point J.

Load	The numerical results of the principal stress of the concrete on point J in [N/mm²]	Maximal allowable shear stress of concrete in [N/mm²]	Ratio
0	0	0	0
400	2.90	7.2	40 %
475	3.40	7.2	47 %

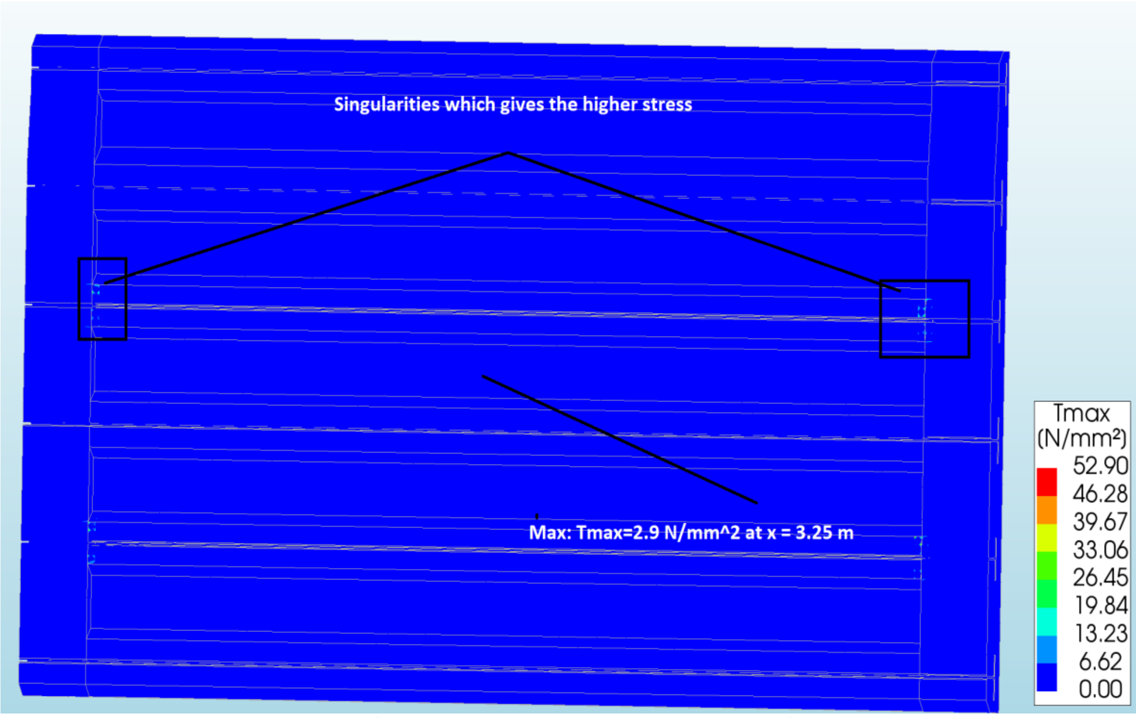

Figure 6-22: The numerical results of the maximal shear stress in the concrete Tmax for a load of 400 kN at the point J.

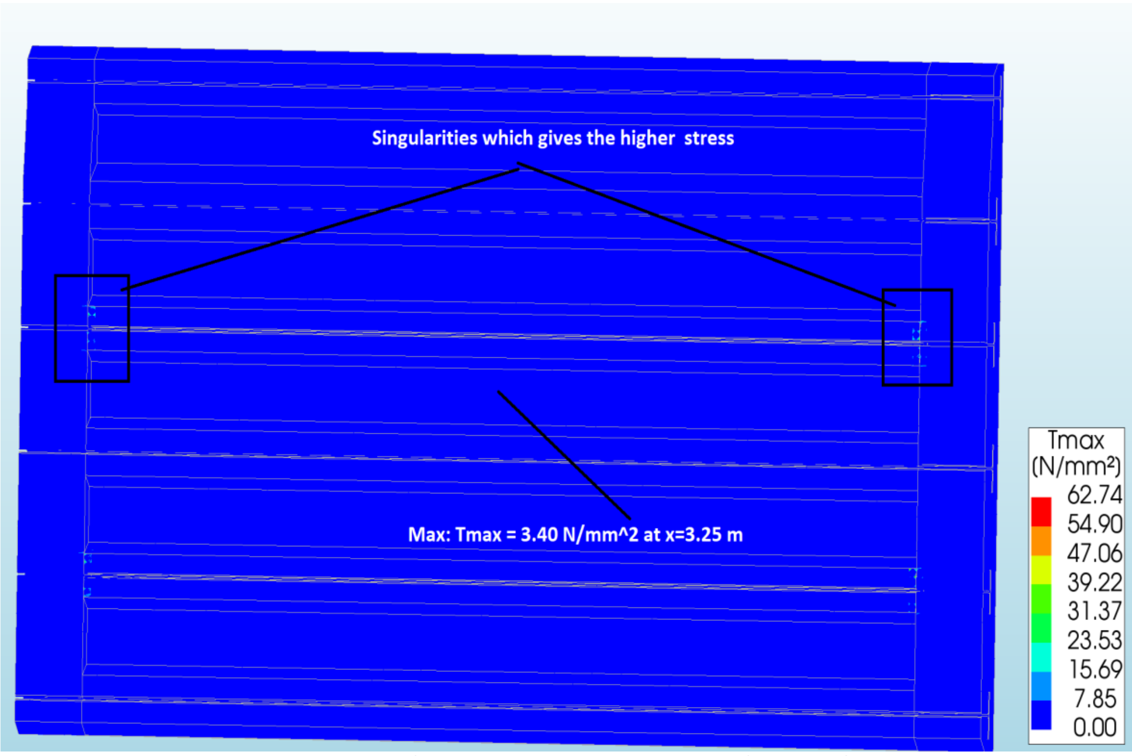

Figure 6-23: The numerical results of the shear stress in the concrete Tmax for a load of 475 kN at the point J.

Comment: The shear stress is under the maximal shear stress of concrete.

6.2.1. Improving load transfer based on the strut and tie model in the transverse direction of bridge deck A

Introduction:

In this section the results of the numerical simulation of the transverse direction will be presented. First, the results of the measured horizontal displacement for each cycle will be presented and compared with previous load cycle. Secondly, the result of the horizontal displacement will be compared with the in-situ-load-test. After that, the strut and tie model will be implemented in the transverse direction based on the analytical calculation and numerical simulation.

The results of the measured horizontal displacement of in-situ-load-test 2 for row J for more than one loading cycle of the transverse direction:

In the figures 6-24 until 6-29 the different cycles of the horizontal displacement for each steel girder of row J are presented. In each figure it can be seen that the horizontal displacement is not the same for each load cycle, for example in figure 6-24 the measured horizontal displacement is not the same for the force of 100 kN of each load cycle. This means that there is slip available in the transverse direction. This will be discussed in the following paragraph of discussions.

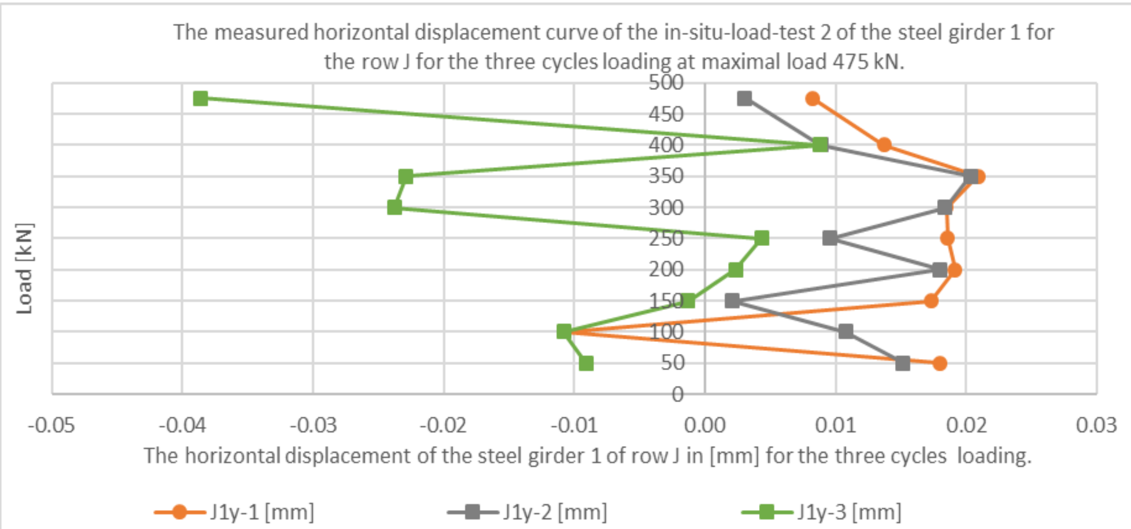

Figure 6-24: The measured horizontal displacement curve of in-situ-load-test 2 of steel girder 1 for row J for the three loading cycles.

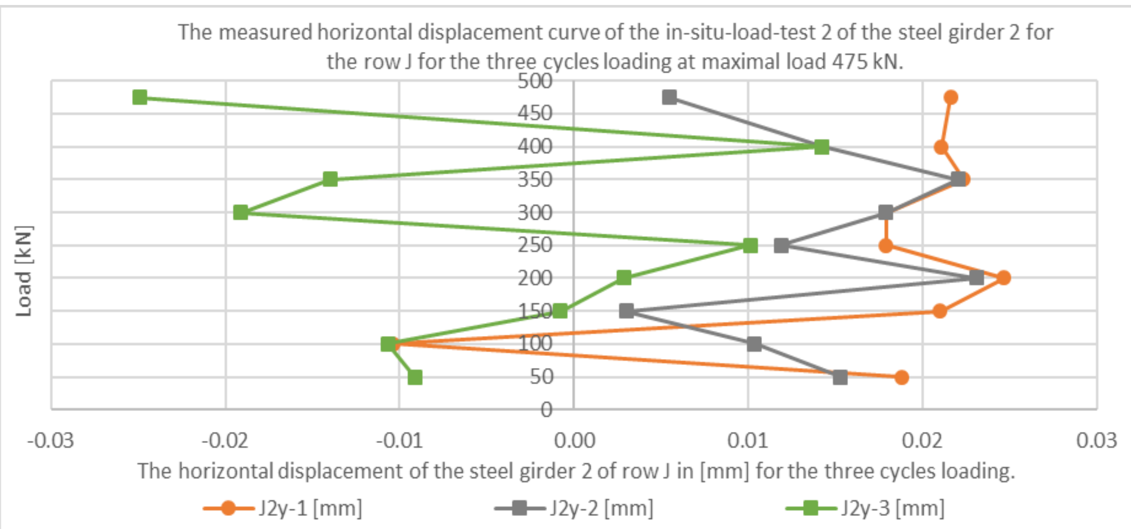

Figure 6-25: The measured horizontal displacement curve of in-situ-load-test 2 of steel girder 2 for row J for the three loading cycles.

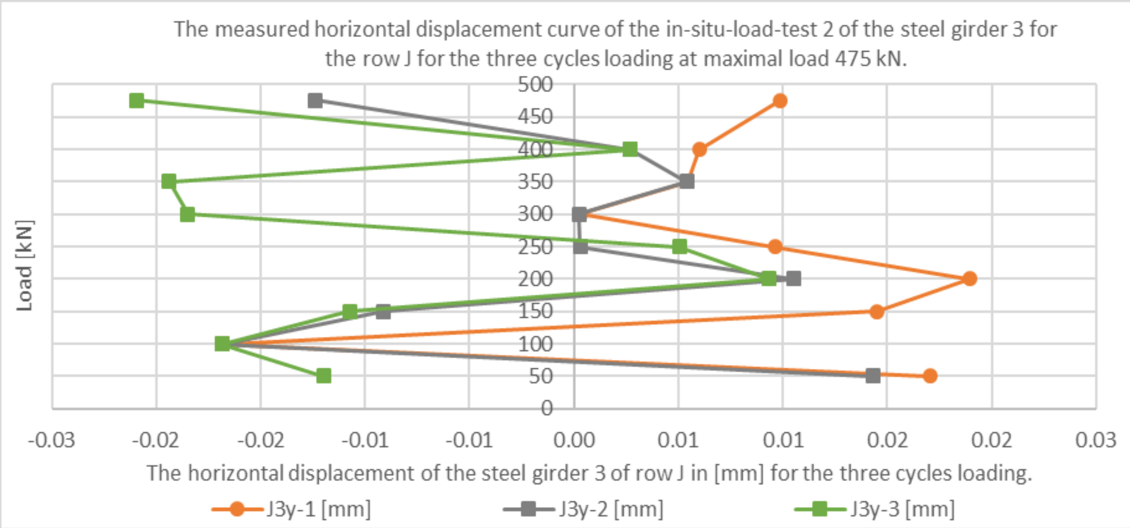

Figure 6-26: The measured horizontal displacement curve of in-situ-load-test 2 of steel girder 3 for row J for the three loading cycles.

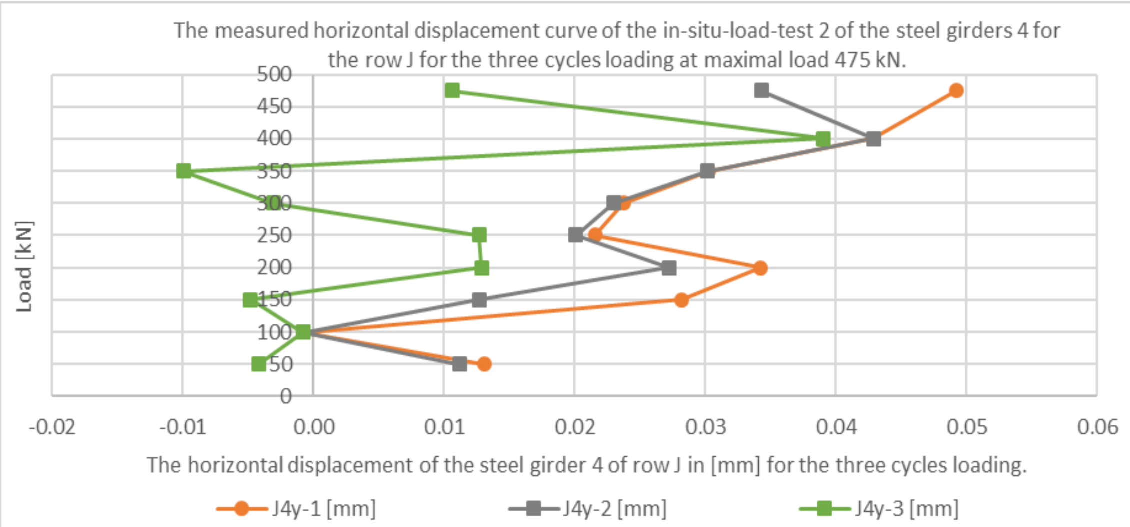

Figure 6-27: The measured horizontal displacement curve of in-situ-load-test 2 of steel girder 4 for row J for the three loading cycles.

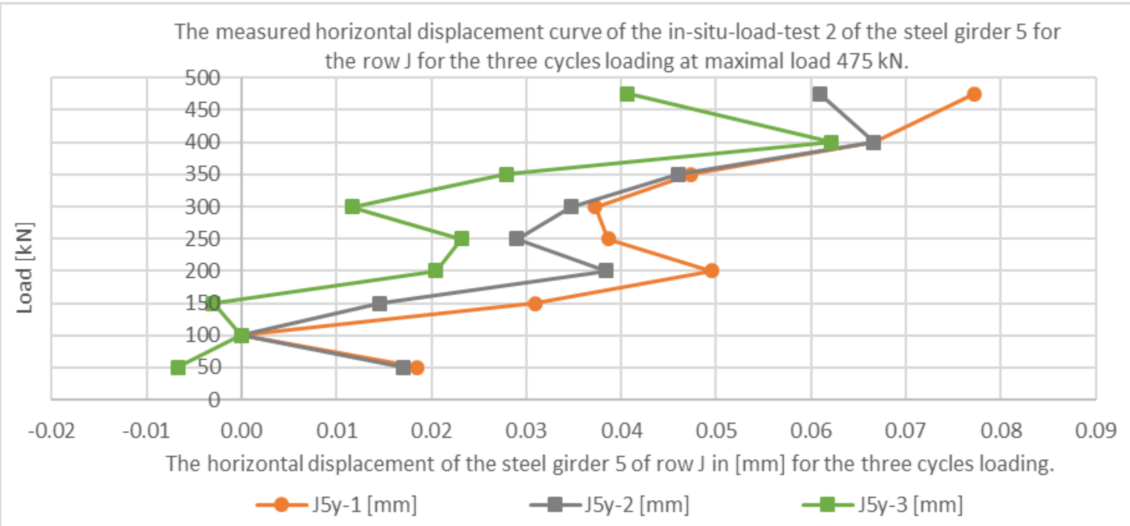

Figure 6-28: The measured horizontal displacement curve of in-situ-load-test 2 of steel girder 5 for row J for the three loading cycles.

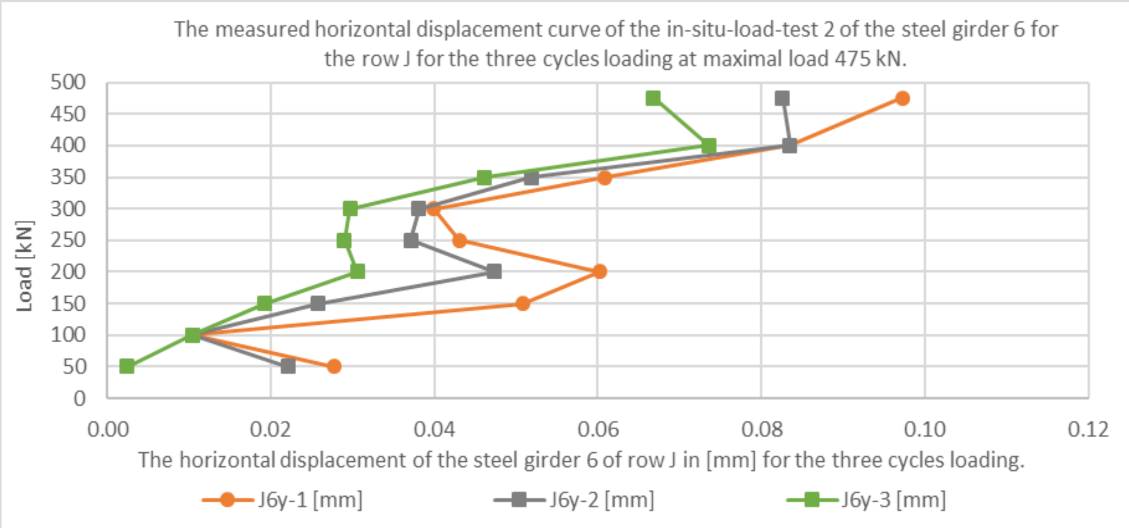

Figure 6-29: The measured horizontal displacement curve of in-situ-load-test 2 of steel girder 6 for row J for the three loading cycles.

<u>The results of the numerical simulation of the transverse direction versus the in-situ-load-test:</u>

In this section the results of the numerical simulation will be added and compared with the in-situ-load-test specifically for the transverse direction and for the mid-span. In figures 6-30 / 6-31 and tables 6-16 until 6-21 the horizontal displacement is presented for row J which is the normative row for bridge deck A. In the tables 6-16 until 6-21 the values of the in-situ-load-test versus the numerical simulation values and their ratio are added for each steel girder in the transverse direction. In the figures 6-30 / 6-31 the measured horizontal displacement versus the numerical simulated values for all the rows is presented. The results will be described a discussed in the sub-paragraph of the discussion part.

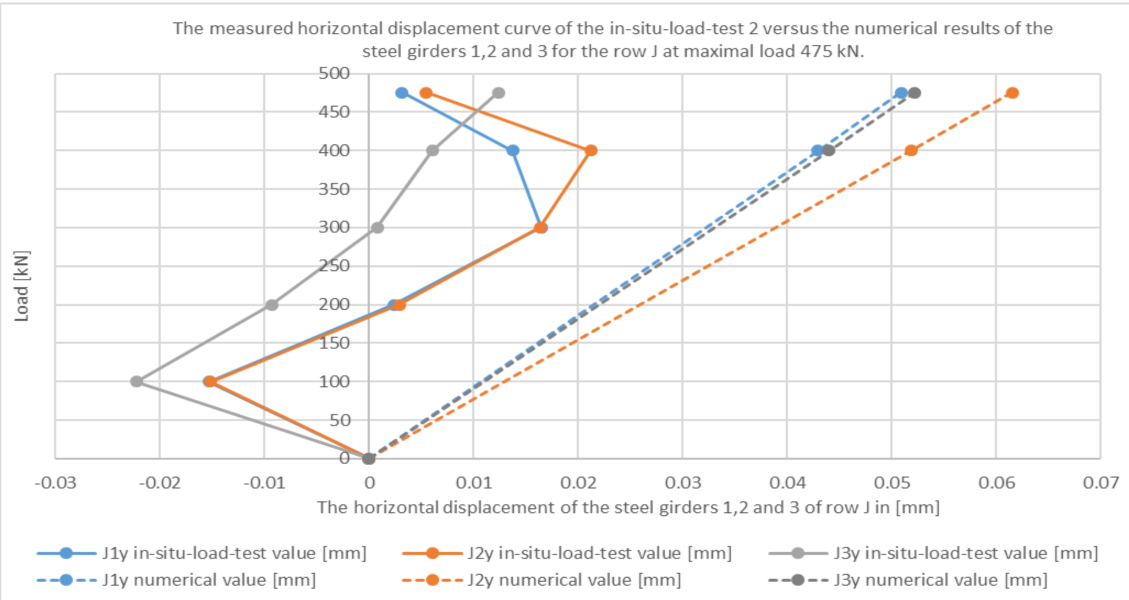

Figure 6-30: The measured horizontal displacement curve of the in-situ-load-test 2 versus the numerical results of the steel girders 1,2 and 3 for the row J at maximal load 475 kN.

Table 6-16: The numerical values versus the in-situ-load and the ratio for steel girder 1.

Load [kN]	J1y numerical values [mm]	J1y in-situ-load-test values [mm]	Ratio
0	0	0	0
400	0.0429	0.01376	32%
475	0.0509	0.00314	6%

Table 6-17: The numerical values versus the in-situ-load and the ratio for steel girder 2.

Load [kN]	J2y numerical values [mm]	J2y in-situ-load-test values [mm]	Ratio
0	0	0	0
400	0.0519	0.02121	41%
475	0.0615	0.00549	9%

Table 6-18: The numerical values versus the in-situ-load and the ratio for steel girder 3.

Load [kN]	J3y numerical values [mm]	J3y in-situ-load-test values [mm]	Ratio
0	0	0	0
400	0.0440	0.00605	14%
475	0.0522	0.01235	24%

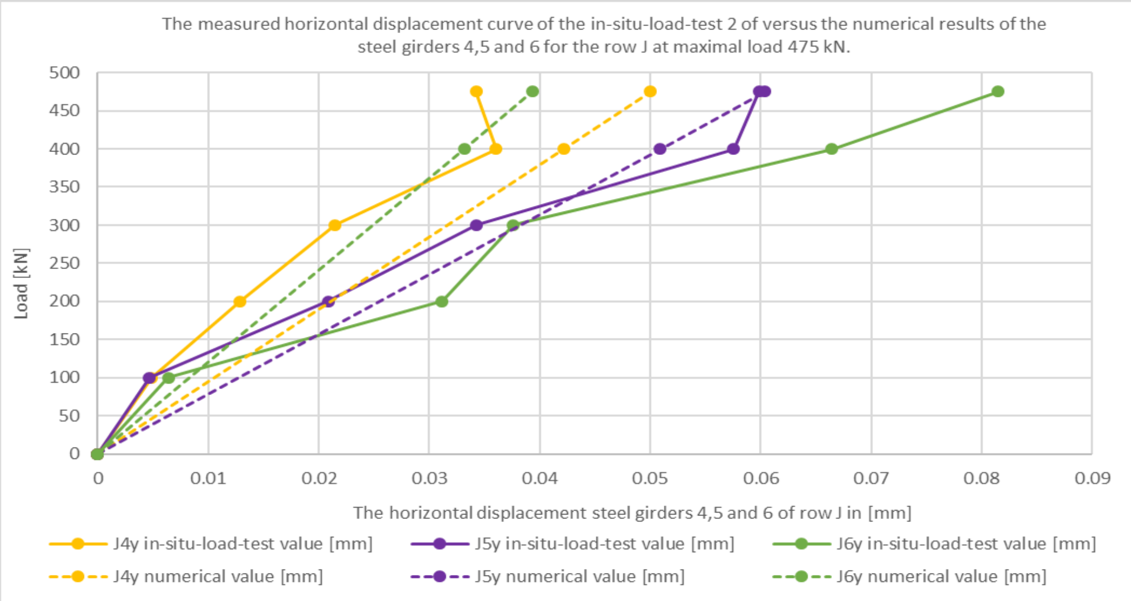

Figure 6-31: The measured horizontal displacement curve of the in-situ-load-test 2 versus the numerical results of the steel girders 4,5 and 6 for the row J at maximal load 475 kN.

Table 6-19: The numerical values versus the in-situ-load and the ratio for steel girder 4.

Load [kN]	J4y numerical values [mm]	J4y in-situ-load-test values [mm]	Ratio
0	0	0	0
400	0.0422	0.03605	85%
475	0.0500	0.03424	68%

Table 6-20: The numerical values versus the in-situ-load and the ratio for steel girder 5.

Load [kN]	J5y numerical values [mm]	J5y in-situ-load-test values [mm]	Ratio
0	0	0	0
400	0.0509	0.05756	113%
475	0.0604	0.05986	99%

Table 6-21: The numerical values versus the in-situ-load and the ratio for steel girder 6.

Load [kN]	J6y numerical values [mm]	J6y in-situ-load-test values [mm]	Ratio
0	0	0	0
400	0.0331	0.06643	200%
475	0.0393	0.08149	207%

Improvement of the strut and tie based on the carried out numerical simulation in the transverse direction:

To improve the strut and tie model in the transverse direction the mid-span of the bridge deck is used. This is done to simulate the load displacement in the plane of the transverse direction. The maximal principal stress (S_3) of concrete and steel which is obtained from the numerical simulation is presented in figures 6-32 / 6-34. The numerical values are compared with the maximal allowable compressive stress of concrete. This is also done for the shear stress of concrete and those results can be seen in figure 6-34 and the table 6-23. In addition to this, the analytical model of strut and tie will be analysed and compared with numerical simulations of the transverse direction. This will be done for the mid-span. The assumption which has been used to calculate the model has been added in this paragraph by including the Eurocode 2.

Table 6-22: The maximal principal stress of concrete versus the compressive stress.

Load	**The numerical results of the principal stress of the concrete in [N/mm^2]**	**Maximal allowable compressive stress of concrete(f_{cd}) in [N/mm^2]**	**Ratio**
0	0	0	0 %
475	-9.5	-36.7	26 %

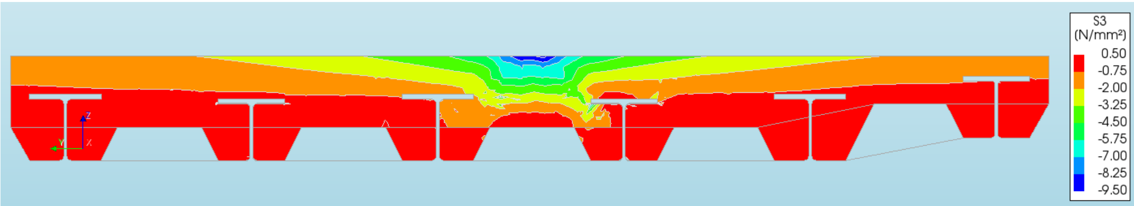

Figure 6-32: The numerical results of the principal stress in the concrete for a load of 475 kN in the z-direction.

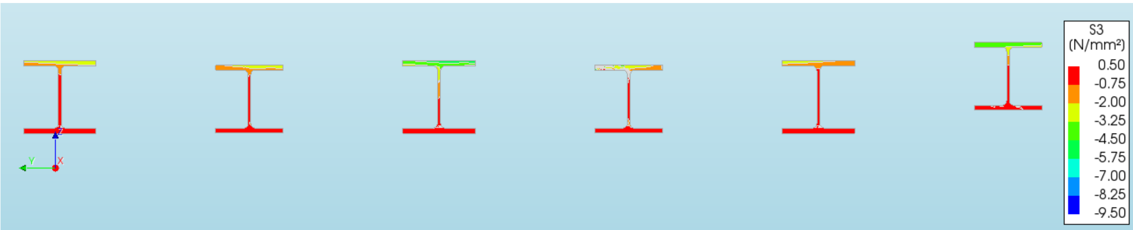

Figure 6-33: The numerical results of the principal stress in the steel girders for a load of 475 kN in the z-direction.

Table 6-23: The maximal shear stress of concrete versus the allowable shear stress of concrete.

Load	**The numerical results of the principal stress of the concrete in [N/mm^2]**	**Maximal allowable shear stress of concrete in [N/mm^2]**	**Ratio**
0	0	0	0 %
475	3.8	7.2	52 %

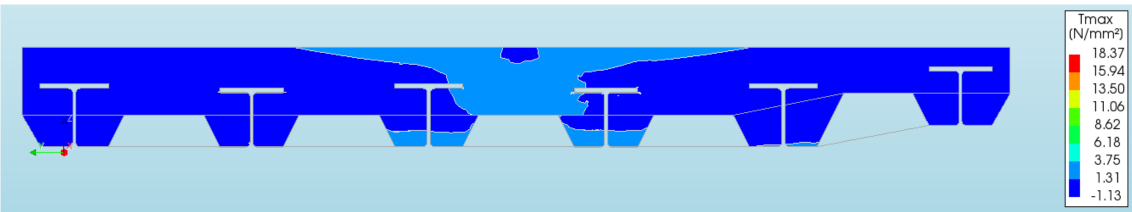

Figure 6-34: The numerical results of the shear stress in the concrete for a load of 475 kN in the z-direction.

The analytical model of the transverse direction:

In this section the analytical model is carried out and the stresses of steel and concrete will be calculated based on the strut and tie model, and those results will be compared with the numerical simulations in the transverse direction. In the figure 6-37 the load transfers in the transverse direction are presented based on the following assumptions:

a) The angle which is needed to reach equilibrium in the nodes will be carried out in the calculations;
b) The length where the load is transferred in the transverse direction can be seen in figure 6-37;

c) The assumed width is based on the spread plane in the longitudinal direction, the made calculation will be presented;
d) The Tie component is ignored because the concrete will not transfer the force, there is no reinforcement available in the cross-section;
e) The allowable strength of concrete in the strut region based on the Eurocode is presented in the figure 6-35 which is obtained from the Eurocode:

The allowable strength for a concrete strut in a region with transverse compressive stress can be calculated based on the formulas which are presented below with the figure 6-35. This is obtained from the Eurocode. In the numerical simulation there is only compressive stress available see figure 6-32 (Het Nederlands Normalisatie-instituut, 2020).

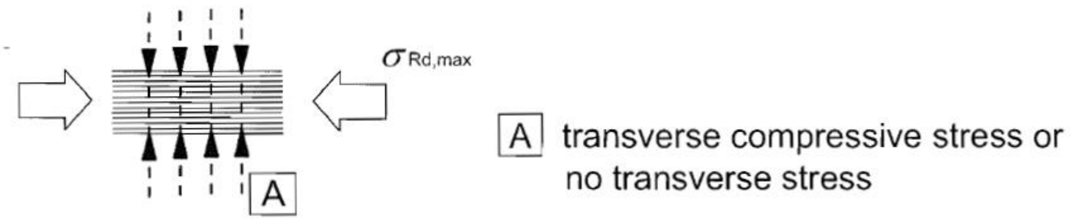

Figure 6-35: The rules to implement the strut conform the Eurocode 2 (Het Nederlands Normalisatie-instituut, 2020).

$$\sigma_{Rd,max} = f_{cd} \quad : (6.1)$$

Note: It may be appropriate to assume a higher allowable strength in regions where multi-axial compression exists (Het Nederlands Normalisatie-instituut, 2020).

f) The design of the node will be done based on the rules from the Eurocode 2 which are described in the figure 6-36. The forces which are defined in the figure are depending on the angle which will lead to equilibrium and this will be carried out in the coming calculation. The allowable strength of concrete depends on the presented formulas 6.4 and 6.5 for concrete (Het Nederlands Normalisatie-instituut, 2020).

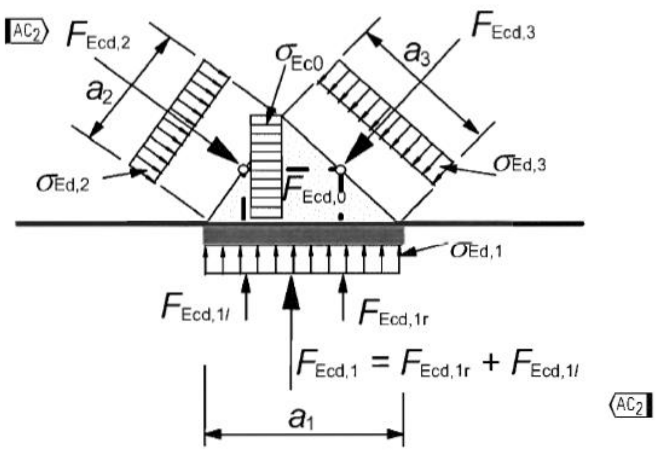

Figure 6-36: The rules to implement the node conform the Eurocode 2 where only compressive stress are available. (Het Nederlands Normalisatie-instituut, 2020).

$$\sigma_{Rd,max} = k_1 * \nu * f_{Ecd} \quad : (6.4)$$

$$\nu = 1 - \frac{f_{cd}}{250} \quad : (6.5)$$

Note: The recommended value of k_1 is 1.0. where $\sigma_{Rd,max}$ is the maximum stress which can be applied at the edges of the node (Het Nederlands Normalisatie-instituut, 2020).

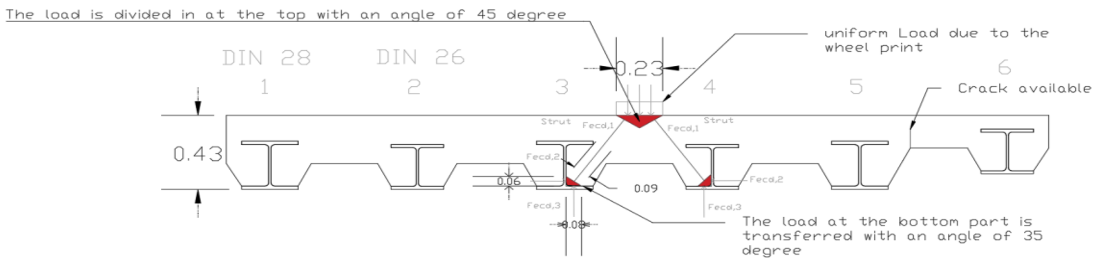

Figure 6-37: Appling the strut and tie model in the transverse direction with an angle of 21.5 degree.

The calculation which will be carried out to validate the strut and tie model will be presented in following formulas for concrete and steel:

a) **Calculating the strut for the concrete region and comparing it with numerical simulations and testing it to the allowable stress of the concrete in the two defined nodes.**

Defining the strut load based on an angle of 45 degrees in the top node in concrete (see figure 6-37):

$$F_{strut(ecd1)} = F_{total} * \cos(45) = 475\ \text{kN} * \cos(45) = 335.88\ \text{kN} \ : (6.6)$$

Defining the component of the strut load based on an angle of 35 degrees (see figure 6-37) which has been assumed from the made sketch (which illustrate the load transfers in transverse direction), in figure 6-37 at the bottom node of the deck:

$$F_{strut(ecd2)} = F_{strut(ecd1)} * \cos(35) = 335.88\ \text{kN} * \cos(35) = 275.14\ \text{kN} : (6.7)$$

$$F_{strut(ecd3)} = F_{strut(ecd1)} * \sin(35) = 335.88\ \text{kN} * \sin(35) = 192.66\ \text{kN} \ : (6.8)$$

The two nodes will be tested based on the obtained stress from the numerical simulations and the calculated stress by assuming the width only. See table 6-31 for the information which is obtained from the sketch in figure 6-37.

The calculated width is shown in the following steps and in figure 6-38:

$$\text{a} = \text{Center to center} = 730\ mm : (6.9)$$

$$\text{b} = \text{Width of the wheel print} = 230\ mm : (6.10)$$

$$\text{c} = \text{Length of the wheel print} = 300\ mm : (6.11)$$

$$x = \frac{a}{2} = \frac{730\ mm}{2} = 365\ mm : (6.12)$$

$$y = x - \frac{b}{2} = 365 - \frac{230}{2} = 250\ mm \ : (6.13)$$

$$w = y \text{ x } 2 + c = 250 \text{ x } 2 + 300 = 800\ mm \ : (6.14)$$

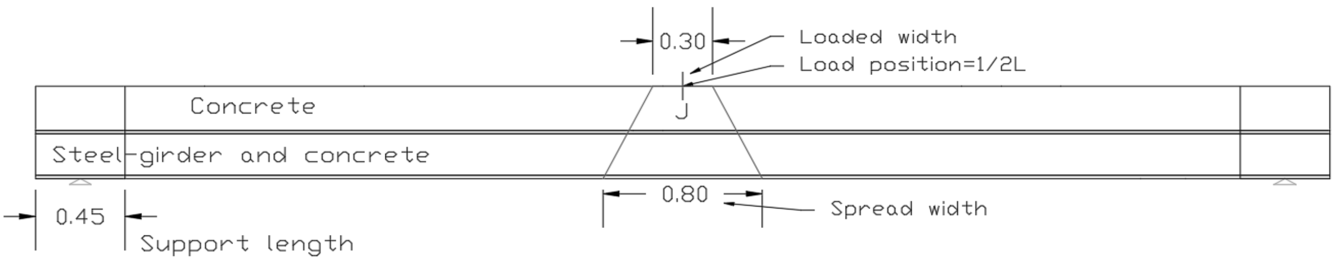

Figure 6-38: The calculated width based on the spread of the load.

Table 6-24: The different distance available in the nodes (Top and bottom).

Material	**Distance in [mm]**		**Width in the longitudinal direction b_{strut} in [mm]**
Top node	a_1	115	300
Bottom node	a_1	90	800
	a_2	60	800
	a_3	80	800

Calculating the strut area for both nodes (top and bottom, see figure 6-37):

$$A_{top} = a_1 * b_{strut} = 115 \text{ mm} * 300 \text{ mm} = 34500 \text{ mm}^2 \quad : (6.15)$$

$$A_{bottum\ 2} = a_2 * b_{strut} = 60 \text{ mm} * 800 \text{ mm} = 48000 \text{ mm}^2 \quad : (6.16)$$

$$A_{bottum\ 3} = a_3 * b_{strut} = 80 \text{ mm} * 800 \text{ mm} = 64000 \text{ mm}^2 \quad : (6.17)$$

Calculating the stress of the strut in the concrete region for both nodes:

$$\sigma_{top} = \frac{F_{strut\,(ecd1)}}{A_{top}} = \frac{335880\ N}{34500\ mm^2} = 9.74\frac{N}{mm^2} \quad : (6.18)$$

$$\sigma_{bottum\ 2} = \frac{F_{strut\,(ecd2)}}{A_{bottum\ 2}} = \frac{275140\ N}{48000\ mm^2} = 5.74\frac{N}{mm^2} \quad : (6.19)$$

$$\sigma_{bottum\ 3} = \frac{F_{strut\,(ecd3)}}{A_{bottum\ 3}} = \frac{192660\ N}{64000\ mm^2} = 3.01\frac{N}{mm^2} \quad : (6.20)$$

Comparing the values with the numerical simulations and the allowable concrete stress for the top node:

Table 6-25: The maximal principal stress of concrete versus the calculated analytical and allowable compressive stress at the top node.

Load	**The numerical results of the principal stress of the concrete in [N/mm2]**	**Result of the analytical model (strut at the concrete region) in [N/mm2]**	**The allowable concrete stress in [N/mm2]**
$F_{strut\,(ecd1)}$	-9.5	-9.74	-36.7

Calculating the allowable maximal stress of concrete based on the previous formulas which are presented in point f:

$$f_{cd} = 36.7 \ \frac{N}{mm^2} : (6.21)$$

$$v = 1 - \frac{f_{cd}}{250} = 1 - \frac{36.7}{250} = 0.8532 : (6.22)$$

$$\sigma_{Rd,max} = 0.6 * v * f_{cd} = 0.6 * 0.8532 * 36.7 = 18.79 \frac{N}{mm^2} \quad : (6.23)$$

Comparing the values with the numerical simulation and the allowable calculated concrete stress for the bottom node:

Table 6-26: The maximal principal stress of concrete versus the calculated analytical and allowable compressive stress at the bottom node.

Load	**The numerical results of the principal stress of the concrete in [N/mm2]**	**Result of the analytical model (strut at the concrete region) in [N/mm2]**	**The allowable concrete stress in [N/mm2]**
$F_{strut\,(ecd2)}$	-1.2	-5.74	-18.79
$F_{strut\,(ecd3)}$	-1.2	-3.01	-18.79

The calculated stresses of concrete from the analytical model and numerical simulation are very low, and lower than the allowable compressive stress.

b) Calculating the strut for the steel region and comparing it with numerical simulations and testing it to the allowable stress of the steel.

Table 6-27: The different distance available in the nodes (Top and bottom).

Material	Distance in [mm]		Width in the longitudinal direction b_{strut} in [mm]
Bottom node	a_2	60	800
	a_3	80	800

Calculating the strut area for the bottom node in the steel region:

$$A_{bottum\ 2} = a_2 * b_{strut} = 60\ \text{mm} * 800\ \text{mm} = 48000\ \text{mm}^2 \ : (6.24)$$

$$A_{bottum\ 3} = a_3 * b_{strut} = 80\ \text{mm} * 800\ \text{mm} = 64000\ \text{mm}^2 \ : (6.25)$$

Calculating the stress of the strut in the steel region:

The loads which have been used are the same as which are defined in the concrete, see formulas 6.6/6.7 and 6.8.

$$\sigma_{bottum\ 2} = \frac{F_{strut(ecd2)}}{A_{bottum\ 2}} = \frac{275140\ N}{48000\ mm^2} = 5.74\frac{N}{mm^2} \ : (6.26)$$

$$\sigma_{bottum\ 3} = \frac{F_{strut(ecd3)}}{A_{bottum\ 3}} = \frac{192660\ N}{64000\ mm^2} = 3.01\frac{N}{mm^2} \ : (6.27)$$

Comparing the values with the numerical simulations and the allowable steel stress:

Table 6-28: The maximal principal stress of steel versus the calculated analytical and allowable compressive stress at the bottom node.

Load	The numerical results of the principal stress of the steel in [N/mm2]	Result of the analytical model on the steel girder in [N/mm2]	The allowable steel stress in [N/mm2]
$F_{strut(ecd2)}$	-1.2	-5.74	-235
$F_{strut(ecd3)}$	-1.2	-3.01	-235

The calculated steel stresses from the analytical model and the obtained results from the numerical simulation for the steel girder web and the flange are lower than the allowable steel stresses.

6.3. Discussion of the linear analysis of bridge deck A

The input to the model as mentioned before can be found in chapter 5. The 3D FEA-model of bridge deck A which has been used in this chapter is validated to the results of the separated beam and the in-situ-load-test. The calibration of the separated beam can be found in the previous chapter.

The numerical results of the vertical displacement and strain of steel girder 4 in the 3D FEA-model of bridge deck A are almost the same as the numerical results of the separated beam and the in-situ-load-test. This is the case for the three in-situ-load-tests which are simulated. For the mid-span this can be seen in tables 6-11 and 6-12. The range of the variation between the results of the vertical displacement of the numerical simulation of the separated beam (steel girder 4) and the FEA-simulation of the 3D bridge deck is 1%. The variation of the vertical displacement between the in-situ-load-tests and the simulated 3D FEA-model of the bridge deck is in the range of 5%.

However, the strains in the simulated 3D FEA-model of the bridge deck are stiffer than the measured strains during the three in-situ-load-tests. This is due to the effect of the restrained supports, which limits the movement of the strains at the supports. There is also a difference between the strain of the 2D model and 3D model, which is around the 20 %. This due to the difference in the used FEA-models.

The results of the steel girder 4 are validated based on the measured data of the three in-situ-load-tests. As mentioned before by steel girder 4, the same results hold also for steel girder 4.

a) The vertical displacements are validated in a range of 5%;
b) The strains are stiffer due to the restrained supports.

These are the results of the longitudinal direction of the 3D bridge deck A model which is validated with the in-situ-load-tests and the simulated separated decisive beam (steel girder 4). The validation of the results of the numerical simulation for loaded point J can be seen in the previous tables for the in-situ-load-test 2, which are presented in sub-chapter 6.2. The other loaded points (H and L) are added in appendix E.

The vertical displacement of the transverse direction for in-situ-load-test 2 is validated in a range of 5%, except for steel girder 5 and 6 because of the available crack between the two beams which can be seen in figure 6-39. The range is higher than 5%, but this is due to the available crack as mentioned before. This can be seen in figures 6-8 and 6-13.

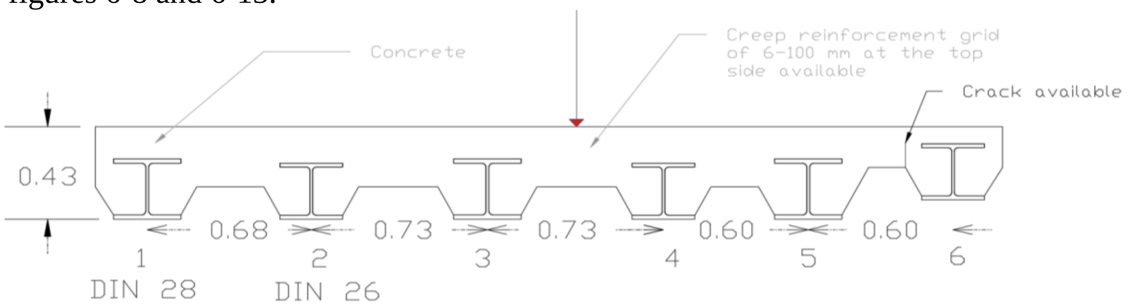

Figure 6-39: The loaded points (H ,J and L) on the bridge deck in the transvers direction of the bridge deck.

For the other in-situ-load-tests this is not the case because the crack is available only in the mid-span and not at the outer side of the bridge deck. The influence of the crack on row H and L is smaller than on row J at the mid-span. Besides that, at the supports there is also a fully integrated concrete beam over the whole length and width of the support (abutment and Pillar). See figure 6-40.
The available concrete beam in the transverse direction has also influence on the vertical displacement of the other made in-situ-load-tests.

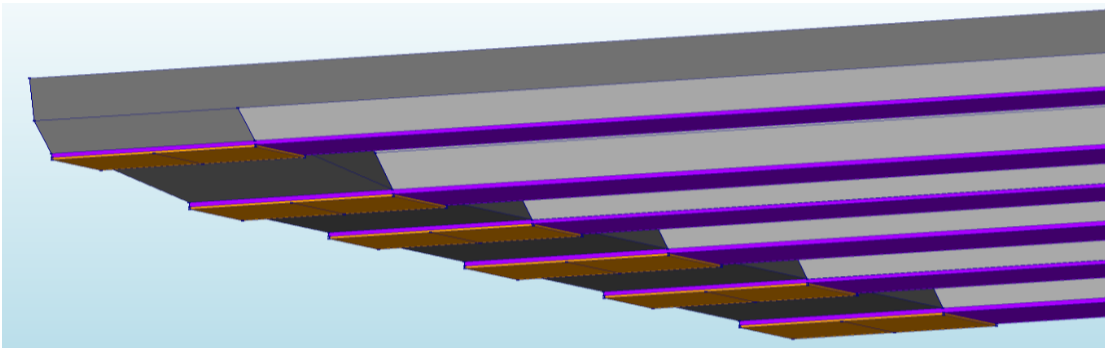

Figure 6-40: The available concrete beam in the transverse direction.

Regarding the strain, the same observation holds as for the three rows in the longitudinal direction of the simulated separated beam in chapter 5. This observation is: the strains of the numerical simulation are stiffer than the measured strains during the three in-situ-load-tests. This is due to the effect of the restrained supports.

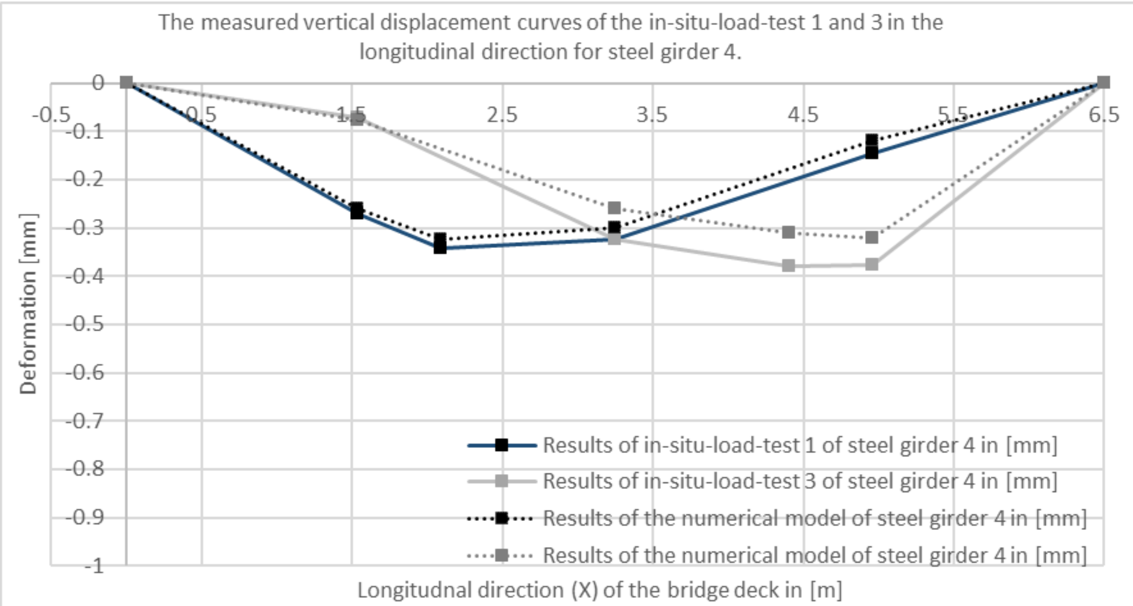

Figure 6-41: The measured vertical displacement curves for the in-situ-load-test 1 (loaded point H) and in-situ-load-test 3 (loaded points L) versus the numerical results in the longitudinal direction for steel girder 4.

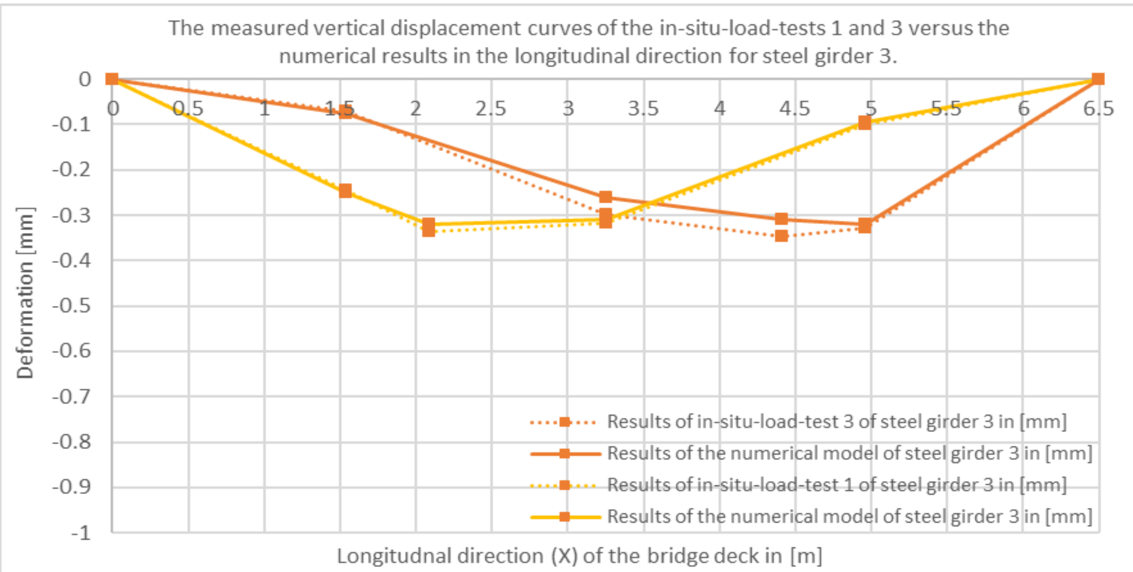

Figure 6-42: The measured vertical displacement curves for the in-situ-load-test 1 (loaded point H) and in-situ-load-test 3 (loaded points L) versus the numerical results in the longitudinal direction for steel girder 4.

In the figures 6-41 and 6-42 the numerical simulation of vertical displacement versus in-situ-load-test 1 and 3 is presented. The two tests are setup to validate the symmetry condition as mentioned before in chapter 4 (the in-situ-load-test). During the in-situ-load-test the measured vertical displacement is not symmetrical at all, this is due to the stuck concrete beam at the abutment. During the FEA-simulation this is also considered and the results are also not symmetrical. The vertical displacement is validated in a range of 5 % in the longitudinal direction. The assumption that the bridge deck is not symmetrical is validated. This is also the case for the separated beam, see previous chapter. The rest of the results of the numerical simulation of the two loaded positions H and L are added in appendix E.

In addition to this, the next step is to analyse the stress state of concrete and steel and to look at the load-bearing capacity of the bridge deck and to define the failure which is available in the concrete and steel. Finally, the goal is to make a comparison between the inspections, in-situ-load-tests and the numerical simulations and to discuss this.

According to the inspection of bridge deck A and specifically on the side where the in-situ-load-test is done, there is no sign of:

a) Corrosions of the steel beams;
b) The material removals;
c) Leakage;
d) Small cracks.

There can be some micro cracks available on the side where the in-situ-load-test is made in the concrete which are not visible for the inspector, and which is therefore not added in the inspection report. During the in-situ-load-test there is an inspection made where it is considered that there is a longitudinal crack between steel girder 5 and 6, which can also be seen in the measured results of the in-situ-load-test and the comparison with the numerical simulation. See the previous discussion.
For the other parts of the deck there are defects available as:

a) Corrosions of the steel beams;
b) The material removals;
c) Leakage;
d) Small cracks.

The stress state of the bridge deck A is analysed and there are singularities available in the model which are mentioned in figures 6-18 and 6-19. In addition to this, the numerical result of the tensile principal stress of concrete is lower than the allowable tensile stress of the assumed concrete from the destructive inspections. The compressive principal stress of concrete which is obtained from the numerical model is also lower than the compressive strength of the assumed concrete from the destructive inspections. The results are not added because they are lower than the allowable stresses of steel and concrete, which leads to ignore them. This observation is made by the maximal 475 kN of the in-situ-load-test.

The maximal shear stress of concrete (which is presented in figures 6-22 and 6-23) is also small, which does not lead to punching shear or other shear failure. This is also validated from the in-situ-load-test, during the in-situ-load-test there is no observation of punching shear failure in the longitudinal direction or transverse direction. This is the case for all the three tests of the in-situ-load-test. See appendix E for the other numerical simulation of loaded point H and L.

The steel-girders are also analysed with the help of the FEA-simulations. From the FEA-simulations it follows that the principal tensile, compression and shear stress is lower than the maximal stress of the steel

based on the assumed steel capacity from destructive inspections of S235. This can be seen in figures 6-20 and 6-21 where the principal stress is presented, for the shear and compression they are very low which leads to ignore them. In addition to this, from the inspection it is observed that the material loss of steel is less than 2%, which is not high. This will not reduce the capacity of the steel-girders. Furthermore, there is corrosion of steel available in the part where the in-situ-load-test is made, and the rest of the bridge and especially the other parts of the bridge deck has shown the defects which are mentioned in chapter 2.3.3.
The available corrosion in steel has not an effect but leads to symptoms that the bottom flange of the steel girders is not in contact with the concrete. This observation leads to take into consideration that there is slip available.

In the figures 6-24 until 6-29 the different cycles of the horizontal displacement for each steel girder of row J are presented. In each figure it can be seen that the horizontal displacement is not the same for each load cycle. This can be explained because there is slip available between the steel girder and concrete. In addition to this, the horizontal displacement goes not back to the origin of the previous cycles, even though the load which has been used is very small and will not lead to yielding of the materials, because the stresses which are obtained from the numerical simulations are smaller than the allowable stresses of concrete and steel. Furthermore, there is a change in stiffness between 400 kN until 475 kN this can be seen for different steel girders. This will be discussed in the following part below.

The results of the displacement are almost in the non-linear range. From the figures 6-30 until 6-31 it can be seen that there is a distortion of the displacements from the load of 400 kN until 475 kN. The most logical interpretation for the horizontal displacement is that the steel girders *(upper flanges)* are sliding until they reach the concrete *(the gap between the flange and the embedded concrete has been assumed to be very small because the measured horizontal displacement is also small),* where the two materials in the transverse direction will be in contact and this leads to activate the concrete where the beam becomes stiffer. This is the explanation of the change in the stiffness of the curve in the horizontal displacement. For steel girder 6 the results are increasing only because of the available crack between steel girder 5 and 6. Comparing the measured results with numerical simulations, the numerical simulations deviate from the measured horizontal displacement and this leads to indicate that there is slip available in the transverse direction and this is validated.

The strut and tie model has been investigated in chapter 3. Based on the investigation which is done, the suspicion that the strut and tie model concept is available in the transverse direction is based on the following aspects:

a) The small effective width which is available in the historical bridge deck;
b) Assessment which is made in chapter 3 over the concept of strut and tie model;
c) The analytical calculation carried out in 6-2-1.

The strut and tie model in the transverse direction is carried out on the mid-span of the bridge deck. The analytical model and the numerical simulation which is made is observed and the materials are also tested to the allowable capacity to check if there is a failure at the load 475 kN.
The following observation is detected:

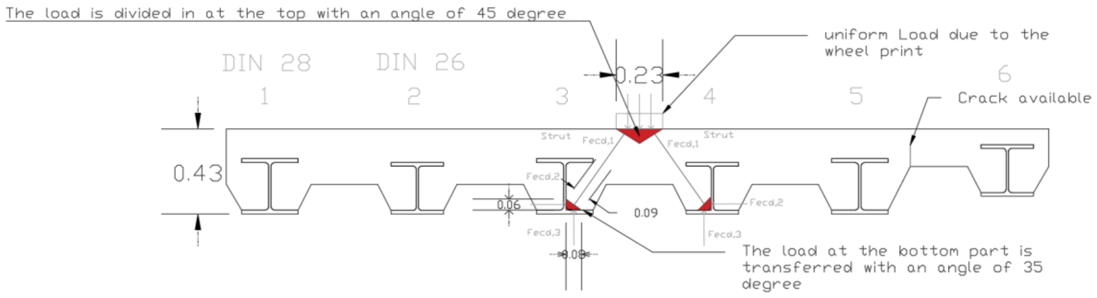

Figure 6-43: The scheme which shows the load transfers in the in the vertical plane of the concrete in the transverse direction of bridge deck A.

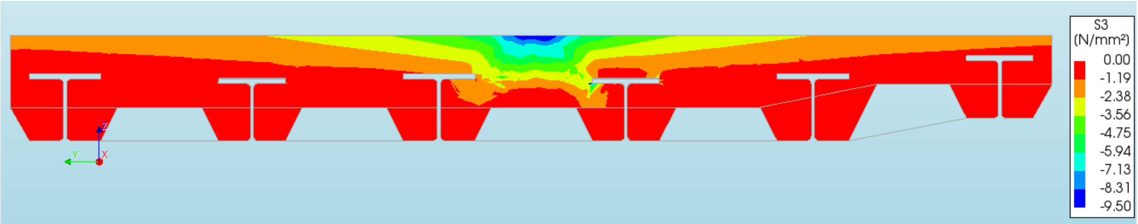

Figure 6-44: The numerical results of the principal stress in the concrete for a load of 475 kN in the z-direction.

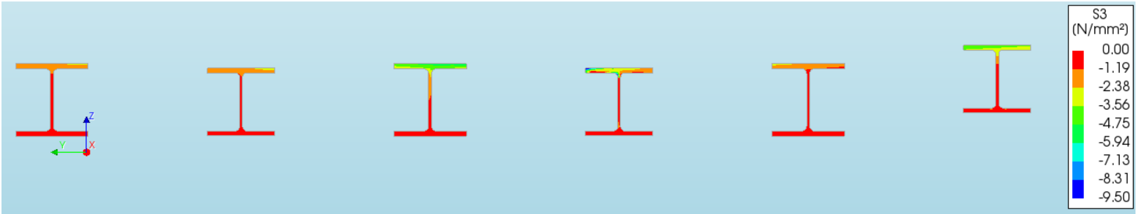

Figure 6-45: Principal stress in the steel in the transverse direction of bridge deck A.

Based on the figures 6-43 and 6-44 and the made analytical calculation in sub-chapter 6-2-1 it can be seen that the load is transferring with the same load path in the numerical simulation as in the exact drawn sketch (figure 6-43). In the numerical simulation, the different colours show how the strut is developing to the below flange of the steel girder. This leads to a validation that the strut and tie model is applicable in the transverse direction, but the tie in the analytical calculation is ignored because of the assumption that there is no reinforcement available in the cross section, see sub-chapter 6-2-1. In addition to this, due to the available slip between steel girders and concrete, which has been validated, the strut force has been directed to the corner of the steel flange and web.

The stress state of the analytical model is higher than stresses of the numerical simulations, because of the width which has been used, see the assumptions in sub-chapter 6-2-1. In addition to this, the stress state for each node in the numerical simulation is also tested to the allowable compressive stress of concrete, steel and compared with the analytical model. The stresses which are predicted in the nodes based on a load of 475 kN are much lower than the allowable stresses of concrete and steel. This can be validated from the in-situ-load-test where punching failure is not observed. The compressive stresses show no presence of crashing of the concrete during the inspection and during the in-situ-load-test. The obtained values can be seen in the sub-chapter 6-2-1 where the analytical model and the numerical simulation are carried out.

6.4. Conclusions of the linear analysis of the bridge deck A

Based on the 3D linear analysis which is made for the bridge deck the following conclusions can be taken for the longitudinal and the transverse direction:

The bridge deck is calibrated in both directions and the results are validated with the in-situ-load-tests. In addition to this, the result of the numerical simulation of the 3D FEA-model of bridge deck A is compared with the numerical separated beam. The comparison is validated in a range of 5%, which is acceptable. The conclusion from the separated beam hold also for bridge deck A in the longitudinal direction. That is:

a) The first part (from 0 kN until 400 kN) shows that there is sliding available. This means that there is no full interaction between that the between steel girder and concrete;
b) In the second part (from 400 kN until 475 kN) the deck becomes stiffer which leads to a change in the behaviour of the slip;
c) These conclusions are validated only for the single point load at the mid-span.

For bridge deck A as well as for the separated beam, the same conclusions about the stress states hold:

a) The difference ratio of the shear, comparison and tensile stresses is very low, and will not lead to failure;
b) This result is also validated based on the input from the in-situ-load-tests and the inspection of bridge A.

In the transverse direction there is slip available until 400 kN. After 400 kN to 475 kN there is change in stiffness which leads to a cooperation between steel girders and concrete. The available slip will influence the transport of the load in the transverse direction.

Finally, the conclusions which can be taken from the numerical simulation and the analytical model is that the strut and tie model is available in the transverse direction, which is validated from the numerical simulation and the analytical model. The force of the strut model is ending in the corner of the steel girder. The steel girders are then taking the force over. In addition to this, the produced stresses are smaller than the allowable stresses of concrete and steel at the nodes. The strut and tie model can be used to test the bridge deck in the transverse direction.

7. Evaluation and applying the behaviour of the historical Amsterdam bridge deck A on bridge deck B and C based on 3D-lineair simulations

7.1. Introduction

In this chapter the comparison between the three bridges is made in the longitudinal and transverse direction. Furthermore, the FEA-models are built up in the same way as the FEA-model of bridge deck A, the only difference is the geometry of the bridge decks and the support length of the bridge decks. This can be seen in chapter 5, where the three bridges are described. In the transverse direction the goal is to improve the strut and tie concept on the other two bridge decks and to present the influence of this model on these two bridge decks based on their configuration. The strut and tie model will also be used on the other two bridge decks (B and C) based on FEA-simulations and the analytical model. Bridge deck A is carried out in the previous chapter, only the main results will be added in this chapter to make the comparison. The stressed state of bridge deck A in the previous chapter is very low; however, bridge deck A is not stiffer than bridge deck B and C.

7.2. Application of the proposed linear elastic model on the other two chosen bridge decks

In this chapter the longitudinal direction will be compared based on the following quantities:

a) Vertical displacement;
b) Principal stress (tensile stress) in the concrete and steel;
c) Maximal shear stress in the concrete.

The quantities of the three bridges are presented in the figures 7-1 until 7-2 and tables 7-1 until 7-2. In the discussion part the comparison will be described and added.

Table 7-1: Results displacement of in-situ-load-test 2 versus numerical results for the three bridges of steel girder 4.

Vertical displacement of steel girder 4 in [mm]				
Load	**Results of in-situ-load-test 2**	**Results of the numerical model of steel girder 4 with a span 6.5 [m]**	**Results of the numerical model of steel girder 4 with a span 10 [m]**	**Results of the numerical model of steel girder 4 with a span 13 [m]**
0	0	0	0	0
400	0.53	0.51	0.90	1.37
475	0.58	0.61	1.07	1.63

Table 7-2: Results displacement of in-situ-load-test 2 versus numerical results for the three bridges of steel girder 4.

	Vertical displacement of steel girder 3in [mm			
Load	**Results of in-situ-load-test 2**	**Results of the numerical model of steel girder 3with a span 6.5 [m]**	**Results of the numerical model of steel girder 3with a span 10 [m]**	**Results of the numerical model of steel girder 3 with a span 13 [m]**
0	0	0	0	0
400	0.53	0.52	0.90	1.37
475	0.58	0.59	1.07	1.63

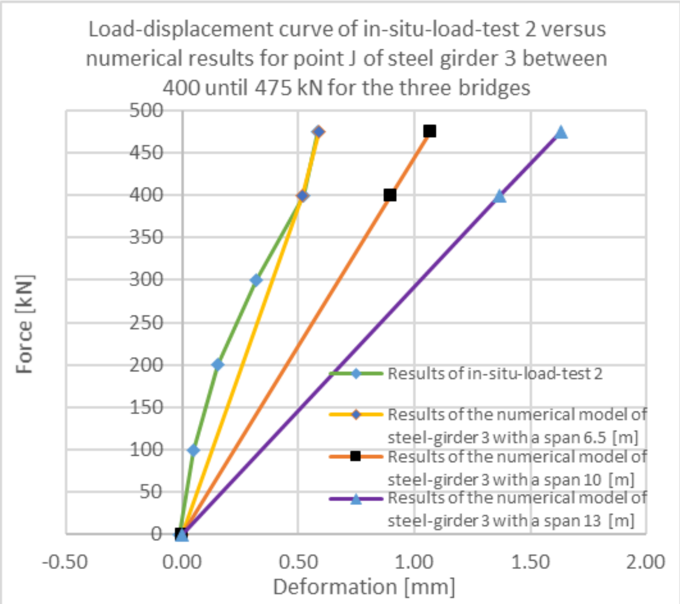

Figure 7-1: Load-displacement curve of in-situ-load-test 2 versus numerical results for point J of steel girder 3 between 400 until 475 kN for the three bridge decks.

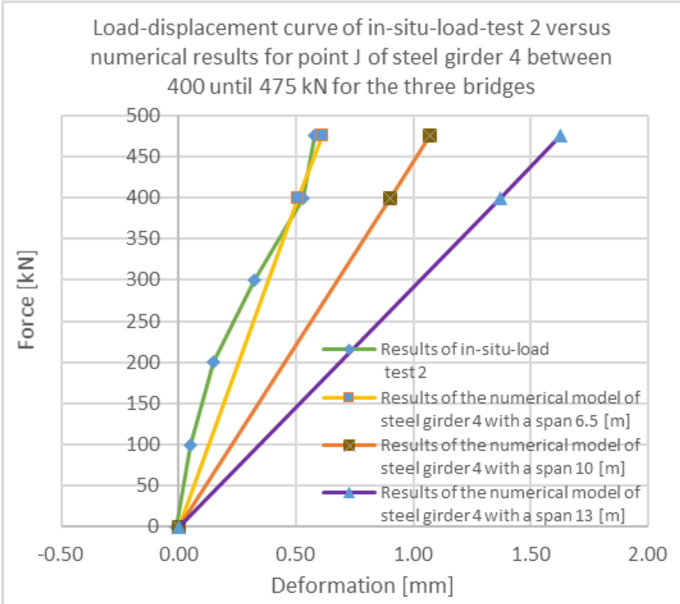

Figure 7-2: Load-displacement curve of in-situ-load-test 2 versus numerical results for point J of steel girder 4 between 400 until 475 kN for the three bridge decks.

Table 7-3: Results maximal principal stress of concrete for the three bridge decks.

Maximal principal stress of concrete in [N/mm²]			
Load	**Results of the maximal principal stress for the span 6.5 [m]**	**Results of the maximal principal stress for the span 10 [m]**	**Results of the maximal principal stress for the span 13 [m]**
0	0	0	0
400	3.03	3.33	3.28
475	3.60	3.95	3.89

Table 7-4: Results maximal shear stress of concrete for the three bridge decks.

Maximal principal stress of steel girder in [N/mm²]			
Load	**Results of the maximal principal stress for the span 6.5 [m]**	**Results of the maximal principal stress for the span 10 [m]**	**Results of the maximal principal stress for the span 13 [m]**
0	0	0	0
400	18.00	15.27	15.53
475	21.00	18.14	18.42

Table 7-5: Results maximal shear stress of concrete for the three bridge decks.

Maximal shear stress of concrete in [N/mm²]			
Load	**Results of the maximal shear stress for the span 6.5 [m]**	**Results of the maximal shear stress for the span 10 [m]**	**Results of the maximal shear stress for the span 13 [m]**
0	0	0	0
400	2.90	1.48	1.73
475	3.40	1.76	2.06

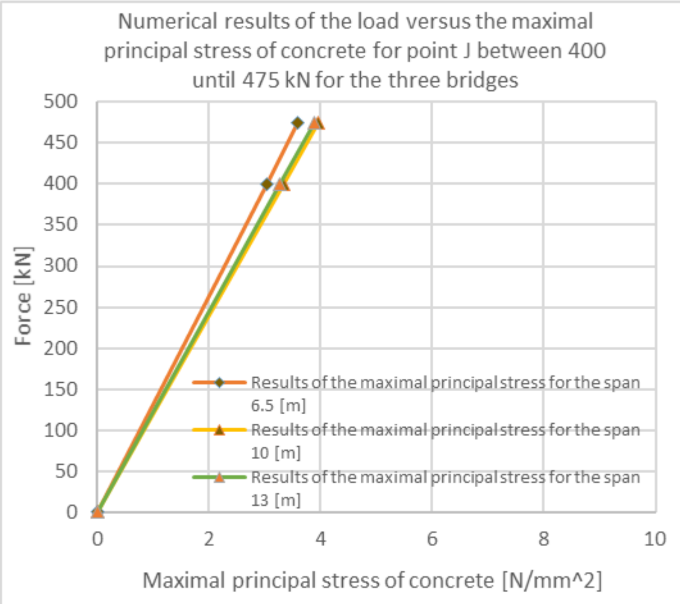

Figure 7-3: Numerical results of the load versus the maximal principal stress of concrete for point J between 400 until 475 kN for the three bridge decks.

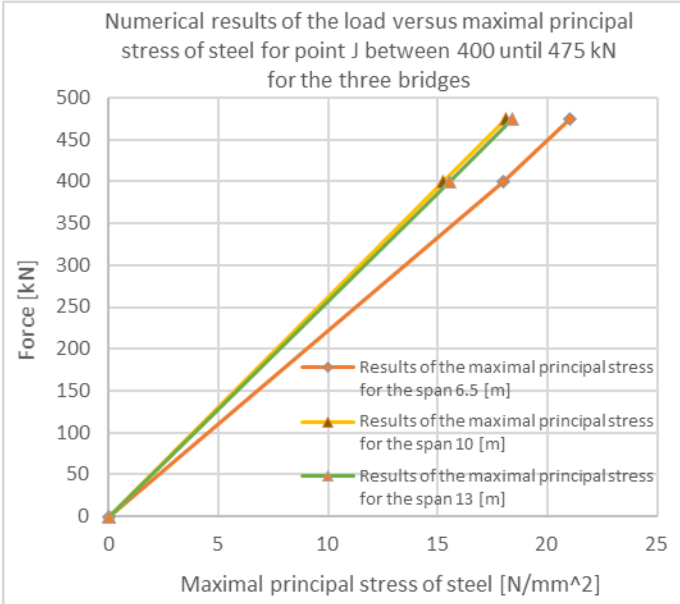

Figure 7-4: Numerical results of the load versus the maximal principal stress of steel for point J between 400 until 475 kN for the three bridge decks.

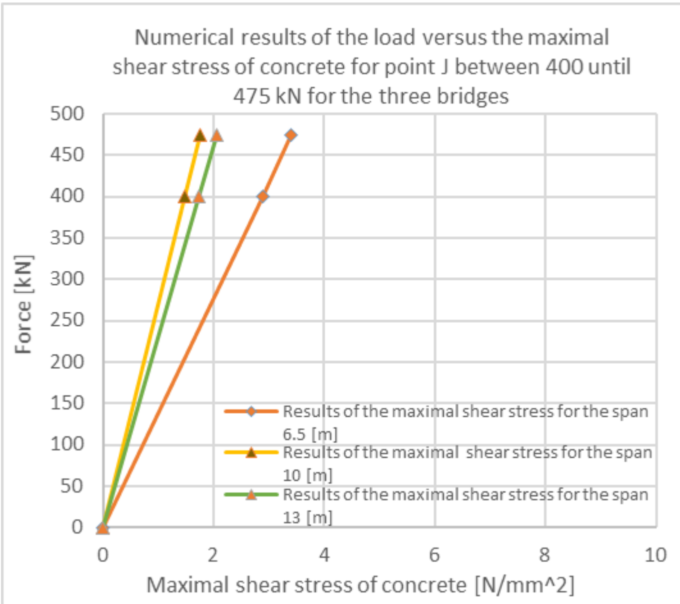

Figure 7-5: Numerical results of the load versus maximal shear stress of concrete for point J between 400 until 475 kN for the three bridge decks.

7.3. Improving the strut and tie model behaviour in the transverse direction compared with the three chosen bridge decks

1. Introduction:

In this section the strut and tie model will be simulated based on the FEA-models of the three bridge decks. The FEA-results will be tested based on the maximal allowable stresses of the material properties. In addition to this, the analytical model which is applied on bridge deck A will be used on the other two bridge decks (B and C) and will be compared with the numerical simulations. This will be carried out and discussed in the coming sub-chapter.

7.3.1. Results of bridge deck A in the transverse direction by using the strut and tie model

The compressive stress in the transverse direction of concrete of bridge deck A will be tested by the allowable compressive stress of concrete and steel.

Table 7-6: The maximal principal stress of concrete versus the compressive stress of bridge deck A.

Load	**The numerical results of the principal stress of the concrete in [N/mm^2]**	**Maximal allowable compressive stress of concrete(f_{cd}) in [N/mm^2]**	**Ratio**
0	0	0	0 %
475	-9.5	-36.7	26 %

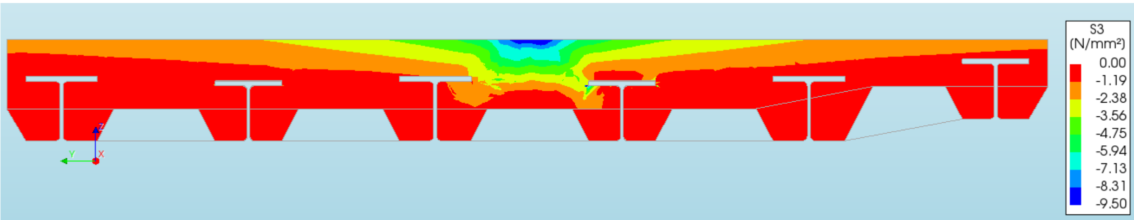

Figure 7-6: The maximal principal stress of concrete of bridge deck A.

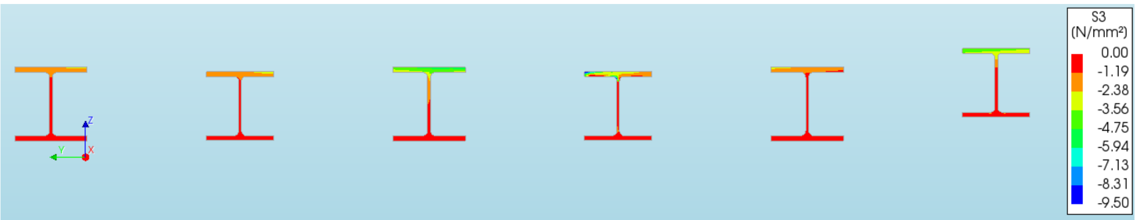

Figure 7-7: The maximal principal stress of steel of bridge deck A.

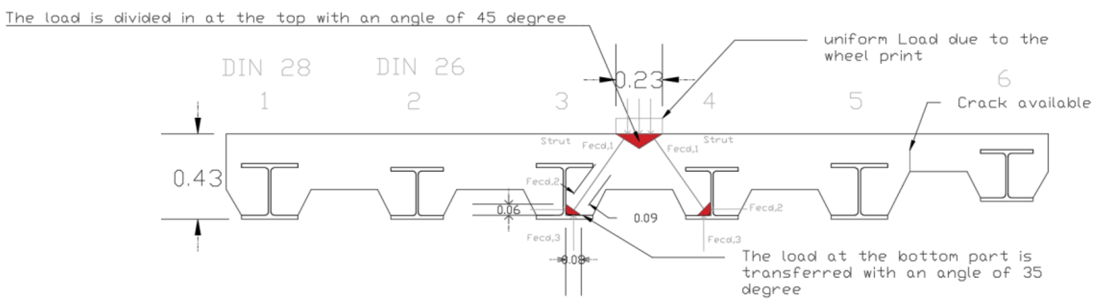

Figure 7-8: The scheme which shows the load transfers in the in the vertical plane of the concrete in the transverse direction of bridge deck B.

a) **Calculating the strut for the concrete region and comparing it with numerical simulations and testing it to the allowable stress of the concrete in the two defined nodes (top and bottom).**

Comparing the values with the numerical simulations and the allowable concrete stress for the top node:

Table 7-7: The maximal principal stress of concrete versus the calculated analytical and allowable compressive stress at the top node.

Load	The numerical results of the principal stress of the concrete in [N/mm2]	Result of the analytical model (strut at the concrete region) in [N/mm2]	The allowable concrete stress in [N/mm2]
$F_{strut(ecd1)}$	-9.5	-9.74	-36.7

Comparing the values with the numerical simulation and the allowable calculated concrete stress for the bottom node:

Table 7-8: The maximal principal stress of concrete versus the calculated analytical and allowable compressive stress at the bottom node.

Load	The numerical results of the principal stress of the concrete in [N/mm2]	Result of the analytical model (strut at the concrete region) in [N/mm2]	The allowable concrete stress in [N/mm2]
$F_{strut(ecd2)}$	-1.2	-5.74	-18.79
$F_{strut(ecd3)}$	-1.2	-3.01	-18.79

The calculated stresses of concrete from the analytical model and numerical simulation are very low, and lower than the allowable compressive stress.

b) **Calculating the strut for the steel region and comparing it with numerical simulations and testing it to the allowable stress of the steel.**

Comparing the values with the numerical simulations and the allowable steel stress:

Table 7-9: The maximal principal stress of steel versus the calculated analytical and allowable compressive stress at the bottom node.

Load	The numerical results of the principal stress of the steel in [N/mm2]	Result of the analytical model on the steel girder in [N/mm2]	The allowable steel stress in [N/mm2]
$F_{strut(ecd2)}$	-1.2	-5.74	-235
$F_{strut(ecd3)}$	-1.2	-3.01	-235

The calculated steel stresses from the analytical model and the obtained results from the numerical simulation for the steel girder web and the flange are lower than the allowable steel stresses.

7.3.2. Results of bridge deck B in the transverse direction by using the strut and tie model

The compressive stress in the transverse direction of concrete of the bridge deck B will be tested by the allowable compressive stress of concrete and steel.

Table 7-10: The maximal principal stress of concrete versus the compressive stress of bridge deck B.

Load	The numerical results of the principal stress of the concrete in [N/mm^2]	Maximal allowable compressive stress of concrete in [N/mm^2]	Ratio
0	0	0	0 %
475	-10	-36.7	28 %

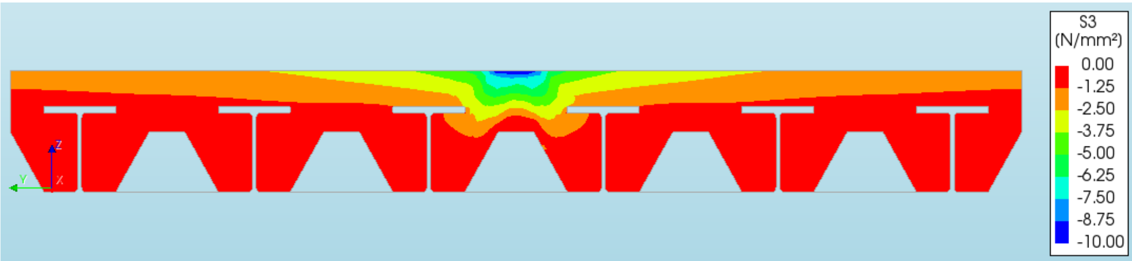

Figure 7-9: The maximal principal stress of concrete of bridge deck B.

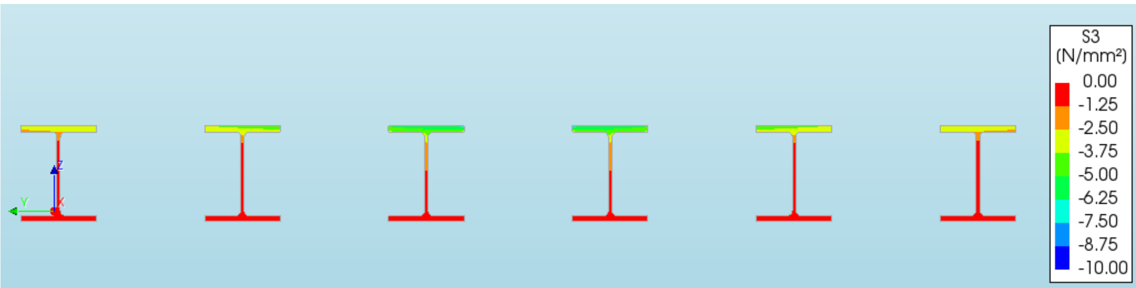

Figure 7-10: The maximal principal stress of steel of bridge deck B.

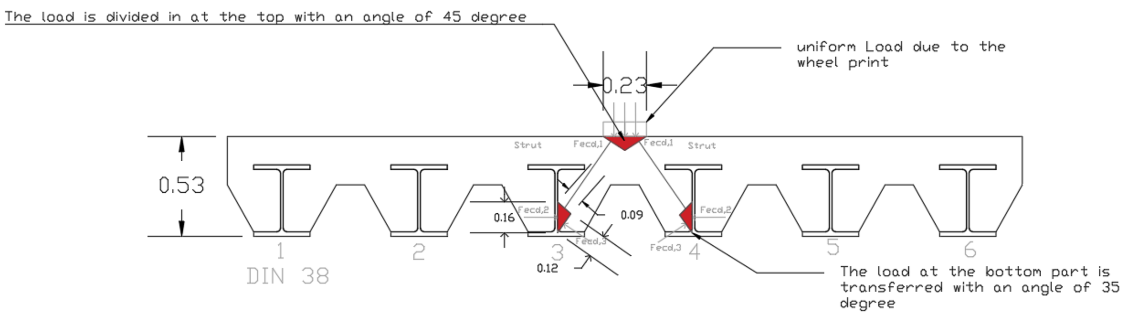

Figure 7-11: The scheme which shows the load transfers in the in the vertical plane of the concrete in the transverse direction of bridge deck B.

Due to the available slip in the transverse direction the force will slide to the corner in the cross section.

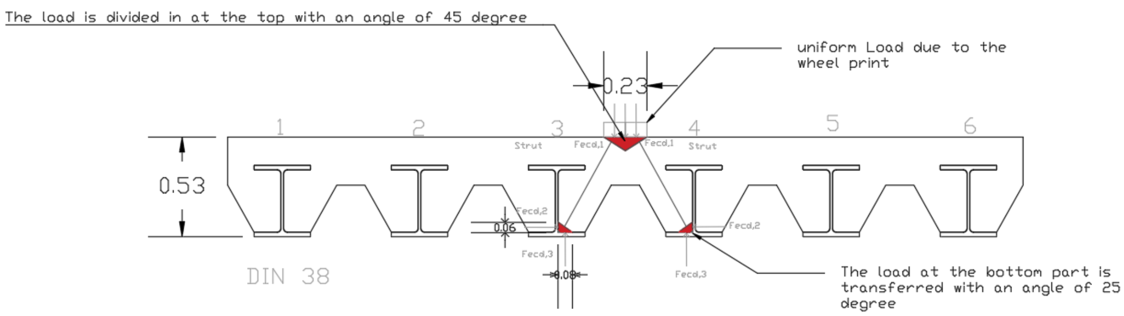

Figure 7-12: The scheme which shows the load transfers in the in the vertical plane of the concrete in the transverse direction of bridge deck B.

The calculation which will be carried out to validate the strut and tie model will be presented in following formulas for concrete and steel:

a) **Calculating the strut for the concrete region and comparing it with numerical simulations and testing it to the allowable stress of the concrete in the two defined nodes (top and bottom).**

Defining the strut load based on an angle of 45 degrees in the top node in concrete (see figure 7-12):

$$F_{strut(ecd1)} = F_{total} * \cos(45) = 475 \text{ kN} * \cos(45) = 335.88 \text{ kN} \; : (7.1)$$

Defining the component of the strut load based on an angle of 25 degrees (see figure 7-12) which has been assumed from the made sketch (which illustrate the load transfers in transverse direction) at the bottom node of the deck:

$$F_{strut(ecd2)} = F_{strut(ecd1)} * \cos(25) = 335.88 \text{ kN} * \cos(25) = 305 \text{ kN} : (7.2)$$

$$F_{strut(ecd3)} = F_{strut(ecd1)} * \sin(25) = 335.88 \text{ kN} * \sin(25) = 142 \text{ kN} \; : (7.3)$$

The two nodes will be tested based on the obtained stress from the numerical simulations and the calculated stress by assuming the width only. See table 7-11 for the information which is obtained from the sketch in figure 7-12. And for the calculation of the width see figure 7-13.

The calculated width is shown in the following steps and in figure 7-13:

$$\text{a} = \text{Center to center} = 730 \; mm : (7.4)$$

$$\text{b} = \text{Width of the wheel print} = 230 \; mm : (7.5)$$

$$\text{c} = \text{Length of the wheel print} = 300 \; mm : (7.6)$$

$$x = \frac{a}{2} = \frac{730 \; mm}{2} = 365 \; mm : (7.7)$$

$$y = x - \frac{b}{2} = 365 - \frac{230}{2} = 250 \; mm \; : (7.8)$$

$$w = y \text{ x } 2 + c = 250 \text{ x } 2 + 300 = 800 \; mm \; : (7.9)$$

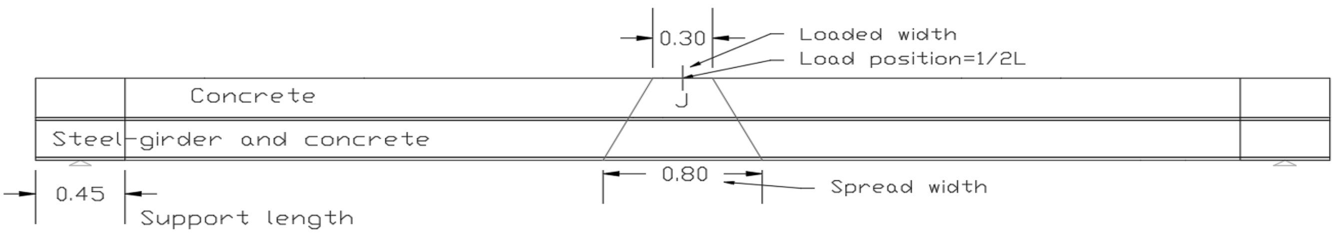

Figure 7-13: The calculated width based on the spread of the load.

Table 7-11: The different distance available in a the nodes (Top and bottom).

Material	Distance in [mm]		Width in the longitudinal direction b_{strut} in [mm]
Top node	a_1	115	300
Bottom node	a_1	90	800
	a_2	60	800
	a_3	80	800

Calculating the strut area for both nodes (top and bottom see figure 7-11):

$$A_{top} = a_1 * b_{strut} = 115 \text{ mm} * 300 \text{ mm} = 34500 \text{ mm}^2 \;:(7.10)$$

$$A_{bottum\ 2} = a_2 * b_{strut} = 60 \text{ mm} * 800 \text{ mm} = 48000 \text{ mm}^2 \;:(7.11)$$

$$A_{bottum\ 3} = a_3 * b_{strut} = 80 \text{ mm} * 800 \text{ mm} = 64000 \text{ mm}^2 \;:(7.12)$$

Calculating the stress of the strut in the concrete region for both nodes:

$$\sigma_{top} = \frac{F_{strut\,(ecd1)}}{A_{top}} = \frac{335880\ N}{34500\ mm^2} = 9.74\frac{N}{mm^2} \;:(7.13)$$

$$\sigma_{bottum\ 2} = \frac{F_{strut\,(ecd2)}}{A_{bottum\ 2}} = \frac{305000\ N}{48000\ mm^2} = 6.35\frac{N}{mm^2} \;:(7.14)$$

$$\sigma_{bottum\ 3} = \frac{F_{strut\,(ecd3)}}{A_{bottum\ 3}} = \frac{142000\ N}{64000\ mm^2} = 2.22\frac{N}{mm^2} \;:(7.15)$$

Comparing the values with the numerical simulations and the allowable concrete stress for the top node:

Table 7-12: The maximal principal stress of concrete versus the calculated analytical and allowable compressive stress at the top node.

Load	**The numerical results of the principal stress of the concrete in [N/mm2]**	**Result of the analytical model (strut at the concrete region) in [N/mm2]**	**The allowable concrete stress in [N/mm2]**
$F_{strut\,(ecd1)}$	-10	-9.74	-36.7

Calculating the allowable maximal stress of concrete based on the previous formulas which are presented in point f previous sub-chapter 6-2-1:

$$f_{cd} = 36.7\ \frac{N}{mm^2} \;:(7.16)$$

$$\nu = 1 - \frac{f_{cd}}{250} = 1 - \frac{36.7}{250} = 0.8532 \;:(7.17)$$

$$\sigma_{Rd,max} = 0.6 * \nu * f_{cd} = 0.6 * 0.8532 * 36.7 = 18.79\ \frac{N}{mm^2} \;:(7.18)$$

Comparing the values with the numerical simulation and the allowable calculated concrete stress for the bottom node:

Table 7-13: The maximal principal stress of concrete versus the calculated analytical and allowable compressive stress at the bottom node.

Load	**The numerical results of the principal stress of the concrete in [N/mm2]**	**Result of the analytical model (strut at the concrete region) in [N/mm2]**	**The allowable concrete stress in [N/mm2]**
$F_{strut\,(ecd2)}$	-1.25	-6.35	-18.79
$F_{strut\,(ecd3)}$	-1.25	-2.22	-18.79

The calculated stresses of concrete from the analytical model and numerical simulation are very low, and lower than the allowable compressive stress.

b) **Calculating the strut for the steel region and comparing it with numerical simulations and testing it to the allowable stress of the steel.**

Defining the component of the strut load based on an angle of 25 degrees which has been assumed from the made sketch (which illustrate the load transfers in transverse direction) in figure 7-12 at the bottom node of the deck:

$$F_{strut(ecd2)} = F_{strut(ecd1)} * \cos(25) = 335.88 \text{ kN} * \cos(25) = 305 \text{ kN} : (7.2)$$

$$F_{strut(ecd3)} = F_{strut(ecd1)} * \sin(25) = 335.88 \text{ kN} * \sin(25) = 142 \text{ kN} : (7.3)$$

Table 7-14: The different distance available in a nodes (Top and bottom).

Material	**Distance in [mm]**		**Width in the longitudinal direction b_{strut} in [mm]**
Bottom node	a_2	60	800
	a_3	80	800

Calculating the strut area for the bottom node in the steel region:

$$A_{bottum\ 2} = a_2 * b_{strut} = 60 \text{ mm} * 800 \text{ mm} = 48000 \text{ mm}^2 : (7.19)$$

$$A_{bottum\ 3} = a_3 * b_{strut} = 80 \text{ mm} * 800 \text{ mm} = 64000 \text{ mm}^2 : (7.20)$$

Calculating the stress of the strut in the steel region:

$$\sigma_{bottum\ 2} = \frac{F_{strut(ecd2)}}{A_{bottum\ 2}} = \frac{275140\ N}{48000\ mm^2} = 5.74 \frac{N}{mm^2} : (7.21)$$

$$\sigma_{bottum\ 3} = \frac{F_{strut(ecd3)}}{A_{bottum\ 3}} = \frac{192660\ N}{64000\ mm^2} = 3.01 \frac{N}{mm^2} : (7.22)$$

Comparing the values with the numerical simulations and the allowable steel stress:

Table 7-15: The maximal principal stress of steel versus the calculated analytical and allowable compressive stress at the bottom node.

Load	**The numerical results of the principal stress of the steel in [N/mm2]**	**Result of the analytical model on the steel girder in [N/mm2]**	**The allowable steel stress in [N/mm2]**
$F_{strut(ecd2)}$	-1.25	-6.35	235
$F_{strut(ecd3)}$	-1.25	-2.22	235

The calculated steel stresses from the analytical model and the obtained results from the numerical simulation for the steel girder web and flange are lower than the allowable steel stresses.

7.3.3. Results of bridge deck C in the transverse direction by using the strut and tie model

The compressive stress in the transverse direction of concrete of the bridge deck C will be tested by the allowable compressive stress of concrete and steel.

Table 7-16: The maximal principal stress of concrete versus the compressive stress of bridge deck C.

Load	The numerical results of the principal stress of the concrete in [N/mm^2]	Maximal allowable compressive stress of concrete in [N/mm^2]	Ratio
0	0	0	0 %
475	-13.5	-36.7	37 %

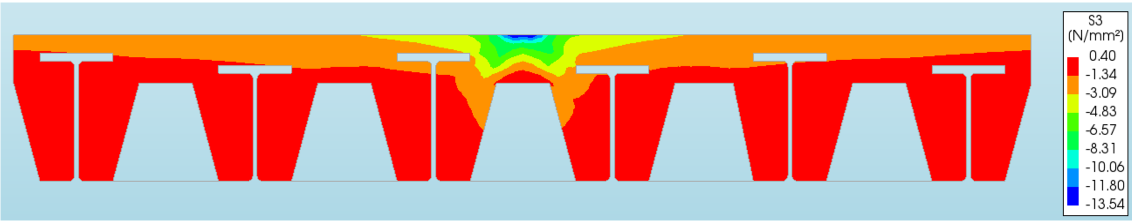

Figure 7-14: The maximal principal stress of concrete of bridge deck C.

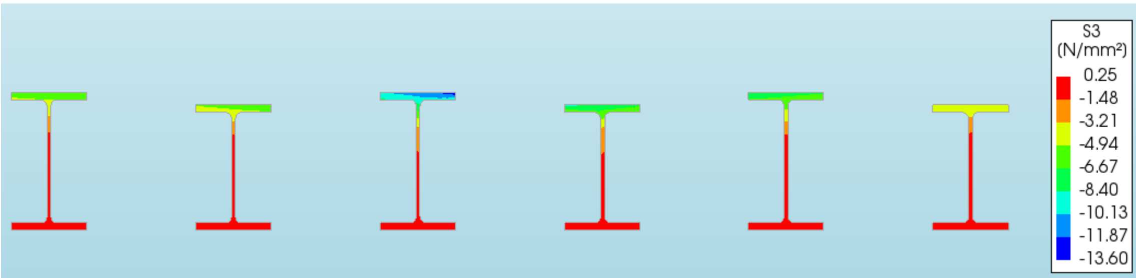

Figure 7-15: The maximal principal stress of steel of bridge deck C.

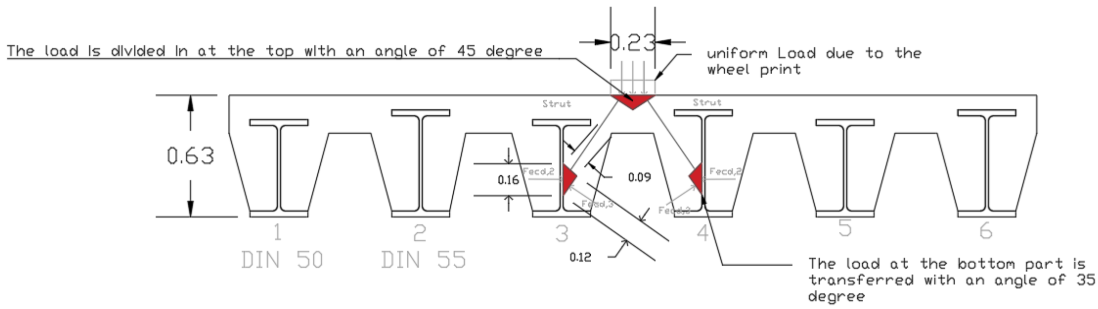

Figure 7-16: The scheme which shows the load transfers in the in the vertical plane of the concrete in the transverse direction of bridge deck C.

Due to the available slip in the transverse direction the force will slide to the corner in the cross section

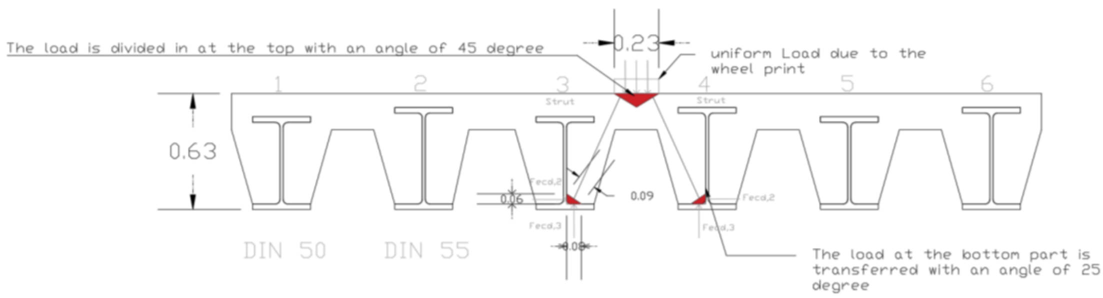

Figure 7-17: The scheme which shows the load transfers in the in the vertical plane of the concrete in the transverse direction of bridge deck C.

The calculation which will be carried out to validate the strut and tie model will be presented in following formulas for concrete and steel:

a) **Calculating the strut for the concrete region and comparing it with numerical simulations and testing it to the allowable stress of the concrete in the two defined nodes (top and bottom).**

Defining the strut load based on an angle of 45 degrees in the top node in concrete (see figure 7-17):

$$F_{strut(ecd1)} = F_{total} * \cos(45) = 475 \text{ kN} * \cos(45) = 335.88 \text{ kN} \; : (7.23)$$

Defining the component of the strut load based on an angle of 25 degrees (see figure 7-17) which has been assumed from the made sketch in figure 7-17 at the bottom node of the deck:

$$F_{strut(ecd2)} = F_{strut(ecd1)} * \cos(25) = 335.88 \text{ kN} * \cos(25) = 305 \text{ kN} : (7.24)$$

$$F_{strut(ecd3)} = F_{strut(ecd1)} * \sin(25) = 335.88 \text{ kN} * \sin(25) = 142 \text{ kN} \; : (7.25)$$

The two nodes will be tested based on the obtained stress from the numerical simulations and the calculated stress by assuming the width only. See table 7-17 for the information which are obtained from the sketch in figure 7-17.

For the calculation of the width see previous bridge deck B.

Table 7-17: The different distance available in a nodes (Top and bottom).

Material	Distance in [mm]		Width in the longitudinal direction b_{strut} in [mm]
Top node	a_1	115	300
Bottom node	a_1	90	800
	a_2	60	800
	a_3	80	800

Calculating the strut area for both nodes (top and bottom see figure 7-17):

$$A_{top} = a_1 * b_{strut} = 115 \text{ mm} * 300 \text{ mm} = 34500 \text{ mm}^2 \; : (7.26)$$

$$wA_{bottum\ 2} = a_2 * b_{strut} = 60 \text{ mm} * 800 \text{ mm} = 48000 \text{ mm}^2 \; : (7.27)$$

$$A_{bottum\ 3} = a_3 * b_{strut} = 80 \text{ mm} * 800 \text{ mm} = 64000 \text{ mm}^2 \; : (7.28)$$

Calculating the stress of the strut in the concrete region for both nodes:

$$\sigma_{top} = \frac{F_{strut\,(ecd1)}}{A_{top}} = \frac{335880\ N}{34500\ mm^2} = 9.74\frac{N}{mm^2} \; : (7.29)$$

$$\sigma_{bottum\ 2} = \frac{F_{strut\,(ecd2)}}{A_{bottum\ 2}} = \frac{305000\ N}{48000\ mm^2} = 6.35\frac{N}{mm^2} \; : (7.30)$$

$$\sigma_{bottum\ 3} = \frac{F_{strut\,(ecd3)}}{A_{bottum\ 3}} = \frac{142000\ N}{64000\ mm^2} = 2.22\frac{N}{mm^2} \; : (7.31)$$

Comparing the values with the numerical simulations and the allowable concrete stress for the top node:

Table 7-18: The maximal principal stress of concrete versus the calculated analytical and allowable compressive stress at the top node.

Load	The numerical results of the principal stress of the concrete in [N/mm2]	Result of the analytical model (strut at the concrete region) in [N/mm2]	The allowable concrete stress in [N/mm2]
$F_{strut\,(ecd1)}$	-13.5	-9.74	-36.7

Calculating the allowable maximal stress of concrete based on the previous formulas which are presented in point f, previous sub-chapter 6-2-1:

$$f_{cd} = 36.7 \ \frac{N}{mm^2} : (7.32)$$

$$\nu = 1 - \frac{f_{cd}}{250} = 1 - \frac{36.7}{250} = 0.8532 : (7.33)$$

$$\sigma_{Rd,max} = 0.6 * \nu * f_{cd} = 0.6 * 0.8532 * 36.7 = 18.79 \ \frac{N}{mm^2} \ : (7.34)$$

Comparing the values with the numerical simulation and the allowable calculated concrete stress for the bottom node:

Table 7-19: The maximal principal stress of concrete versus the calculated analytical and allowable compressive stress at the bottom node.

Load	The numerical results of the principal stress of the concrete in [N/mm2]	Result of the analytical model (strut at the concrete region) in [N/mm2]	The allowable concrete stress in [N/mm2]
$F_{strut(ecd2)}$	-1.35	-6.35	-18.79
$F_{strut(ecd3)}$	-1.35	-2.22	-18.79

The calculated stresses of concrete from the analytical model and numerical simulation are very low, and lower than the allowable compressive stress.

b) Calculating the strut for the steel region and comparing it with numerical simulations and testing it to the allowable stress of the steel.

Defining the component of the strut load based on an angle of 25 degrees which has been assumed from the made sketch in figure 7-17 at the bottom node of the deck:

$$F_{strut(ecd2)} = F_{strut(ecd1)} * \cos(25) = 335.88 \text{ kN} * \cos(25) = 305 \text{ kN} : (7.24)$$
$$F_{strut(ecd3)} = F_{strut(ecd1)} * \sin(25) = 335.88 \text{ kN} * \sin(25) = 142 \text{ kN} : (7.25)$$

Table 7-20: The different distance available in a nodes (Top and bottom).

Material	Distance in [mm]		Width in the longitudinal direction b_{strut} in [mm]
Bottom node	a_2	60	800
	a_3	80	800

Calculating the strut area for the bottom node in the steel region:

$$A_{bottum\ 2} = a_2 * b_{strut} = 60 \text{ mm} * 800 \text{ mm} = 48000 \text{ mm}^2 \ : (7.35)$$

$$A_{bottum\ 3} = a_3 * b_{strut} = 80 \text{ mm} * 800 \text{ mm} = 64000 \text{ mm}^2 \ : (7.36)$$

Calculating the stress of the strut in the steel region:

$$\sigma_{bottum\ 2} = \frac{F_{strut(ecd2)}}{A_{bottum\ 2}} = \frac{305000\ N}{48000\ mm^2} = 6.35 \frac{N}{mm^2} \ : (7.37)$$

$$\sigma_{bottum\ 3} = \frac{F_{strut(ecd3)}}{A_{bottum\ 3}} = \frac{142000\ N}{64000\ mm^2} = 2.22 \frac{N}{mm^2} \ : (7.38)$$

Comparing the values with the numerical simulations and the allowable steel stress:

Table 7-21: The maximal principal stress of steel versus the calculated analytical and allowable compressive stress at the bottom node.

Load	The numerical results of the principal stress of the steel in [N/mm2]	Result of the analytical model on the steel girder in [N/mm2]	The allowable steel stress in [N/mm2]
$F_{strut(ecd2)}$	-1.35	-6.35	235
$F_{strut(ecd3)}$	-1.35	-2.22	235

The calculated steel stresses from the analytical model and the obtained results from the numerical simulation for the steel girder web and the flange are lower than the allowable steel stresses.

7.3.4. Comparing the results of the bridge decks A, B and C

In figures 7-18 until 7-20 the development of the strut can be seen. In bridge deck A, the strut is developing to the bottom flange and the web of the steel girder. In bridge deck B the development of the strut goes more or less to the web instead of the bottom flange and this holds also for bridge deck C. The observation which is made: How thicker the cross-section, the more force is transported to the web instead of the flange. This observation can be seen in figures 7-18 until 7-20. But due to the slip the force ends in the corner of the steel girder between the web and the flange.

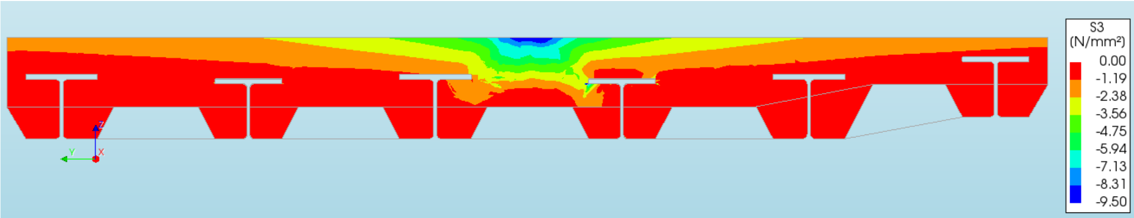

Figure 7-18: The maximal principal stress of concrete of bridge deck A.

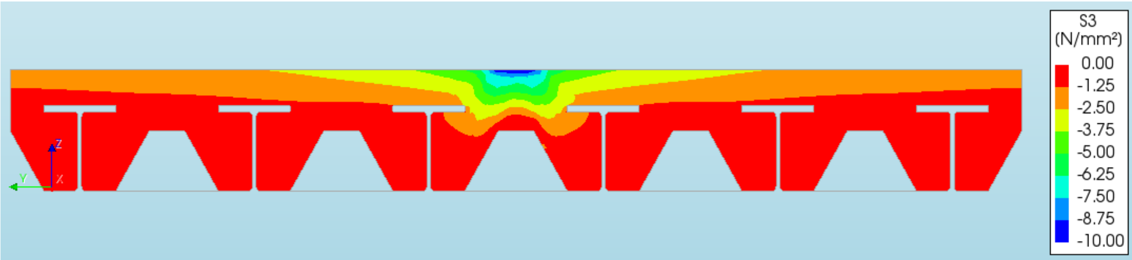

Figure 7-19: The maximal principal stress of concrete of bridge deck B.

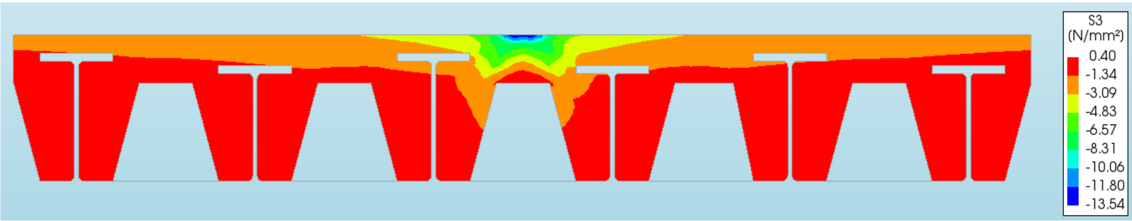

Figure 7-20: The maximal principal stress of concrete of bridge deck C.

In the tables 7-22 until 7-24 the results of the numerical simulation, analytical calculation and the allowable stress of concrete and steel are presented. The general observation which can be made is that the stress state is lower than the maximal allowable stress in the top and bottom nodes. At the top node the stress state which is obtained from the numerical simulations is a bit higher than the calculated stress in the analytical model. In the bottom node the stress state of the numerical simulation is lower than the stress state of the analytical model. This is for the concrete part. For the steel part, the stresses which are transferred into the steel girder are from the numerical simulations lower than from the analytical model. The reason is that the spreading plane which has been assumed in the longitudinal direction for the analytical model is lower than for he numerical simulation, this has to do with the calculated width in the longitudinal direction. These are the main things which can be mentioned from the comparison of the results of the three bridge decks.

Table 7-22: The maximal principal stress of concrete versus the calculated analytical and allowable compressive stress at the top node for the three bridge decks.

Bridges	Load	The numerical results of the principal stress of the concrete in [N/mm2]	Result of the analytical model (strut at the concrete region) in [N/mm2]	The allowable concrete stress in [N/mm2]
Bridge A	$F_{strut(ecd1)}$	-9.5	-9.74	-36.7
Bridge B		-10		
Bridge C		-13.5		

Table 7-23: The maximal principal stress of concrete versus the calculated analytical and allowable compressive stress at the bottom node for the three bridge decks.

Bridges	**Load**	**The numerical results of the principal stress of the concrete in [N/mm2]**	**Result of the analytical model (strut at the concrete region) in [N/mm2]**	**The allowable concrete stress in [N/mm2]**
Bridge A	$F_{strut(ecd2)}$	-1.2	-5.74	-18.79
	$F_{strut(ecd3)}$		-3.01	
Bridge B	$F_{strut(ecd2)}$	-1.25	-6.35	
	$F_{strut(ecd3)}$		-2.22	
Bridge C	$F_{strut(ecd2)}$	-1.35	-6.35	
	$F_{strut(ecd3)}$		-2.22	

Table 7-24: The maximal principal stress of steel versus the calculated analytical and allowable compressive stress at the bottom node for the three bridge decks.

Bridges	**Load**	**The numerical results of the principal stress of the steel in [N/mm2]**	**Result of the analytical model on the steel girder in [N/mm2]**	**The allowable steel stress in [N/mm2]**
Bridge A	$F_{strut(ecd2)}$	-1.2	-5.74	235
	$F_{strut(ecd3)}$		-3.01	
Bridge B	$F_{strut(ecd2)}$	-1.25	-6.35	
	$F_{strut(ecd3)}$		-2.22	
Bridge C	$F_{strut(ecd2)}$	-1.35	-6.35	
	$F_{strut(ecd3)}$		-2.22	

7.4. Discussion of the three bridge decks A, B and C

The two bridge decks B and C are both modelled like bridge deck A, which is presented in chapter 6. The difference between the three bridges is:

a) The span of the bridge (see chapter 2);
b) The steel-girders (see paragraph of 5.1.2);
c) The thickness of the bridge decks (see paragraph of 5.1.2);
d) The support length (see paragraph of 5.1.2).

The other bridge deck properties are the same. Furthermore, the assumption which is made when modelling the bridge decks is that there is sliding available until 400 kN, after 400 kN until 475 kN the deck becomes stiffer which leads to a full cooperation between the two materials steel and concrete. A comparison is made between steel girder 3 and 4 of the three chosen bridges. This can be seen in figure 7-1 and 7-2. The numerical values of the three bridge decks are added in tables 7-1 and 7-2.

Furthermore, the stress state of the materials (concrete and steel) of the three bridges is below the maximal allowable stress of the named materials. Concrete and steel aren't yielding at this stage until 475 kN in the longitudinal direction. This can be seen in figures 7-3/7-4 and 7-5. The numerical values of the stresses are also added in the tables 7-3/7-4 and 7-5.

In the transverse direction the same holds for the stress state of the two materials (concrete and steel) in the simulated three bridge decks. Steel and concrete aren't yielding in the transverse direction.

The second step is to look at the strut and tie model in the transverse direction. This concept is improved and validated based on the analytical model and the numerical simulations. In the figures 7-18 until 7-20 the development of the strut can be seen. In bridge deck A, the strut is developing to the bottom flange and the web. In bridge deck B the development of the strut goes more or less to the web instead of the bottom flange and this holds also for bridge deck C. The following observation which is made: How thicker the cross-section is, the more force is transported to the web instead of the flange. This observation can be seen in figures 7-18 until 7-20. But due to the slip the force ends in the corner of the steel girder between the web and flange, and this is visualized in the figures 7-18, 7-12 and 7-17.

In the tables 7-22 until 7-24 the results of the numerical, analytical and the allowable stress of concrete and steel are presented. The general observation which can be made is that the stress state is lower than the maximal allowable stress in the top and bottom nodes. At the top node, the stress state which is obtained from the numerical simulations is a bit higher than the calculated stress in the analytical model. In the bottom node, the stress state of the numerical simulation is lower than the stress state of the analytical model. This is for the concrete part. For the steel part, the stresses which are transferred into the steel girder are from the numerical simulations lower than from the analytical model. The reason is that the spreading plane which has been assumed in the longitudinal direction for the analytical model is lower than for he numerical simulation, this has to do with the calculated width in the longitudinal direction. These are the main things which can be mentioned from the comparison of the results of the three bridge decks.

7.5. Conclusion of the three bridge decks

Based on the 3D linear analysis which is made for the three bridge decks the following conclusion can be made for the longitudinal and the transverse direction:

The stresses which are predicted from the numerical simulation are smaller than the allowable stresses of concrete and steel for the longitudinal as well as the transverse direction.

The conclusion which can be taken from the numerical simulation and the used analytical model of the bridge decks is that the strut and tie model is validated. The strut and tie model can be used to test the bridge decks in the transverse direction.

At last, another conclusion that can be taken by comparing the bridge decks in the transverse direction is based on the used strut and tie model: The force of the strut is transported directly to the web of the steel girder in the numerical simulations. But based on the available slip the force is transported from the web to the corner between flange and web of the steel girder.

8. Conclusion and Recommendation

8.1. Conclusion

This thesis studies the structural behaviour of historical steel-concrete-composite-bridge-decks in Amsterdam. This type of bridge decks does not have sufficient load bearing capacity according to the current Eurocode 4. The issue with these type of bridge decks is that the capacity of the bridge deck is almost not determined in the longitudinal and completely not determined in the transversal direction. The goal of this investigation is to gain more insights in both the longitudinal and transverse direction of the historical steel-concrete-composite-bridge-decks, such that a more accurate model on the possible residual capacity in both directions may be developed. The study consists of three steps:

1. An investigation of a selection of 32 existing historical bridges and selection of 3 typical bridges for further research;
2. A study on the measurement data from the proof loading test of one of the selected bridges;
3. Develop numerical models of the selected 3 bridges and investigate the possibility of using analytical models such as strut and tie models.

Detailed conclusions of each study steps can be find in the separate conclusion of chapter 2, 4, 5, 6 and 7 respectively. A summary of the main findings are listed below:

From the investigation on the state of the 32 historical steel-concrete-composite-bridge-decks the following conclusions are derived:

a) The current Eurocode 4, does not provide an answer to calculate the load-bearing capacity of historical steel-concrete-composite-bridge-decks, because the typical cross sections that the current Eurocode 4 models is significantly different from that of the historical model;
b) The strut and tie model is potentially applicable on the historical steel-concrete-composite-bridge-decks to model the bearing capacity of the deck in the transverse direction.

From the study of the measurement data obtained during the proof loading test, the following conclusions are derived:

a) In the in-situ-tests 1, 2 and 3 at loaded point H(1/6L), J(1/2L) and L(5/6L), non-linear load deflection curves were observed. One may conclude that the bridge was in the non-linear stage;
b) There was no occurrence of punching shear failure behaviour or other failure during all the three loading tests of the bridge deck.

From comparing the numerical models with the three proof loading tests, we may confirm the following assumptions:

a) Slip occurs from 0 kN until 400 kN, and between 400 kN until 475 kN the deck becomes stiffer which leads to a change in the absolute value of the slip;
b) Slip behaviour occurs at least in the transverse direction based on the measurement results of the in-situ tests, probably there is also slip behaviour in the longitudinal direction, but that is not measured in the in-situ-load-tests;
c) In the transverse direction the strut and tie model is applicable on the historical steel-concrete composite bridge deck based on the performed analysis.

8.2. Recommendation

The goal of the thesis is to gain insights in the longitudinal and transverse direction of the historical steel-concrete-composite-bridge-decks. The investigation in the longitudinal direction is not satisfying, because the goal was to develop a cooperation factor. The cooperation factor will describe the interaction level between the steel girder and concrete. To study the interaction level between steel and concrete, it is recommended to set-up an additional lab experiment where the bridge deck or a part of the deck will be tested and the measured data will be used to define and to gain insight in the behaviour of the historical bridge deck without shear connectors.

The steps needed to define the interaction level in the longitudinal direction is formulated in the following steps:

1. Setting up the FEA-model to simulate the behaviour of the bridge deck in the longitudinal direction. In the model, the following interface models are recommended:

    a) Bond-slip;
    b) Coulomb friction;
    c) Non-linear elastic friction.

    These models can be used to simulate the interface between steel and concrete.

2. Calibrating and validating the FEA-simulation based on the measurements which will be obtained from the additional lab experiment. The advice is to validate the model first in the linear stage and to use this model in the non-linear stage, to model the interaction level between steel and concrete. In addition to that, use the analytical model (see sub-chapter 3.2.2) to validate the FEA-models and to define the interaction factor;

3. Finally, the advice is to follow the named steps above to define the factor which describes the composite action in the longitudinal direction.

In the transverse direction there are no recommendations because the conclusion is satisfying.

9. Bibliography

(2002), U. H. (2002). *UK HA BD81/02 (2002).* UK: UK.

(2005)., t. H. (sd). *Contributions to horizontal translational restraint stiffness .*

1975, H. a. (sd). *classification of the restrained slab .*

1984, K. e. (sd). *Main concept of the figures inspired by Kirkpatrick et al. 1984.*

Agrawal, A. K. (2020, May 24). *Quora*. Opgehaald van Quora: https://www.quora.com/What-is-the-neutral-axis-of-a-beam

Amsterdam, G. (2019, 10 25). *IB gemeente Amsterdam*. Opgehaald van Programma Bruggen en Kademuren: https://www.betonvereniging.nl/media/16587/61-bruggen-en-kademuren-amsterdam-annemarij-kooistra.pdf

Antea Group B.V. (2016). *Inspection reports.* Amsterdam: Gemeente van Amsterdam.

Asin, M. (2000). *The Behaviour of Reinforced Concrete Continuous Deep Beams.* Delft: Delft University Press.

CAN/CSA-S6-06 2006. (2006). *Canadian Highway Bridge Design Code.* Canadian : the Ontario Ministry of Transportation's OHBDC-91-01, Ontario Highway Bridge Design Code.

DENORMALISATION, A. C. (2006). *Commentary on CAN/CSA-S6-06,Canadian Highway Bridge Design Code.* Canada: ASSOCIATION CANADIENNE DENORMALISATION.

Dr. C. C. Fu, P. P. (August 21, 2001). *THE STRUT-AND-TIE MODEL OF CONCRETE STRUCTURES.* Maryland: The Maryland State Highway Administration.

FEA, D. (sd). Opgehaald van https://dianafea.com/faq-tangent-normal-stiffness

Gemeente Amsterdam. (sd). *Archiefinformatie.*

Google Street View. (2021). Amsterdam. Opgehaald van https://www.google.com/maps/d/u/0/viewer?mid=1JEkfH9bJtMKrVCMHrKGPP_QmMys&ll=37.731904282056874%2C-92.97047165000001&z=5

Het Nederlands Normalisatie-instituut. (2020). *NEN-EN 1992-1-1:2005+A1:2015+NB:2016+A1:2020/NEN-EN 1991-1-1:2005+A1:2015+NB:2016+A1:2020.* Nederland: Het Nederlands Normalisatie-instituut.

Het NederlandsNormalisatie-instituut, . (2012). *NEN-EN 1994-1-1:2005+C1:2009+NB:2012.* Nederland: NEN.

Hon, A. T.-M. (2005). Strength of reinforced concrete bridge decks under compressive membrane action.

Jianguo Nie1 and C. S. Cai, P. M. (2003). Steel–Concrete Composite Beams Considering Shear Slip Effects. *JOURNAL OF STRUCTURAL ENGINEERING © ASCE .*

Kirkpatrick. (1984). Main concept of the figures and tekst.

Municipality of Amsterdam. (1950). Calculation of the archive.

Municipality of Amsterdam. (1950, 10 23). *Drawing Archiive.* Amsterdam. Opgehaald van https://www.volksgezondheidenzorg.info/onderwerp/influenza/cijfers-context/huidige-situatie#node-aantal-ziektegevallen-van-influenza

Osman, B. H. (2008). *SHEAR IN R.C DEEP BEAMS.* Khartoum: University of Khartoum.

Reniers , L. (2021, Oktober). Bruggen van Amsterdam. Amsterdam. Opgehaald van https://www.bruggenvanamsterdam.nl/prinsengracht_hoek_vijzelstraat.htm

Roosen, M. H. (2020, April 2). *RTD.* Opgehaald van Guidelines for Nonlinear Finite Element Analysis of Concrete Structures: http://homepage.tudelft.nl/v5p05/RTD

ŞAMHÂL, E. (april 2005). *Lecture 1.1: Composite Construction.* SSEDTA(European Steel Computer Aided Learning).

List of figures

List of tables

A Annex – Input for research about the historical Amsterdam bridge decks

A.1. Below is a summary of the procedure which is used at the structural department of the IB

1. There is no cooperation between the concrete deck and the steel beams in *verbundträger* bridge decks without mechanical connections, the loads are carried separately by the two construction parts in proportion to their bending stiffness;
2. Because there is no reinforcing steel reinforcement in the bottom (chamfered parts) of the concrete deck in the longitudinal direction, those parts are considered inactive and also do not contribute to both the bridge stiffness and the resistance (bearing capacity) of the bridge deck (they are dead weight applied to steel);
3. The stiffness of the bridge deck in the transverse direction is entirely derived from the concrete deck, namely the part with the smallest thickness and the thickness is constantly assumed over the entire width of the bridge deck;
4. The concrete deck is assumed to be cracked and the modulus of elasticity of cracked concrete is between 10000 N /mm^2 and 15000 N /mm^2;
5. The calculation of the force distribution in the bridge deck is based on the linear elastic calculation method;
6. In the global force distribution, the steel beams absorb the summed force distribution in both steel and concrete in the longitudinal direction and in the transverse direction, the concrete deck absorbs the transverse moments;
7. The local effect is not tested because there is a direct payment (of load) to the steel beams;
8. Because there is no reinforcing steel reinforcement in the tensile zone of the concrete deck, the concrete always does not meet the ULS requirements at the global transverse moments. The concrete deck cannot absorb the moments occurring in the transverse direction of the bridge deck.

A.2. Input from drawing of the Historical Amsterdam bridges

1. Analysing the obtained data of the Amsterdam bridges:

The obtained data from the drawing will be analysed. The goal is to look of there is a correlation between the properties of the historic steel-concrete-composite-bridge-decks. This is done for number of items which are obtained from the drawing. Based on the results of the analysed items, the conclusion which can be taking is. There is no correlation between the data items. This leads to take all the items of the dataset, which are named in the paragraph 2.2 in consideration. See the figures A-1 until A-4 which give an illustration of the results of a view items.

1 Figure A-2-1: Analysis of the correlation between concrete properties (N/mm^2) and the span of bridges (m);
2 Figure A-2-2: Analysis of the correlation between reinforcement in the lane in (mm^2/m) and the span of bridges (m);
3 Figure A-2-3: Analysis of the correlation between center -to-center in (mm) and the span of bridges (m);
4 Figure A-2-4: Analysis of the correlation between layout of the bridge foot/bike deck in (m) and the span of bridges (m).

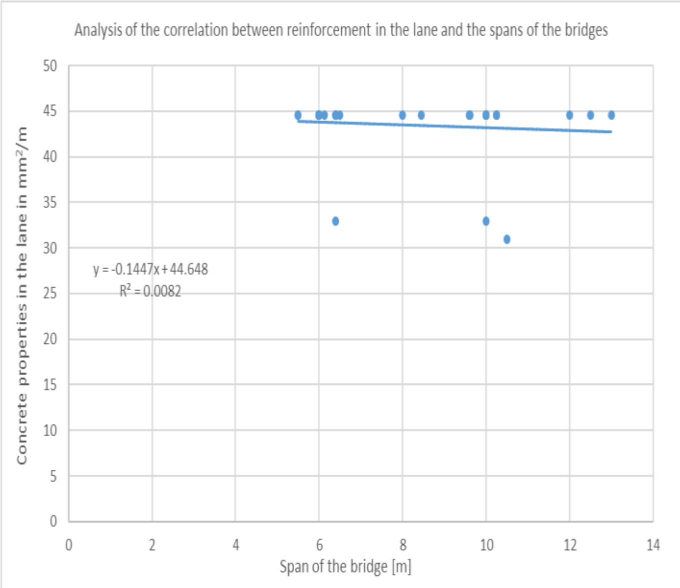

Figure A-2-1: Analysis of the correlation between concrete properties (N/mm2) and the span of bridge decks (m).

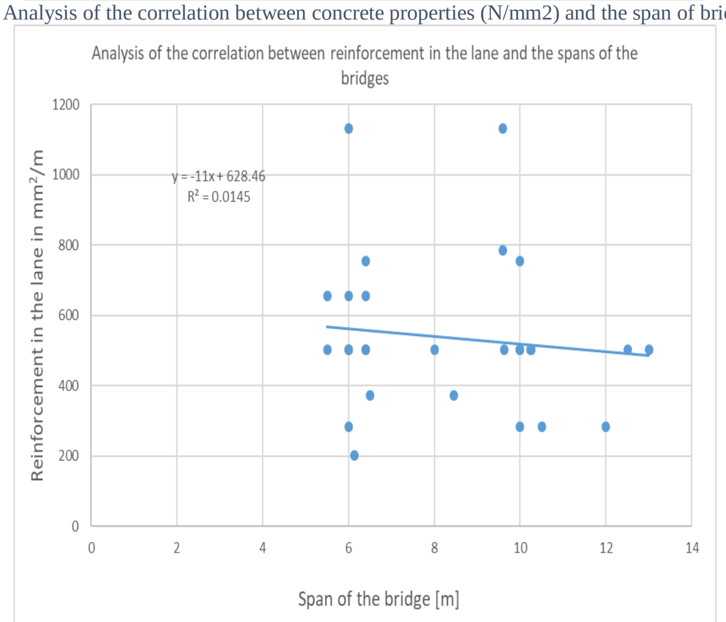

Figure A-2-2: Analysis of the correlation between reinforcement in the lane in mm2/m and the span of bridge decks.

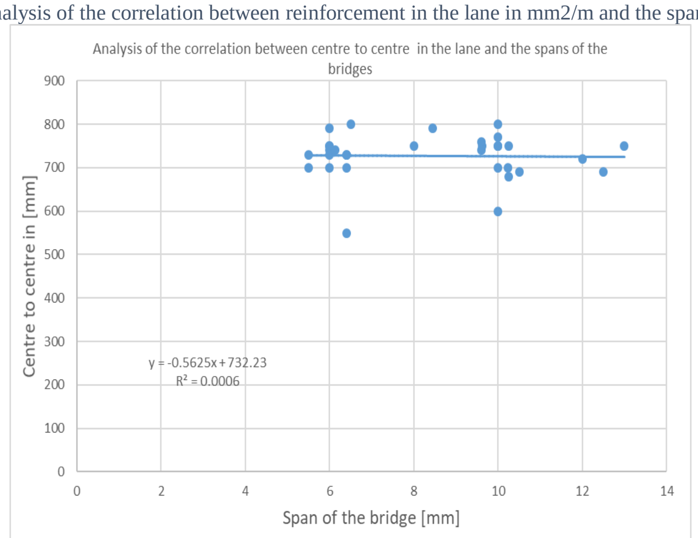

Figure A-2-3: Analysis of the correlation between center -to-center in (mm) and the span of bridge decks.

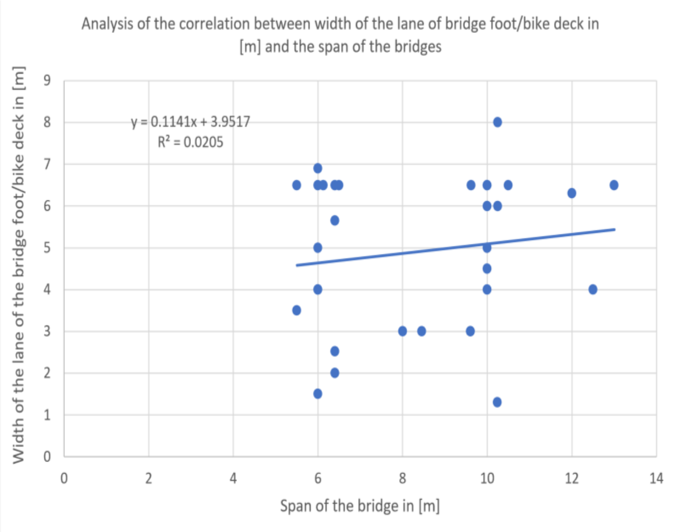

Figure A-2-4: Analysis of the correlation between layout of the bridge foot/bike deck in (m) and the span of bridge decks.

In the figures above the correlation is presented for different items from the database. In the figures the values R^2 gives an indication about the correlation between the data items. For example, the span of the bridge is plotted behind the width of the lane of the bridge foot/bike deck in (m), and other figures which are mentioned above. Based on the value of the R^2 men can see if there is some correlation or not and on the line which in the most figures a straight-line. The conclusion is, there is no correlation between data items. This leads to take each items of the database into consideration separately. The database is added later on in this appendix.

2. Analysing the distance between the steel profile (center -to-center):

In this paragraph, the cross-section properties center -to-center will be analysed. The properties of the cross-sections of the Amsterdam bridges are not uniform at all. The variation is seen in all the items which are obtained in the database. But the focus will invest only on the item center -to-center distance which is the distance between the steel profiles in the transverse direction of the historic steel-concrete-composite-bridge-deck. From the investigation of the drawing which is made there are three distances obtained per lane (foot/bike, vehicle, or the tramway). The goal is to transform the three distances to an average distance which will be used during the calculation of the cross-section properties. See figure A-2-5: (different distance between steel profile). First full the deck will be explained. Most of the bridges of Amsterdam contains the foot/bike lane and the vehicles lane. However, some of them have the tramrails also. The database is dividing on this perspective to full up the difference information which is obtained from the data. See the figures A-2-5 until A-2-8.

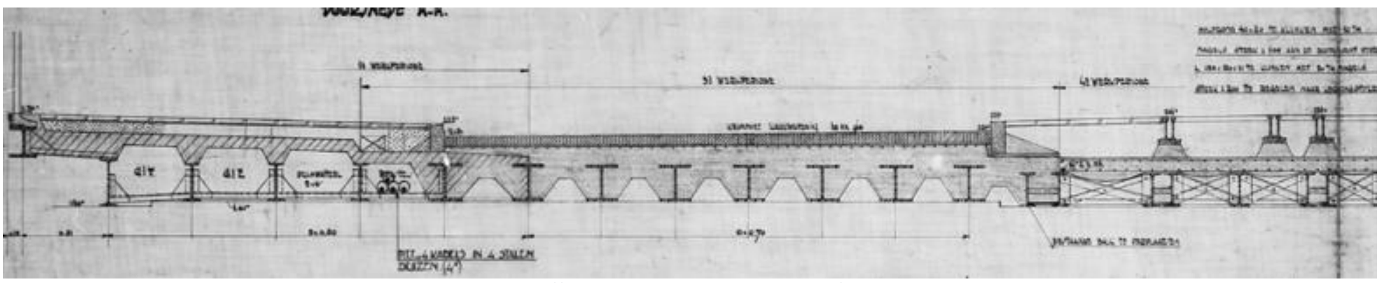

Figure A-2-5: Different distance between steel profile bridge deck.

1 Figure A-2-6: Three center -to-center in (mm) distance Foot/Bike lane;
2 Figure A-2-8: Three center -to-center in (mm) distance for tram lane on the bridge;
3 Figure A-2-7: Three center -to-center in (mm) distance for vehicle lane on the bridge.

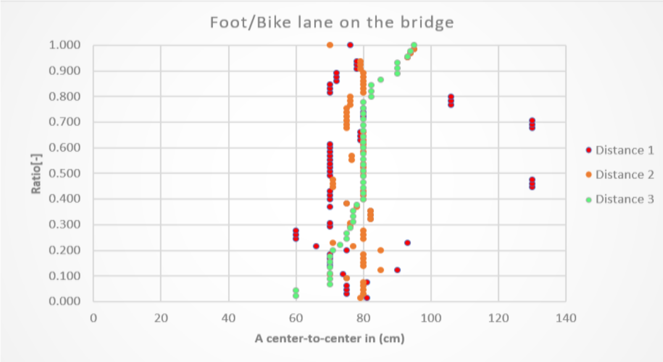

Figure A-2-6: Three center -to-center in (mm) distance Foot/Bike Lane.

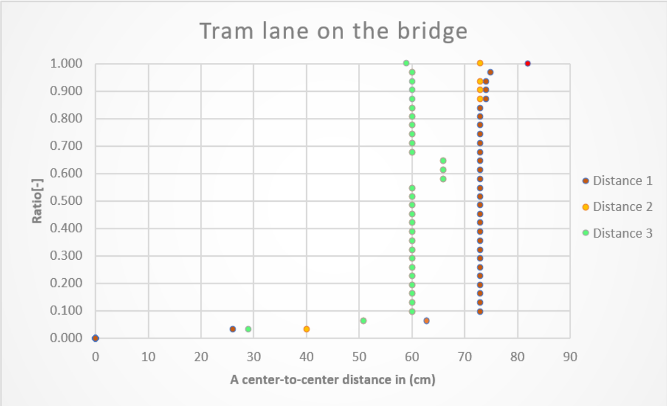

Figure A-2-7: Three center -to-center in (mm) distance for tram lane on the bridge deck.

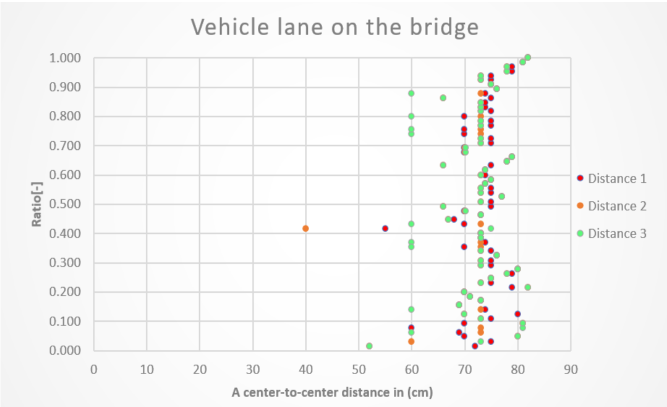

Figure A-2-8: Three center -to-center in (mm) distance for vehicle lane on the bridge deck.

In the figures above are three different “center -to-center distance” presented. The center -to-center distance is the distance between the steel profile (definition see paragraph 2.2) for the three lanes (foot/bike, vehicle, and tram) and all the thirty-two bridges presented. The distance has a variation in the three lanes, to optimize this to one uniform distance. Is chosen to plot the dataset and to evaluated to a specific distance for the three and the thirty-two bridges. The chosen distance is average for the thirty-two bridges and three different distances. The following distance are choosing to be used to calculate the stiffness of the cross-section.

Table A-1: The center -to-center which are chosen.

Specific lane	A center -to-center distance in (cm)
foot bike	80
vehicle	75
the tram	65

Based on the presented table the cross-section property will be determined.

3. Minimal height cross-section:

The cross-section dependence on the height of the concrete including the steel profile. The bridges deck is built up as a curved in the transverse and longitudinal direction. Which make it imposable to have a constant height. In addition to this there is also asphalt which is not taking into consideration by depending on the height. To avoid this, the decision is made to take the minimal height of each lane of the historic steel-concrete-composite-bridge-deck for the thirty-two bridges. This height is presented in the database. See figure A-2-5.

4. Steel profile which are available in the historic steel-concrete-composite-bridge-decks:

Figure A-2-9 below is an example of the section view of bridge A for the description of the figure see paragraph 2.2. The goal of the figure A-2-9 is to mention that there is different steel profile in the cross-section of the historic steel-concrete-composite-bridge-deck. This lead to take more than one steel profile in consideration to have an overview about the stiffness of the historic steel-concrete-composite-bridge-deck. All the profile which are available in the section of the thirty-two bridges are brought in the database. The model where the stiffness (EI) can be calculated in an analytical way is included in the database. In the table A-2 the different steel profile (German steel-profile) which are available in the cross-section, can be seen. The database can be found in this appendix.

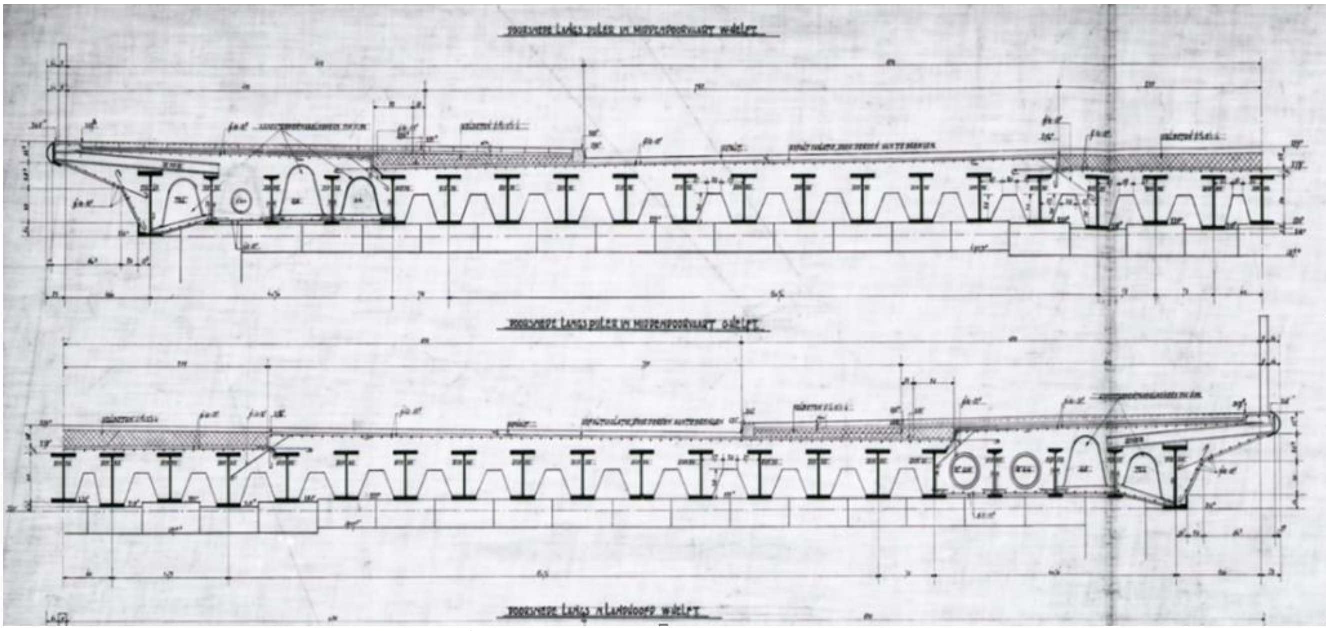

Figure A-2-9: Layout of the bridge deck A in the transverse direction (Gemeente Amsterdam).

Table A-2: Profile which are comment in thirty-two historic steel-concrete-composite-bridge-deck.

Germany type profile	The type of profile
DIN (Differdange normal)	DIN24/25/26/28/30/34/36/40/50/55
NP (Deutsche Normal profile: für 1)	NP30/34/38/40/45/50/55
B (Breitilanschige Differdinger Spezial-Träger)	B40/45
DIR (Differdange renforcé)	DIR 60
DIE (Differdange économique)	DIE 40

Based on the steel profile which are obtained in the database the cross-section properties will be calculated and the numerical model will be setup.

5. Selecting three bridges from the thirty-two bridges

The available spans and the analysis to select the 3 representative bridges in Amsterdam. There is a need to choose three bridges which will give the overview of all the historic steel-concrete-composite-bridge-deck in Amsterdam. To satisfy the goal, there is only one item from the dataset selected and that is the span of the bridges. The bridge span consists of two types of spans, the main span, and the side-span. The main span is decisive. Because the length is more spreader than the side-span and the main span has a larger span, see Figure A-2-10: for the difference between the two spans is presented. There is only on exception and that is the bridge A where the experience is made. The experience is made on the side-span because of restriction which will be explained in the chapter 4 of the experiment.

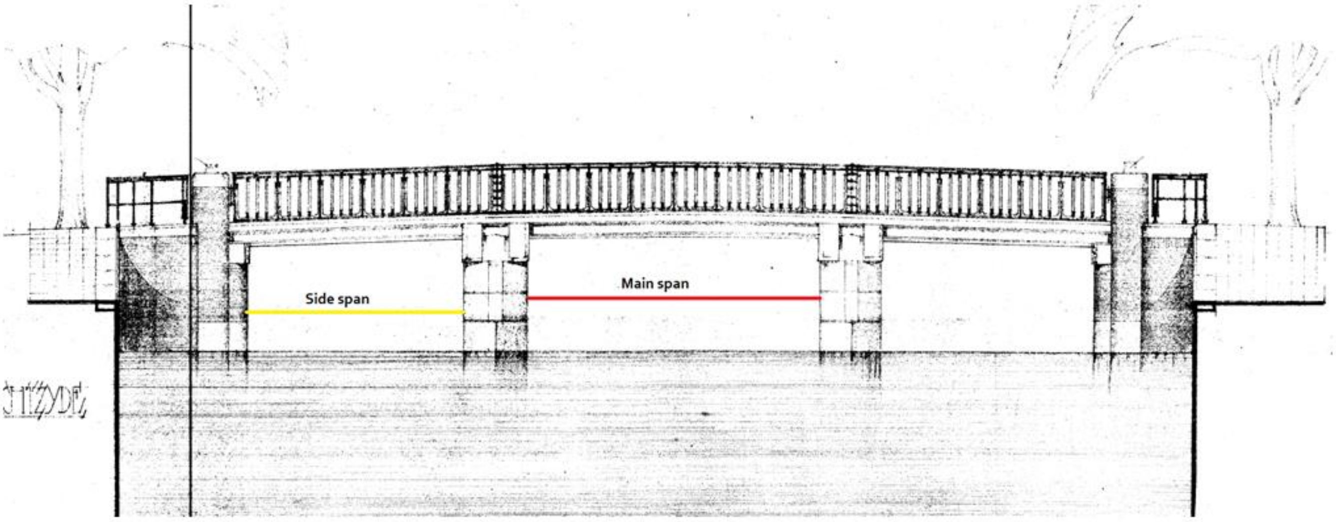

Figure A-2-10: The difference between the main/side-span.

In the figure A-11 (visualization of the data the main/side-span), can be seen conclude that the bandwidth of the main span is larger than the side-span. The variation in the main span leads to select three different populations. The selected populations will be used to choose two the device bridges which will be used in in this research, see figure A-2-12 (The three population). The third bridge is fixed as mentioned before because of the experiment.

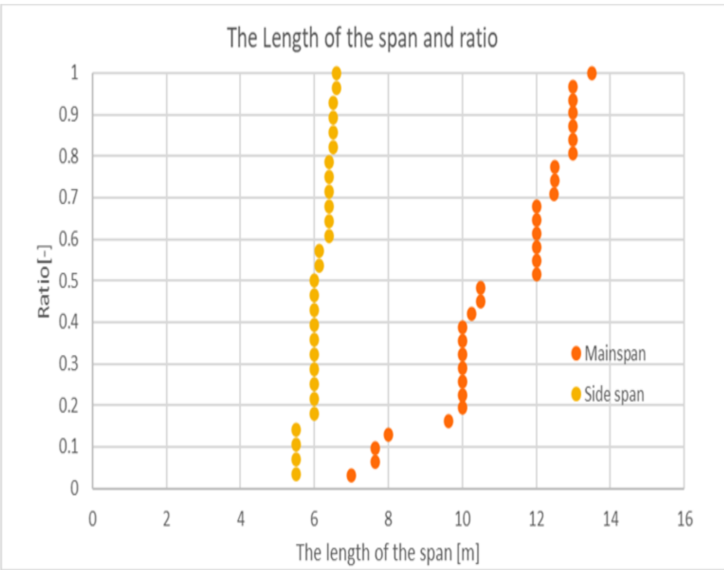

Figure A-2-11: Visualization of the data the main/side-span.

The data of the main span has some repetition, but that is not an issue. In figure A-2-12 (The three population), the selected population are presented. The three-population are located in the following ranges.

1. The first range is: 6 to 8 m and ratio of 0 to 13 %;
2. The second range is: 9 to 11 m and ratio of 13 to 48 %;
3. The third range is: 6 to 8m and ratio of 48 to 100 %.

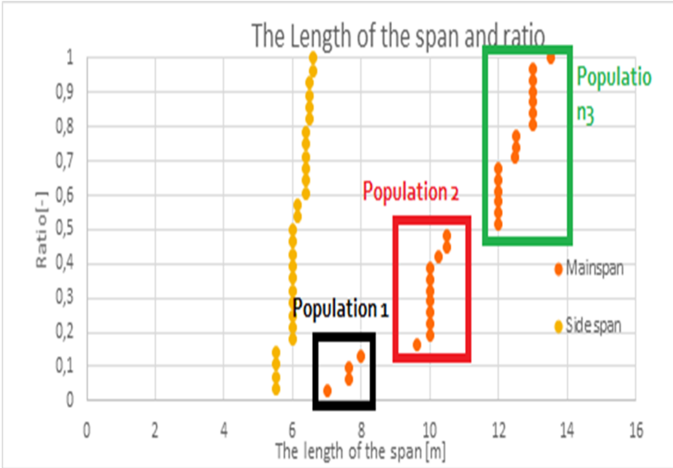

Figure A-2-12: The three population.

From the investigation, the total bridge collection is split into three groups. For each group, a bridge is selected. The three chosen bridges based on the named population above are:

1 Bridge A: 20 %;
2 Bridge B: 40 %;
3 Bridge C: 80 %.

Bridge A is a representative bridge in main span because the length on the main span is 8 m, but due to restriction during the in-situ-load-test is chosen to use the side-span and that will be the case also in this thesis assignment. The second bridge is bridge B because this bridge does not contain any tramway and is from the category 10 m span. The third bridge is based on the configuration of the cross-section properties and is from the category 13 m span. This is the same for some other bridges in the collection of the 32 bridges.

The percentage of the choosing bridges are:

1 Bridge A: span = 6.5 m: 20% (is bridge where the in-situ-load-test is done);
2 Bridge B: span = 10 m: 40 % (is from the category of the 10 m span);
3 Bridge C: span = 13 m: 88 % (is from the category of the 13 m span).

6. Statically determinate or indeterminate and the available reinforcement on the cross-section
During the investigation of the different drawing of the selected 32 bridges is highlighting that the available reinforcement on the cross-section is only the shrinkage reinforcement the variation of this reinforcement is between the diameter of 6 until 10 in some cases. The reinforcement is available only on the top of the cross-section as can be seen in Figure A-2-13. The available reinforcement will not lead to a statically indeterminate case in the longitudinal direction as can be seen in Figure A-2-14. The historic steel-concrete-composite-bridge-deck in Amsterdam is a statically determined slab.

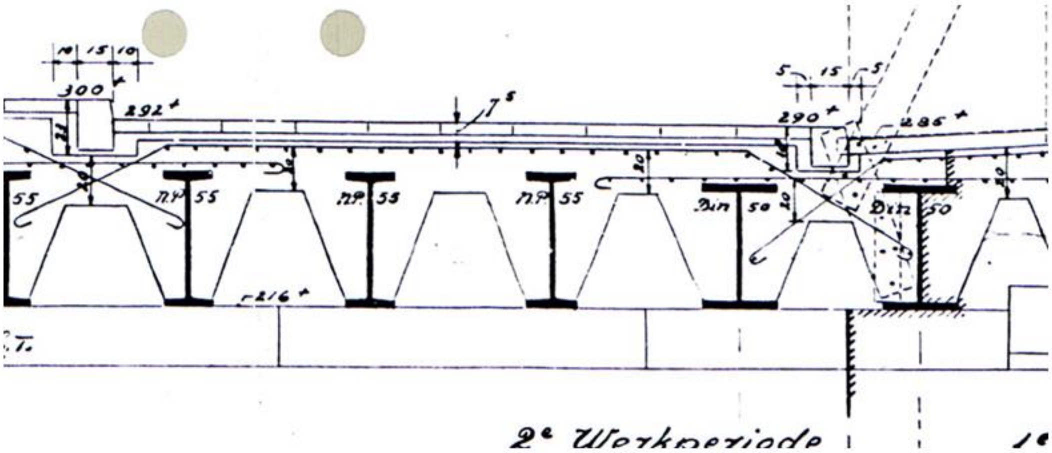

Figure A-2-13: Transverse direction.

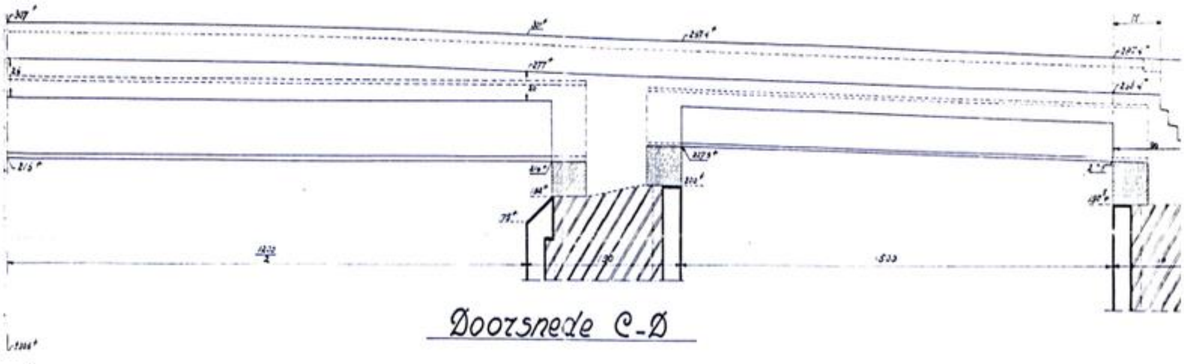

Figure A-2-14: The longitudinal direction of one of the bridge decks.

7. Database of the 32 bridges which are been investigated

Bridgenumber	TYPE span	Number of Spans	Length Span	Width bridge deck	Construction year	Statically in/determinate	Material quality(bestek)				Current material quality based on the inspections		Cracks in the deck							
							Steel/N/mm2	concrete			Steel	concrete	Longitudinal	Crackwidth in the longitudinal	Comment	Transverse	Crackwidth the transvere	Comment	Transvers	
								Cement/KG	Grind/KG	Sand/KG									Reinforcement	Reinforcement in mm^2/m
Bridge D	Mainspan	1	10,24	20,34	1928	Statically determinate	200	100	2,4	3,8	S235	44,58	Cracks are present	is not clere of the cracks are located in the longitudinal only	In the inspection, rapport is tolled that There e is a leakage at the underside of the deck. There is lime bloom at the underside.	Cracks are present	is not clere of the cracks are located in the transvere only	In the inspection, rapport is tolled that There e is a leakage at the underside of the deck. There is lime bloom at the underside.	8-100 mm	503
Bridge A	Side span Mainspan Side span	3	6,4 8 6,4	26	1934	Statically determinate	200	100	2,4	3,8	S235	31	Cracks are present	The cracks are located longitudinal direction.	In the inspection, rapport is tolled that There e is a leakage at the underside of the deck. There e is lime bloom at the underside.	Cracks are present	No	No	8-100 mm	503
Bridge E	Mainspan	1	9,62	26,6	1927	Statically determinate	200	100	2,4	3,8	S235	44,58	Cracks are present	The cracks are located longitudinal direction.	In the inspection, rapport is tolled that There e is a leakage at the underside of the deck. There e is lime bloom at the underside.	Cracks are present	No	No	12-150 mm	754
Bridge F	Mainspan	1	10	16	1971	Statically determinate	200	100	2,4	3,8	S235	44,58	Cracks are present	The cracks are located longitudinal direction.	The reinforcement is corroded.	Cracks are present	The cracks are located transverse direction.	The reinforcement is corroded.	6-100 mm	284
Bridge G	Mainspan	1	10	20	1936	Statically determinate	200	100	2,4	3,8	S235	44,58	Cracks are present	The cracks are located longitudinal direction.	The reinforcement is corroded./There e is lime bloom at the underside.	Cracks are present	The cracks are located transverse direction.	The reinforcement is corroded./There is lime bloom at the underside.	8-100 mm	503
Bridge H	Mainspan	1	10,5	20,39	1892	Statically determinate	200	0	0	0	S235	32,99	Cracks are present	The cracks are located longitudinal direction.	The reinforcement is corroded./There is lime bloom at the underside.	Cracks are present	The cracks are located transverse direction.	The reinforcement is corroded./There is lime bloom at the underside.	10-120 mm	654
Bridge I	Side span Mainspan Side span	3	6 12 6	30	1928	Statically determinate	200	100	2,5	1,5	S235	44,58	Cracks are present	The cracks are located longitudinal direction	The reinforcement is corroded./There is lime bloom at the underside.	Cracks are present	The cracks are located transverse direction	The reinforcement is corroded./There is lime bloom at the underside.	8-100 mm	503
Bridge J	Mainspan	1	10	22	1936	Statically determinate	200	1	3	2	S235	44,58	Cracks are present	The cracks are located longitudinal direction.	The reinforcement is corroded./ There is lime bloom at the underside	Cracks are present	The cracks are located transverse direction.	The reinforcement is corroded./There is lime bloom at the underside	8-100 mm	503
Bridge K	Mainspan	1	10	15	1936	Statically determinate	200	100	2,3	1,6	S235	44,58	Cracks are present	The cracks are located longitudinal direction.	The reinforcement is corroded./ There is lime bloom at the underside	Cracks are present	The cracks are located longitudinal direction.	The reinforcement is corroded./ There is lime bloom at the underside	8-100 mm	503
Bridge L	Mainspan	1	10	30	1937	Statically determinate	200	1	3	2	S235	44,58	Cracks are present	The cracks are located longitudinal direction.	The reinforcement is corroded./ There is lime bloom at the underside	Cracks are present	The cracks are located longitudinal direction.	The reinforcement is corroded./ There is lime bloom at the underside	8-100 mm	503
Bridge B	Mainspan	1	10	8	1951	Statically determinate	200	350 kg portland cement B per m3	0	0	S235	44,58	No cracks are present	No	No	No cracks are present	No	No	12-150 mm	754
Bridge M	Side span Mainspan Side span	3	9,6 12,48 9,6	8,5	1881	Statically determinate	200	0	0	0	S235	32,99	No cracks are present	No	No	Cracks are present	No	No	6-100 mm	284
Bridge N	Mainspan	1	12	30	1954	Statically determinate	200	0	0	0	S235	44,58	Cracks are present	The cracks are located longitudinal direction.	There is lime bloom at the underside	Cracks are present	The cracks are located longitudinal direction.	There is lime bloom at the underside	8-100 mm	503
Bridge O	Mainspan	1	12	30	1929	Statically determinate	200	0	0	0	S235	44,58	Cracks are present	The cracks are located longitudinal direction.	There is lime bloom at the underside	Cracks are present	The cracks are located longitudinal direction.	There is lime bloom at the underside	8-100 mm	503
Bridge P	Side span Mainspan Side span	3	10,25 10,5 10,25	8,5	1961	Statically determinate	200	1	3	2	S235	44,58							8-100 mm	503
Bridge Q	Mainspan	1	12	30	1932	Statically determinate	200	1	4	2	S235	44,58							8-100 mm	503
Bridge R	Mainspan	1	12	21,6	1936	Statically determinate	200	1	5	2	S235	44,58	No	No	No	No	No	No	10-100 mm	785
Bridge S	Side span Mainspan Side span	3	5,5 13,5 5,5	30	1921	Statically determinate	200	1	5	2	S235	44,58	Cracks are present	The cracks are located longitudinal direction.	In the inspection, rapport is tolled that There e is a leakage at the underside of the deck. There is lime bloom at the underside.	Cracks are present	The cracks are located transverse direction.	In the inspection, rapport is tolled that There e is a leakage at the underside of the deck. There is lime bloom at the underside.	8-100 mm	503
Bridge T	Side span Mainspan Side span	3	6,13 7 6,13	20,6	1936	Statically determinate	200	1	5	2	S235	44,58	Cracks are present	The cracks are located longitudinal direction.	The reinforcement is corroded./ There is lime bloom at the underside	Cracks are present	The cracks are located transverse direction.	The reinforcement is corroded./ There is lime bloom at the underside	12-100 mm	1131
Bridge U	Mainspan	1	12	15	1928	Statically determinate	200	1	5	2	S235	44,58	Cracks are present	The cracks are located longitudinal direction.	There is lime bloom at the underside	Cracks are present	The cracks are located transverse direction.	There is lime bloom at the underside	8-100 mm	503
Bridge V	Side span Mainspan Side span	3	5,5 12,5 5,5	27	1926	Statically determinate	200	1	5	2	S235	44,58	Cracks are present	The cracks are located longitudinal direction.	There is lime bloom at the underside	Cracks are present	The cracks are located transverse direction.	There is lime bloom at the underside	8-100 mm	503
Bridge W	Side span Side span	2	8,45 8,45	25	1927	Statically determinate	200	1	5	2	S235	44,58	Cracks are present	The cracks are located longitudinal direction.	There is lime bloom at the underside	Cracks are present	The cracks are located transverse direction.	There is lime bloom at the underside	8-100 mm	503
Bridge X	Side span Mainspan Side span	3	6 13 6	30	1925	Statically determinate	200	1	5	2	S235	44,58	Cracks are present	The cracks are located longitudinal direction	In the inspection, rapport is tolled that There e is a leakage at the underside of the deck. There is lime bloom at the underside.	Cracks are present	The cracks are located transverse direction.	In the inspection, rapport is tolled that There e is a leakage at the underside of the deck. There is lime bloom at the underside.	8-100 mm	503
Bridge Y	Side span Mainspan Side span	3	6 13 6	20	1927	Statically determinate	200	1	5	2	S235	44,58	Cracks are present	The cracks are located longitudinal direction	In the inspection, rapport is tolled that There e is a leakage at the underside of the deck. There is lime bloom at the underside.		The cracks are located longitudinal direction	In the inspection, rapport is tolled that There e is a leakage at the underside of the deck. There is lime bloom at the underside.	6-100 mm	284
Bridge C	Side span Mainspan Side span	3	6 13 6	30	1936	Statically determinate	200	1	5	2	S235	44,58							10-120 mm	654
Bridge Z	Side span Mainspan Side span	3	6,5 13 6,5	30	1940	Statically determinate	200	1	5	3	S235	44,58							12-250 mm	754
Bridge AA	Side span Mainspan Side span	3	6,5 12,5 6,5	30	1939	Statically determinate	200	1	3	2	S235	44,58	Cracks are present	The cracks are located longitudinal direction	In the inspection, rapport is tolled that There e is a leakage at the underside of the deck. There is lime bloom at the underside.	Cracks are present	The cracks are located transverse direction.	In the inspection, rapport is tolled that There e is a leakage at the underside of the deck. There is lime bloom at the underside.	12-100 mm	1131
Bridge AB	Side span Mainspan Side span	3	6,6 13 6,6	30	1930	Statically determinate	200	B35 CEMIII/B42,5 LH HS			S235	44,58	Cracks are present	The cracks are located longitudinal direction	In the inspection, rapport is tolled that There e is a leakage at the underside of the deck. There is lime bloom at the underside.	Cracks are present	The cracks are located transverse direction.	In the inspection, rapport is tolled that There e is a leakage at the underside of the deck. There is lime bloom at the underside.	8-100 mm	503
Bridge AC	Side span Mainspan Side span	2	6 13 6	30	1931	Statically determinate	200	1	3	2	S235	44,58	Cracks are present	The cracks are located longitudinal direction	In the inspection, rapport is tolled that There e is a leakage at the underside of the deck. There is lime bloom at the underside.	Cracks are present	The cracks are located transverse direction.	In the inspection, rapport is tolled that There e is a leakage at the underside of the deck. There is lime bloom at the underside.	8-100 mm	503
Bridge AD	Side span Mainspan Side span	3	6,4 7,65 6,4	8,8	1938	Statically determinate	200	B35 CEMIII/B42,5 LH HS			S235	44,58	Cracks are present	The cracks are located longitudinal direction	In the inspection, rapport is tolled that There e is a leakage at the underside of the deck. There is lime bloom at the underside.	Cracks are present	The cracks are located transverse direction.	In the inspection, rapport is tolled that There e is a leakage at the underside of the deck. There is lime bloom at the underside.	8-135 mm	372
Bridge AE	Side span Mainspan Side span	3	6,4 7,65 6,4	1044	1938	Statically determinate	200	B35 CEMIII/B42,5 LH HS			S235	44,58	Cracks are present	The cracks are located longitudinal direction	In the inspection, rapport is tolled that There e is a leakage at the underside of the deck. There is lime bloom at the underside.	Cracks are present	The cracks are located transverse direction.	In the inspection, rapport is tolled that There e is a leakage at the underside of the deck. There is lime bloom at the underside.	8-135 mm	372
Bridge AF	Mainspan	1	10	12,45	1947	Statically determinate	200	1	3	2	S235	44,58	Cracks are present	The cracks are located longitudinal direction	In the inspection, rapport is tolled that There e is a leakage at the underside of the deck. There is lime bloom at the underside.	Cracks are present	The cracks are located transverse direction.	In the inspection, rapport is tolled that There e is a leakage at the underside of the deck. There is lime bloom at the underside.	10-120 mm	654

Reinforcement layout foot/Bike path						Reinforcement layout Lanes				Reinforcement layout tramway			
e direction		Longitudinal direction				Transverse direction		Longitudinal direction		Transverse direction		Longitudinal direction	
Reinforcement	Reinforcement in mm^2/m	Reinforcement	Reinforcement in mm^2/m	Reinforcement	Reinforcement in mm^2/m	Reinforcement	Reinforcement in mm^2/m	Reinforcement	Reinforcement in mm^2/m	Reinforcement	Reinforcement in mm^2/m	Reinforcement	Reinforcement in mm^2/m
8-100 mm	503	8-100 mm	503	8-100 mm	503	6-100 mm	284	6-100 mm	284	6-100 mm	284	6-100 mm	284
6-100 mm	284	8-100 mm	284	6-100 mm	284	6-100 mm	284	6-100 mm	284	6-100 mm	284	6-100 mm	284
12-150 mm	754	12-150 mm	754	12-150 mm	754	6-100 mm	284	6-100 mm	284	6-100 mm	284	6-100 mm	284
6-100 mm	284	6-100 mm	284	6-100 mm	284	6-100 mm	284	6-100 mm	284	None	0	None	0
8-100 mm	503	8-100 mm	503	8-100 mm	503	8-100 mm	503	8-100 mm	503	None	0	None	0
10-120 mm	654	10-120 mm	654	10-120 mm	654	10-120 mm	654	10-120 mm	654	10-120 mm	654	10-120 mm	654
8-100 mm	503	8-100 mm	503	8-100 mm	503	6-100 mm	284	6-100 mm	284	6-100 mm	284	6-100 mm	284
8-100 mm	503	8-100 mm	503	8-100 mm	503	8-100 mm	503	8-100 mm	503	8-100 mm	503	8-100 mm	503
8-100 mm	503	8-100 mm	503	8-100 mm	503	8-100 mm	503	8-100 mm	503	8-100 mm	503	8-100 mm	503
8-100 mm	503	8-100 mm	503	8-100 mm	503	8-100 mm	503	8-100 mm	503	None	0	None	0
12-150 mm	754	12-150 mm	754	12-150 mm	754	12-150 mm	754	12-150 mm	754	none	0	none	0
6-100 mm	284	6-100 mm	284	6-100 mm	284	6-100 mm	284	6-100 mm	284	None	0	None	0
8-100 mm	503	8-100 mm	503	8-100 mm	503	6-100 mm	284	6-100 mm	284	6-100 mm	284	6-100 mm	284
8-100 mm	503	8-100 mm	503	8-100 mm	503	6-100 mm	284	6-100 mm	284	6-100 mm	284	6-100 mm	284
8-100 mm	503	8-100 mm	503	8-100 mm	503	8-100 mm	503	8-100 mm	503	None	0	None	0
8-100 mm	503	8-100 mm	503	8-100 mm	503	6-100 mm	284	6-100 mm	284	6-100 mm	284	6-100 mm	284
10-100 mm	785	10-100 mm	785	10-100 mm	785	10-100 mm	785	10-100 mm	785	none	0	none	0
8-100 mm	503	8-100 mm	503	8-100 mm	503	6-100 mm	284	6-100 mm	284	6-100 mm	284	6-100 mm	284
12-100 mm	1131	12-100 mm	1131	12-100 mm	1131	12-100 mm	1131	12-100 mm	1131	None	0	None	0
8-100 mm	503	8-100 mm	503	8-100 mm	503	6-100 mm	284	6-100 mm	284	6-100 mm	284	6-100 mm	284
8-100 mm	503	8-100 mm	503	8-100 mm	503	6-100 mm	284	6-100 mm	284	None	0	None	0
8-100 mm	503	8-100 mm	503	8-100 mm	503	6-100 mm	284	6-100 mm	284	none	0	none	0
8-100 mm	503	8-100 mm	503	8-100 mm	503	6-100 mm	284	6-100 mm	284	none	0	none	0
6-100 mm	284	6-100 mm	284	6-100 mm	284	6-100 mm	284	6-100 mm	284	none	0	none	0
10-120 mm	654	10-120 mm	654	10-120 mm	654	10-120 mm	654	10-120 mm	654	none		none	0
8-250 mm	201	12-250 mm	754	8-250 mm	201	12-250 mm	452	8-250 mm	201	none	754	none	0
12-100 mm	1131	12-100 mm	1131	12-100 mm	1131	12-100 mm	1131	12-100 mm	1131	12-100 mm	1131	12-100 mm	1131
8-100 mm	503	8-100 mm	503	8-100 mm	503	6-100 mm	284	6-100 mm	284	6-100 mm	284	6-100 mm	284
8-100 mm	503	8-100 mm	503	8-100 mm	503	6-100 mm	284	6-100 mm	284	6-100 mm	284	6-100 mm	284
8-135 mm	372	8-135 mm	372	8-135 mm	372	8-135 mm	372	8-135 mm	372	None	0	None	0
8-135 mm	372	8-135 mm	372	8-135 mm	372	8-135 mm	372	8-135 mm	372	None	0	None	0
10-120 mm	654	10-120 mm	654	10-120 mm	654	10-120 mm	654	10-120 mm	654	None	0	None	0

layout of the bridge deck in (m)			The minimal width of bridge deck in (m)			A centre-to-centre distance in (mm)								
foot/Bike path	Lanes	Tramway	foot/Bike path	Lanes	Tramway	foot/ Bikepath			Lanes			Tramway		
						Distance 1	Distance 2	Distance 3	Distance 1	Distance 2	Distance 3	Distance 1	Distance 2	Distance 3
4	3,65	2,35	200	570	570	810	790	None	790	820	None	820	730	590
4,5	5	7	200	500	360	750	800	None	690	None	None	730	600	None
4	4,2	5,75	200	500	400	810	800	None	800	700	None	628	508	None
3	5	None	200	400	None	750	None	None	720	520	None	None	None	None
4	4	None	200	500	None	740	700	730	600	730	810	None	None	None
2,52	4,5	2,5	600	600	520	900	850	None	550	400	750	260	400	290
6,5	6,26	4,5	200	570	570	700	800	None	750	730	None	730	600	None
5	5	3,5	300	430	none	700	800	None	750	600	730	None	None	None
3	4,5	none	100	430	none	750	850	None	700	800	None	None	None	None
6,5	8,5	none	100	440	none	660	770	760	690	730	600	None	None	None
1,3	5,35	none	560	560	none	930	710	None	730	None	None	None	None	None
2	4,5	None	580	580	None	600	800	None	770	None	None	None	None	None
6,5	3	3	200	600	600	700	760	600	730	730	None	730	600	None
6,5	4,5	4	200	600	600	700	760	600	730	730	None	730	600	None
1,5	5,5	None	600	600	None	820	821	822	700	701	702	None	None	None
6,5	6	4,73	100	650	650	700	780	None	680	670	None	730	600	None
6,5	6	none	200	580	none	750	750	750	760	760	760	None	None	None
6,5	6	5	100	580	580	700	800	None	750	730	None	730	600	None
4	6	none	200	600	none	1300	710	None	700	730	600	None	None	None
5,65	6	3,5	100	570	570	700	800	None	750	None	None	750	600	None
6,5	6	none	100	580	none	700	800	None	750	730	None	None	None	None
6	7,5	none	100	500	none	700	765	700	700	730	600	None	None	None
6,5	5,5	6	100	580	580	700	800	None	750	730	None	730	600	None
5	5	none	570	570	none	790	800	None	740	730	None	None	None	None
8	6	5	690	690	600	1300	750	770	750	660	None	730	660	None
6,5	6	none	620	500	none	800	750	900	740	730	600	None	None	None
6,9	5	3	600	550	380	1060	760	700	740	None	None	740	730	600
6	6,5	2,5	100	650	630	700	800	None	730	None	None	730	600	None
6,3	3,75	6,5	100	500	430	720	800	None	750	730	None	730	600	None
3	5	None	200	570	None	780	790	None	790	780	None	None	None	None
3	5	None	200	570	None	930	None	None	800	None	None	None	None	None
3,5	2	None	600	500	None	760	700	None	700	810	None	None	None	None

Steel profile of the bridge										
foot/Bikepath						Lanes				
Profile 1	properties Ixx cm4	Profile 2	properties Ixx cm4	Profile 3	properties Ixx cm4	Profile 1	properties Ixx cm4	Profile 2	properties Ixx cm4	Profile 3
B32	30 119	NP40	20 173	None	0	B40	57894	None	0	None
DIN24 DIN25 DIN26	11690 13300 15050	DIN30 DIN30 DIN30	25760 25760 25760	NP28 NP34 NP28	7675 15070 0	DIN26 DIN30 DIN26	15050 25760 15050	DIN26 DIN30 DIN26	15050 25760 15050	DIN26 DIN30 DIN26
BP26 = HEA 260	10455	INP42	36973	INP34	605	DIN34	36940	BP32 = HEA 320	22929	None
BP29		None	0	None	0	BP34 = HEA 340	27693	BP29 = HEA 290	13673	None
DIN30	25760	DIN34	36940	NP40	29173	DIN36	45120	DIN32	32250	None
INP450	49649	None	0	None	0	DIN38	50950	INP40	29213	None
DIN 32 DIN 32 DIN 32	32250 32250 32250	DIN 36 DIN 36 DIN 36	45120 45120 45120	NP30 NP45 NP30	9785 45888 9785	DIN28 DIN40 DIN28	20720 60640 20720	NP34 None NP34	15070 15070	None None None
DIN 30	25760	DIN 36	45120	None	0	DIN 36	45120	None	0	None
DIN 30	25760	DIN 34	36940	NP43	36056	DIN 36	45120	None	0	None
DIN 30	25760	DIN 34	36940	DIN 32	32250	DIN 36	45120	DIN 32	45120	None
DIN 34	36940	None	0	None	0	DIN 38	50950	None	0	None
NP45	45888	NP46	50410	NP47	50410	BP45 = HEA450	63722	BP46 = HEA460	63722	BP47 = HEA470
B36	42479	NP45	45 888	NP50	68730	B45	80887	None	0	None
B36	42479	NP45	45 888	NP50	68730	B46	94811	None	0	None
DIN42	69480	DIN35	45120	None	0	DIN35	36940	DIN35	36940	DIN35
DIN38	50950	DIN45	84220	NP50	68736	DIN50	113180	DIN50	113180	None
DIN45	84220	NP55	00 064	None	0	DIN50	113180	None	0	None
BP32 = HEA320	22929	BP36 = HEA 360	33090	NP30 NP45	9785 45888	BP45 = HEA450	63722	None	0	None
DIR65	216780	NP45	45 888	NP36	19578	NP36	19578	NP38	23 978	None
BP32 = HEA 320	22929	BP36 = HEA 360	33090	NP45	45888	BP45 = HEA450	63722	None	0	None
BP32 = HEA 320	22929	BP3 = HEA 300	18263	NP30 NP45	9785 45888	BP40 = HEA400	45069	BP45 = HEA450	63722	BP50 = HEA500
BP26 = HEA 260	10455	BP28 = HEA 280	13673	NP34	15070	BP28 = HEA280	13673	BP30		BP34
BP32 = HEA 320	22929	BP36 = HEA 360	33090	NP30 NP45	 45888	BP28 = HEA280 BP45 = HEA450	13673 63722	NP34 BP45 = HEA450	15070 63722	NP38 BP50 = HEA500
DIN38	50950	NP30 DIN40	9 785 60640	None	0	NP30 DIN45	9785 84220	None	0	None
DIN65	216780	NP38 DIN50	23 078 113180	None	0	NP36 DIN50	19578 113180	NP36 DIN55	19578	None
DIR65	216780	DIN40 DIN48	60640 95120	DIN40 DIN50	60640 113180	DIN40 DIN50	60640 113180	DIN28 DIN50	20720 113180	DIN30 DIN55
DIR66	216780	DIN56 DIN64	140340 216780	DIN60 DIN70	180830 270290	DIN60 DIN70	180830 270290	DIN72 DIN94	270290 572950	DIN80 DIN105
DIN36	45120	DIN40	60640	NP30 NP50	 68730	NP34 NP50	 68730	NP40 NP50	 68736	None
DIN26	15050	DIN28	20720	NP36	19570	DIN32	32250	DIN36	45120	None
DIN32	32250	NP36	19570	None	0	DIN30 DIN32	25760 32250	None	0	None
DIN28	20720	NP30 NP34	9785 15070	None	0	DIN26 DIN28	15050 20720	None	0	None
DIN47	95120	DIN36	45120	DIE40	45210	DIE40	45210	DIE40	45210	None

	Tramway					
properties Ixx cm4	Profile 1	properties Ixx cm4	Profile 2	properties Ixx cm4	Profile 3	properties Ixx cm4
0	B45	80887	B40	111283	None	0
15050	DIN26	15050	DIN28	20720	None	0
25760	DIN30	25760	DIN34	36940		
15050	DIN26	15050	DIN28	20720		
0	BP26 = HEA260		INP42	36973	DIN34	36940
0	None	0	None	0	None	0
0	None	0	None	0	None	0
0	INP40	29213	INP40	29213	None	0
0	NP34	15070	NP36	19576	None	0
0	DIN40	60640	DIN45	84220	None	0
0	NP34	15070	NP36	19576	None	0
0	None	0	None	0	None	0
0	None	0	None	0		0
0	None	0	None	0	None	0
0	None	0	None	0	None	0
63722	None	0	None	0	None	0
0	B45	80887	B50	111283	None	0
0	B45	80887	B50	111283	None	0
36940	None	0	None	0	None	0
0	DIN 55	140340	DIN 50	113180	None	0
0	None	0	None	0	None	0
0	BP45 = HEA450	63722	BP50 = HEA500	86975	None	0
0	None	0	None	0	None	0
0	BP45		BP50		None	0
86975	None	0	None	0	None	0
	None	0	None	0	None	0
23978	NP34	15070	NP38	23978	None	0
86975	BP45 = HEA450	63722	BP50 = HEA500	86975		
0	None	0	None	0	None	0
0	NP38	23978	NP36	19578	None	0
	DIN50	113180	DIN55	19578		
25760	None	0	None	0	None	0
140340						
366390	None	0	None	0	None	0
644750						
0	NP34		NP40	29173	None	0
	NP50	68736	NP55	99054		
0	None	0	None	0	None	0
0	None	0	None	0	None	0
0	None	0	None	0	None	0
0	None	0	None	0	None	0

8. The drawing of the three selected bridges

DOORSNEDE E.E
DOORSNEDE F.F
AANZICHT WALMUREN VANAF Nwe PRINSENGRACHT
DOORSNEDE G.G
DOORSNEDE H.H
7 VAKKEN VAN 1.40 m.
OUDE TOESTAND
SLOOPLYN
vL. B
vL. C
ZYAANZICHT VANAF ONBEKENDE GRACHT
vL. D
vL. A
MIDDENDOORSNEDE VERBREDE BRUG
MIDDENDOORSNEDE OUDE BRUG
DETAIL VLEUGELS
BOVENAANZICHT vL. D
vL. A IS HET SPIEGELBEELD
BOVENAANZICHT vL. C
vL. B IS HET SPIEGELBEELD
AANZICHT WALMUUR vL. A
5 VAKKEN VAN 1.40 m
BOVENAANZICHT
TROTTOIRBANDEN VAN SPECIALE BETON IN LENGTEN VAN 1.15 m.
VOORAANZICHT
VOORAANZICHT
DETAIL BRUGEINDE T.P.V. RUWEG
2 STUKS
1 RECHTS 1 LINKS
TE BEHAKKEN BLOKKEN
1 RECHTS 1 LINKS
2 STUKS
2 STUKS
1 RECHTS 1 LINKS
ALLE MATEN NAUWKEURIG IN HET WERK TE CONTROLEREN
DOORSNEDE K-K
DOORSNEDE J.J
DOORSNEDE K.K
KOPPELING EINDBALK EN BEVESTIGING LEUNING
DETAIL RYPLAATJES
6 + 2 STUKS
DEKSTENEN vL. A EN D
2 STUKS, 1 RECHTS 1 LINKS
DE AFMETINGEN DER STENEN MOETEN IN HET WERK NADER WORDEN BEPAALD.
DEKSTENEN vL. B EN C
4 STUKS, 2 RECHTS 2 LINKS
DSN I-I
NIEUWE PRINSENGRACHT
ONBEKENDE GRACHT
SITUATIE
VOORAANZICHT LANDHOOFD
HET ANDERE LANDHOOFD IS HET SPIEGELBEELD


Doorsnede Langs pijler in middendoorvaart.
Alle krimpnetten ϕ10-12
Westzijde
2e Werkperiode
1e Werkperiode
Wegprofiel tijdens 2e werkperiode
IN DIT BUISVAK LIGGEN
3-4" BUIZEN
Doorsnede Langs Landhoofd Noordzijde
Westzijde
Liggerverdeeling. Schaal 1 a 50.
Zijde Stadionplein
2e Werkperiode
1e Werkperiode
Doorsnede A-B.
Doorsnede C-D
16" Gas
Doorsnede over het midden van de hoofddoorvaart. 1a10.
Trottoir Westzijde.
Bitume isolatie
Dekistingconstructie
aan buitenligger
en in telefoonvak
Doorsnede over Westelijk trottoir zijdoorvaart 1a10.
Zie voor wapening de doorsn: op schaal 1a20
Buitenkant trottoir W.Gr.
Leuning te maken door derden.
Doorsn: E-F
L 200-100-14

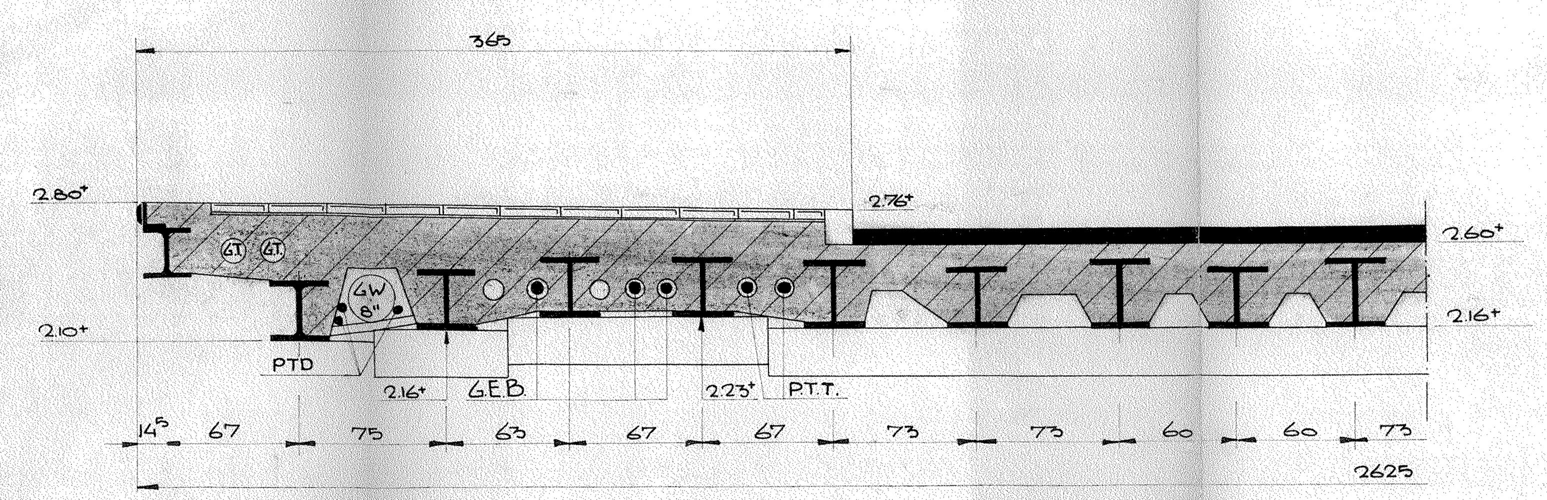

DOORSNEDE A-A BESTAANDE TOESTAND

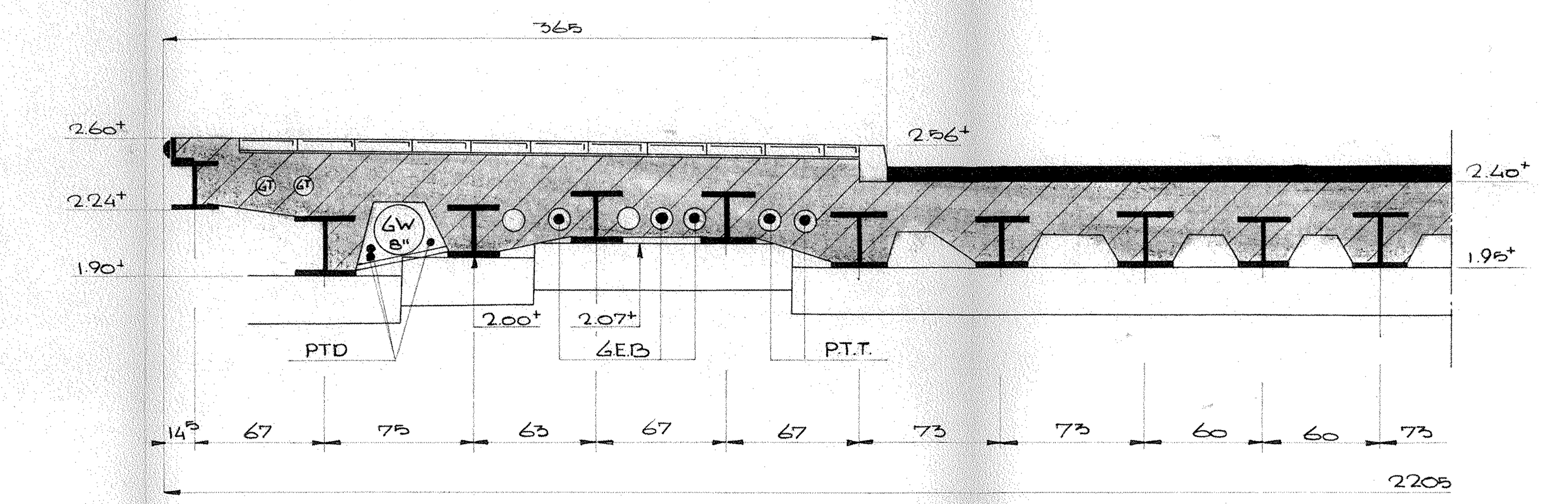

DOORSNEDE B-B BESTAANDE TOESTAND

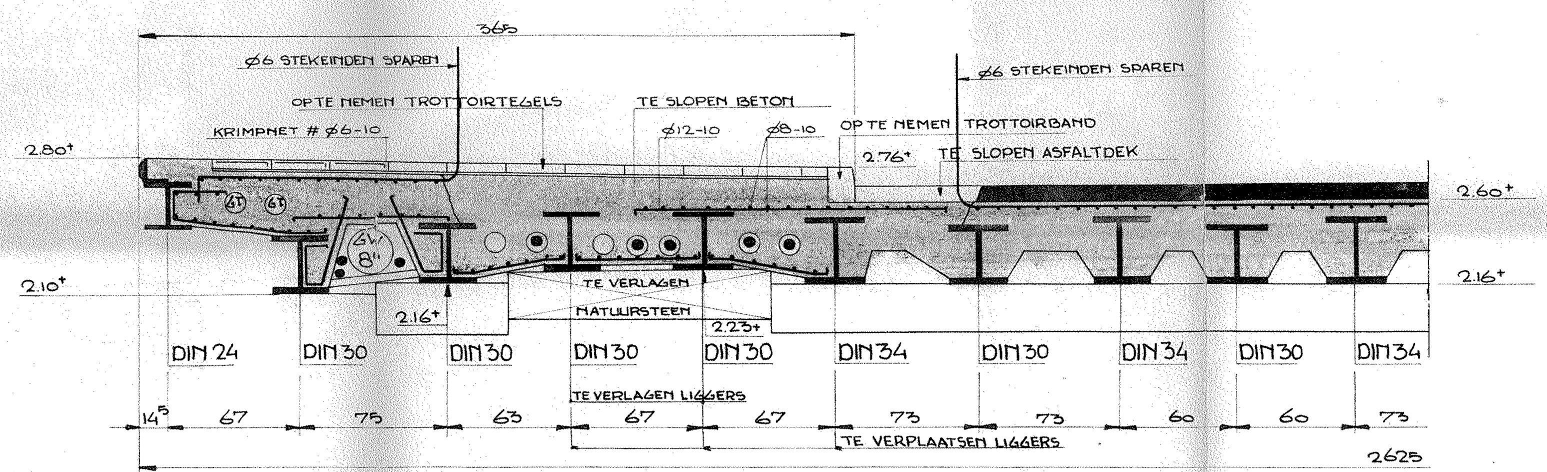

DOORSNEDE A_A SLOOPWERK

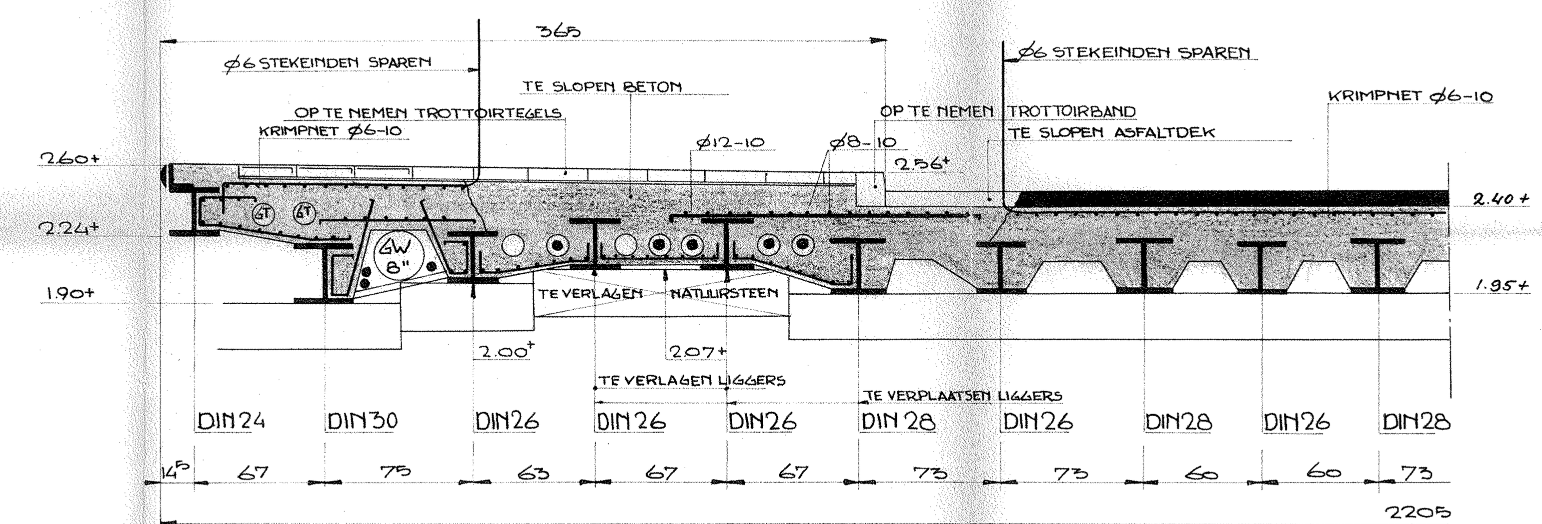

DOORSNEDE B-B SLOOPWERK

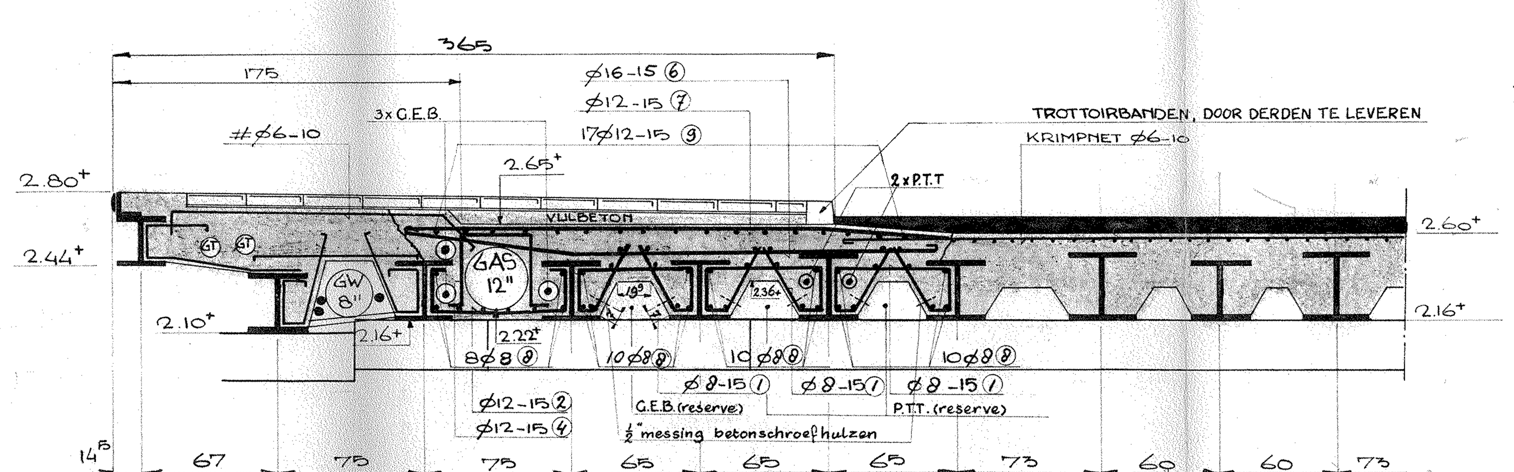

DOORSNEDE A-A NIEUWE TOESTAND.

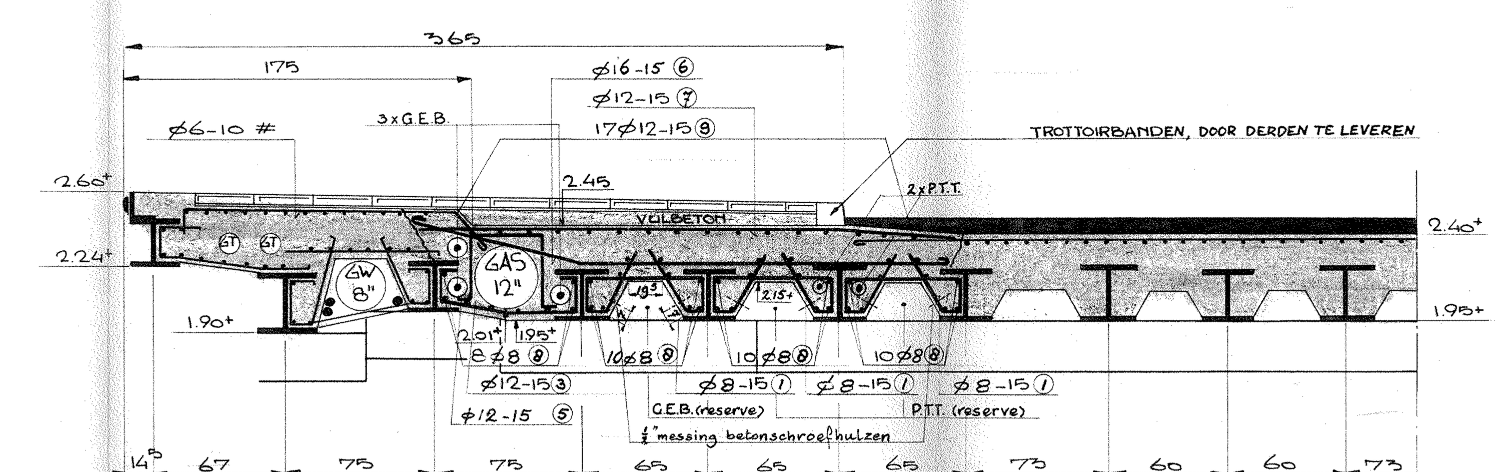

DOORSNEDE B_B NIEUWE TOESTAND.

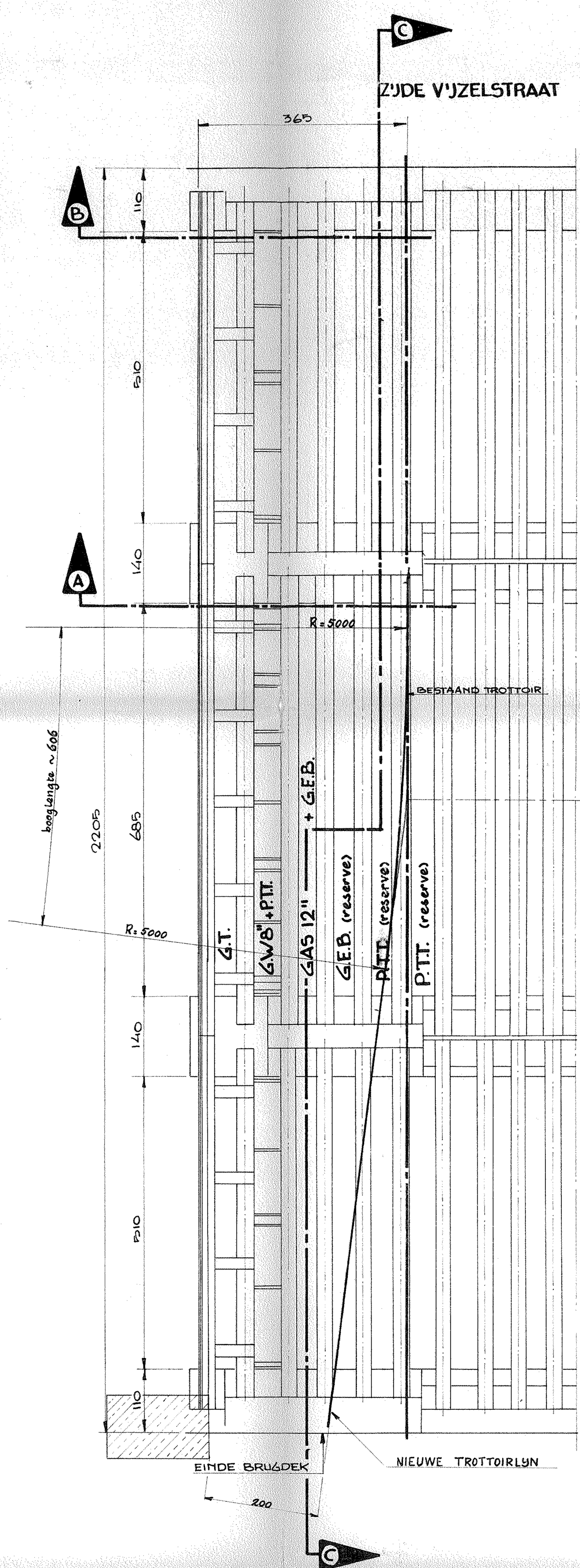

PLATTEGROND.

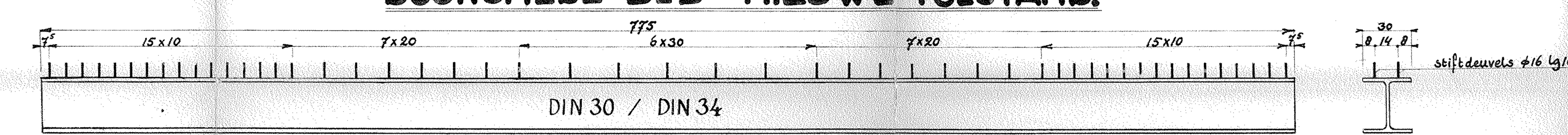

DEUVELVERDELING BALKEN MIDDENOVERSPANNING (3 stuks)

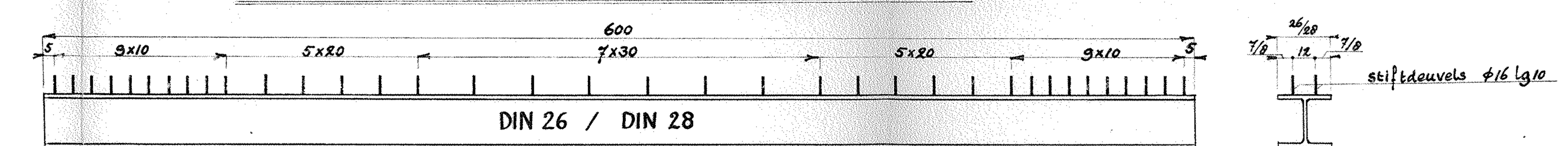

DEUVELVERDELING BALKEN ZYDOORVAARTEN (6 stuks)

Totaal aantal stiftdeuvels 738 stuks

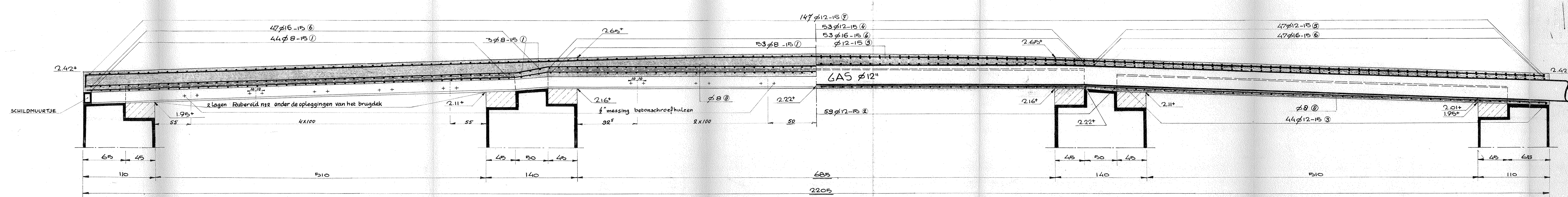

DOORSNEDE C-C NIEUWE TOESTAND

VULBETON EN TROTTOIR WEGGELATEN

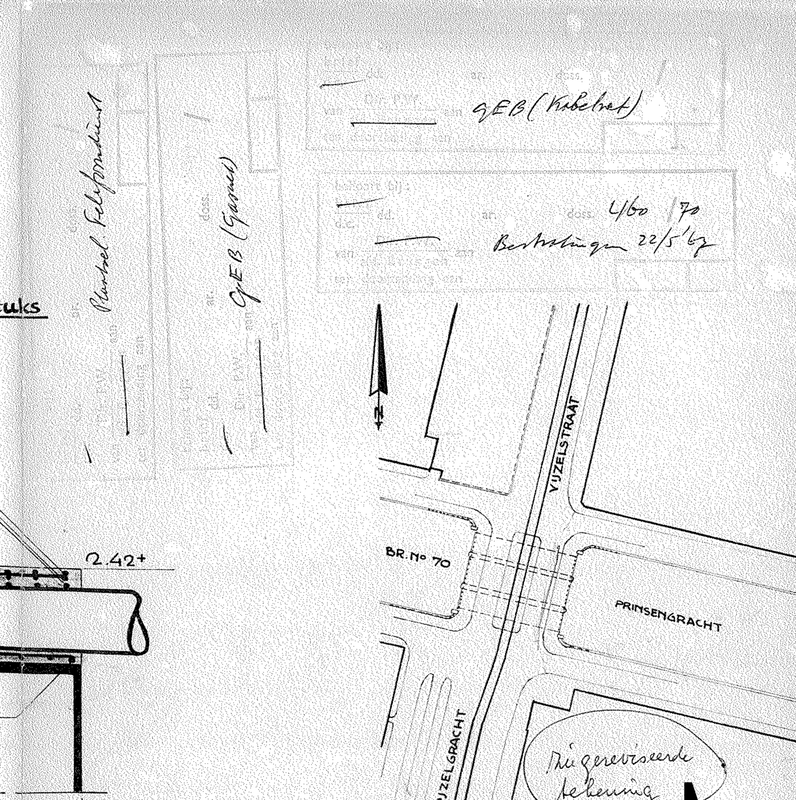

Reserve kabelnet G.E.B. 17-3-'67

[redacted]

DOORSNEDE E.E
DOORSNEDE F.F
AANZICHT WALMUREN VANAF Nwe PRINSENGRACHT
DOORSNEDE G.G
DOORSNEDE H.H
OUDE TOESTAND
SLOOPLYN
MIDDENDOORSNEDE VERBREDE BRUG
ZYAANZICHT VANAF ONBEKENDE GRACHT
MIDDENDOORSNEDE OUDE BRUG
DETAIL VLEUGELS
BOVENAANZICHT vL. D
vL. A IS HET SPIEGELBEELD
BOVENAANZICHT vL. C
vL. B IS HET SPIEGELBEELD
AANZICHT WALMUUR vL. A
vL. D
vL. C
vL. A
vL. B
BOVENAANZICHT
DETAIL BRUGEINDE T.P.V. RUWEG
VOORAANZICHT
VOORAANZICHT
TE BEHAKKEN BLOKKEN
2 STUKS 1 RECHTS 1 LINKS
1 RECHTS 1 LINKS 2 STUKS
2 STUKS 1 RECHTS 1 LINKS
ALLE MATEN NAUWKEURIG IN HET WERK TE CONTROLEREN
DOORSNEDE K-K
DOORSNEDE J.J
DOORSNEDE K.K
DETAIL RYPLAATJES 6+2 STUKS
DEKSTENEN vL. A EN D 2 STUKS, 1 RECHTS 1 LINKS
DEKSTENEN vL. B EN C 4 STUKS, 2 RECHTS 2 LINKS
KOPPELING EINDBALK EN BEVESTIGING LEUNING
VOORAANZICHT LANDHOOFD
HET ANDERE LANDHOOFD IS HET SPIEGELBEELD
NIEUWE PRINSENGRACHT
ONBEKENDE GRACHT
SITUATIE

A.3. Input of the numerical calculation

Length of the beam

Length Span (mm)	Effective width (Bef) (mm)
6500.00	690.63

Geometry of the cross-section

Concrete			Steel		
width 1 in (mm)	width 2(mm)	width 3 (mm)	Profile 1	Heigth above the steel flange (mm)	Height (mm)
730.00	335.00	335.00	DIN26	170.00	260.00
Heighte part1	Heighte part 2 (mm)	Heighte part 3 (mm)			
260.00	80.00	80.00			

Material properties of the cross section

E=concrete (N/mm^2)	50 % E=concrete (N/mm^2)	30 % E = concrete (N/mm^2)	Section steel E= steel in (N/mm^2)
3.80E+04	3.80E+04	3.80E+04	2.10E+05

Calculating the stiffness of the cross-section

Moment of inertia of concrete			Moment of inertia of steel
Moment of inertia concrete part 1	Moment of inertia concrete part 2	Moment of inertia concrete part 3	Moment of inertia steel
1.07E+09	1.43E+07	1.43E+07	1.48E+08

Area of concrete			Area of steel
Area section 1 A1 (mm^2)	Area section 2 A2 (mm^2)	Area section 3 A3 (mm^2)	Area steel A (mm^2)
1.90E+05	2.68E+04	2.68E+04	1.19E+04

Calucalting the NC

Differance between the NC on the cross-section for height 1 (mm)	Differance between the NC on the cross-section for height 2 (mm)	Differance between the NC on the cross-section for height 3 (mm)	height above the steel (mm)
-72.57	97.43	177.43	97.43

EI1 (Nmm^2)	EI2 (Nmm^2)	EI3 (Nmm^2)	EI4 (Nmm^2)
4.06E+13	5.43E+11	5.43E+11	3.10E+13

EA1 (N)	EA2 (N)	EA3(N)	EA4 (N)
7.21E+09	1.02E+09	1.02E+09	2.50E+09

EA*a^2	EA*a^3	EA*a^4	EA*a^5
3.80E+13	9.67E+12	3.21E+13	2.37E+13

Calucalting the NC and the total EI/EA

Totaal EAz	Totaal EA	NC of the cross-section (mm)	The total EI cross-section
2.38E+12	1.17E+10	202.57	1.76E+14

Verification with forget me nots

F	Span	F*l^3	SpanL^3	The total EI cross-section	48EI	W1
83000.00	6050.00	1.84E+16	2.21E+11	1.76E+14	8.45E+15	2.17
Q	Span	5*Q*l^4	SpanL^4	The total EI cross-section	384EI	W2
1.00	6050.00	6.70E+15	1.34E+15	1.76E+14	6.76E+16	0.10
					W T	2.27

B Annex – Analytical way to predict the interaction level between steel and concrete

> restart :

> $EI_c := 1.21\mathrm{E}{+}14 : EI_s := 5.47\mathrm{E}{+}13 : y_{cb} := 160 : y_{st} := 130 : G := 215550000 : L := 5600 :$
$EA_s := 5.53\mathrm{E}{+}13 : EA_c := 9.98\mathrm{E}{+}09 :$

> $q(x) := 100554 \cdot \mathrm{Dirac}(x - 0.5 \cdot L) :$

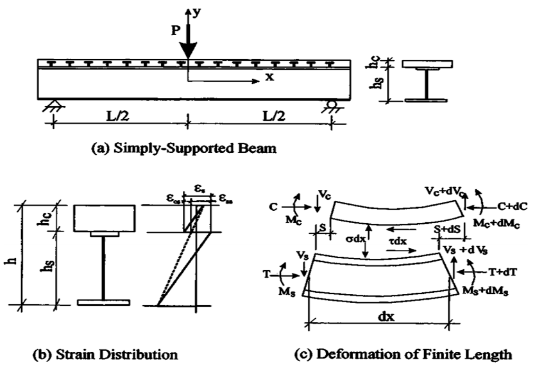

Fig. 1. Calculation model for simply supported beam

$\#diff\left(V_c(x), x\right) + diff\left(V_s(x), x\right) = q(x)$

$\#V_c(x) + V_s(x) = -\left(diff\left(M_c(x), x\right) + diff\left(M_s(x), x\right)\right) + \frac{1}{2} \cdot \mathrm{tau}(x) \cdot \left(y_{cb} + y_{st}\right)$

$\#M_s(x) + M_c(x) = \left(EI_s + EI_c\right) \cdot \mathrm{kappa}(x)$

> $DV1 := diff\left(-diff\left(\left(EI_s + EI_c\right) \cdot diff(w(x), x\$2), x\right) + 0.5 \cdot \left(y_{cb} + y_{st}\right) \cdot \frac{G}{L} \cdot s(x), x\right) = q(x);$

$$DV1 := -1.757\ 10^{14}\ \frac{d^4}{dx^4}\ w(x) + 5.581205357\ 10^{6}\ \frac{d}{dx}\ s(x) = 100554\ \mathrm{Dirac}(x - 2800.0) \qquad \textbf{(1)}$$

> $DV2 := diff(s(x), x\$2) = diff(diff(w(x), x\$2), x) \cdot \left(y_{cb} + y_{st}\right) + \left(\frac{1}{EA_s} + \frac{1}{EA_c}\right) \cdot \frac{G}{L} \cdot s(x);$

$$DV2 := \frac{d^2}{dx^2}\ s(x) = 290\ \frac{d^3}{dx^3}\ w(x) + 3.857516827\ 10^{-6}\ s(x) \qquad \textbf{(2)}$$

> $sys\_ode := DV1, DV2 :$

> $assign(dsolve([\ sys\_ode]))$

> $w := (w(x)) : s := (s(x)) :$

> $eq1 := evalf(subs(x = 0, w = 0)) :$

> $eq2 := evalf(subs(x = 0, diff(s, x))) = 0 :$

> $eq3 := evalf\left(\left(EI_s + EI_c\right) \cdot subs(x = 0, diff(w, x\$2))\right) = 0 :$

> $eq4 := evalf(subs(x = L, w = 0)) :$

> $eq5 := evalf(subs(x = L, diff(s, x))) = 0 :$

> $eq6 := evalf\left(\left(EI_s + EI_c\right) \cdot subs(x = L, diff(w, x\$2))\right) = 0 :$

> $bcs := eq1, eq2, eq3, eq4, eq5, eq6 :$

> $con := \_C1, \_C2, \_C3, \_C4, \_C5, \_C6 :$

> $assign(solve(\{bcs\}, \{con\}))$

> $plot(w, x = 0 ..L)$

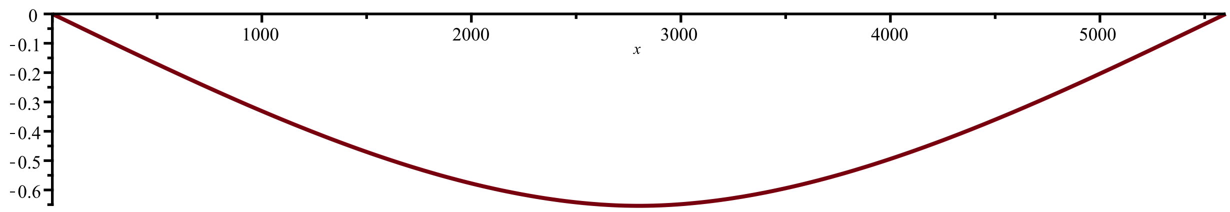

>

> $plot(s, x = 0 ..L)$

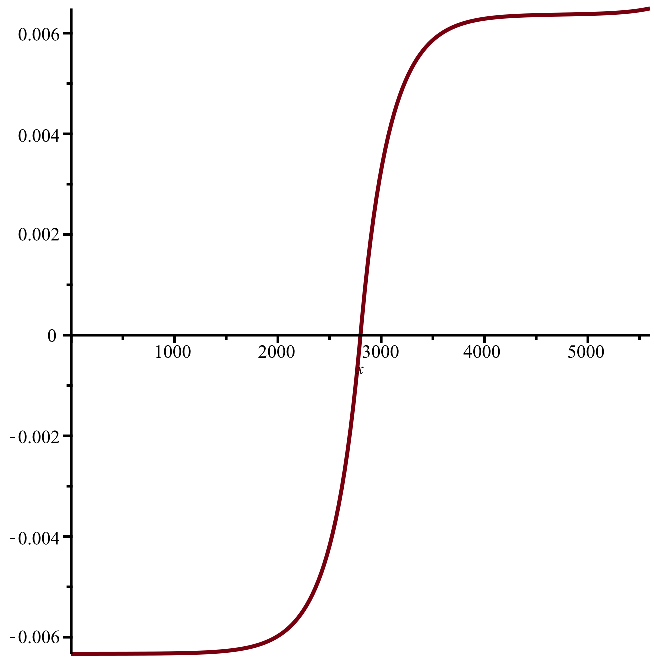

> $plot(diff(s, x), x = 0 ..L)$

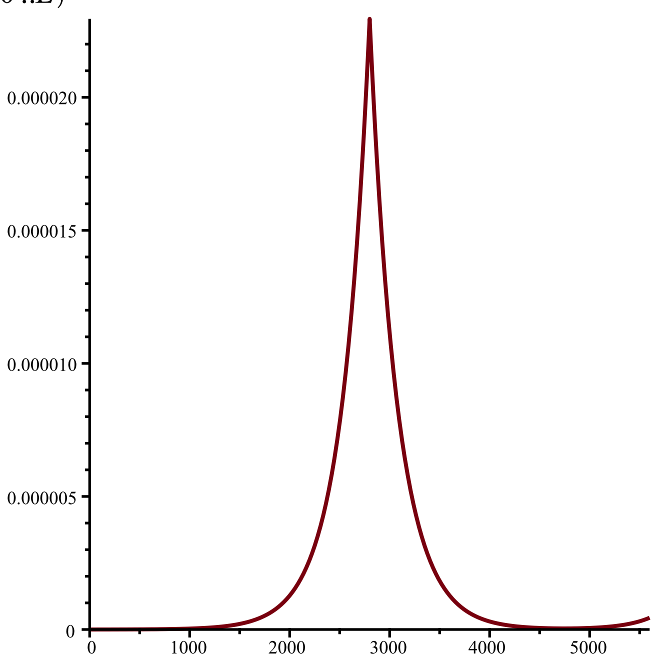

>

C Annex – The measured data for each test and the made analysis

C.1. Measured data for test 1 including the analysis

In the figure C-1 the configuration of test 1 is presented. The description, discussion and the conclusion can be can found in paragraph 4.2 and 4.3. In this section only the tables will be adding with the made analysis which is described can be found in paragraph 4.2.2.

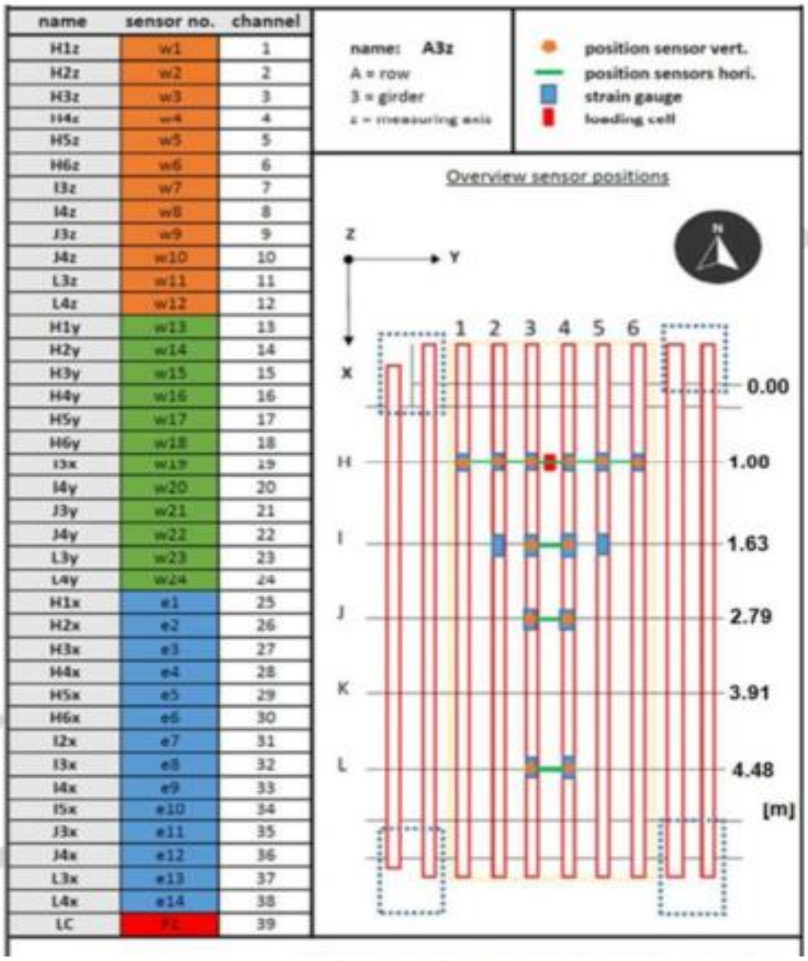

Figure C-1: Configuration of in-situ-load-test 1.

In table C-1 and C-4 can be found the measured strain and displacement during test 1 due to cyclic loading (traffic load) + the residual deformations. The table C-2 and C-5 can be found the measured strain and displacement due to the effect of the residual deformations. In table C-3 and C-6 the total measured strain and displacement due to cyclic loading (traffic load) is available. This procedure is being used for all the three tests. In the following section only the data and the configuration will be presented. See the tables C-1 until C-6.

Table C-1: The measured displacement due to cyclic loading (traffic load) + residual displacement.

Load [kN]	H6z [mm]	H5z [mm]	H4z [mm]	H3z [mm]	H2z [mm]	H1z [mm]	I4z [mm]	I3z [mm]	J4z [mm]	J3z [mm]	L4z [mm]	L3z [mm]
0	0	-0,002	-0,002	-0,003	-0,003	-0,004	-0	-0	-0	-0	-0	0
100	0,018	0,039	0,059	0,057	0,038	0,015	0,075	0,074	0,073	0,069	0,036	0,03
200	0,076	0,116	0,159	0,152	0,109	0,059	0,2	0,192	0,187	0,179	0,094	0,08
300	0,13	0,20	0,26	0,26	0,19	0,12	0,33	0,33	0,32	0,31	0,16	0,15
400	0,13	0,23	0,32	0,31	0,22	0,12	0,41	0,40	0,39	0,38	0,20	0,19
475	0,15	0,26	0,38	0,36	0,25	0,14	0,49	0,47	0,46	0,45	0,24	0,22

Table C-2: The measured residual displacement.

Load cyclus	H6z [mm]	H5z [mm]	H4z [mm]	H3z [mm]	H2z [mm]	H1z [mm]	I4z [mm]	I3z [mm]	J4z [mm]	J3z [mm]	L4z [mm]	L3z [mm]
3	0,04	0,05	0,07	0,07	0,06	0,05	0,08	0,08	0,08	0,08	0,05	0,07
6	0,08	0,09	0,10	0,11	0,09	0,08	0,13	0,13	0,12	0,13	0,08	0,10
9	0,06	0,07	0,10	0,11	0,09	0,08	0,13	0,12	0,12	0,12	0,09	0,10
12	0,06	0,08	0,11	0,12	0,1	0,09	0,14	0,14	0,14	0,14	0,09	0,11

Table C-3: The measured displacement due to cyclic loading (traffic load).

Load [kN]	H6z [mm]	H5z [mm]	H4z [mm]	H3z [mm]	H2z [mm]	H1z [mm]	I4z [mm]	I3z [mm]	J4z [mm]	J3z [mm]	L4z [mm]	L3z [mm]
0	0,00	0,00	0,00	0,00	0,00	0,00	0,00	0,00	0,00	0,00	0,00	0,00
100	0,02	0,04	0,06	0,06	0,04	0,02	0,08	0,07	0,07	0,07	0,04	0,03
200	0,04	0,06	0,09	0,08	0,05	0,01	0,12	0,11	0,11	0,10	0,05	0,02
300	0,05	0,11	0,16	0,15	0,10	0,04	0,20	0,20	0,19	0,18	0,08	0,05
400	0,08	0,15	0,22	0,20	0,13	0,04	0,28	0,28	0,27	0,26	0,12	0,08
475	0,09	0,18	0,27	0,25	0,15	0,04	0,34	0,34	0,33	0,32	0,15	0,10

Table C-4: The measured strain due to cyclic loading (traffic load) + the residual strain.

Load [kN]	H6x [µm/m]	H5x [µm/m]	H4x [µm/m]	H3x [µm/m]	H2x [µm/m]	H1x [µm/m]	I2x [µm/m]	I4x [µm/m]	I3x [µm/m]	I5x [µm/m]	J4x [µm/m]	J3x [µm/m]	L4x [µm/m]	L3x [µm/m]
0	0,1	0,2	0,1	0,0	0,1	0,0	0,1	0,0	0,0	0,1	0,0	0,3	0,4	0,7
100	2,7	10,8	15,7	15,6	10,5	6,6	11,4	11,0	11,3	8,6	6,8	7,5	1,1	1,2
200	0,6	21,2	32,5	32,3	20,7	12,6	23,4	22,9	23,1	17,8	13,1	15,0	1,2	0,3
300	3,2	33,4	50,6	50,4	31,6	19,7	36,3	35,4	35,0	27,0	20,7	23,2	1,1	0,6
400	6,1	47,3	69,4	69,2	43,2	26,9	49,6	48,0	47,3	36,2	28,2	31,0	1,9	2,5
475	6,2	57,7	84,1	84,1	52,2	31,9	59,8	57,8	56,7	43,0	33,9	37,2	2,2	2,2

Table C-5: The measured residual strain.

Load cyclus	H6x [µm/m]	H5x [µm/m]	H4x [µm/m]	H3x [µm/m]	H2x [µm/m]	H1x [µm/m]	I2x [µm/m]	I4x [µm/m]	I3x [µm/m]	I5x [µm/m]	J4x [µm/m]	J3x [µm/m]	L4x [µm/m]	L3x [µm/m]
3	-1,3	4,6	8,6	8,6	5,0	2,7	6,3	6,2	6,2	4,6	3,1	4,5	0,0	-0,9
6	-1,5	5,7	9,8	10,1	5,6	2,6	7,1	7,2	6,7	4,7	3,5	5,2	-0,2	-1,3
9	-2,9	8,9	12,3	12,9	7,3	3,3	8,6	8,5	7,4	4,9	4,3	6,0	-0,7	-1,8
12	4,3	8,6	12,6	13,4	7,3	2,3	8,6	8,4	7,7	4,6	4,6	5,9	-0,6	-1,6

Table C-6: The measured strain due to cyclic loading (traffic load).

Load [kN]	H6x [µm/m]	H5x [µm/m]	H4x [µm/m]	H3x [µm/m]	H2x [µm/m]	H1x [µm/m]	I2x [µm/m]	I4x [µm/m]	I3x [µm/m]	I5x [µm/m]	J4x [µm/m]	J3x [µm/m]	L4x [µm/m]	L3x [µm/m]
0	0,1	0,2	0,1	0,0	0,1	0,0	0,1	0,0	0,0	0,1	0,0	0,3	0,4	0,7
100	2,7	10,8	15,7	15,6	10,5	6,6	11,4	11,0	11,3	8,6	6,8	7,5	1,1	1,2
200	1,9	16,6	23,9	23,7	15,7	9,9	17,1	16,7	16,9	13,2	10,0	10,5	1,2	1,2
300	4,7	27,7	40,8	40,3	26,0	17,1	29,2	28,2	28,3	22,3	17,2	18,0	1,3	1,9
400	9,0	38,4	57,1	56,3	35,9	23,6	41,0	39,5	39,9	31,3	23,9	25,0	2,6	4,3
475	1,9	49,1	71,5	70,7	44,9	29,6	51,2	49,4	49,0	38,4	29,3	31,3	2,8	3,8

C.2. Measured data for test 2 including the analysis

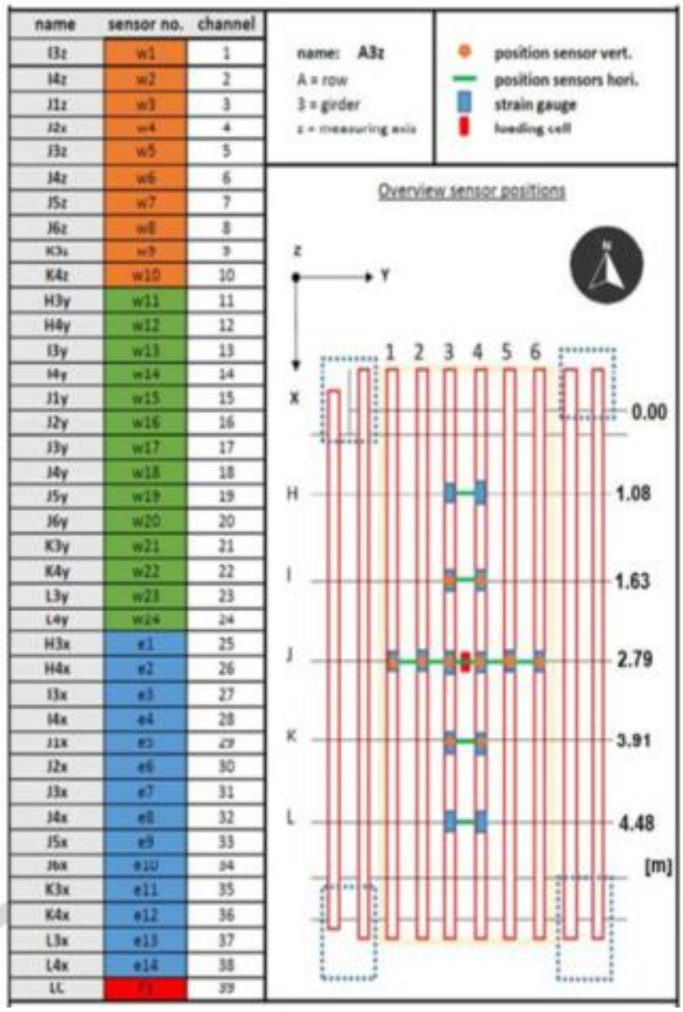

Figure C-2: Configuration of in-situ-load-test 2.

Table C-7: The measured displacement due to cyclic loading (traffic load) + the residual displacement.

Load [kN]	J6z [mm]	J5z [mm]	J4z [mm]	J3z [mm]	J2z [mm]	J1z [mm]	I4z [mm]	I3z [mm]	K4z [mm]	K3z [mm]
0	-0,01	-0,01	-0,01	-0,01	-0,01	0,00	-0,01	-0,01	0,00	0,00
100	0,05	0,09	0,12	0,12	0,11	0,06	0,08	0,08	0,10	0,11
200	0,17	0,24	0,29	0,29	0,26	0,15	0,20	0,21	0,25	0,24
300	0,31	0,42	0,51	0,51	0,46	0,30	0,37	0,39	0,43	0,43
400	0,42	0,57	0,68	0,68	0,61	0,39	0,50	0,52	0,58	0,58
475	0,55	0,70	0,83	0,83	0,74	0,48	0,62	0,64	0,71	0,70

Table C-8: The measured residual displacement.

Load cyclus	J6z [mm]	J5z [mm]	J4z [mm]	J3z [mm]	J2z [mm]	J1z [mm]	I4z [mm]	I3z [mm]	K4z [mm]	K3z [mm]
3	0,03	0,05	0,07	0,07	0,07	0,04	0,05	0,05	0,07	0,07
6	0,10	0,12	0,14	0,14	0,14	0,11	0,11	0,12	0,12	0,13
9	0,15	0,17	0,18	0,19	0,18	0,14	0,16	0,17	0,16	0,17
12	0,13	0,14	0,16	0,15	0,14	0,09	0,13	0,13	0,14	0,14
15	0,22	0,23	0,25	0,25	0,24	0,18	0,23	0,22	0,22	0,22

Table C-9: The measured displacement due to cyclic loading (traffic load).

Load [kN]	J6z [mm]	J5z [mm]	J4z [mm]	J5z [mm]	J2z [mm]	J1z [mm]	I4z [mm]	I3z [mm]	K4z [mm]	K3z [mm]
0	-0,01	-0,01	-0,01	-0,01	-0,01	0,00	-0,01	-0,01	0,00	0,00
100	0,02	0,04	0,05	0,05	0,04	0,02	0,03	0,03	0,04	0,04
200	0,07	0,12	0,15	0,15	0,12	0,04	0,09	0,10	0,13	0,12
300	0,17	0,25	0,32	0,32	0,27	0,16	0,21	0,23	0,27	0,27
400	0,29	0,42	0,53	0,53	0,46	0,30	0,37	0,40	0,44	0,44
475	0,33	0,47	0,58	0,58	0,49	0,30	0,39	0,41	0,49	0,48

Table C-10: The measured strain due to cyclic loading (traffic load) + the residual strain.

Load [kN]	J6x [µm/m]	J5x [µm/m]	J4x [µm/m]	J3x [µm/m]	J2x [µm/m]	J1x [µm/m]	H4x [µm/m]	H3x [µm/m]	I4x [µm/m]	I3x [µm/m]	K4x [µm/m]	K3x [µm/m]	L4x [µm/m]	L3x [µm/m]
0	-0,2	-0,3	-0,5	-0,3	-0,4	-0,3	-0,5	-0,5	-0,5	-0,4	-0,2	-0,1	*	-0,2
100	14	17	21,9	23,2	19	11	4,4	4,1	13	12	12	12	*	3,4
200	27	32	45,1	47,6	37	22	8,1	7,9	26	25	22	24	*	5,8
300	41	49	66,1	72,7	56	34	12	12	39	37	32	37	*	9,1
400	58	69	93,2	99,9	76	47	17	17	52	51	47	51	*	16
475	70	84	114	122	92	56	21	21	63	61	55	62	*	18

Table C-11: The measured residual strain.

Load cyclus	J6x [µm/m]	J5x [µm/m]	J4x [µm/m]	J3x [µm/m]	J2x [µm/m]	J1x [µm/m]	H4x [µm/m]	H3x [µm/m]	I4x [µm/m]	I3x [µm/m]	K4x [µm/m]	K3x [µm/m]	L4x [µm/m]	L3x [µm/m]
3	6,9	7,8	11,8	12,5	9,5	5,3	2	1,9	6,5	6,4	5,7	6,3	*	1,5
6	6,1	5,7	8,7	13	10	5,5	1,5	1,8	6,4	6,4	4	6,1	*	-0,8
9	6	4,9	8,7	14,9	11	6,1	2	2,1	7	6,7	3,4	6,4	*	-0,9
12	8,6	9,2	13,5	18,1	13	7,1	2,8	3	8	8	5,6	8,2	*	1,1
15	7,2	6,8	11,1	20,6	15	8	5,5	3,6	8,7	8,7	5,7	6,3	*	1,5

Table C-12: The measured strain due to cyclic loading (traffic load).

Load [kN]	J6x [µm/m]	J5x [µm/m]	J4x [µm/m]	J3x [µm/m]	J2x [µm/m]	J1x [µm/m]	H4x [µm/m]	H3x [µm/m]	I4x [µm/m]	I3x [µm/m]	K4x [µm/m]	K3x [µm/m]	L4x [µm/m]	L3x [µm/m]
0	-0,2	-0,3	-0,5	-0,3	-0,4	-0,3	-0,5	-0,5	-0,5	-0,4	-0,2	-0,1	*	-0,2
100	7,5	9,5	10,1	10,7	9	5,2	2,4	2,2	6,2	6	5,9	6	*	1,9
200	21	27	36,4	34,6	26	16	6,6	6,1	19	18	18	18	*	6,6
300	35	44	57,4	57,8	45	28	10	10	32	31	29	31	*	10
400	49	60	79,7	81,8	63	39	14	14	44	43	42	43	*	15
475	63	77	103	101	78	48	15	17	55	52	49	55	*	17

C.3. Measured data for test 3 including the analysis

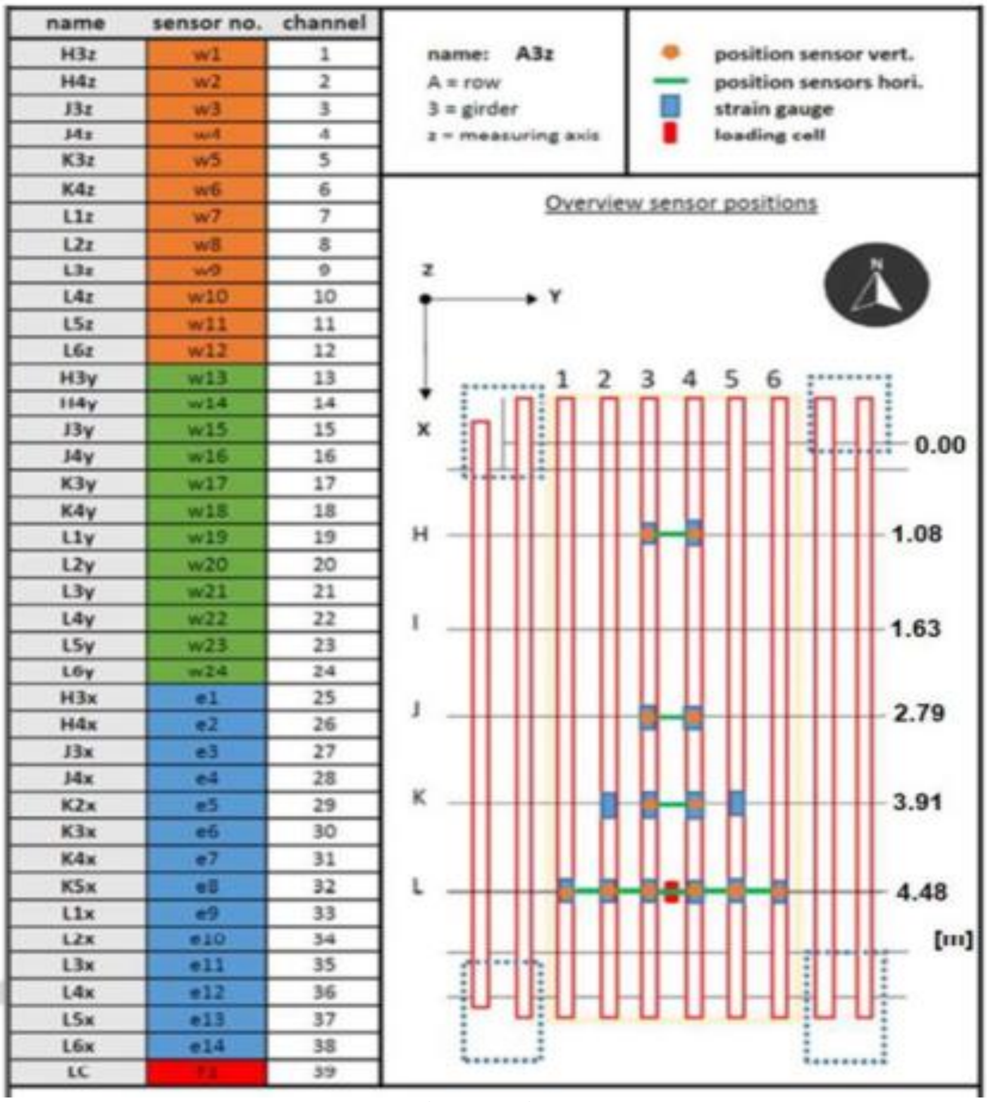

Figure C-3: Configuration of in-situ-load-test 3.

Table C-13: The measured displacement due to cyclic loading (traffic load) + the residual displacement.

Load [kN]	L6z [mm]	L5z [mm]	L4z [mm]	L3z [mm]	L2z [mm]	L1z [mm]	H4z [mm]	H3z [mm]	J4z [mm]	J3z [mm]	K4z [mm]	K3z [mm]
0	0	0	0	0	0	0	-0	-0	0	0	0	0
100	0,03	0,06	0,07	0,06	0,03	0,00	0,01	0,01	0,05	0,05	0,06	0,06
200	0,11	0,15	0,17	0,15	0,10	0,01	0,05	0,05	0,15	0,15	0,17	0,16
300	0,18	0,24	0,28	0,26	0,18	0,06	0,09	0,09	0,25	0,25	0,29	0,28
400	0,26	0,34	0,40	0,38	0,28	0,11	0,13	0,14	0,37	0,37	0,42	0,41
475	0,33	0,43	0,51	0,49	0,40	0,22	0,22	0,23	0,50	0,51	0,54	0,55

Table C-14: The measured residual displacement.

Load [kN]	L6z [mm]	L5z [mm]	L4z [mm]	L3z [mm]	L2z [mm]	L1z [mm]	H4z [mm]	H3z [mm]	J4z [mm]	J3z [mm]	K4z [mm]	K3z [mm]
3	0,03	0,04	0,05	0,04	0,03	0,002	0,014	0,015	0,04	0,04	0,04	0,04
6	0,05	0,06	0,06	0,06	0,06	0,026	0,039	0,041	0,07	0,07	0,07	0,07
9	0,05	0,06	0,08	0,08	0,08	0,061	0,049	0,051	0,08	0,09	0,09	0,09
12	0,08	0,09	0,12	0,14	0,16	0,152	0,113	0,116	0,15	0,16	0,14	0,17
15	0,08	0,1	0,14	0,17	0,2	0,187	0,143	0,156	0,17	0,21	0,17	0,2

Table C-15: The measured displacement due to cyclic loading (traffic load).

Load [kN]	L6z [mm]	L5z [mm]	L4z [mm]	L3z [mm]	L2z [mm]	L1z [mm]	H4z [mm]	H3z [mm]	J4z [mm]	J3z [mm]	K4z [mm]	K3z [mm]
0	0	0	0	0	0	0	-0	-0	0	0	0	0
100	0,01	0,02	0,03	0,02	0,003	-0,002	-0,01	-0	0,01	0,01	0,02	0,02
200	0,06	0,1	0,11	0,09	0,04	-0,01	0,01	0,011	0,08	0,07	0,1	0,09
300	0,13	0,18	0,21	0,18	0,1	-0,003	0,036	0,042	0,17	0,16	0,2	0,19
400	0,18	0,25	0,29	0,24	0,12	-0,04	0,019	0,023	0,23	0,21	0,28	0,24
475	0,25	0,33	0,38	0,33	0,20	0,032	0,072	0,071	0,33	0,3	0,38	0,35

Table C-16: The measured strain due to cyclic loading (traffic load) + the residual strain.

Load [kN]	L6x [µm/m]	L5x [µm/m]	L4x [µm/m]	L3x [µm/m]	L2x [µm/m]	L1x [µm/m]	H4x [µm/m]	H3x [µm/m]	J4x [µm/m]	J3x [µm/m]	K5x [µm/m]	K4x [µm/m]	K3x [µm/m]	K2x [µm/m]
0	0	0	0	0	0	0	-0,2	-0,1	-0,1	-0,1	0,2	0	0	0
100	6,6	8,5	14	4,5	4,4	13	-0,2	-0,1	4,6	5,3	8,7	7,8	9	8,9
200	13	17	29	14	9,5	27	0,4	0,5	9,9	12	18	16	19	19
300	20	27	45	23	16	43	0,4	0,8	16	18	28	25	29	29
400	26	36	63	32	22	59	-1,9	1,1	21	24	37	31	39	40
475	31	43	77	40	26	68	-2	0,6	26	28	44	35	47	48

Table C-17: The measured residual strain.

Load [kN]	L6x [µm/m]	L5x [µm/m]	L4x [µm/m]	L3x [µm/m]	L2x [µm/m]	L1x [µm/m]	H4x [µm/m]	H3x [µm/m]	J4x [µm/m]	J3x [µm/m]	K5x [µm/m]	K4x [µm/m]	K3x [µm/m]	K2x [µm/m]
3	3,9	4,6	8,2	-0,1	2,7	6,3	0,0	0,1	2,0	3,1	4,7	4,4	5,1	5,1
6	2,7	3,3	8,4	-2,2	2,2	5,2	-0,7	-0,3	1,3	2,6	3,9	2,4	4,6	4,8
9	2,9	3,1	9,3	-4,0	2,1	5,0	-0,9	0,0	1,0	2,7	3,8	1,6	4,6	4,8
12	2,3	2,7	11,0	-4,6	2,3	3,3	-4,3	-1,0	-0,3	1,7	3,2	-1,0	5,8	5,6
15	1,7	3,5	12,0	-4,5	2,0	3,4	-4,2	-0,9	1,3	2,3	3,0	-2,2	5,4	5,4

Table C-18: The measured strain due to cyclic loading (traffic load).

Load [kN]	L6x [µm/m]	L5x [µm/m]	L4x [µm/m]	L3x [µm/m]	L2x [µm/m]	L1x [µm/m]	H4x [µm/m]	H3x [µm/m]	J4x [µm/m]	J3x [µm/m]	K5x [µm/m]	K4x [µm/m]	K3x [µm/m]	K2x [µm/m]
0	0	0	0	0	0	0	-0,2	-0,1	-0,1	-0,1	0,2	0	0	0
100	2,7	3,9	5,5	4,6	1,7	6,8	0,5	0,2	3,3	2,7	4	3,4	3,9	3,8
200	11	14	20,7	16	7,3	22	1,3	0,5	8,9	8,8	13,9	13,4	13,9	14
300	17	24	36,1	26,5	13	38	4,7	1,8	16,5	16	23,9	23,2	23,9	24,4
400	24	33	51,7	36,9	19	56	2,3	2	20,1	21,4	33,5	32,2	33,3	34,4
475	29	40	64,7	44,1	24	64	-2	0,6	25,5	27,9	40,6	37,6	41,8	42,5

D Annex – The numerical results versus in-situ-load-test 1 and 3 for the separated beam

D.1. Defined load and results of the calibration for the numerical models

Table D-1: Defined loads based on the measured vertical displacement during in-situ-load-test 1 at row H.

Load [kN]	**H6 [mm]**	**H5 [mm]**	**H4 [mm]**	**H3 [mm]**	**H2 [mm]**	**H1 [mm]**	**Sum of the total deformation [mm]**
400	0.08	0.15	0.22	0.20	0.13	0.04	0.82
475	0.09	0.18	0.27	0.25	0.15	0.04	0.97
Percentage	10%	19%	27%	25%	16%	5%	
load is obtained from a maximal load of 400 kN	38.3 [kN]	74.3 [kN]	107.8[kN]	98.5 [kN]	62.6 [kN]	18.4 [kN]	
Percentage	0.09	0.18	0.28	0.25	0.16	0.04	
Load is obtained from a maximal load of 475 kN	41.5 [kN]	87.3 [kN]	131.7 [kN]	119.5 [kN]	74.1 [kN]	21.0 [kN]	

Table D-2: Defined loads based on the measured vertical displacement during in-situ-load-test 2 at row J.

Load [kN]	**J5 [mm]**	**J6 [mm]**	**J4 [mm]**	**J3 [mm]**	**J2 [mm]**	**J1 [mm]**	**Sum of the total deformation [mm]**
400	0.29	0.42	0.53	0.53	0.46	0.30	2.53
475	0.33	0.47	0.58	0.58	0.49	0.30	2.75
Percentage	11%	17%	21%	21%	18%	12%	
Load is obtained from a maximal load of 400 kN	45.8 [kN]	66.8 [kN]	82.9 [kN]	83.3 [kN]	73.1 [kN]	48 [kN]	
Percentage	0.1	0.2	0.2	0.2	0.2	0.1	
Load is obtained from a maximal load of 475 kN	56.9 [kN]	80.7 [kN]	100.6 [kN]	99.3 [kN]	85.0 [kN]	52.4 [kN]	

Table D-3: Defined loads based on the measured vertical displacement during in-situ-load-test 3 at row L.

Load [kN]	**L6 [mm]**	**L5 [mm]**	**L4 [mm]**	**L3 [mm]**	**L2 [mm]**	**L1 [mm]**	**Sum of the total deformation [mm]**
400	0.18	0.25	0.29	0.24	0.12	0.04	1.12
475	0.25	0.33	0.38	0.33	0.2	0.03	1.52
Percentage	16%	23%	26%	21%	11%	3%	
Load is obtained from a maximal load of 400 kN	65 [kN]	91 [kN]	103 [kN]	85 [kN]	43 [kN]	14 [kN]	
Percentage	17%	22%	25%	22%	13%	2%	
Load is obtained from a maximal load of 475 kN	79 [kN]	103 [kN]	118 [kN]	102 [kN]	63 [kN]	10 [kN]	

Table D-4: Calibration due to the support length for the vertical displacement.

Poin t	**X**	**1 line support**	**2 line support**	**3 line support**	**4 line support**	**5 line support**	**6 line support**	**7 line support**	**8 line support**	**9 line support**	**Deformatio n results of in-situ-load-test 3 of steel girder 4**	**Ratio**
*******	**0**	0	0	0	0	0	0	0	0	0	0	0 %
I	**2.09**	-1.26	-1.01	-0.78	-0.64	-0.55	-0.49	-0.46	-0.44	-0.43	-0.37	116%
J	**3.25**	-1.62	-1.32	-1.05	-0.88	-0.77	-0.70	-0.66	-0.64	-0.63	-0.53	120%
K	**4.41**	-1.26	-1.01	-0.78	-0.64	-0.55	-0.49	-0.46	-0.44	-0.43	-0.44	98%
*******	**6.5**	0	0	0	0	0	0	0	0	0	0	0 %

Table D-5: Calibration due to the support length for the strain.

Point	**X**	**1 line support**	**2 line support**	**3 line support**	**4 line support**	**5 line support**	**6 line support**	**7 line support**	**8 line support**	**9 line support**	**Strain results of in-situ-load test 3 of steel girder 4**	**Ratio**
***	**0**	0	0	0	0	0	0	0	0	0	0	0 %
H	**1.54**	4.82E-05	3E-05	1.5E-05	4.9E-06	-1E-06	-5E-06	-7E-06	-8E-06	-9E-06	1.40E-05	-61%
I	**2.09**	7.87E-05	6E-05	4.5E-05	3.5E-05	3E-05	3E-05	2.4E-05	2E-05	2E-05	4.44E-05	49%
J	**3.25**	1.38E-04	0.0001	0.0001	9.5E-05	9E-05	9E-05	8.3E-05	8E-05	8E-05	7.97E-05	102%
K	**4.41**	7.87E-05	6E-05	4.5E-05	3.5E-05	3E-05	3E-05	2.4E-05	2E-05	2E-05	4.15E-05	53%
L	**4.96**	4.82E-05	3E-05	1.5E-05	4.9E-06	-1E-06	-5E-06	-7E-06	-8E-06	-9E-06	1.40E-05	-61%
***	**6.5**	0	0	0	0	0	0	0	0	0	0	0 %

Table D-6: Calibration due to the elastic model of concrete for the vertical displacement.

Point	**X**	**38000 N/mm^2**	**40000 N/mm^2**	**42000 N/mm^2**	**44000 N/ mm^2**	**46000 N/mm^2**	**48000 N/mm^2**	**50000 N/mm^2**	**Deformation results of in-situ-load test 3 of steel girder 4**	**Ratio**
***	**0**	0	0	0	0	0	0	0	0	0 %
I	**2.09**	-0.43	-0.42	-0.40	-0.39	-0.38	-0.37	-0.36	-0.37	97%
J	**3.25**	-0.63	-0.61	-0.59	-0.57	-0.55	-0.54	-0.52	-0.53	99%
K	**4.41**	-0.43	-0.42	-0.40	-0.39	-0.38	-0.37	-0.36	-0.44	82%
***	**6.5**	0	0	0	0	0	0	0	0	0 %

Table D-7: Calibration due to the elastic model of concrete for the strain.

Point	**X**	**38000 N/mm^2**	**40000 N/mm^2**	**42000 N/mm^2**	**44000 N/mm^2**	**46000 N/mm^2**	**48000 N/mm^2**	**50000 N/mm^2**	**Strain results of in-situ-load test 3 of steel girder 4**	**Ratio**
***	**0**	0	0	0	0	0	0	0	0	0 %
H	**1.54**	-8.56E-06	-8.29E-06	-8.03E-06	-7.79E-06	-7.56E-06	-7.33E-06	-7.47E-06	1.40E-05	-52%
I	**2.09**	2.19E-05	2.12E-05	2.06E-05	2.01E-05	1.95E-05	1.90E-05	1.83E-05	4.44E-05	43%
J	**3.25**	8.11E-05	7.87E-05	7.64E-05	7.43E-05	7.23E-05	7.04E-05	6.84E-05	7.97E-05	88%
K	**4.41**	2.19E-05	2.12E-05	2.06E-05	2.01E-05	1.95E-05	1.90E-05	1.86E-05	4.15E-05	46%
L	**4.96**	-8.57E-06	-8.29E-06	-8.04E-06	-7.79E-06	-7.56E-06	-7.33E-06	-7.05E-06	1.40E-05	-52%
***	**6.5**	0	0	0	0	0	0	0	0	0 %

D.2. Numerical results of steel girder 4 for the loaded point H at 1.54 m

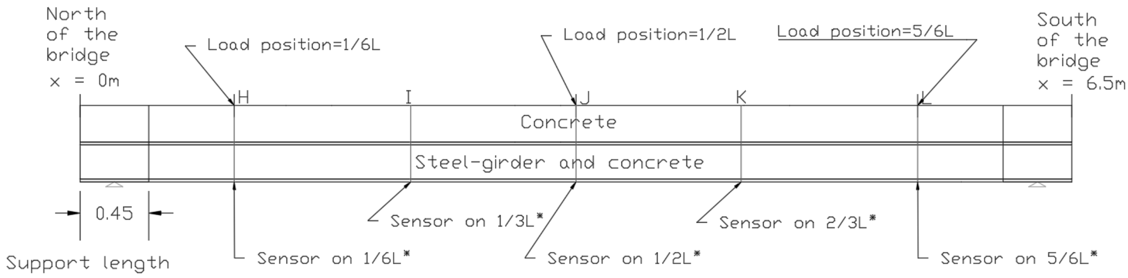

Figure D-1: The loaded point H on the beam.

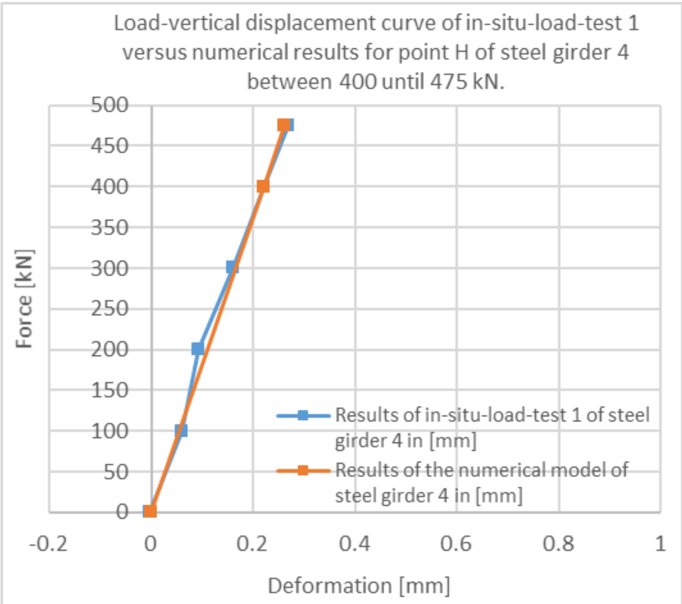

Figure D-2: Load-displacement curve of the in-situ-load of test 1 versus numerical results for point H of steel girder 4 between 400 until 475 kN.

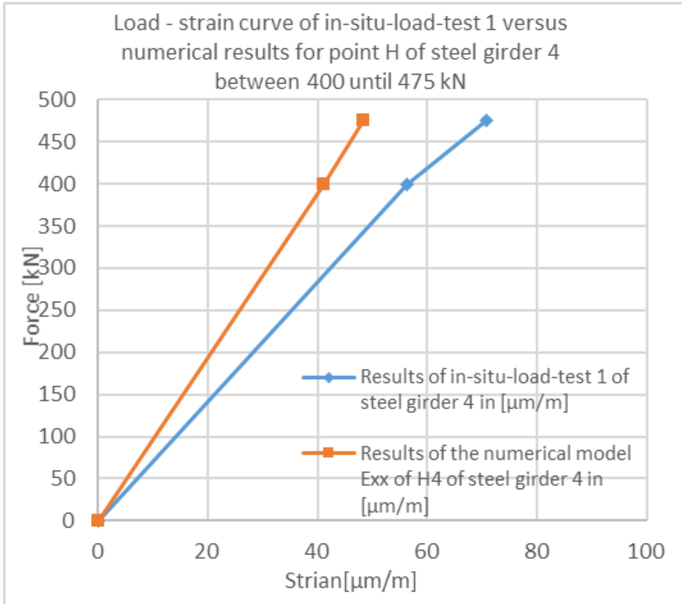

Figure D-3: Load - strain curve in-situ-load-test 1 versus numerical results for point H of steel girder 4 between 400 until 475 kN.

Table D-8: Load-displacement of in-situ-load-test 1 versus numerical results for points of steel girder 4.

Point	**X**	**Results of in-situ-load-test 1 of steel girder 4 in [mm]**	**Results of the numerical model of steel girder 4 in [mm]**	**Ratio**
*******	**0**	0	0	0%
H	**1.5**	-0.27	-0.28	104%
I	**2.09**	-0.34	-0.35	103%
J	**3.25**	-0.33	-0.34	103%
L	**4.96**	-0.15	-0.11	73%
*******	**6.5**	0	0	0%

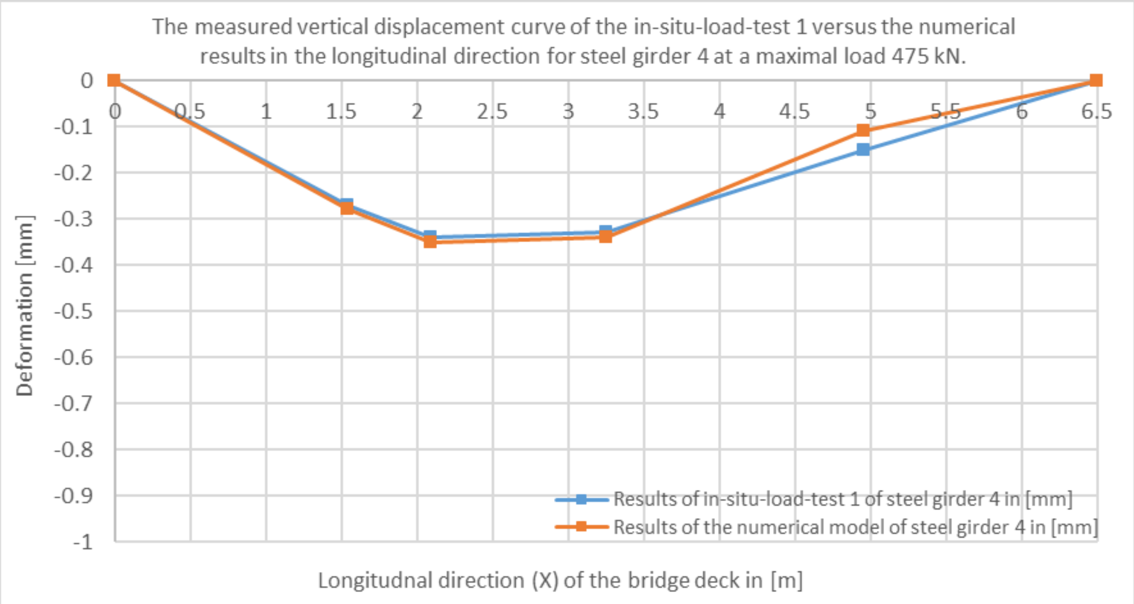

Figure D-4: The measured displacement curves for the in-situ-load-test 1 versus the numerical results in the longitudinal direction of the load 475 kN.

Table D-9: Load-strain of in-situ-load-test 1 versus numerical results for points of steel girder 4.

Point	X	Results of in-situ-load-test 1 of steel girder 4 in [μm/m]	Results of the numerical model of steel girder 4 in [μm/m]	Ratio
***	0	0	0	0
H	1.5	-72	-41	57%
I	2.09	-49	-28	57%
J	3.25	-29	-10	33%
L	4.96	-3	-1	27%
***	6.5	0	0	0

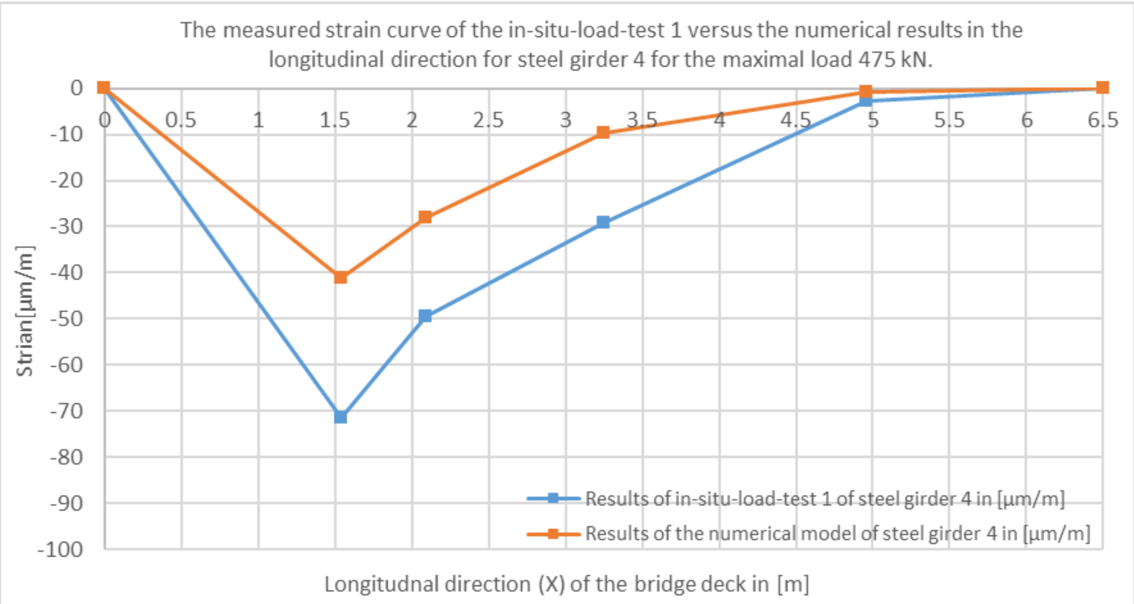

Figure D-5: The measured strain curves for the in-situ-load-test 1 versus the numerical results of the load 475 kN in the longitudinal direction.

Table D-10: The maximal vertical displacement of the in-situ-load-test versus the numerical results and the ratio.

Load	Results of in-situ-load-test 3 of steel girder 4 on point H in[mm]	Results of the numerical model of steel girder 4 on point H in [mm]	Ratio
0	0	0	0 %
400	-0,22	-0,23	104 %
475	-0,27	-0,28	104 %

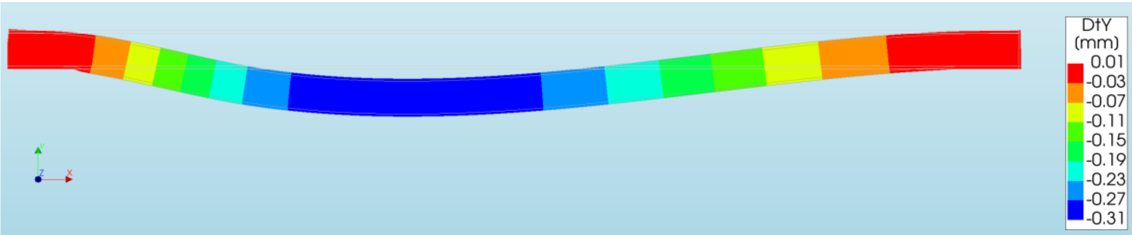

Figure D-6: The numerical results of the vertical displacement of steel girder 4 for a load of 400 kN at point H.

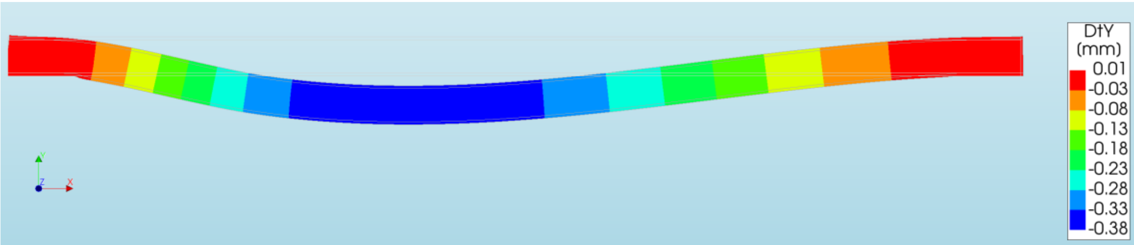

Figure D-7: The numerical results of the vertical displacement of steel girder 4 for a load of 475 kN at point H.

Table D-11: The maximal strain of the in-situ-load-test versus the numerical results and the ratio.

Load	Results of in-situ-load-test 3 of steel girder 4 on point H in [µm/m]	Results of the numerical model of steel girder 4 on point H in [µm/m]	Ratio
0	0	0.0	0
400	56.30	41.0	73%
475	70.70	48.3	68%

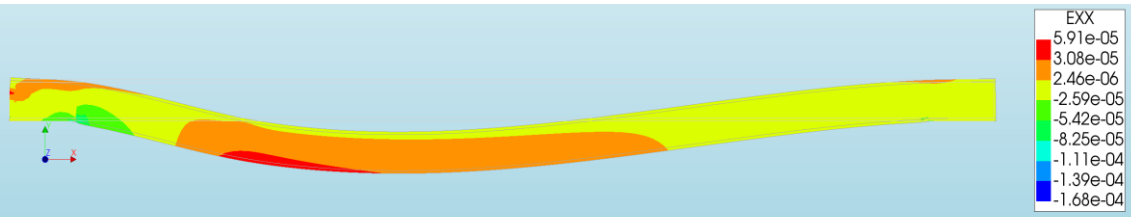

Figure D-8: The numerical results of the strain of steel girder 4 for a load of 400 kN in the point H.

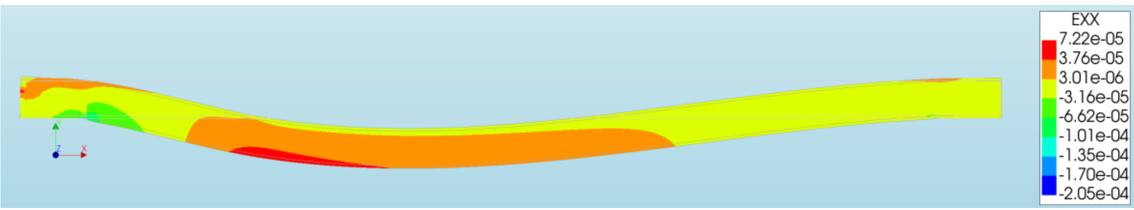

Figure D-9: The numerical results of the strain of steel girder 4 for a load of 475 kN in the point H.

Table D-12: The maximal principal stress of concrete at point H.

Load	The numerical results of the principal stress of the concrete on point H in [N/mm2]	Maximal allowable tensile stress of concrete in [N/mm2]	Ratio
0	0	0	0 %
400	1.90	4.2	45 %
475	2.32	4.2	55 %

Figure D-10: The numerical results of the principal stress in the concrete (S1) of steel girder 4 for a load of 400 kN at the point H.

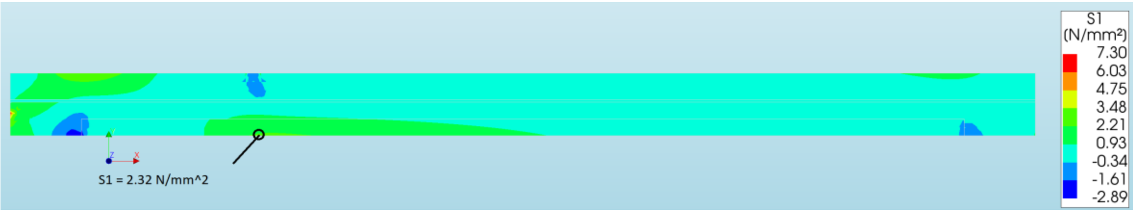

Figure D-11: The numerical results of the principal stress in the concrete (S1) of steel girder 4 for a load of 475 kN at the point H.

Comment: The principal stress is under the maximal tensile stress of concrete.

Table D-13: The maximal principal stress of steel at point H.

Load	The numerical results of the principal stress of the concrete on point H in [N/mm2]	Maximal allowable tensile /compressive stress of steel in [N/mm2]	Ratio
0	0	0	0 %
400	121	235	52 %
475	148	235	63 %

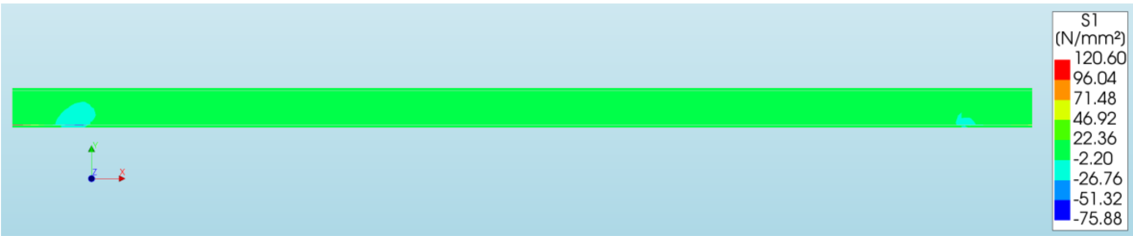

Figure D-12: The numerical results of the principal stress in the steel S1 of steel girder 4 for a load of 400 kN at the point H.

Figure D-13: The numerical results of the principal stress in the steel S1 of steel girder 4 for a load of 475 kN at the point H.

Comment: The principal stress is under the maximal tensile stress of steel-girders.

Table D-14: The maximal principal shear stress in concrete at point H.

Load	The numerical results of the principal stress of the concrete on point H in [N/mm2]	Maximal allowable shear stress of concrete in [N/mm2]	Ratio
0	0	0	0 %
400	1.02	7.2	14 %
475	1.24	7.2	18 %

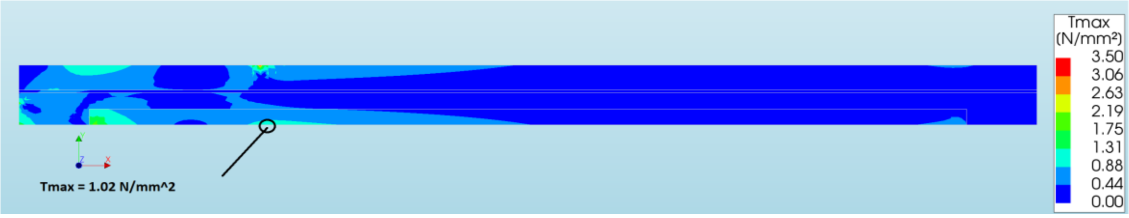

Figure D-14: The numerical results of the principal stress in the concrete Tmax of steel girder 4 for a load of 400 kN at the point H.

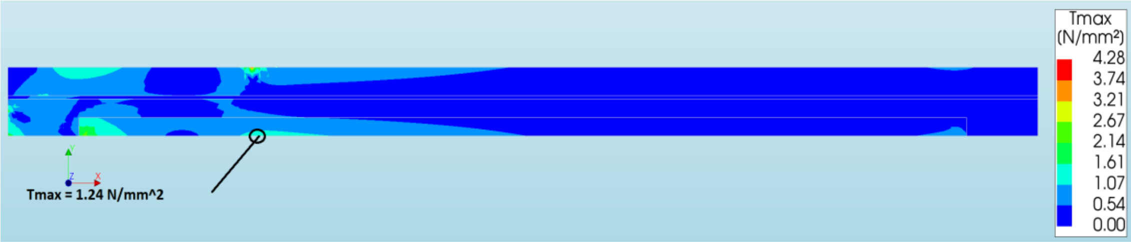

Figure D-15: The numerical results of the principal stress in the concrete Tmax of steel girder 4 for a load of 475 kN at the point H.

Comment: The principal shear stress is under the maximal shear stress of concrete.

D.3. Numerical results of steel girder 4 for the loaded point L at 4.96 m

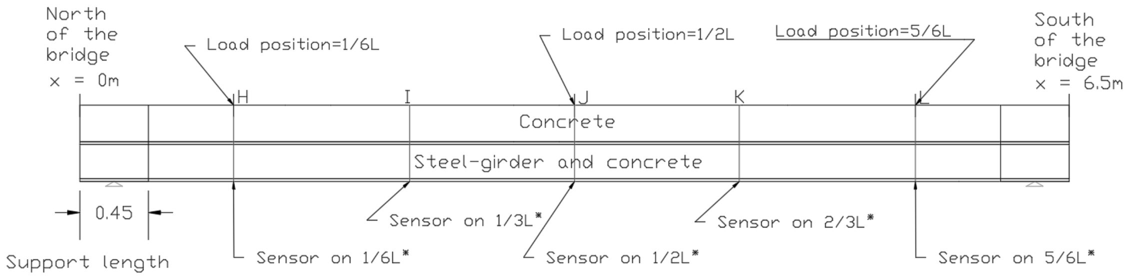

D-20: The loaded point L on the beam.

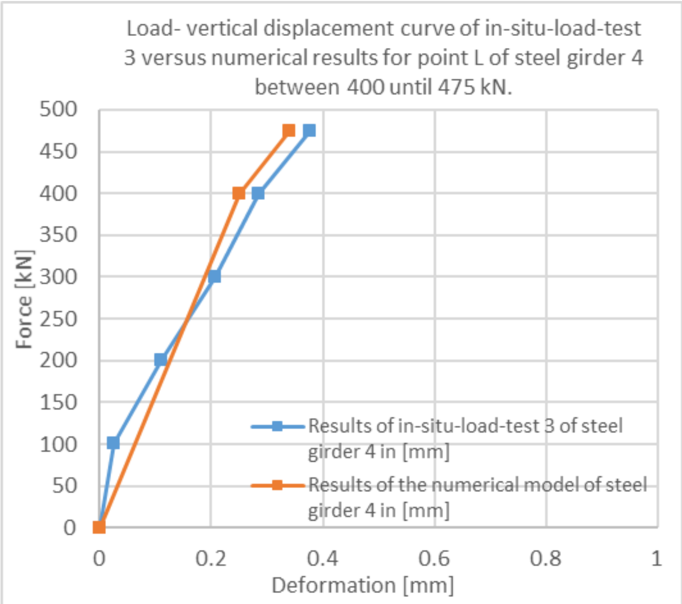

Figure D-16: Load-displacement curve of the in-situ-load-test 3 versus numerical results for point L on steel girder 4 between 400 until 475 kN.

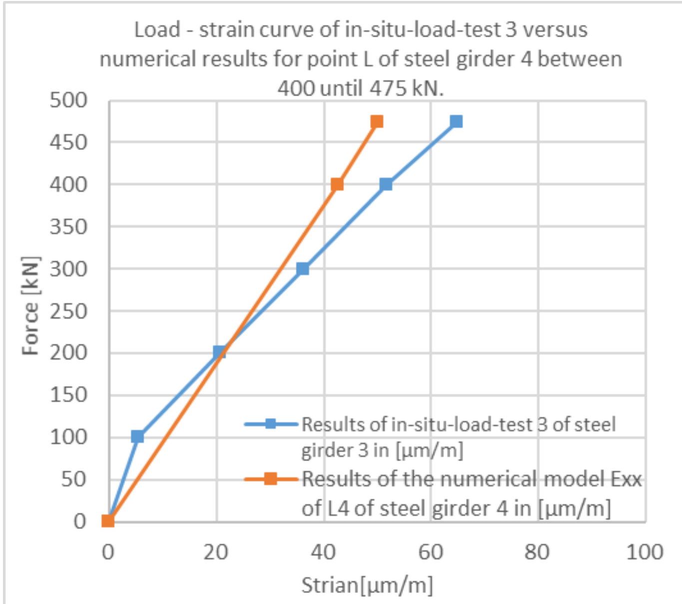

Figure D-17: Load - strain curve in-situ-load of test 3 versus numerical for point L on steel girder 4 between 400 until 475 kN.

Table D-15: Load-displacement of in-situ-load-test 1 versus numerical results for points of steel girder 4.

Point	X	Results of in-situ-load-test 3 of steel girder 3 in [mm]	Results of the numerical model of steel girder 3 in [mm]	Ratio
***	0	0	0	0
H	1.54	-0.07	-0.08	114%
J	3.25	-0.33	-0.26	79%
K	4.41	-0.38	-0.31	82%
L	4.96	-0.38	-0.34	89%
***	6.5	0	0	0

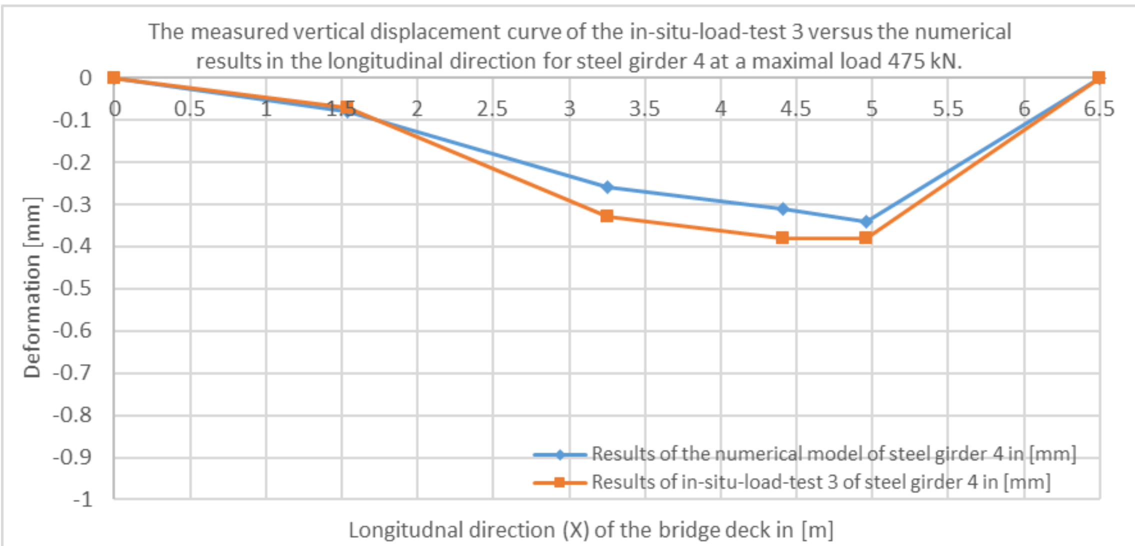

Figure D-18: The measured displacement curves for the in-situ-load-test 3 versus the numerical results of the load 475 kN in the longitudinal direction.

Table D-16: Load-strain of in-situ-load-test 3 versus numerical results for points of steel girder 4.

Point	X	Results of in-situ-load test 3 of steel girder 4 in [µm/m]	Results of the numerical model of steel girder 4 in [µm/m]	Ratio
***	0	0	0	0 %
H	1.54	-2	-4	209%
J	3.25	-26	-8	33%
K	4.41	-38	-17	44%
L	4.96	-65	-21	32 %
***	6.5	0	0	0 %

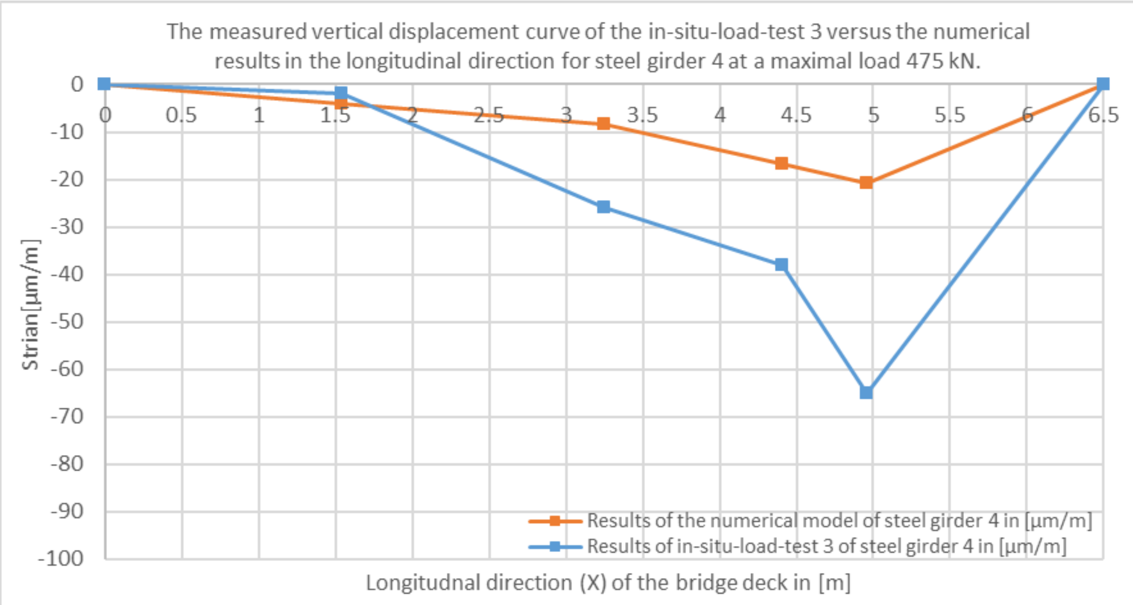

Figure D-19: The measured strain curves for the in-situ-load-test 3 versus the numerical results of the load 475 kN in the longitudinal direction.

Table D-17: The maximal vertical displacement of the in-situ-load-test versus the numerical results and the ratio.

Load	Results of in-situ-load-test 3 of steel girder 4 on point L [mm]	Results of the numerical model of steel girder 4 on point L [mm]	Ratio
0	0	0	0 %
400	-0,28	-0,25	90 %
475	-0,38	-0,34	90 %

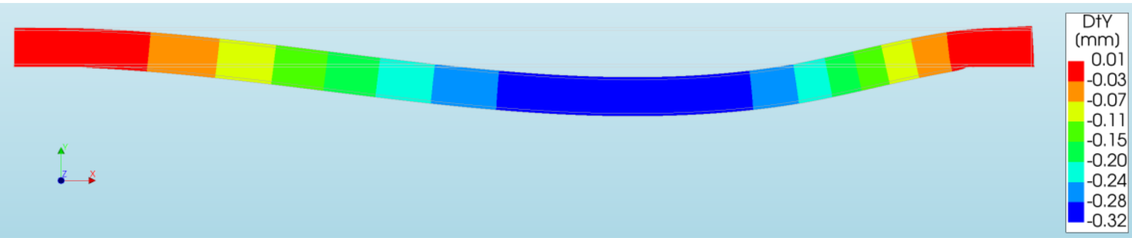

Figure D-20: The numerical results of the displacement for a load of 400 kN in the point L.

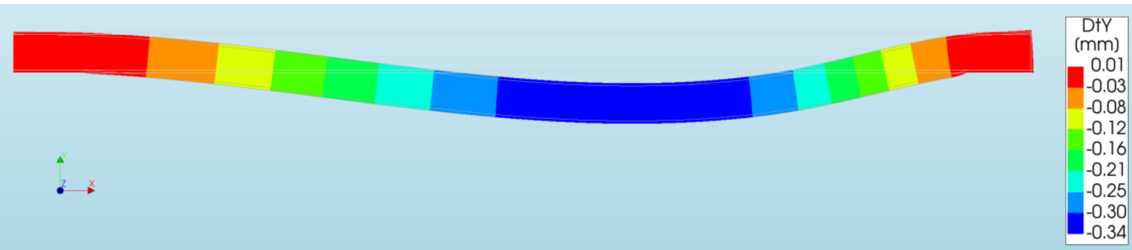

Figure D-21: The numerical results of the displacement for a load of 475 kN in the point L.

Table D-18: The maximal strain of the in-situ-load-test versus the numerical results and the ratio.

Load	Results of in-situ-load-test 3 of steel girder 4 on point L in [µm/m]	Results of the numerical model of steel girder 4 on point L in [µm/m]	Ratio
0	0	0	0 %
400	51.7	42	82 %
475	64.7	50	77 %

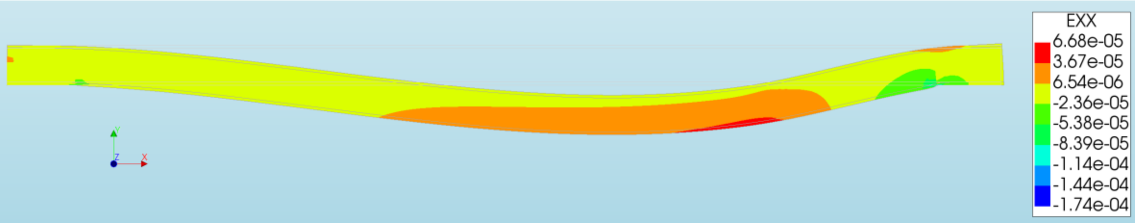

Figure D-22: The numerical results of the strain for a load of 400 kN in the point L.

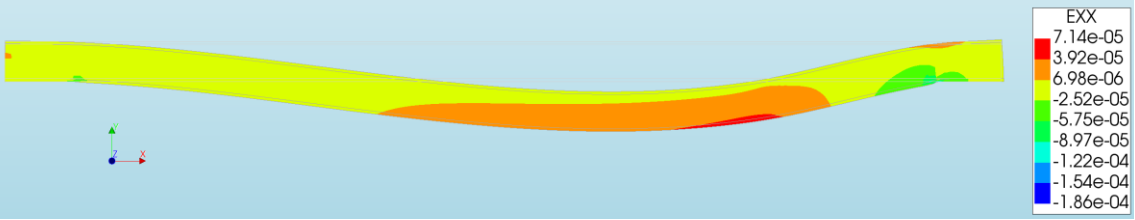

Figure D-23: The numerical results of the strain for a load of 475 kN in the point L.

Table D-19: The maximal principal stress of the concrete.

Load	The numerical results of the principal stress of the concrete on point L in [N/mm2]	Maximal allowable tensile stress of concrete in [N/mm2]	Ratio
0	0	0	0%
400	1.95	4.2	48 %
475	2.06	4.2	50 %

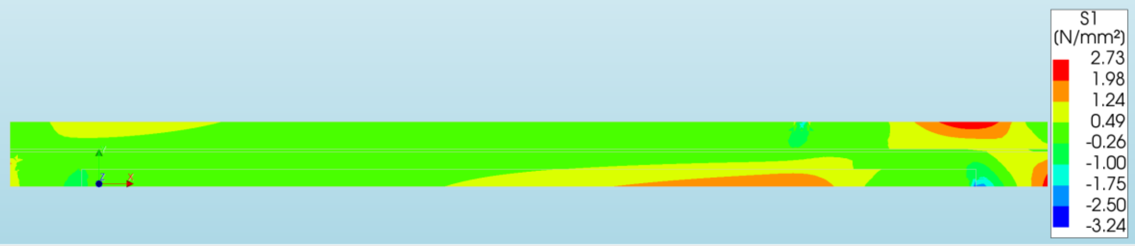

Figure D-24: The numerical results of the principal stress in the concrete S1 for a load of 400 kN at the point L.

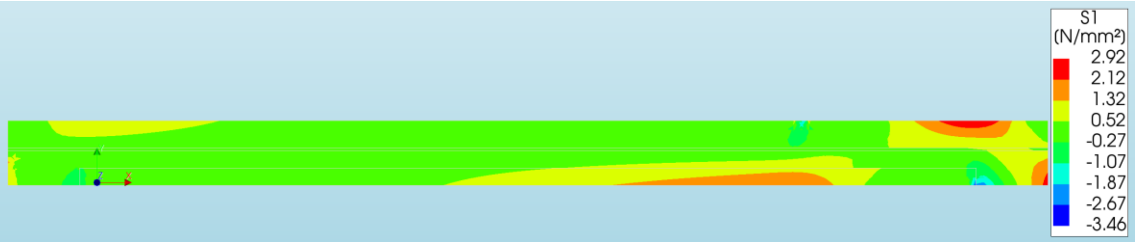

Figure D-25: The numerical results of the principal stress in the concrete S1 for a load of 475 kN at the point L.

Comment: The principal stress is under the maximal tensile stress of concrete

Table D-20: The maximal principal stress of the steel at point L.

Load	The numerical results of the principal stress of the concrete on point L in [N/mm2]	Maximal allowable tensile /compressive stress of steel in [N/mm2]	Ratio
0	0	0	0
400	173	235	73 %
475	185	235	78 %

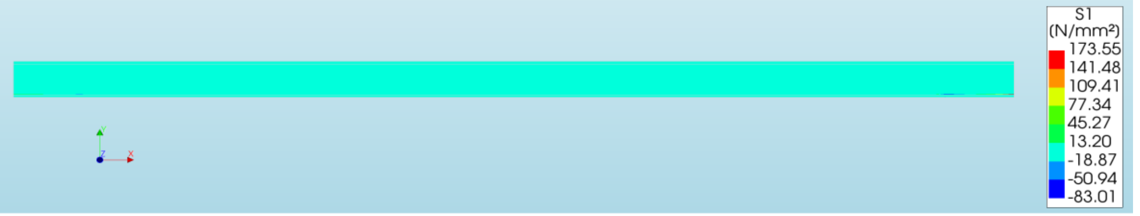

Figure D-26: The numerical results of the principal stress in the steel S1 for a load of 400 kN at the point L.

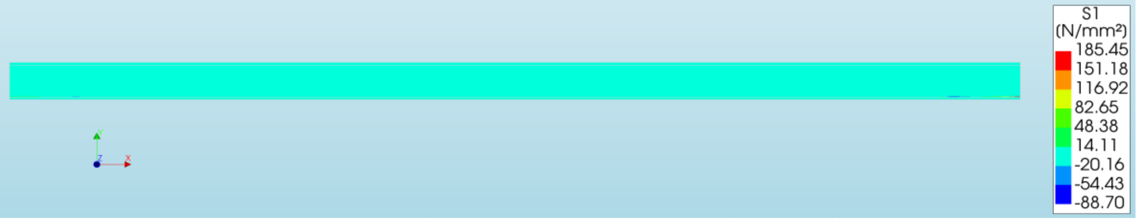

Figure D-27: The numerical results of the principal stress in the steel S1 for a load of 475 kN at the point L.

Comment: The principal stress is under the maximal tensile stress of concrete

Table D-21: The maximal principal stress of the steel.

Load	The numerical results of the principal stress of the concrete on point L in [N/mm2]	Maximal allowable shear stress of concrete in [N/mm2]	Ratio
0	0	0	0
400	1.00	7.2	13 %
475	1.07	7.2	15 %

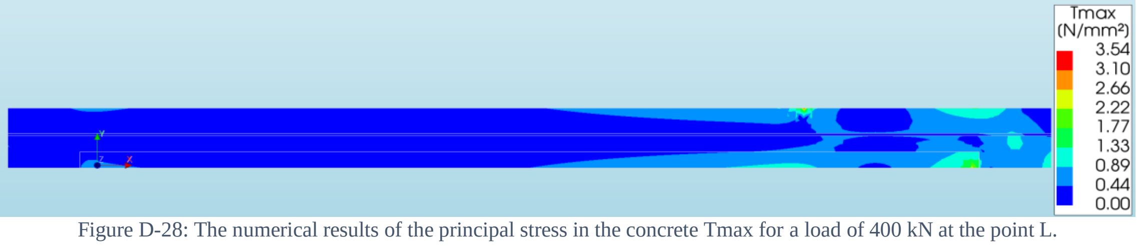

Figure D-28: The numerical results of the principal stress in the concrete Tmax for a load of 400 kN at the point L.

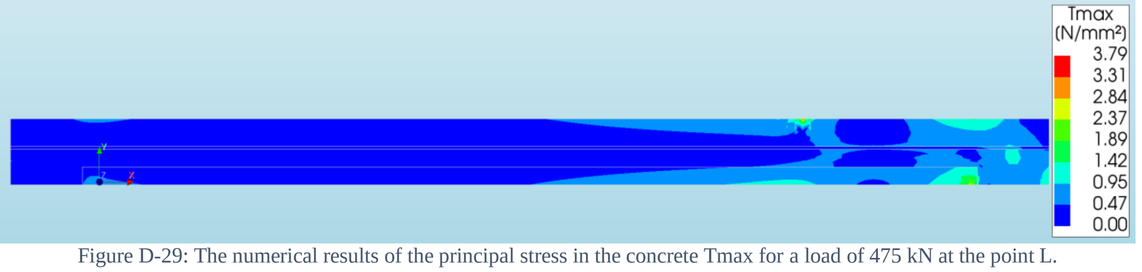

Figure D-29: The numerical results of the principal stress in the concrete Tmax for a load of 475 kN at the point L.

Comment: The principal stress is under the maximal tensile stress of concrete.

E Annex – The numerical results versus in-situ-load-test 1 and 3 for the bridge deck

E.1. Numerical results of bridge deck for the loaded point H at 1.54 m

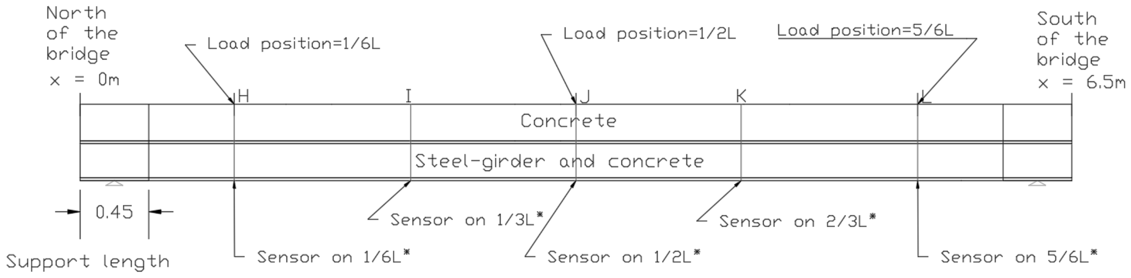

Figure E-1: The loaded point H on the beam.

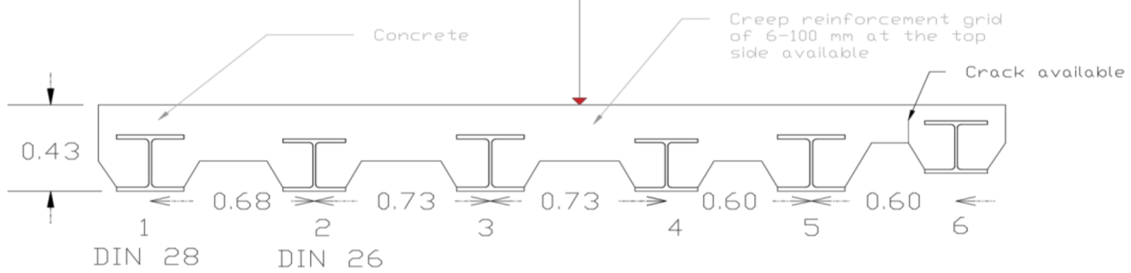

Figure E-2: The loaded points (H, J and L) on the bridge deck in the transvers direction of the bridge deck.

Table E-1: Load-displacement of in-situ-load-test 1 versus numerical results for point H of steel girder 4.

Load	Results of in-situ-load test 1 of steel girder 4 in [mm]	Results of the numerical model of steel girder 4 in [mm]	Ratio
0	0	0	0 %
400	0.22	0.21	97 %
475	0.27	0.24	90 %

Table E-2: Load-displacement of in-situ-load-test 1 versus numerical results for point H of steel girder 3.

Load	Results of in-situ-load-test 1 of steel girder 3 in [mm]	Results of the numerical model of steel girder 3 in [mm]	Ratio
0	0	0	0 %
400	0.20	0.21	102 %
475	0.25	0.24	96 %

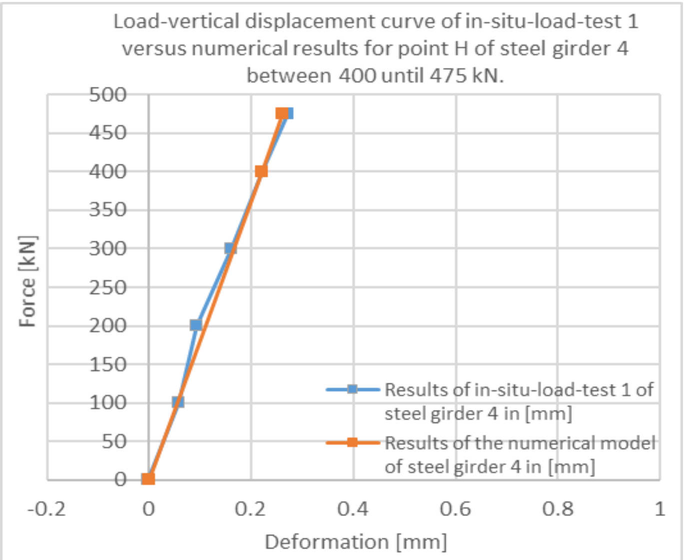

Figure E-3: Load-displacement curve of in-situ-load-test 1 versus numerical results for point H of steel girder 4 between 400 until 475 kN.

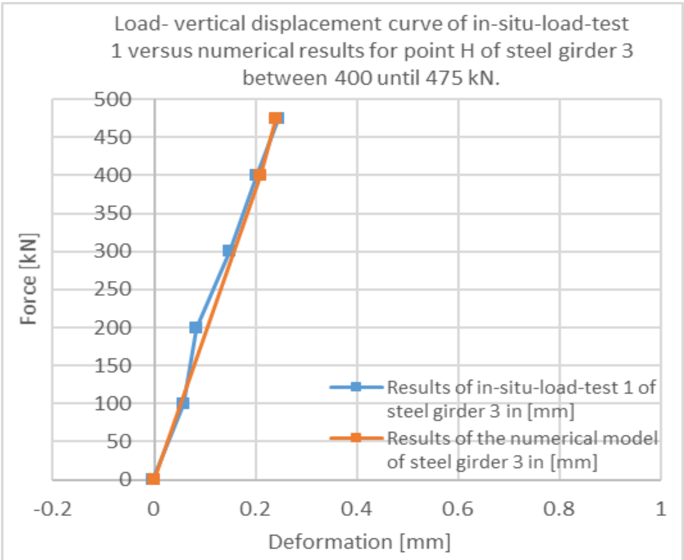

Figure E-4: Load-displacement curve of in-situ-load-test 1 versus numerical results for point H of steel girder 3 between 400 until 475 kN.

Table E-3: Load-displacement of in-situ-load-test 1 versus numerical results for points of steel girder 4.

Point	X	Results of in-situ-load-test 1 of steel girder 4 in [mm]	Results of the numerical model of steel girder 4 in [mm]	Ratio
***	0	0	0	0 %
H	1.540	-0.27	-0.26	96 %
I	2.090	-0.34	-0.32	94 %
J	3.25	-0.33	-0.30	92 %
L	4.96	-0.15	-0.12	82 %
***	6.5	0	0.0	0 %

Table E-4: Load-displacement of in-situ-load-test 1 versus numerical results for points of steel girder 3.

Point	X	Results of in-situ-load-test 1 of steel girder 3 in [mm]	Results of the numerical model of steel girder 3 in [mm]	Ratio
***	0	0	0	0 %
H	1.540	-0.25	-0.25	102 %
I	2.090	-0.34	-0.32	95 %
J	3.25	-0.32	-0.31	98 %
L	4.96	-0.10	-0.09	95 %
***	6.5	0	0	0 %

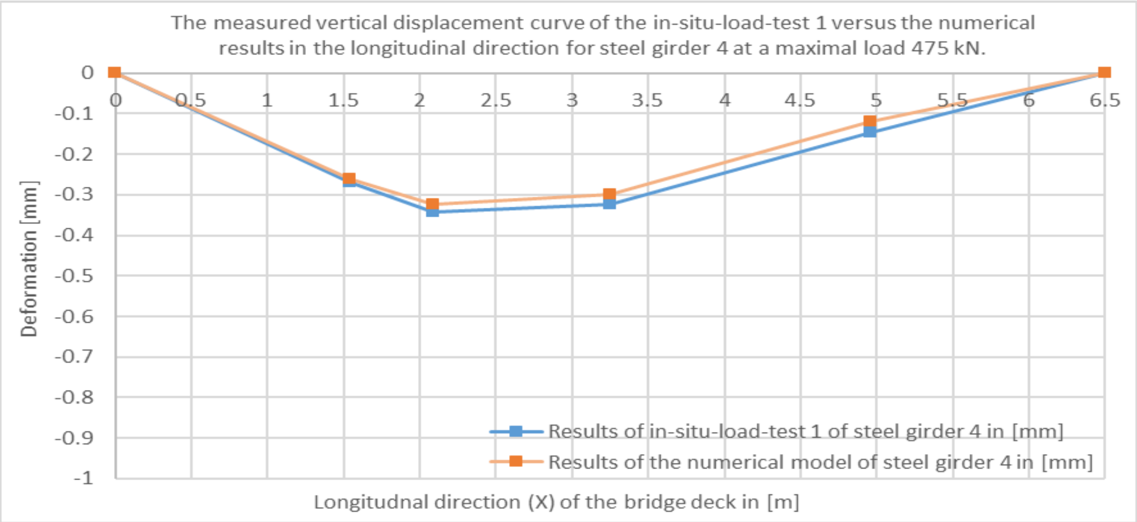

Figure E-5: The measured vertical displacement curves for in-situ-load-test 1 versus the numerical results for the steel girder 4 in the longitudinal direction of the load 475 kN.

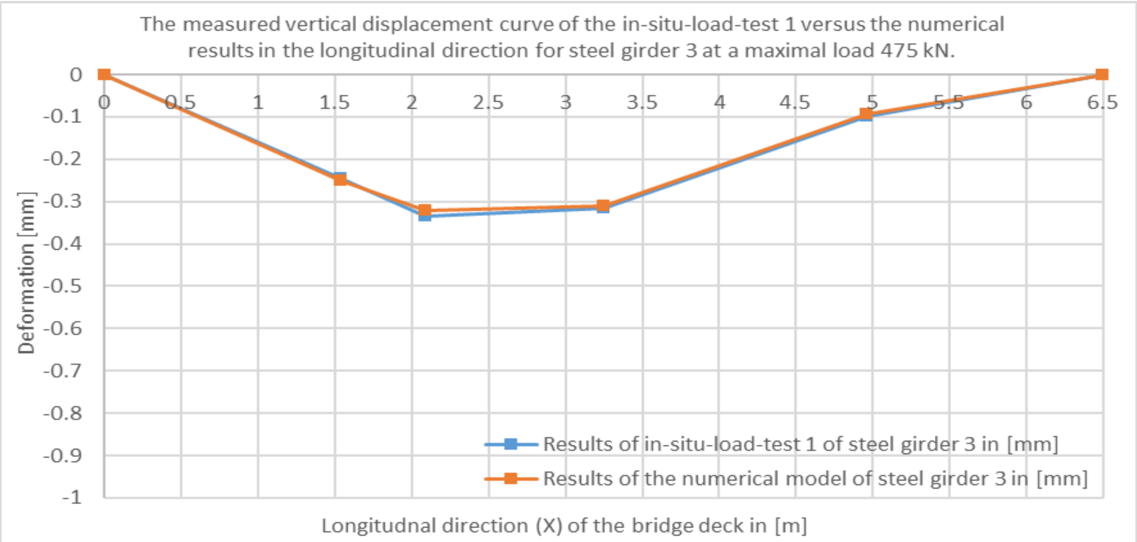

Figure E-6: The measured vertical displacement curves for in-situ-load-test 1 versus the numerical results for the steel girder 3 in the longitudinal direction of the load 475 kN.

Table E-5: Load-displacement of in-situ-load-test 1 versus numerical results of the row H.

Point	Y	Results of in-situ-load-test 1 of row H in [mm]	Results of the numerical model of row H in [mm]	Ratio
H1	**0**	-0.08	-0.08	105%
H2	**0.73**	-0.15	-0.14	90%
H3	**1.46**	-0.22	-0.21	97%
H4	**2.19**	-0.20	-0.21	102%
H5	**2.92**	-0.13	-0.13	99%
H6	**3.65**	-0.04	-0.07	190%

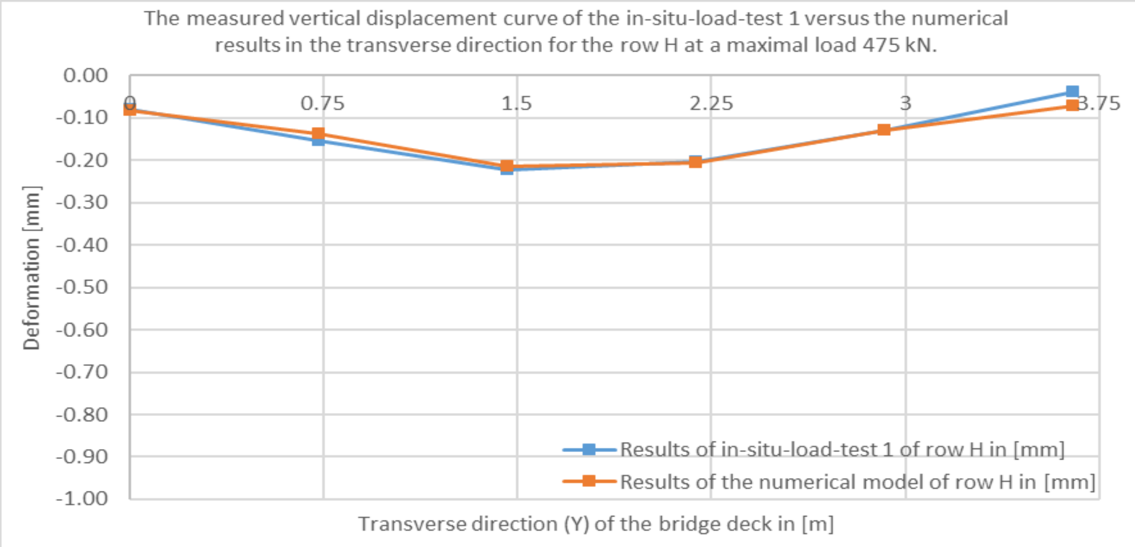

Figure E-7: The measured vertical displacement curves for in-situ-load-test 1 versus the numerical results in the transverse direction for the row H of the load 475 kN.

Table E-6: Load-strain of in-situ-load-test 1 versus numerical results for point H of steel girder 4.

Load	Results of in-situ-load-test 1 of steel girder 4 in[μm/m]	Results of the numerical model Exx of H4 of steel girder 4 in [μm/m]	Ratio
0	0	0	0 %
400	57.1	41	73 %
475	71.5	48	67 %

Table E-7: Load-strain of in-situ-load-test 1 versus numerical results for point H of steel girder 3.

Load	Results of in-situ-load-test 1 of steel girder 3 in [μm/m]	Results of the numerical model Exx of H3 of steel girder 3 in [μm/m]	Ratio
0	0	0	0%
400	57.1	41	73%
475	71.5	48	67%

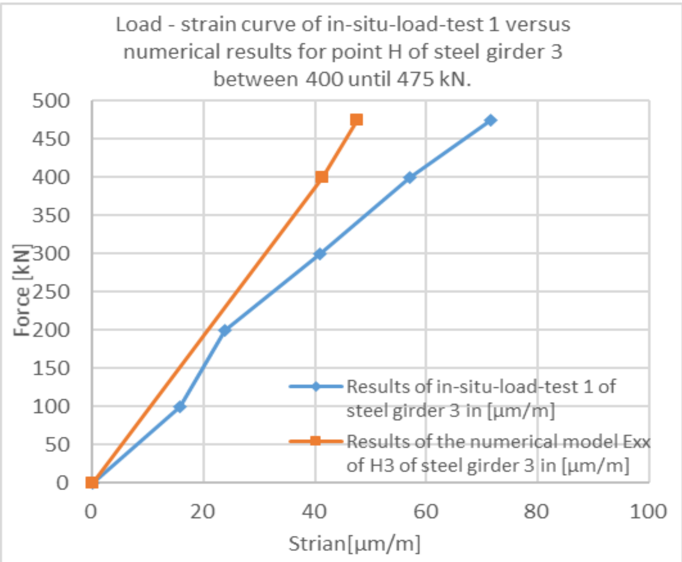

Figure E-8: Load-strain curve of in-situ-load-test 1 versus numerical results for point H of steel girder 3 between 400 until 475 kN.

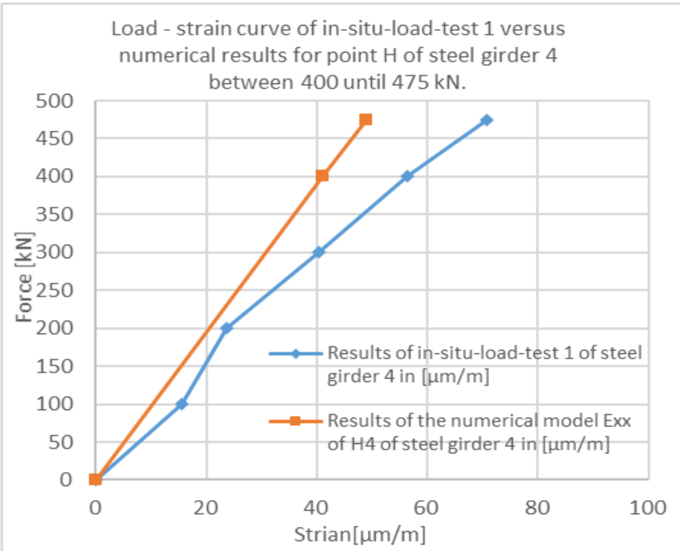

Figure E-9: Load-strain curve of in-situ-load-test 1 versus numerical results for point H of steel girder 4 between 400 until 475 kN.

Table E-8: Load-strain of in-situ-load-test 1 versus numerical results for points of steel girder 4.

Point	X	Results of in-situ-load-test 1 of steel girder 4 in [µm]	Results of the numerical model of steel girder 4 in [µm]	Ratio
***	0	0	0	0 %
H	1.54	-71.5	-41.0	57 %
I	2.09	-49.4	-28.0	57 %
J	3.25	-29.3	-9.8	33 %
L	4.96	-28.0	-4.8	17 %
***	6.5	0	0	0 %

Table E-9: Load-strain of in-situ-load-test 1 versus numerical results for points of steel girder 3.

Point	X	Results of in-situ-load-test 1 of steel girder 3 in [µm/m]	Results of the numerical model of steel girder 3 in [µm/m]	Ratio
***	0	0	0	0 %
H	1.54	-71.0	-41.5	58 %
I	2.09	-49.5	-27.5	56 %
J	3.25	-31.3	-9.1	29 %
L	4.96	-38.0	-4.7	12 %
***	6.5	0	0	0 %

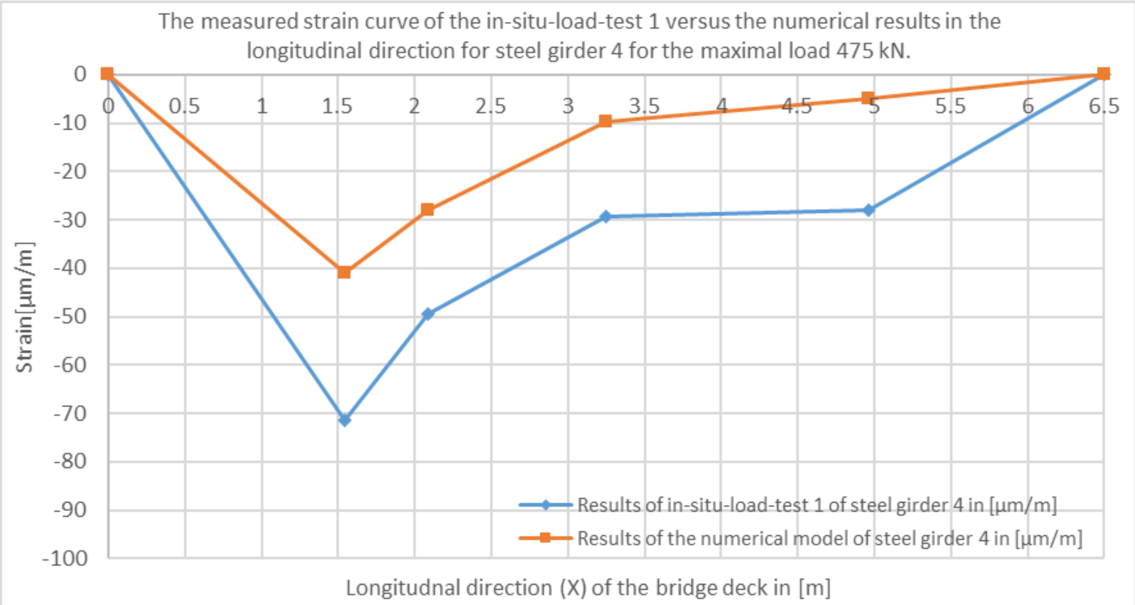

Figure E-10: The measured strain curves for in-situ-load-test 1 versus the numerical results for the steel girder 4 in the longitudinal direction of the load 475 kN.

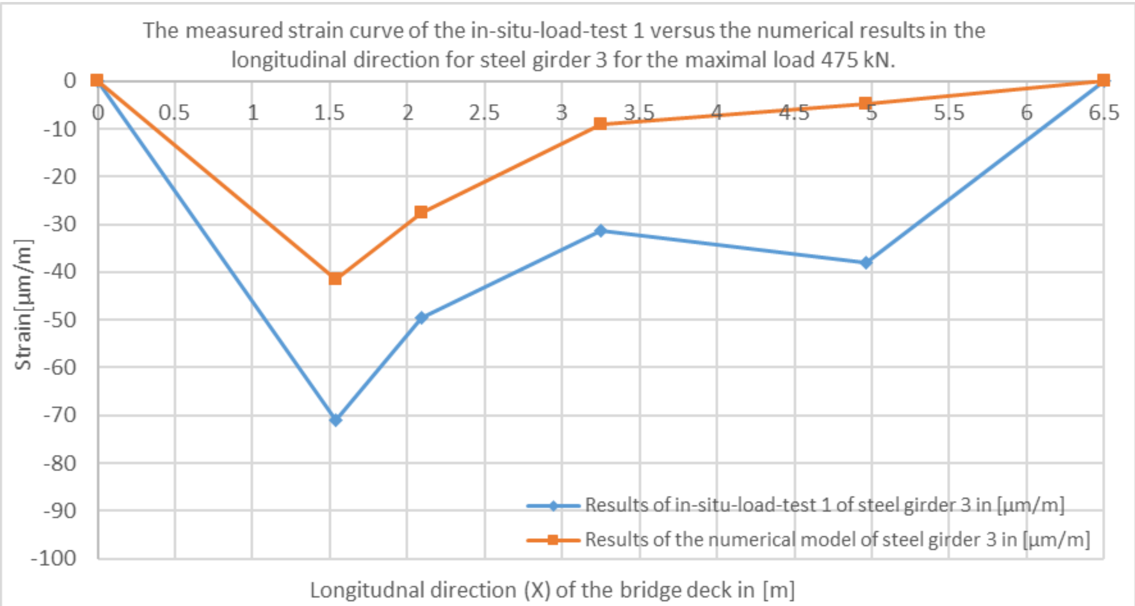

Figure E-11: The measured strain curves for in-situ-load-test 1 versus the numerical results for the steel girder 3 in the longitudinal direction of the load 475 kN.

Table E-10: Load-strain of in-situ-load-test 1 versus numerical results for the row H in the transvers direction.

Point	Y	Results of in-situ-load-test 1 of row H in [µm/m]	Results of the numerical model of row H in [µm/m]	Ratio
H1	**0**	-9.00	-4.80	53%
H2	**0.73**	-38.40	-16.70	43%
H3	**1.46**	-57.10	-41.00	72%
H4	**2.19**	-56.30	-42.00	75%
H5	**2.92**	-36.00	-14.00	39%
H6	**3.65**	-24.00	-5.30	22%

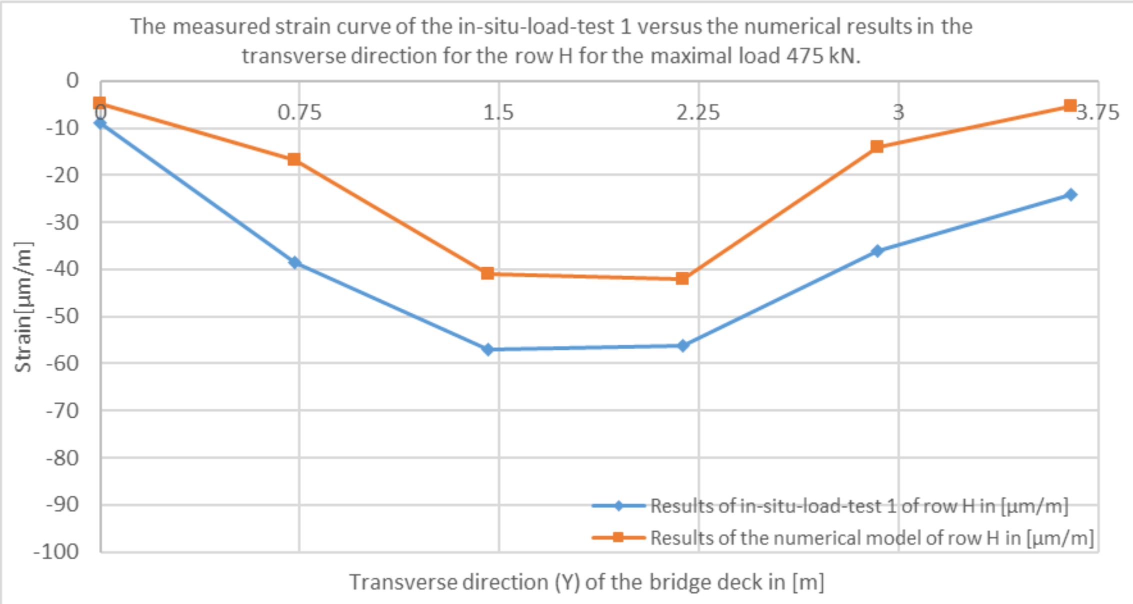

Figure E-12: The measured strain curve of the in-situ-load-test 1 versus the numerical results in the transverse direction for the row H for the maximal load 475 kN.

Table E-11: The maximal vertical displacement of the in-situ-load-test 3 versus the numerical results of steel girder 4.

Load	**Results of in-situ-load-test 1 of steel girder 4 in [mm]**	**Results of the numerical model of steel girder 4 in [mm]**	**Ratio**
0	0	0	0%
400	0.22	0.22	100%
475	0.27	0.26	96%

Table E-12: The maximal vertical displacement of the in-situ-load-test 3 versus the numerical results of steel girder 3.

load	**Results of in-situ-load-test 1 of steel girder 3 in [mm]**	**Results of the numerical model of steel girder 3 in [mm]**	**Ratio**
0	0	0	**0%**
400	0.20	0.21	**103%**
475	0.25	0.24	**98%**

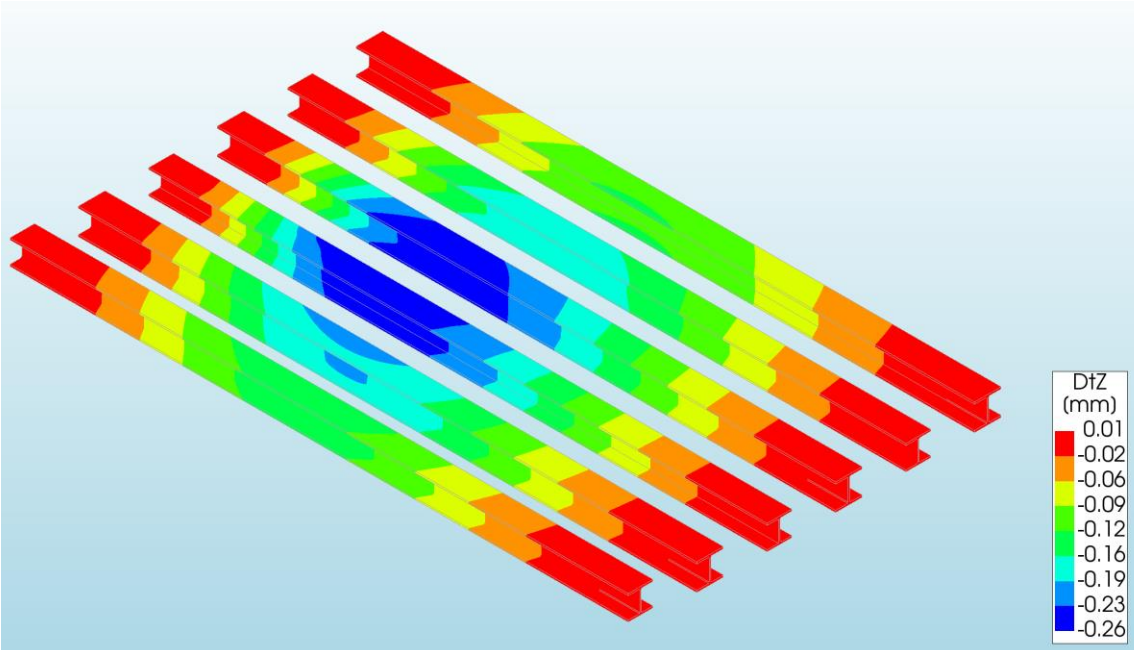

Figure E-13: The numerical results of the vertical displacement of steel-girders for a load of 475 kN at point H.

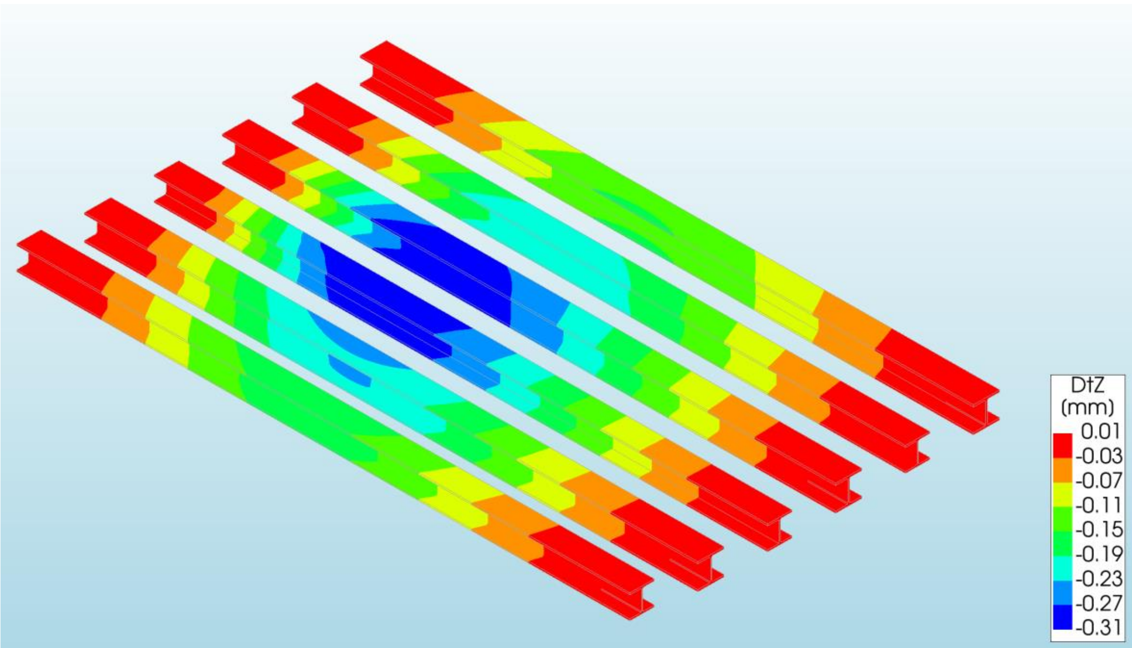

Figure E-14: The numerical results of the vertical displacement of steel-girders for a load of 475 kN at point H.

Table E 13: The maximal strain of the in-situ-load-test 1 versus the numerical results of steel girder 4.

Load	**Results of in-situ-load-test 1 of steel girder 4 in [mm]**	**Results of in-situ-load-test 1 of steel girder 4 in [mm]**	**Ratio**
0	0	0	0 %
400	56.30	41.0	73%
475	70.70	49.0	69%

Table E 14: The maximal strain of the in-situ-load-test 1 versus the numerical results of steel girder 3.

load	**Results of in-situ-load-test 1 of steel girder 3 in [μm/m]**	**Results of the numerical model Exx of H3 of steel girder 3 in [μm/m]**	**Ratio**
0	**0**	**0**	**0%**
400	**57.1**	**41**	**73%**
475	**71.5**	**48**	**67%**

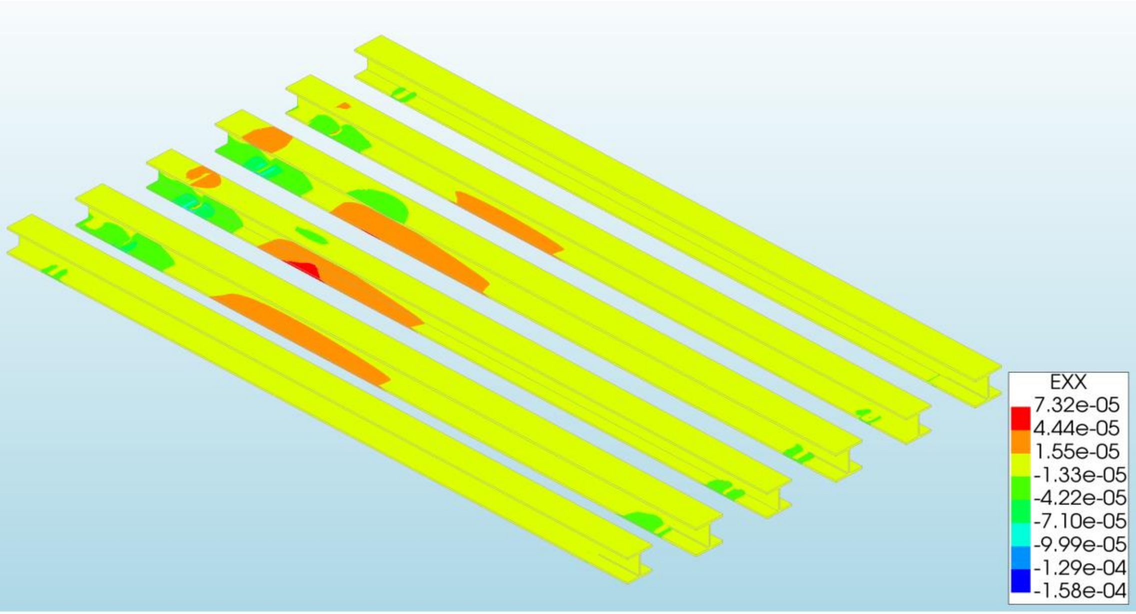

Figure E-15: The numerical results of the strain of steel-girders for a load of 400 kN in the point H.

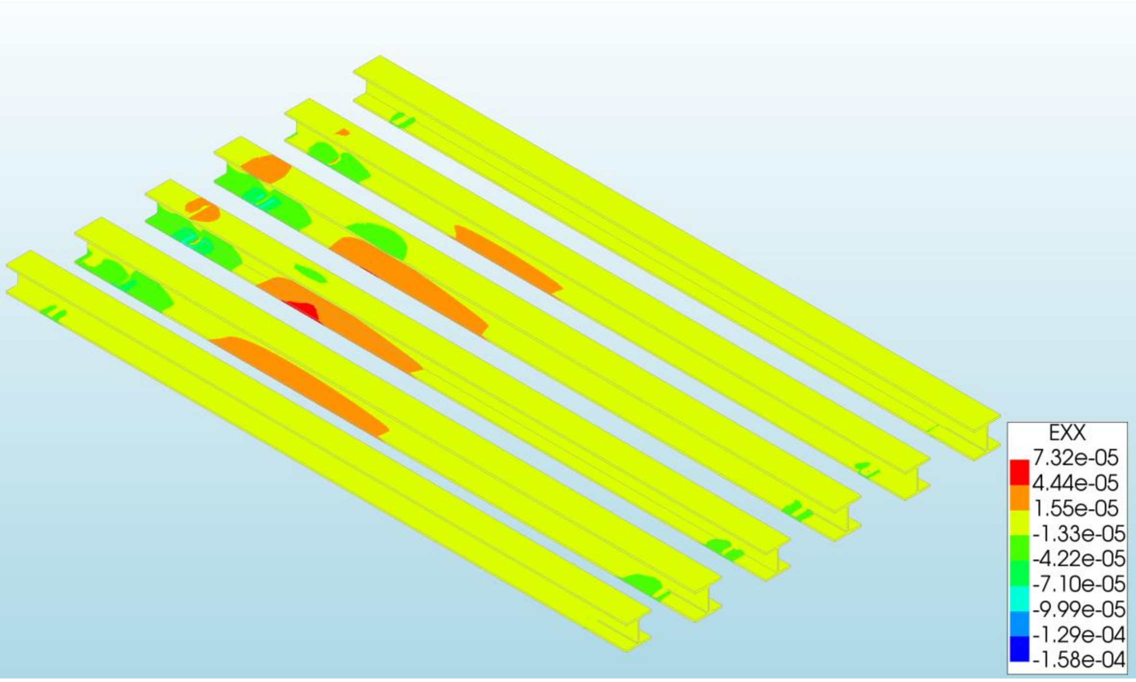

Figure E-16: The numerical results of the strain of steel-girders for a load of 475 kN in the point H.

Table E-15: The maximal principal stress of concrete at point H.

Load	The numerical results of the principal stress of the concrete on point H in [N/mm2]	Maximal allowable tensile stress of concrete in [N/mm2]	Ratio
0	0	0	0 %
400	3.10	4.2	73 %
475	3.62	4.2	87 %

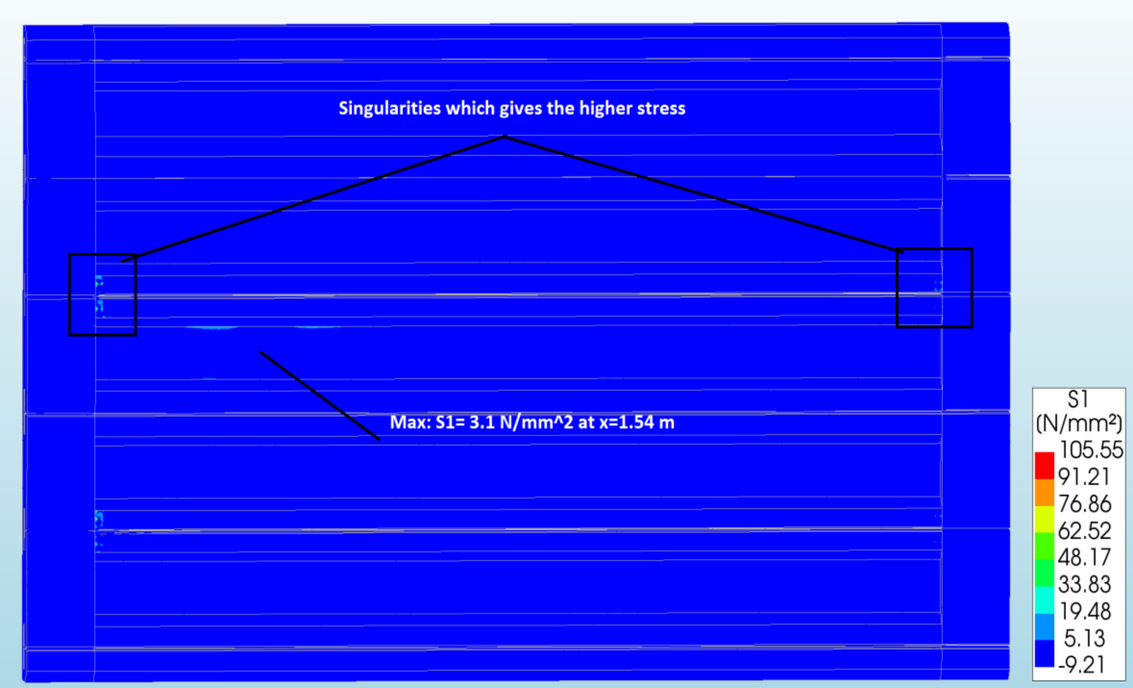

Figure E-17: The numerical results of the principal stress in the concrete for a load of 400 kN at the point H.

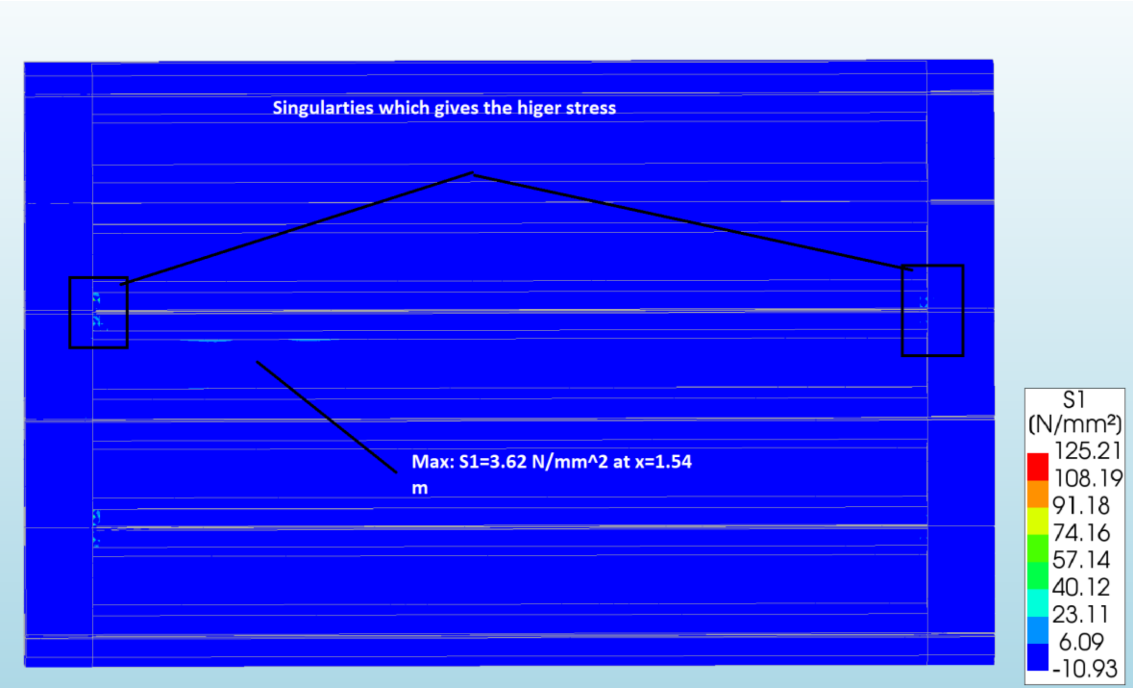

Figure E-18: The numerical results of the principal stress in the concrete for a load of 475 kN at the point H.

Comment: The principal stress is under the maximal tensile stress of concrete.

Table E-16: The maximal principal stress of steel at point H.

Load	The numerical results of the principal stress of the concrete on point H in [N/mm2]	Maximal allowable tensile /compressive stress of steel in [N/mm2]	Ratio
0	0	0	0 %
400	11	235	4.7 %
475	12	235	5.2 %

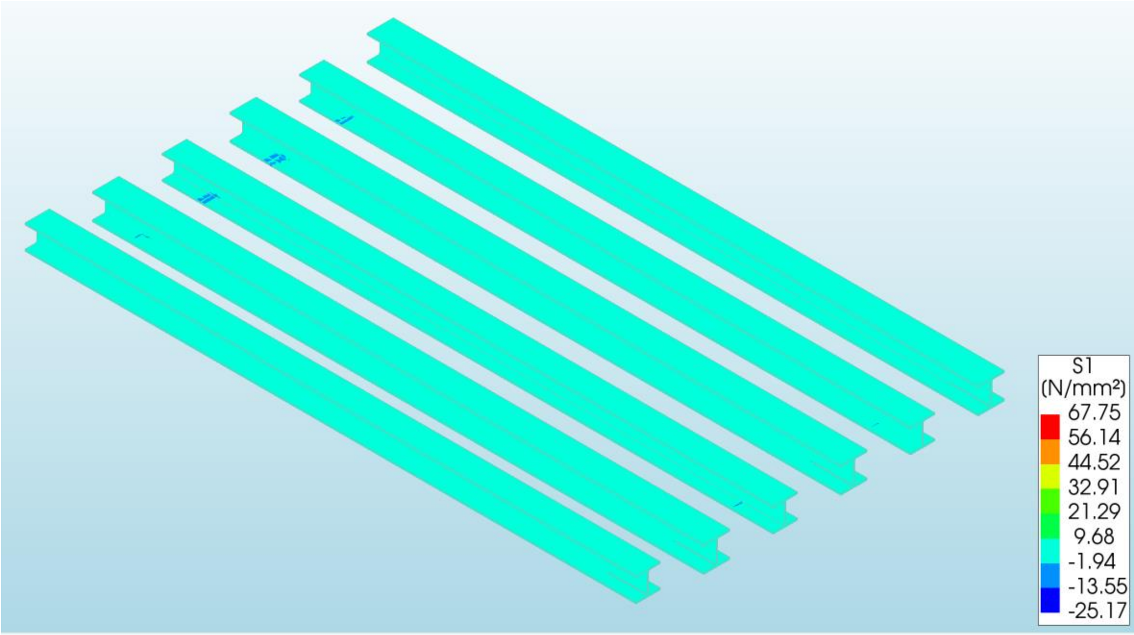

Figure E-19: The numerical results of the principal stress in the steel for a load of 400 kN at the point H.

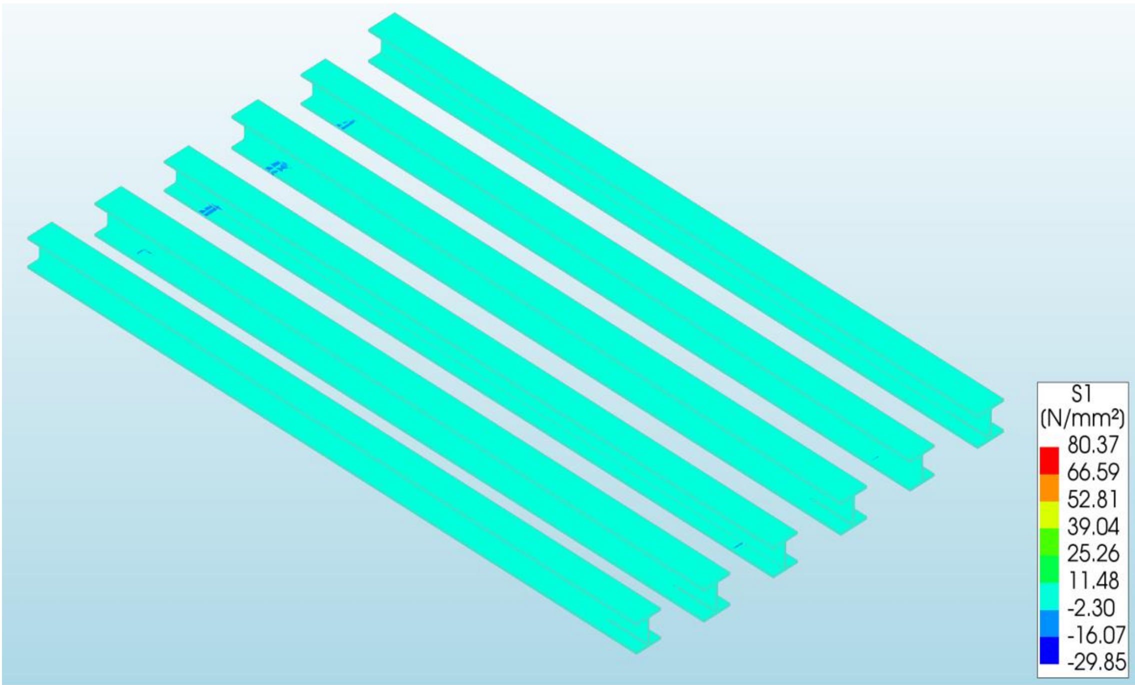

Figure E-20: The numerical results of the principal stress in the steel for a load of 475 kN at the point H.

Comment: The principal stress is under the maximal tensile stress of steel-girders.

Table E-17: The maximal shear stress in concrete at point H.

Load	The numerical results of the principal stress of the concrete on point H in [N/mm2]	Maximal allowable shear stress of concrete in [N/mm2]	Ratio
0	0	0	0 %
400	2.40	7.2	34 %
475	3.00	7.2	42 %

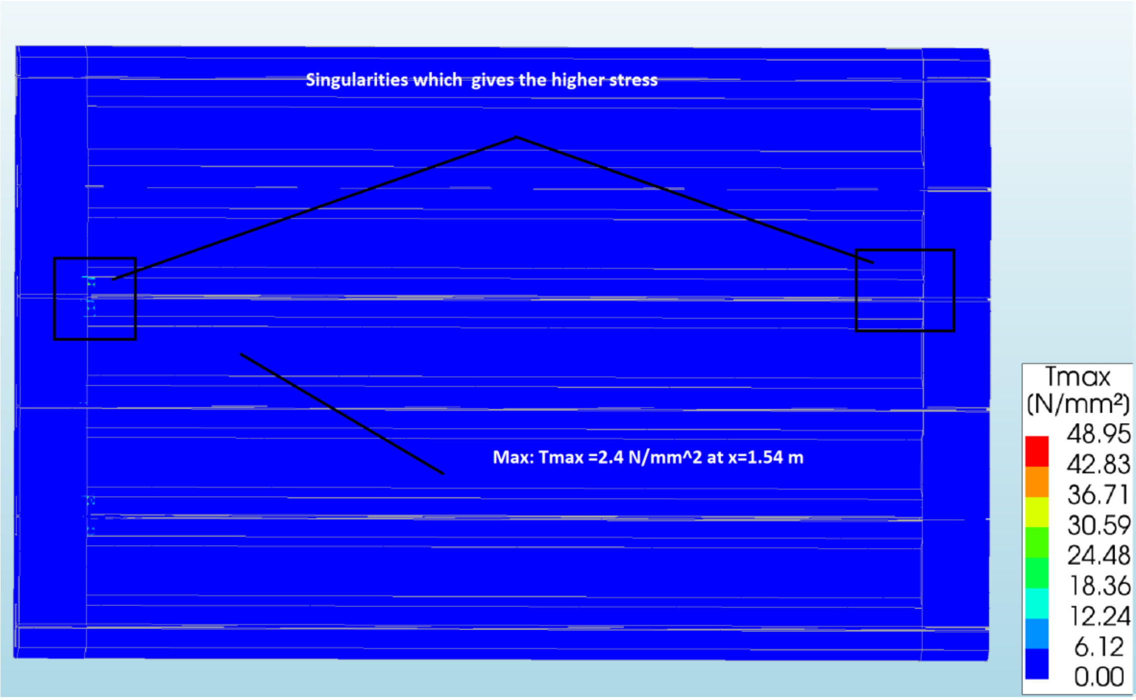

Figure E-21: The numerical results of the maximal shear stress in the concrete Tmax for a load of 400 kN at the point H.

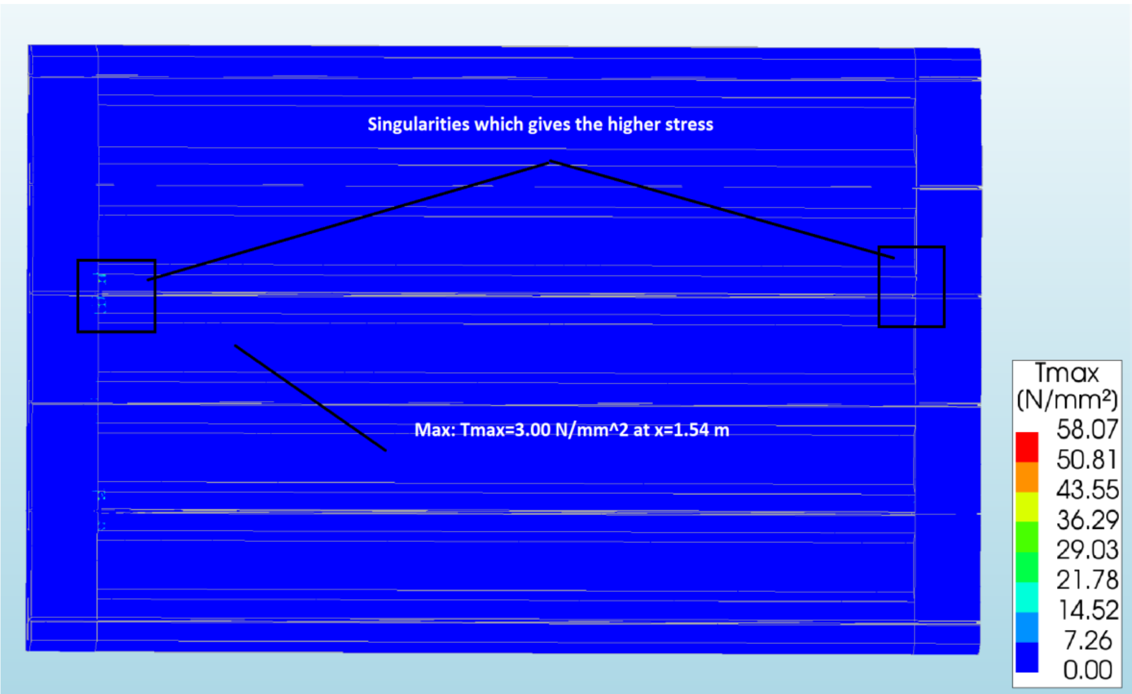

Figure E-22: The numerical results of the shear stress in the concrete Tmax for a load of 475 kN at the point H.

Comment: The shear stress are under the maximal shear stress of concrete.

E.2. Numerical results of steel girder 4 on point L at 4.96 m

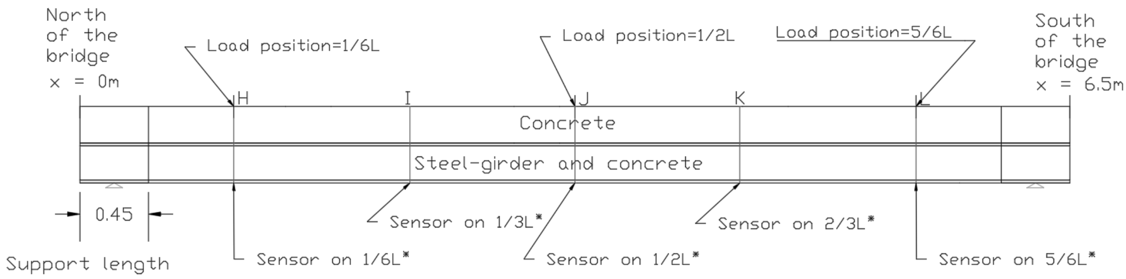

E-23: The loaded point L on the beam.

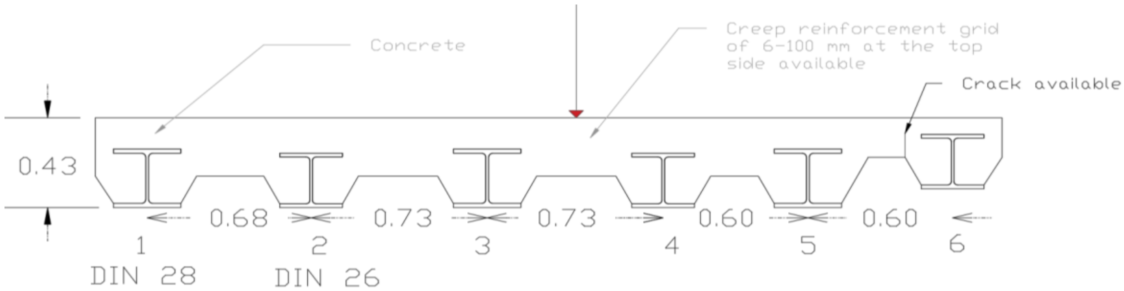

E-24: The loaded points (H, J and L) on the bridge deck in the transvers direction of the bridge deck.

Table E-18: Load-displacement of in-situ-load-test 3 versus numerical results for point L of steel girder 4.

Load	Results of in-situ-load-test 3 of steel girder 4 in [mm]	Results of the numerical model of steel girder 4 in [mm]	Ratio
0	0	0	0%
400	0.29	0.22	77%
475	0.376	0.32	85%

Table E-19: Load-displacement of in-situ-load-test 3 versus numerical results for point L of steel girder 3.

Load	Results of in-situ-load-test 3 of steel girder 3 in [mm]	Results of the numerical model of steel girder 3 in [mm]	Ratio
0	0	0	0%
400	0.24	0.21	89%
475	0.33	0.32	98%

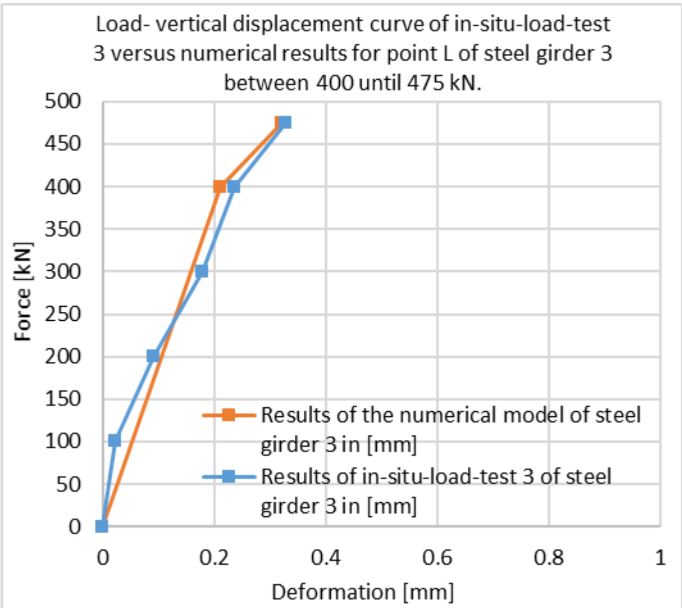

Figure E-25: Load-displacement curve of the in-situ-load-test 3 versus numerical results for point L on steel girder 3 between 400 until 475 kN.

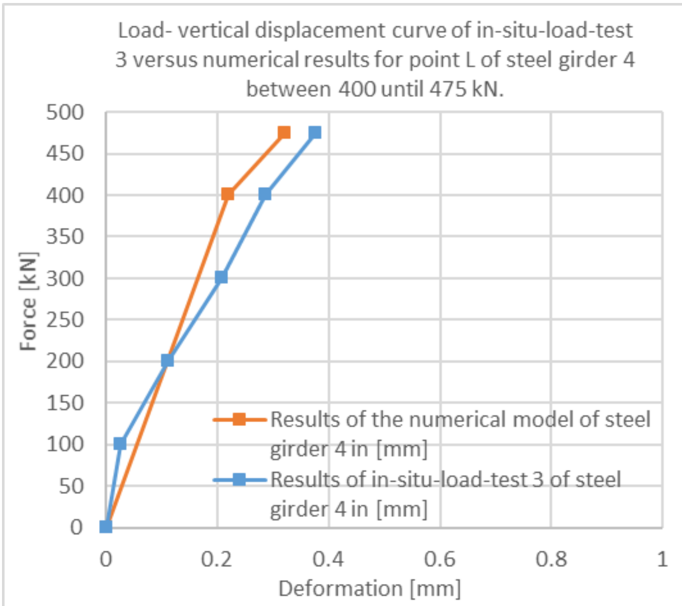

Figure E-26: Load-displacement curve of in-situ-load-test 3 versus numerical results for point L of steel girder 4 between 400 until 475 kN.

Table E-20: Load-displacement of in-situ-load-test 3 versus numerical results for points of steel girder 4.

Point	X	Results of in-situ-load-test 3 of steel girder 4 in [mm]	Results of the numerical model of steel girder 4 in [mm]	Ratio
***	0.00	0	0	0%
H	1.54	-0.07	-0.08	106%
J	3.25	-0.33	-0.26	80%
K	4.41	-0.38	-0.31	82%
L	4.96	-0.38	-0.32	85%
***	6.50	0	0	0%

Table E-21: Load-displacement of in-situ-load-test 3 versus numerical results for points of steel girder 3.

Point	X	Results of in-situ-load-test 3 of steel girder 3 in [mm]	Results of the numerical model of steel girder 3 in [mm]	Ratio
***	0.00	0	0	0%
H	1.54	-0.07	-0.08	107%
J	3.25	-0.30	-0.26	87%
K	4.41	-0.35	-0.31	89%
L	4.96	-0.33	-0.32	98%
***	6.50	0	0	0%

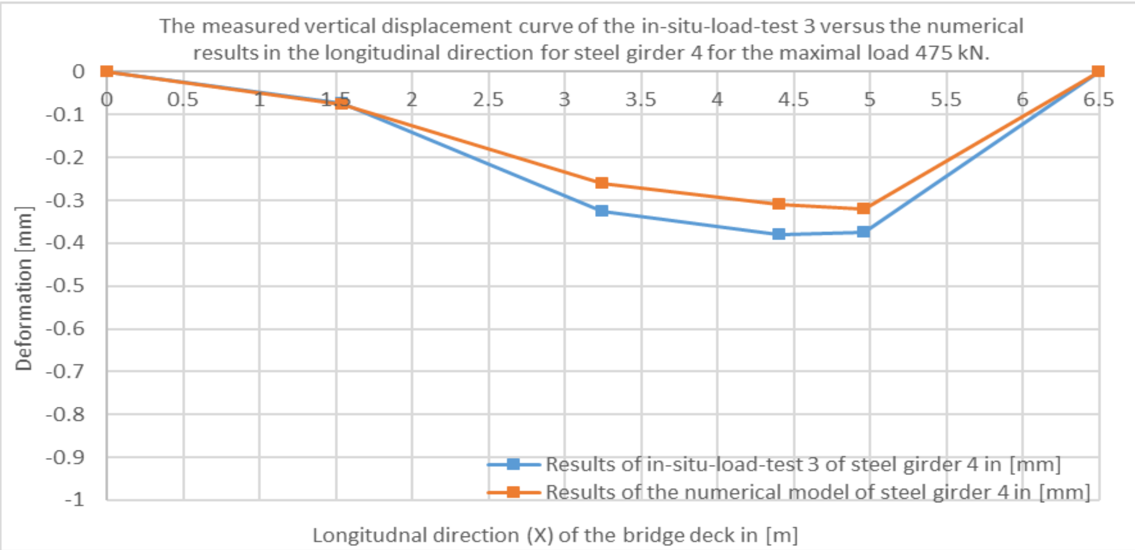

Figure E-27: The measured vertical displacement curves for in-situ-load-test 3 versus the numerical results for the steel girder 4 in the longitudinal direction of the load 475 kN.

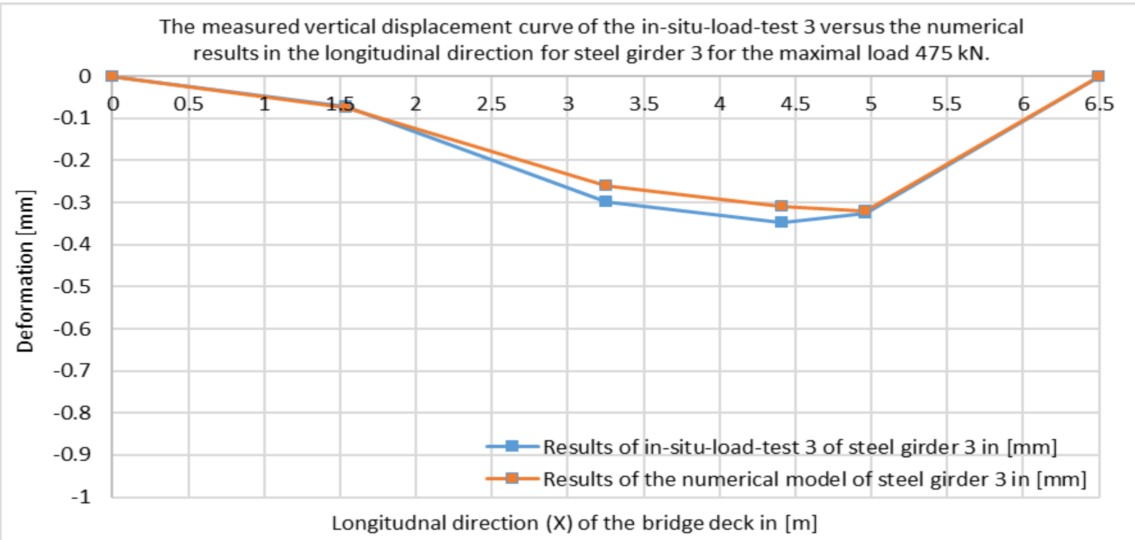

Figure E-28: The measured vertical displacement curves for in-situ-load-test 3 versus the numerical results for the steel girder 3in the longitudinal direction of the load 475 kN.

Table E-22: Load-displacement of in-situ-load-test 3 versus numerical results of the row L.

Point	Y	Results of in-situ-load-test 3 of row L in [mm]	Results of the numerical model of row L in [mm]	Ratio
L1	**0**	-0.25	-0.10	40%
L2	**0.73**	-0.33	-0.18	55%
L3	**1.46**	-0.38	-0.32	85%
L4	**2.19**	-0.33	-0.32	98%
L5	**2.92**	-0.20	-0.17	85%
L6	**3.65**	-0.03	-0.08	250%

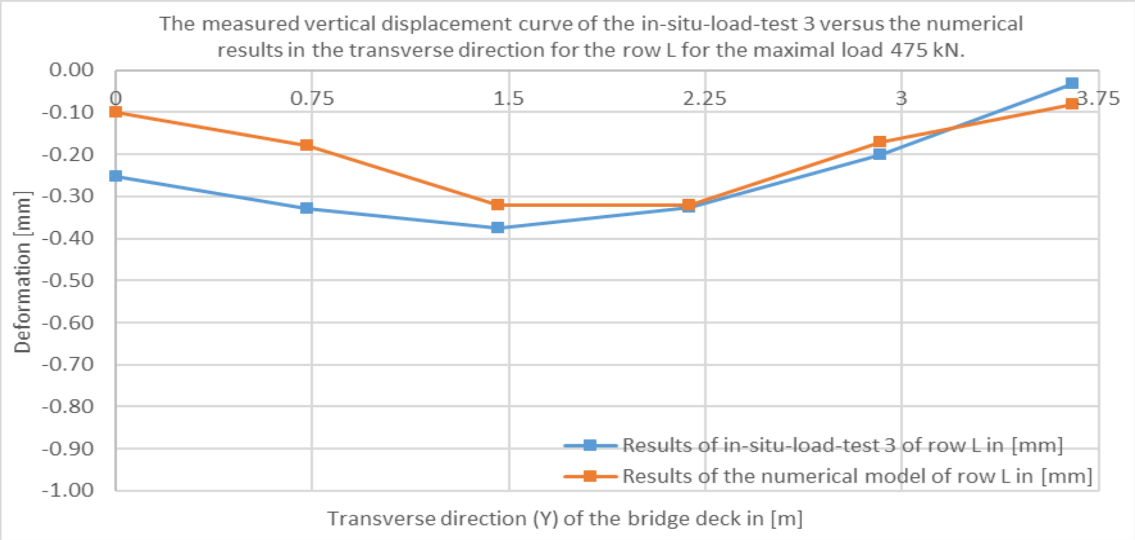

Figure E-29: The measured vertical displacement curves for in-situ-load-test 3 versus the numerical results in the transverse direction for the row L of the load 475 kN.

Table E-23: Load-strain of in-situ-load-test 3 versus numerical results for point L of steel girder 4.

Load	Results of in-situ-load-test 3 of steel girder 4 in [µm/m]	Results of the numerical model Exx of H4 of steel girder 4 in [µm/m]	Ratio
0	0	0	0%
400	51.7	42	82%
475	64.7	51	79%

Table E-24: Load-strain of in-situ-load-test 3 versus numerical results for point L of steel girder 3.

Load	Results of in-situ-load-test 3 of steel girder 3 in [µm/m]	Results of the numerical model Exx of H3 of steel girder 3 in [µm/m]	Ratio
0	0	0.0	0
400	36.90	42.8	116%
475	44.10	50.5	114%

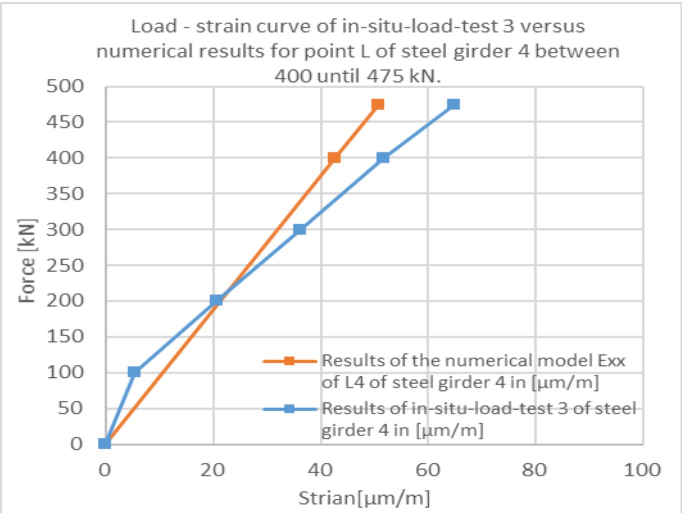

Figure E-30: Load-strain curve of in-situ-load-test 3 versus numerical results for point L of steel girder 4 between 400 until 475 kN.

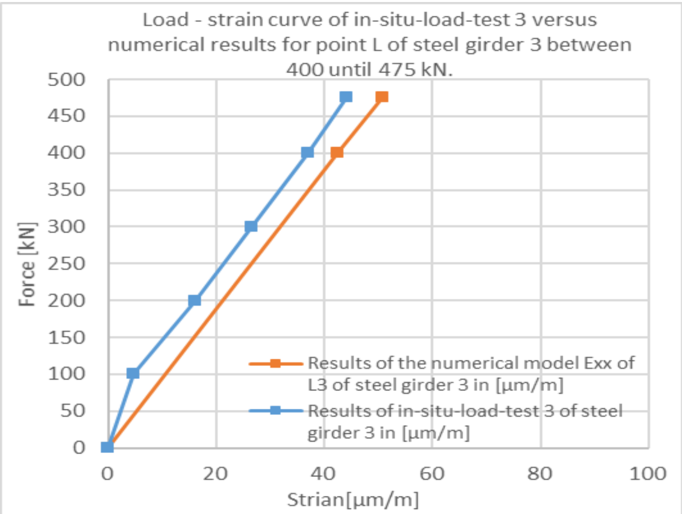

Figure E-31: Load-strain curve of in-situ-load-test 3 versus numerical results for point L of steel girder 3 between 400 until 475 kN.

Table E-25: Load-strain of in-situ-load-test 3 versus numerical results for point L of steel girder 4.

Point	X	Results of in-situ-load-test 3 of steel girder 4 in [µm/m]	Results of the numerical model of steel girder 4 in [µm/m]	Ratio
***	0	0	0	0
H	1.54	-2.00	-5.30	265%
J	3.25	-26.00	-10.00	38%
K	4.41	-38.00	-21.00	55%
L	4.96	-65.00	-43.00	66%
***	6.5	0	0	0

Table E-26: Load-strain of in-situ-load-test 3 versus numerical results for point L of steel girder 3.

Point	X	Results of in-situ-load-test 3 of steel girder 3 in [µm/m]	Results of the numerical model of steel girder 3 in [µm/m]	Ratio
***	0	0	0	0
H	1.54	-0.60	-5.00	833%
J	3.25	-28.00	-10.00	36%
K	4.41	-42.00	-20.00	48%
L	4.96	-42.00	-43.00	102%
***	6.5	0	0	0

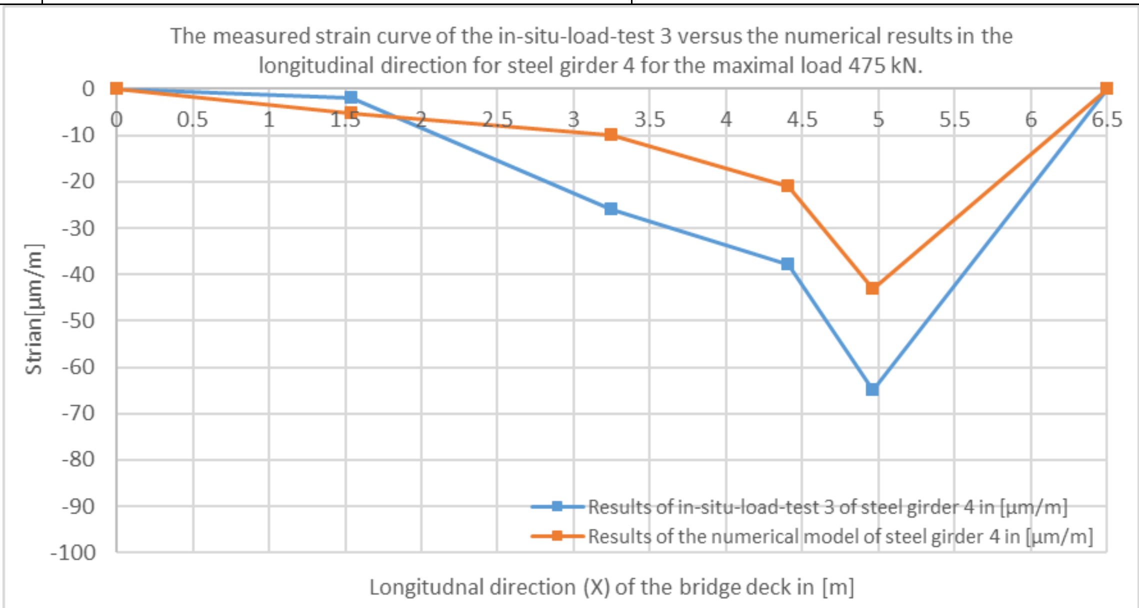

Figure E-32: The measured strain curves for in-situ-load-test 3 versus the numerical results for the steel girder 4 in the longitudinal direction of the load 475 kN.

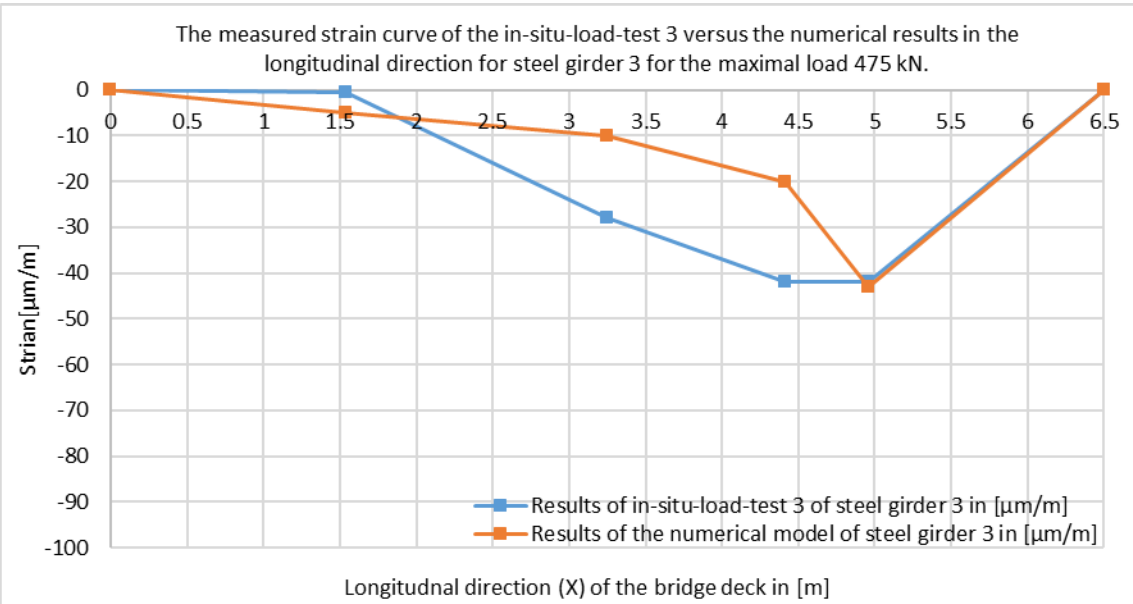

Figure E-33: The measured strain curves for in-situ-load-test 3 versus the numerical results for the steel girder 3 in the longitudinal direction of the load 475 kN.

Table E-27: Load-strain of in-situ-load-test 3 versus numerical results for the row L in the transverse direction.

Point	Y	Results of in-situ-load-test 3 of row L in [μm/m]	Results of the numerical model of row L in [μm/m]	Ratio
L1	**0**	-29.10	-3.00	10%
L2	**0.73**	-40.00	-17.00	43%
L3	**1.46**	-64.70	-42.50	66%
L4	**2.19**	-44.10	-42.50	96%
L5	**2.92**	-23.70	-14.00	59%
L6	**3.65**	64.40	20.00	31%

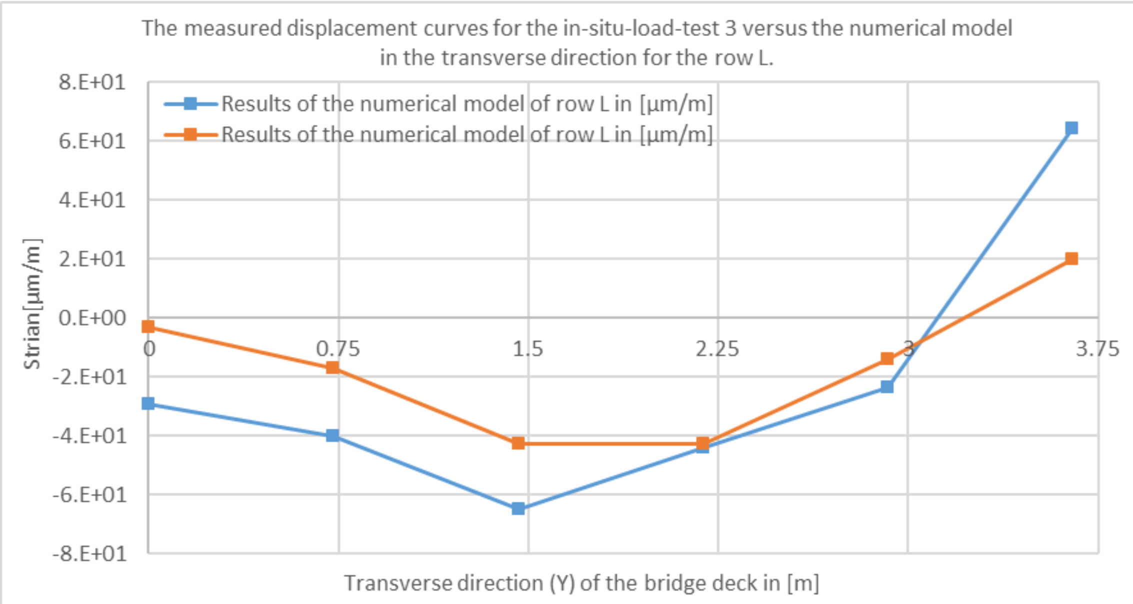

Figure E-34: The measured displacement curves for the in-situ-load-test 3 versus the numerical model in the transverse direction for the row L.

Table E-28: The maximal vertical displacement of the in-situ-load-test versus the numerical results and the ratio.

Load	Results of in-situ-load-test 3 of steel girder 4 on point L in [mm]	Results of the numerical model of steel girder 4 on point L in [mm]	Ratio
0	0	0	0 %
400	-0,28	-0,25	90 %
475	-0,38	-0,34	90 %

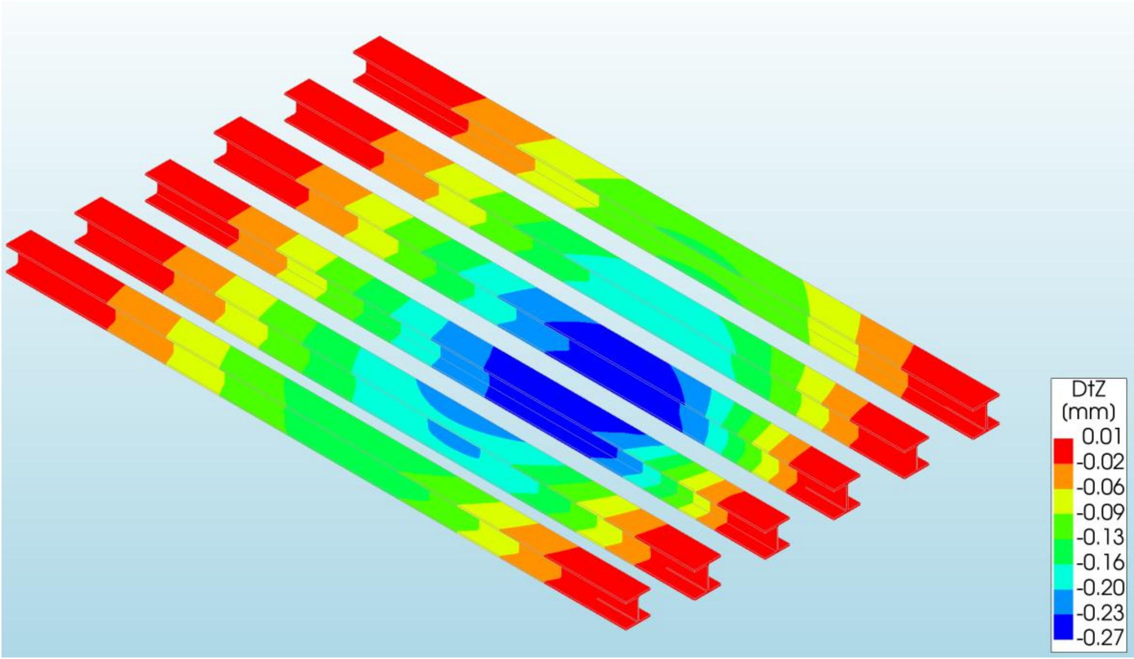

Figure E-35: The numerical results of the vertical displacement of steel-girders for a load of 400 kN at point L.

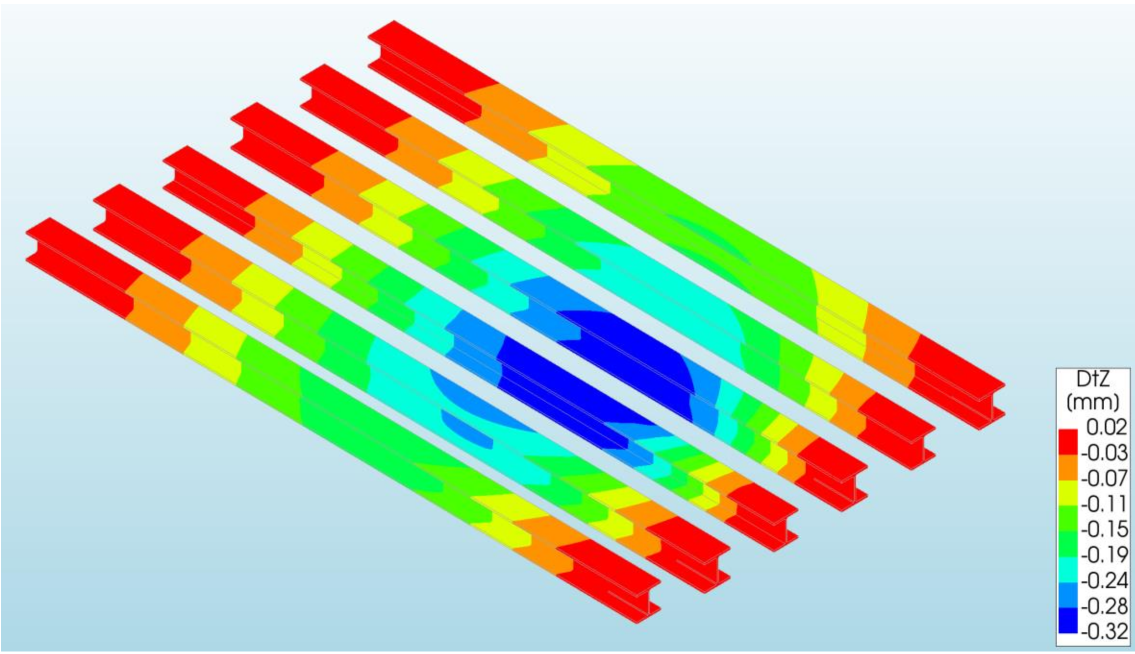

Figure E-36: The numerical results of the vertical displacement of steel-girders for a load of 475 kN at point L.

Table E-29: The maximal strain of the in-situ-load-test 3 versus the numerical results and the ratio.

Load	Results of in-situ-load-test 3 of steel girder 4 on point L in [N/mm2]	Results of the numerical model of steel girder 4 on point L in [N/mm2]	Ratio
0	0	0	0 %
400	79.7*10^-5	4.16*10^-5	87 %
475	102.7*10^-5	4.40*10^-5	81 %

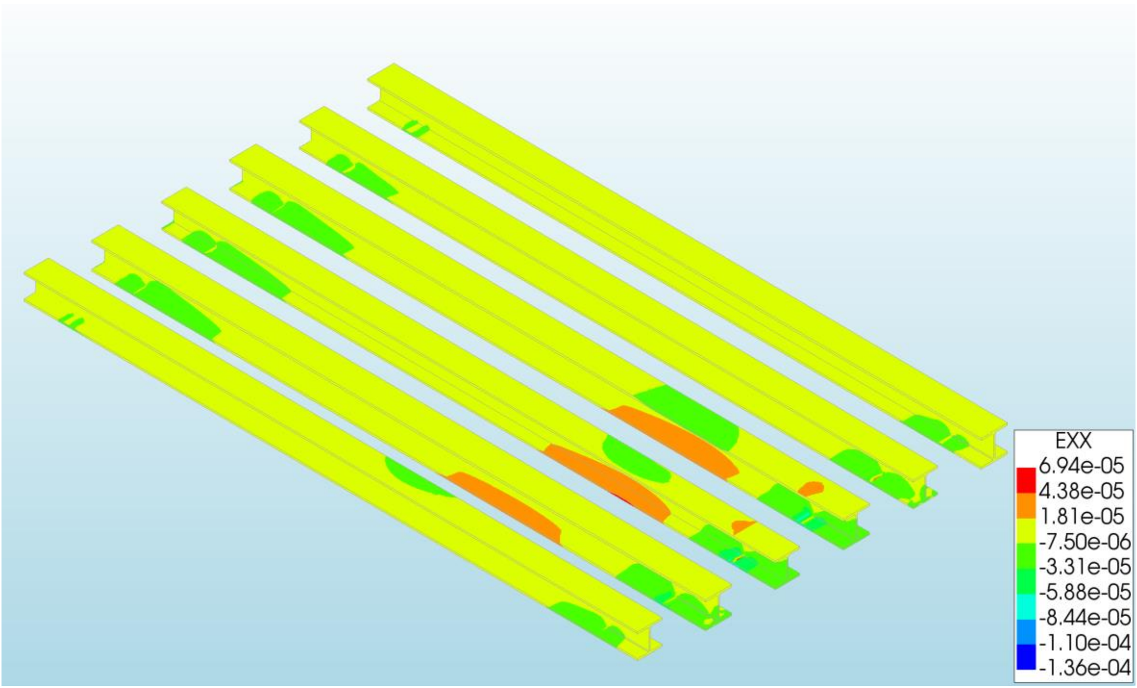

Figure E-37: The numerical results of the strain of steel-girders for a load of 400 kN in the point L.

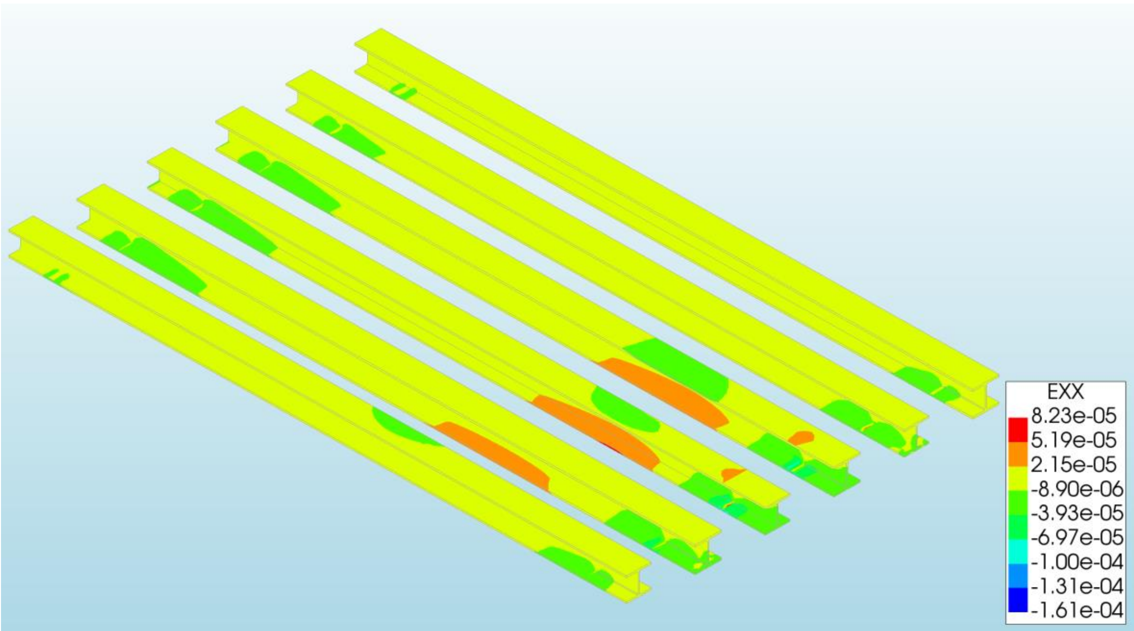

Figure E-38: The numerical results of the strain of steel-girders for a load of 475 kN in the point L.

Table E-30: The maximal principal stress of the concrete.

Load	The numerical results of the principal stress of the concrete on point L in [N/mm2]	Maximal allowable tensile stress of concrete in [N/mm2]	Ratio
0	0	0	0%
400	2.98	4.2	71 %
475	3.54	4.2	85 %

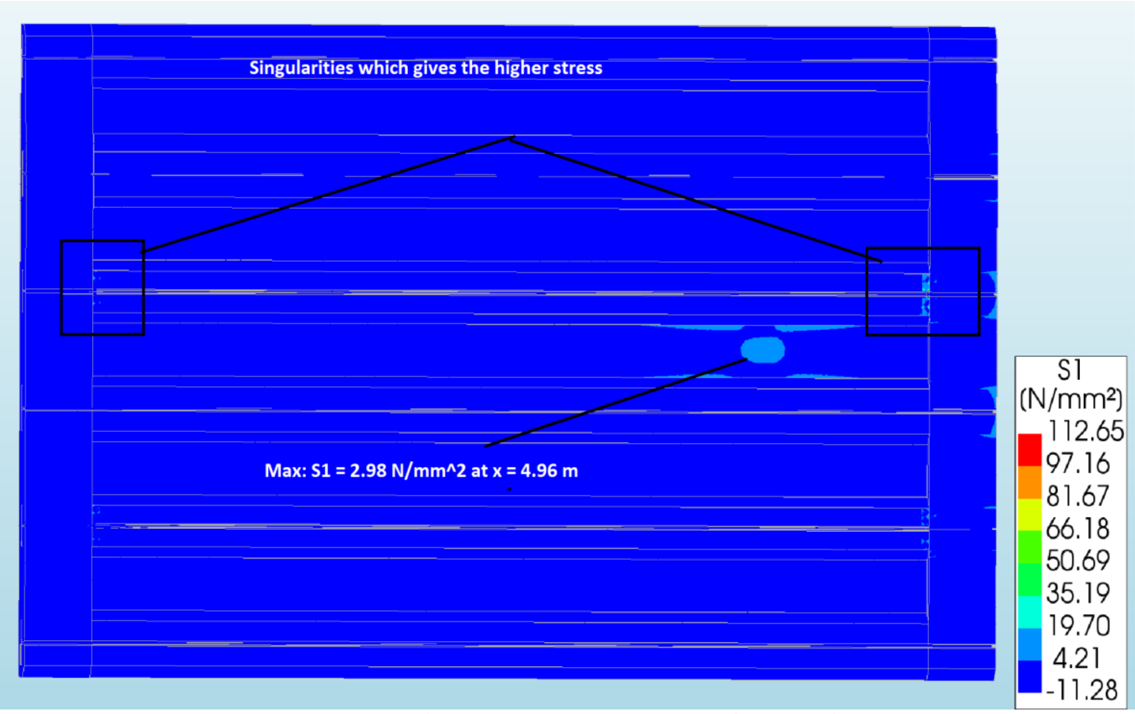

Figure E-39: The numerical results of the principal stress in the concrete for a load of 400 kN at the point L.

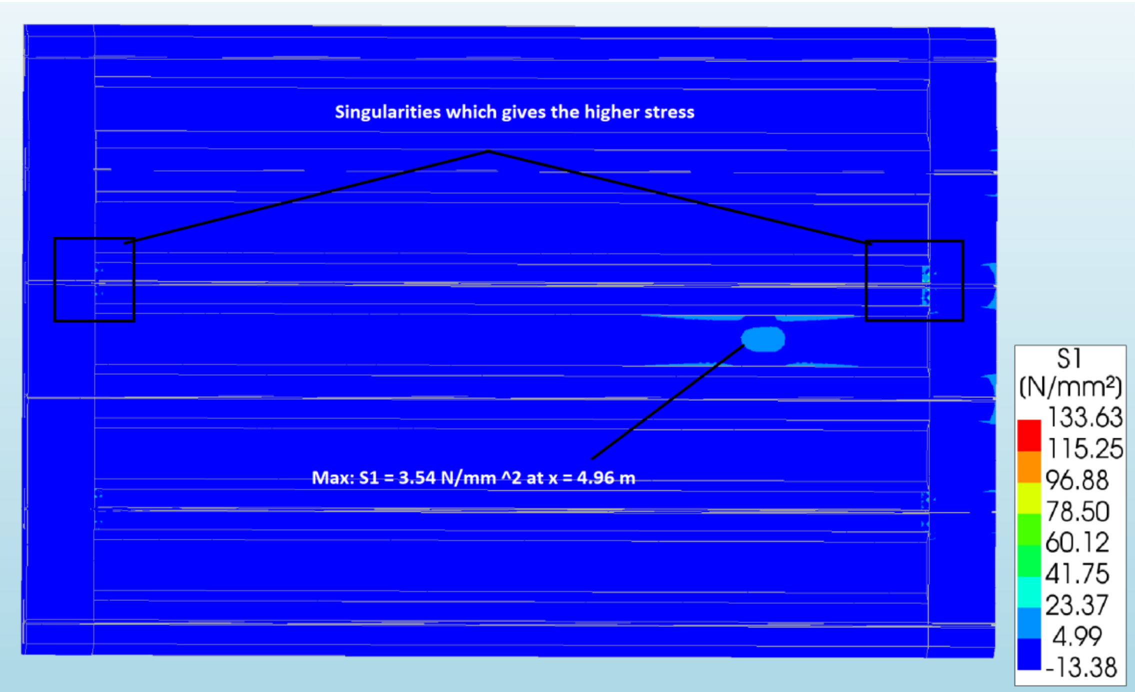

Figure E-40: The numerical results of the principal stress in the concrete for a load of 475 kN at the point L.

Comment: The principal stress is under the maximal tensile stress of concrete.

Table E-31: The maximal principal stress of the steel at point L.

Load	The numerical results of the principal stress of the concrete on point L in [N/mm2]	Maximal allowable tensile /compressive stress of steel in [N/mm2]	Ratio
0	0	0	0
400	11	235	4.6 %
475	13	235	5.5 %

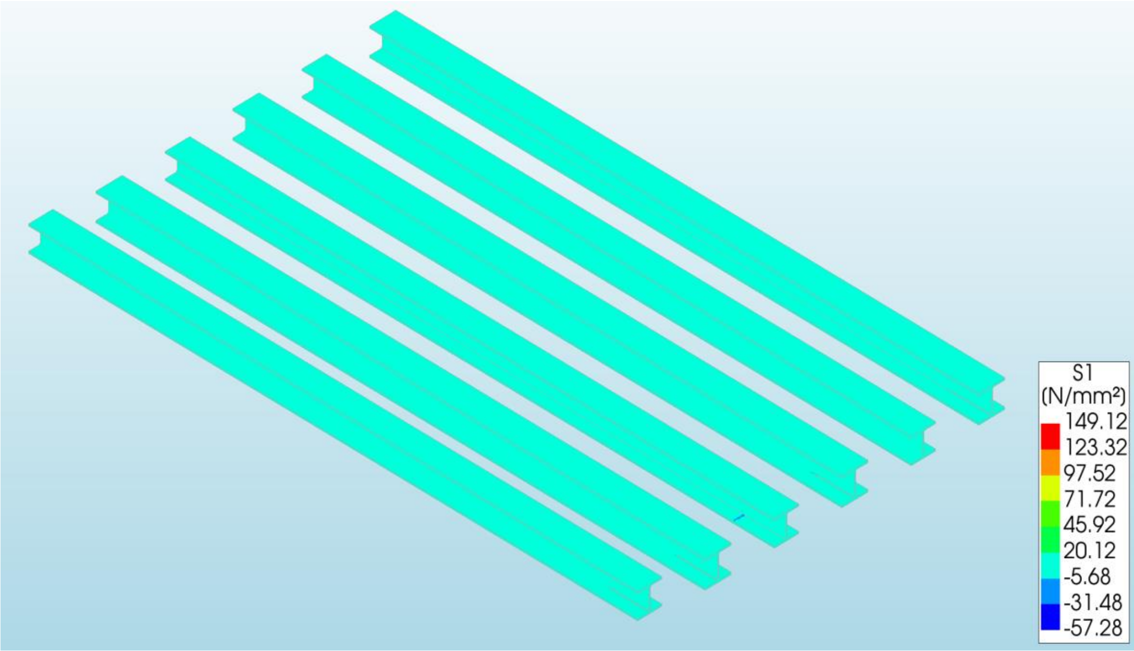

Figure E-41: The numerical results of the principal stress in the steel for a load of 400 kN at the point L.

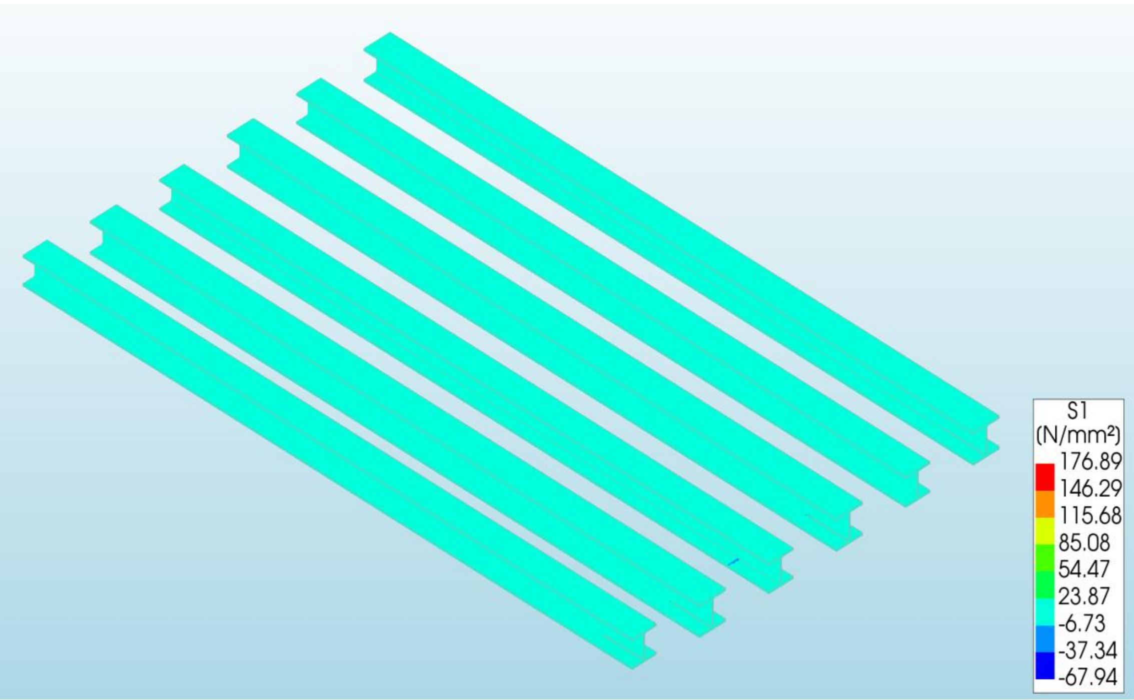

Figure E-42: The numerical results of the principal stress in the steel for a load of 475 kN at the point L.

Comment: The principal stress is under the maximal tensile stress of steel.

Table E-32: The maximal shear stress of the concrete.

Load	The numerical results of the principal stress of the concrete on point L in [N/mm^2]	Maximal allowable shear stress of concrete in [N/mm^2]	Ratio
0	0	0	0
400	1.50	7.2	21 %
475	1.80	7.2	25 %

Figure E-43: The numerical results of the principal stress in the concrete Tmax for a load of 400 kN at the point L.

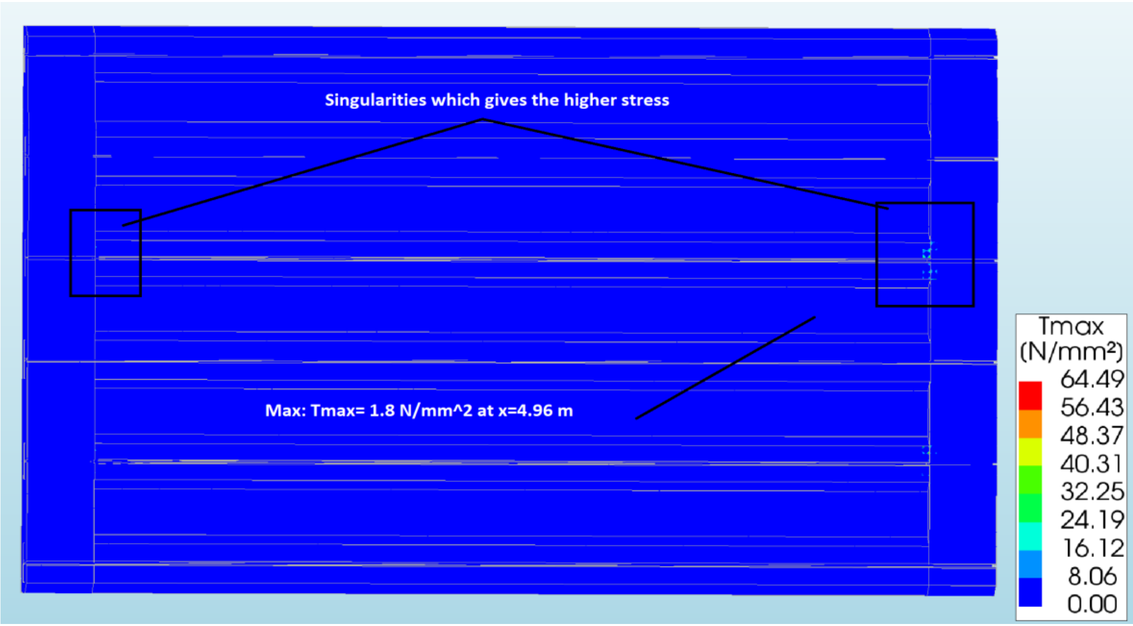

Figure E-44: The numerical results of the principal stress in the concrete Tmax for a load of 475 kN at the point L.

Comment: The shear stress is under the maximal shear stress of concrete.

F Annex – The numerical results of the other bridges decks compared with bridge A

F.1. Numerical results for the loaded point H of three bridge decks

Table F-1: Results displacement of in-situ-load-test 1 versus numerical results for the three bridges of steel girder 4.

Vertical displacement of steel girder 4 in [mm]				
Load	**Results of in-situ-load test 1**	**Results of the numerical model of steel girder 4 with a span 6.5 [m]**	**Results of the numerical model of steel girder 4 with a span 10 [m]**	**Results of the numerical model of steel girder 4 with a span 13 [m]**
0	0	0	0	0
400	0.22	0.21	0.28	0.53
475	0.27	0.24	0.33	0.63

Table F-2: Results displacement of in-situ-load-test 1 versus numerical results for the three bridges of steel girder 3.

Vertical displacement of steel girder 3 in [mm]				
Load	**Results of in-situ-load test 1**	**Results of the numerical model of steel girder 3 with a span 6.5 [m]**	**Results of the numerical model of steel girder 3 with a span 10 [m]**	**Results of the numerical model of steel girder 3 with a span 13 [m]**
0	0	0	0	0
400	0.20	0.21	0.28	0.53
475	0.25	0.24	0.33	0.63

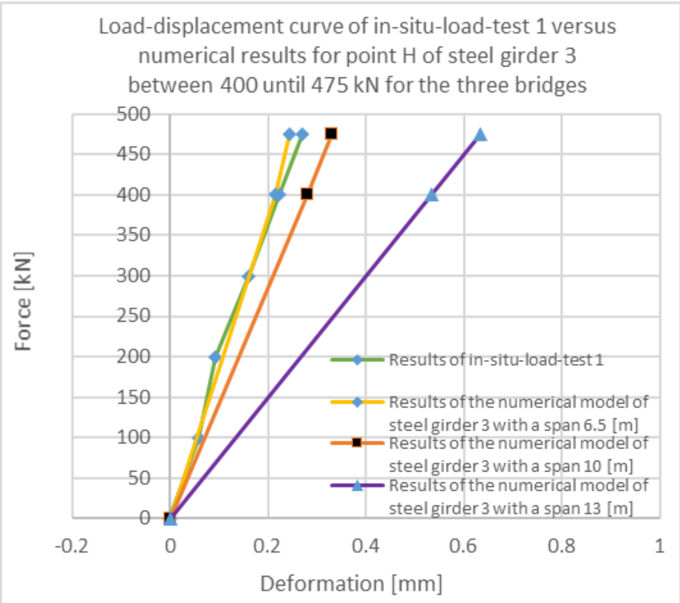

Figure F-1: Load-displacement curve of in-situ-load-test 1 versus numerical results for point H of steel girder 3 between 400 until 475 kN for the three bridge decks.

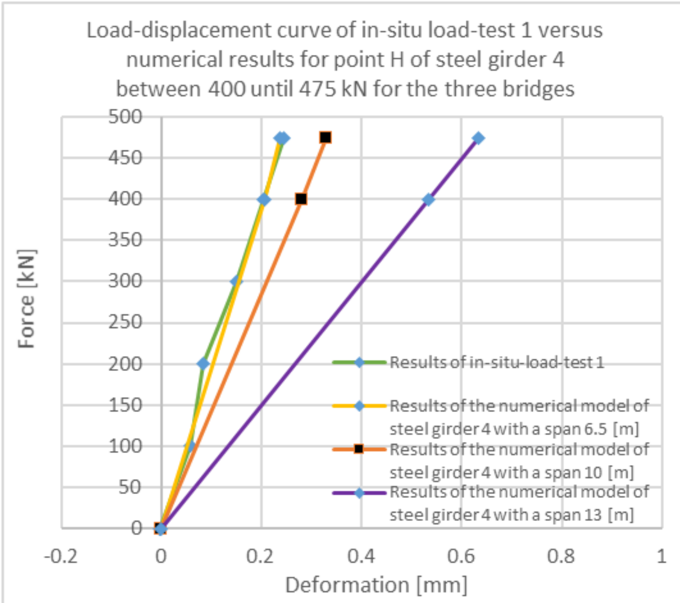

Figure F-2: Load-displacement curve of in-situ-load-test 1 versus numerical results for point H of steel girder 4 between 400 until 475 kN for the three bridge decks.

Table F-3: Results maximal principal stress of concrete for the three bridge decks.

Maximal principal stress of concrete in [N/mm^2]			
Load	**Results of the maximal principal stress for the span 6.5 [m]**	**Results of the maximal principal stress for the span 10 [m]**	**Results of the maximal principal stress for the span 13 [m]**
0	0	0	0
400	3.1	3.22	3.27
475	3.62	3.82	3.88

Table F-4: Results maximal shear stress of concrete for the three bridge decks.

Maximal shear stress of concrete in [N/mm^2]			
Load	**Results of the maximal shear stress for the span 6.5 [m]**	**Results of the maximal shear stress for the span 10 [m]**	**Results of the maximal shear stress for the span 13 [m]**
0	0	0	0
400	2.40	1.52	1.73
475	3.00	1.80	2.06

Table F-5: Results maximal principal stress of steel for the three bridge decks.

Maximal principal stress of steel in [N/mm^2]			
Load	**Results of the maximal principal stress for the span 6.5 [m]**	**Results of the maximal principal stress for the span 10 [m]**	**Results of the maximal principal stress for the span 13 [m]**
0	0	0	0
400	11	5.54	4.56
475	12	6.57	5.41

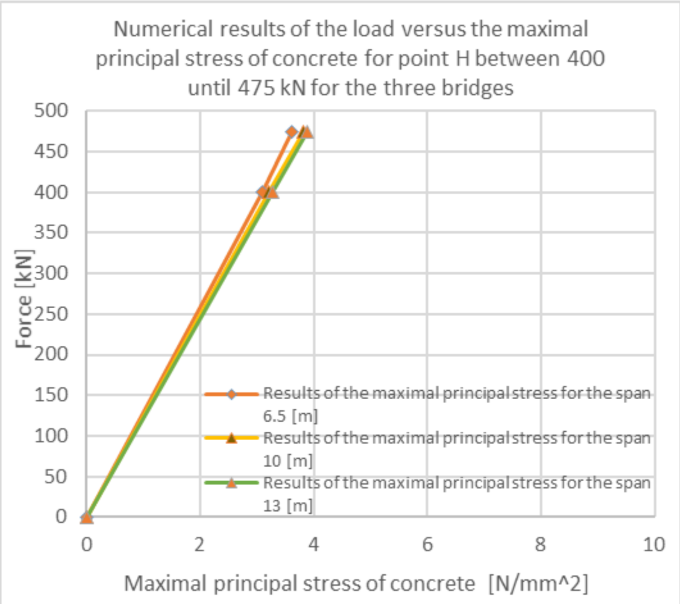

Figure F-3: Numerical results of the load versus the maximal principal stress of concrete for point H between 400 until 475 kN for the three bridge decks.

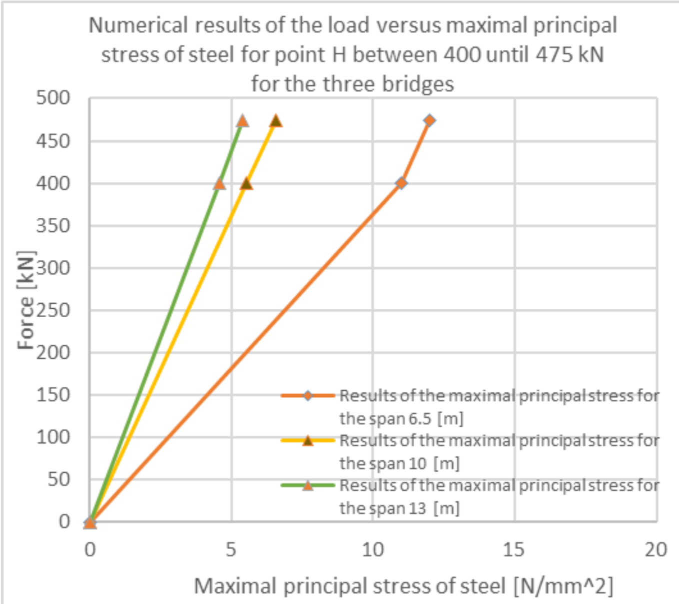

Figure F-4: Numerical results of the load versus the maximal principal stress of steel for point H between 400 until 475 kN for the three bridge decks.

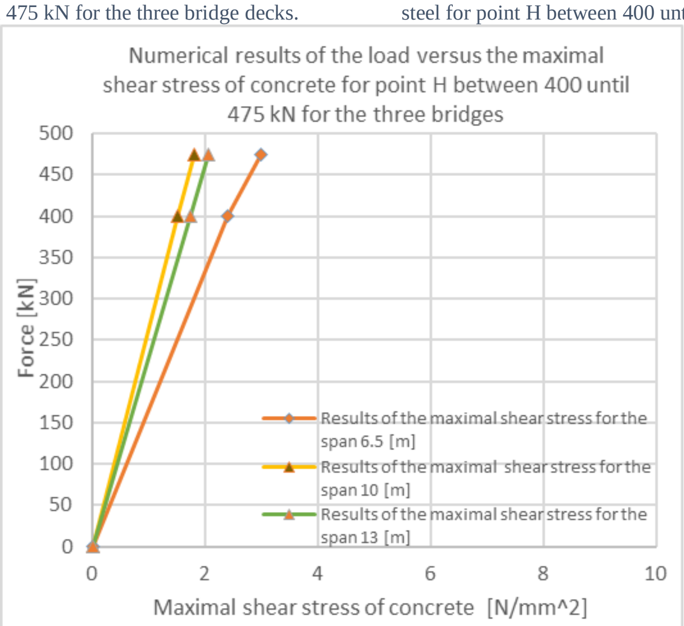

Figure F-5: Numerical results of the load versus the maximal shear stress of concrete for point H between 400 until 475 kN for the three bridge decks.

F.2. Numerical results for the loaded point L of three bridge decks

Table F-6: Results of the vertical displacement of in-situ-load-test 3 versus numerical results for the three bridges of steel girder 4.

Vertical displacement of steel girder 4 in [mm]				
Load	**Results of in-situ-load test 3**	**Results of the numerical model of steel girder 4 with a span 6.5 [m]**	**Results of the numerical model of steel girder 4 with a span 10 [m]**	**Results of the numerical model of steel girder 4 with a span 13 [m]**
0	0	0	0	0
400	0.29	0.21	0.23	0.53
475	0.38	0.25	0.27	0.63

Table F-7: Results of the vertical displacement of in-situ-load-test 3 versus numerical results for the three bridges of steel girder 3.

Vertical displacement of steel girder 3 in [mm]				
Load	**Results of in-situ-load test 3**	**Results of the numerical model of steel girder 3 with a span 6.5 [m]**	**Results of the numerical model of steel girder 3 with a span 10 [m]**	**Results of the numerical model of steel girder 3 with a span 13 [m]**
0	0	0	0	0
400	0.24	0.22	0.23	0.53
475	0.33	0.26	0.27	0.63

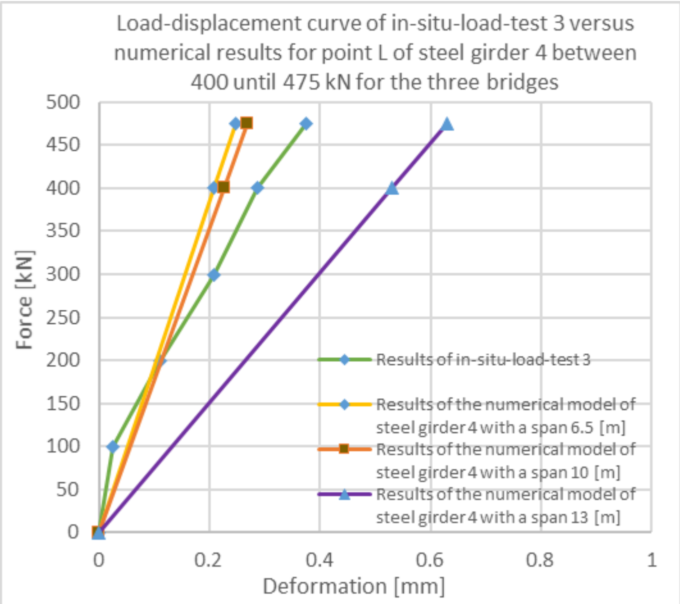

Figure F-6: Load-displacement curve of in-situ-load-test 3 versus numerical results for point L of steel girder 4 between 400 until 475 kN for the three bridge decks.

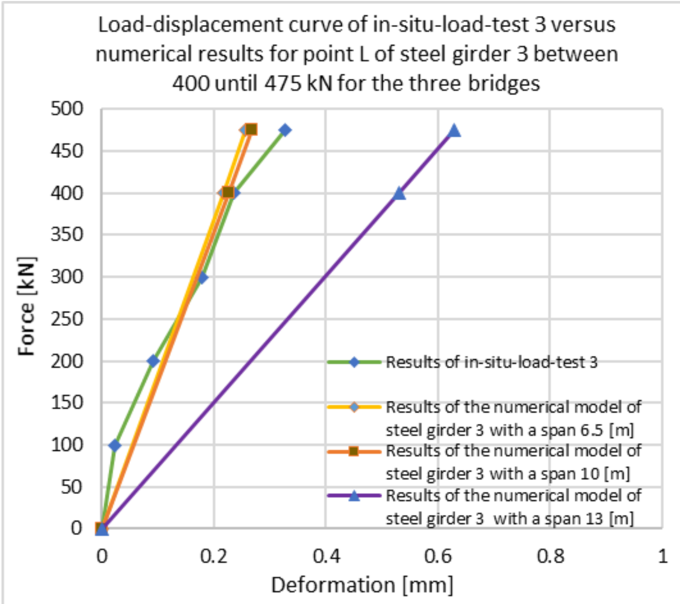

Figure F-7: Load-displacement curve of in-situ-load-test 3 versus numerical results for point L of steel girder 3 between 400 until 475 kN for the three bridge decks.

Table F-8: Results maximal principal stress of concrete for the three bridge decks.

Maximal principal stress of concrete in [N/mm^2]			
Load	**Results of the maximal principal stress for the span 6.5 [m]**	**Results of the maximal principal stress for the span 10 [m]**	**Results of the maximal principal stress for the span 13 [m]**
0	0	0	0
400	2.98	3.36	3.29
475	3.54	3.98	3.90

Table F-9: Results maximal shear stress of concrete for the three bridge decks.

Maximal shear stress of concrete in [N/mm^2]			
Load	**Results of the maximal shear stress for the span 6.5 [m]**	**Results of the maximal shear stress for the span 10 [m]**	**Results of the maximal shear stress for the span 13 [m]**
0	0	0	0
400	1.50	1.49	1.79
475	1.80	1.79	2.12

Table F-10: Results maximal principal stress of steel for the three bridge decks.

Maximal principal stress of steel in [N/mm²]			
Load	**Results of the maximal principal stress for the span 6.5 [m]**	**Results of the maximal principal stress for the span 10 [m]**	**Results of the maximal principal stress for the span 13 [m]**
0	0	0	0
400	11	5.68	7.14
475	13	6.73	8.47

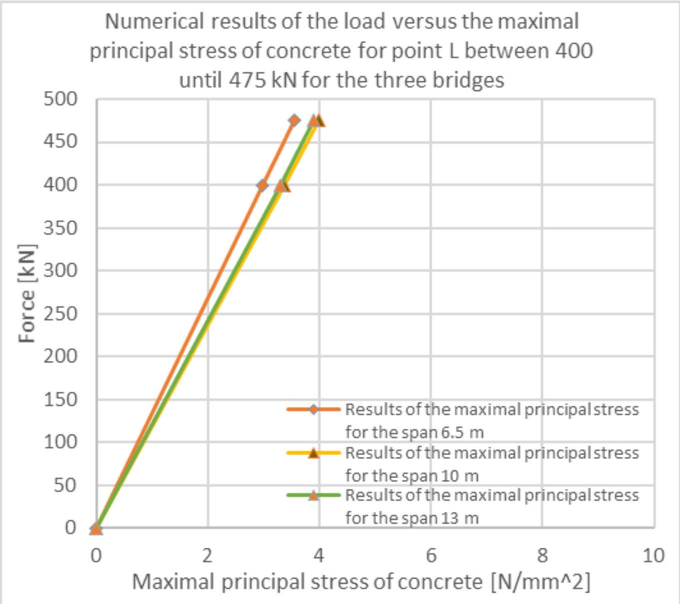

Figure F-8: Numerical results of the load versus the maximal principal stress of concrete for point L between 400 until 475 kN for the three bridge decks.

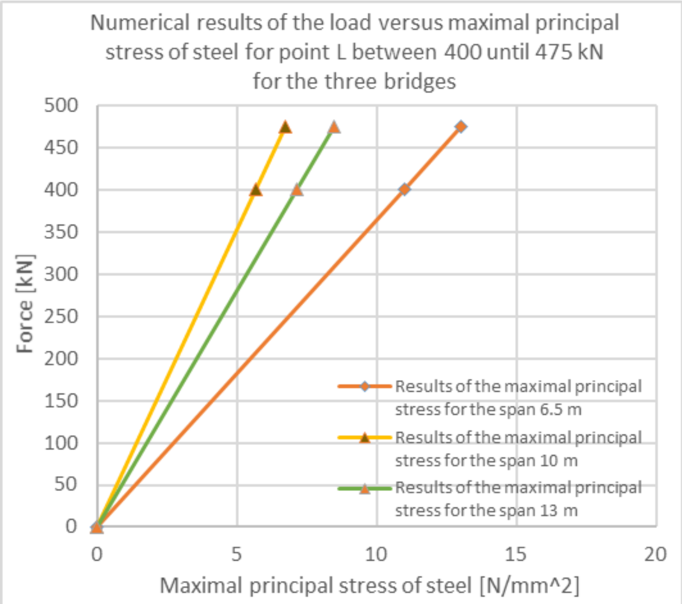

Figure F-9: Numerical results of the load versus maximal principal stress of steel for point L between 400 until 475 kN for the three bridge decks.

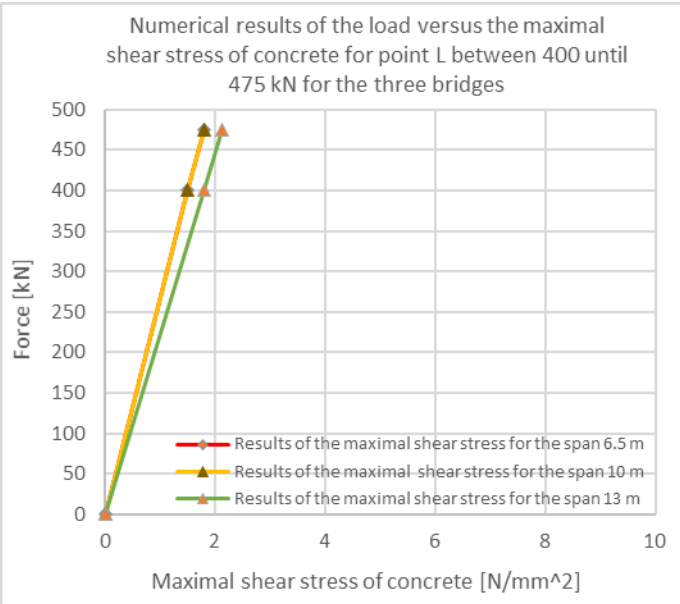

Figure F-10: Numerical results of the load versus the maximal shear stress of concrete for point L between 400 until 475 kN for the three bridge decks.